

**ELECTRON  
FRACTOG-  
RAPHY**

**American Society for Testing and Materials**

**ASTM**

**STP 436**

# ELECTRON FRACTOGRAPHY

A symposium  
presented at the  
Seventieth Annual Meeting  
AMERICAN SOCIETY FOR  
TESTING AND MATERIALS  
Boston, Mass., 25-30 June, 1967

ASTM SPECIAL TECHNICAL PUBLICATION NO. 436

List price \$11.00; 20 per cent discount to members



*published by the*  
AMERICAN SOCIETY FOR TESTING AND MATERIALS  
1916 Race Street, Philadelphia, Pa. 19103

© BY AMERICAN SOCIETY FOR TESTING AND MATERIALS 1968  
Library of Congress Catalog Card Number: 68-15547

NOTE

The Society is not responsible, as a body,  
for the statements and opinions  
advanced in this publication.

Printed in Rahway, N.J.  
July, 1968

# Foreword

The Symposium on Electron Fractography was presented during the Seventieth Annual Meeting of the Society held in Boston, Mass., 25-30 June 1967. The symposium was sponsored by Committee E-24 on Fracture Testing of Metals. The symposium chairman was C. D. Beachem, Naval Research Laboratory.

## **Related ASTM Publications**

**Techniques of Electron Microscopy Diffraction  
Microprobe Analysis, STP 372 (1965), \$3.75**

**Fracture Toughness Testing and Its Applications,  
STP 381 (1965), \$19.50**

**Advances in Electron Metallography, Vol. 6,  
STP 396 (1966), \$7.00**

**Fatigue Crack Propagation, STP 415 (1967), \$30.00**

# Contents

Introduction . . . . .	1
Electron Fractography—Tools and Techniques—J. L. MCCALL . . . . .	3
A Fractographic Analysis of the Relationships Between Fracture Toughness and Surface Topography in Ultrahigh-Strength Steels—W. A. SPITZIG, G. E. PELLISSIER, C. D. BEACHEM, M. HILL, AND W. R. WARKE . . . . .	13
Discussion . . . . .	30
Cleavage Phenomena and Topographic Features—H. C. BURGHARD, JR., AND N. S. STOLOFF . . . . .	32
Fracture by Microscopic Plastic Deformation Processes—C. D. BEACHEM AND D. A. MEYN . . . . .	59
Application of Electron Fractography to Fatigue Studies—J. C. MCMILLAN AND R. W. HERTZBERG . . . . .	89
Environmental Effects on Fracture Morphology—N. A. NIELSEN . . . . .	124
Special Fractographic Techniques for Failure Analysis—B. V. WHITE-SON, A. PHILLIPS, V. KERLINS, AND R. A. RAWE . . . . .	151
Engineering Applications of Fractography—A. J. BROTHERS AND S. YUKAWA . . . . .	179
Fractography and Microstructure of Aluminum Alloys 7075-T651 and 7075-T7351—M. S. HUNTER AND J. C. MCMILLAN . . . . .	196
Techniques for Electron Microscopic Fractography—W. R. WARKE, N. A. NIELSEN, R. W. HERTZBERG, M. S. HUNTER, AND M. HILL . . . . .	212

## Introduction

---

The purpose of this symposium is to describe the present "state-of-the-art" of electron fractography, and report the results of activity sponsored by Subcommittee II on Fractography of ASTM Committee E-24 on Fracture Testing of Metals. It is hoped that future symposia on this subject will benefit from contributions from invited authors from laboratories throughout the world where excellence of electron fractographic usage in research and failure analyses has been proved.

As the papers in the volume indicate, a great deal has been learned about the mechanisms of crack propagation, and the correlation of fine-scale fracture surface features with macroscopic stress and environment conditions.

This volume, however, does not cover all of the fractography subjects presently being studied, because this tool is versatile and is being used to complement other research tools in a variety of disciplines. Neither have the subjects discussed herein been fully explored. Therefore, this volume should serve as a progress report, and one should expect future symposia in electron fractography to include significant new applications of the tool and further refinements of existing theory and techniques.

*C. D. Beachem*

Head, Micro-Mechanical Metallurgy Section,  
Physical Metallurgical Branch, Metallurgical Div.,  
Naval Research Laboratory, Washington, D.C.;  
symposium chairman.

## Electron Fractography—Tools and Techniques

---

**REFERENCE:** McCall, J. L., “**Electron Fractography—Tools and Techniques,**” *Electron Fractography, ASTM STP 436*, American Society for Testing and Materials, 1968, pp. 3–16.

**ABSTRACT:** Electron fractography has recently become a valuable tool for studying the topographic features of fractures, and from it much new theoretical and applied information regarding the micromechanisms of fractures has been obtained. Prior to the use of electron microscopes, the unaided eye, optical microscopes, and metallographic cross sections were used to study fractures. These methods, however, have distinct limitations such as low resolution and small depth of field. Both of these limitations have been overcome with the electron microscope. Other tools are now being applied to fracture studies to complement the electron microscope. These include deep-focusing microscopes, electron microprobe analyzers, and scanning and reflection electron microscopes. The combination of all these tools has provided much new information, but it must be realized that electron microscopy as a tool for studying fractures is still essentially in its infancy, and it offers tremendous opportunities which, as yet, have not been fully explored.

**KEY WORDS:** fractography, fracture, electron microscopy

Valuable information has long been known to exist in the fracture surfaces of materials, and, through the years, various approaches have been employed to obtain and interpret this information. One of the earliest accounts of fractographic studies is the report of the French scientist, DeReaumur, who studied fractured facets of steel by microscopy in 1722 [1].<sup>2</sup> In the latter part of the 19th Century, Martens [2], generally considered as the one who originated metallography, performed some limited fracture studies of metals in his work; however, he is reported to have been somewhat discouraged because of the small depth of focus of his microscope, which allowed him to see clearly only a small portion of the fracture at any one time. Around the turn of the century, Ewing and Humfrey [3] and Ewing and Rosenhain [4–6]

<sup>1</sup> Division chief, Structure of Metals, Battelle Memorial Institute, Columbus Laboratories, Columbus, Ohio.

<sup>2</sup> The italic numbers in brackets refer to the list of references appended to this paper.

were able to provide some significant information regarding the behavior of metals from studies of fractures. For example, they showed that the crystalline appearance of certain fatigue fractures was not related to the grain size of the material but rather to the type of fracture. Furthermore, they were the first to show that metals remained crystalline when deformed and to describe deformation markings which we now know as slip lines.

Except for some studies by Howe [7], most of the microscopic studies of metals in the early 1900's were limited to examinations of polished sections. Somewhat later, a number of investigators recognized that the properties of steels could be correlated with the coarseness or fineness of the fracture surface. For example, it was found that fractured specimens could be used as a means of evaluating the grain size of a metal. In 1927, Arpi [8] developed a set of standard fractures which were believed to cover the full range from coarse to fine grain size. Some time later, Shepherd [9], working in this country, developed a similar set of standards for evaluating grain sizes of hardened steels. His method is still in somewhat limited use today.

The most significant and detailed studies of fractures were performed approximately 20 years ago by Zappfe and Clogg [1]. For their work, they developed techniques for using the optical microscope to study fractures. Although they were bothered by the relatively small depth of focus of the optical microscope, they were able to orient the facets of a fracture with the axis of the microscope such that examinations could be made at a relatively high magnification. As a result of their work, the term "fractography" was coined. Most of their work was done on brittle fractures, from which they described in considerable detail the appearance and crystallography of cleavage facets.

Since Zappfe and Clogg's work, except for routine examinations of the fractures of service failures, another lull occurred in fractographic studies until the advent of the application of electron microscopy to fracture studies [10,11]. With this new tool, there has been a resurgence of effort in research studies concerning the micromechanisms of fracture, and, as a result, much new information regarding fracture has been developed.

## **Use of Optical Microscopes**

### *Examination of Fracture Surfaces*

Prior to the development of the electron microscope as a tool for studying fracture, fractographers were limited essentially to the use of their unaided eyes and to light microscopes. With the unaided eye, it is possible to group fractures into rather broad categories, such as fibrous and shear. In many instances, it is possible to positively recognize

certain types of fractures by certain characteristic markings. For example, fatigue failures are characterized by their normally flat appearance and by the presence of stop rings or beach marks. Sometimes, the origin of fracture can be determined by examinations with the unaided eye.

The optical microscope has made it possible to distinguish the fracture mechanisms more precisely and to study such features as individual grain facets, cleavage facets, fatigue striations, and fracture origins. However, the optical microscope is severely limited for this type of study by its restricted depth of field. The maximum depth of field (defined as the vertical displacement of the object that can be tolerated without loss of focus) [12] of optical microscopes in use today is approximately  $0.2 \mu\text{m}$ . This means that features on a fracture that are displaced vertically by more than this amount cannot be observed simultaneously.

In an attempt to overcome the small-depth-of-field problem, McLachlin [13] has recently developed a microscope that allows rather high-magnification photography of extremely rough specimens. Figure 1 is a photograph of a commercial model of this instrument. This instrument, called a deep-field photographic microscope, uses a very thin beam of light to illuminate the specimen. The light beam is at a constant distance from the microscope objective and is at the focal plane. While the photograph is being made, the specimen is moved at a constant rate through the beam of light. Since only the illuminated portions of the specimen will be recorded on the photographic film, and

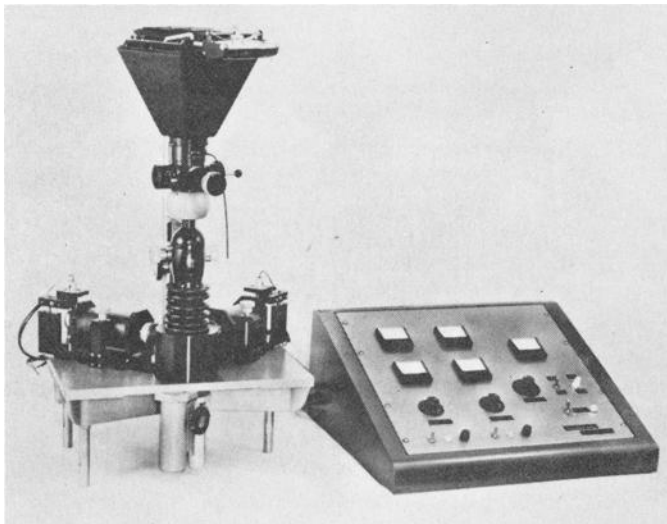


FIG. 1—Deep field photographic microscope developed by McLachlin [13].

since all of the illuminated portions will be in focus, the entire photograph will also be in focus. Figure 2 is an example of the type of result that can be obtained from this microscope. If the fracture shown in Fig. 2 had been photographed at the same magnification ( $\times 100$ ) through a normal microscope, only a small portion of the surface would have been in focus because of the roughness of the surface. When this instrument is fully developed, it should have wide application in the field of fractography.

#### *Examination of Metallographic Cross Sections*

Because of the limitations of optical microscopes, a common technique for studying fractures has been to prepare and examine metallographic cross sections through the fractured faces. Often the two halves of the fracture are matched and mounted together. To preserve the edge the fracture is often plated prior to mounting. The mounted fractures can be examined by optical microscopy, or, when details of the fine structure of interest, electron microscopy can be used. Certain types of significant information can be obtained from cross-sectional analyses; in fact, prior to the use of electron fractography, this was about the only method of determining whether a fracture occurred intergranularly or transgranularly. One drawback of this type of examination is that it presents only a one-dimensional view of the fractured surface. As a result, only a limited amount of the fracture is seen at any one time. Furthermore, the cross section often makes it

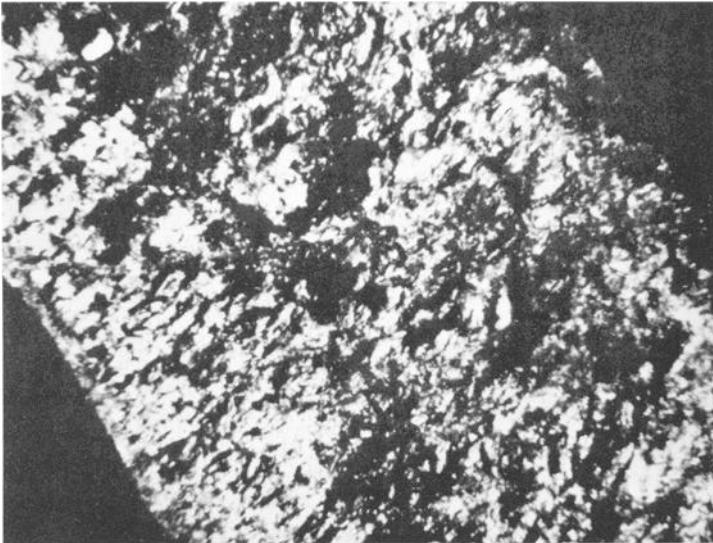


FIG. 2—Fracture of a steel specimen photographed with a deep-field photographic microscope ( $\times 100$ ).

difficult to relate the features seen in the microscope to those macroscopic features of the failed part. Of course, this type of examination is destructive to the fracture.

### **Use of Transmission Electron Microscopes**

Approximately 10 years ago [10,11] electron microscopes were first used to study fractures of materials. Electron microscopic studies of fractures have overcome many of the limitations of the other means of fracture examination [14-17]. Aside from the abilities of electron microscopes to permit high magnification and high-resolution examinations of materials, they also have much higher depths of field than do optical microscopes for the magnifications employed.

#### *The Replication Technique*

Transmission electron microscopes, however, are not capable of examining a fracture directly. Rather, it is necessary to employ a replica of the fractured surface, much the same as that used for microstructural studies.

Before a fracture can be replicated, the fracture surface must be clean and undisturbed. It can never be emphasized too strongly that, from the time of fracture until the time of replication, the fracture must be handled very carefully if maximum information is to be obtained from it. People always seem to have an uncontrollable impulse to see if two halves of a fracture fit exactly together. Only occasionally is such information significant, but the process of mating the fractures can severely damage the microtopographic features of a fracture to the extent that its usefulness for electron fractographic study may be limited. In addition to mechanical damage, the surface can be destroyed, or at least the examination hindered, by chemical and atmospheric attack. Acceptable methods of coating and protecting fractures have been developed [15],<sup>3</sup> and these should be used when fractographic work is anticipated. In fact, it is recommended that these procedures be used whenever possible when a fracture occurs, since unanticipated fractographic work may be required. Often a fracture is intentionally exposed to a media which may be corrosive, such as certain types of crack-detection fluids. In these instances, the effects of these media on the fracture should be thoroughly understood before fractographic work is to be performed.

For fractures produced intentionally in the laboratory, it is normally possible to exercise the required precautions of handling and surface preservation. For failures that occur in service, however, this is seldom possible; fractures often become severely oxidized, corroded, me-

<sup>3</sup> See p. 212.

chanically abraded, or in other ways damaged. As a result, their usefulness for fractographic studies is limited. A number of acceptable procedures for cleaning fractures have been developed, the best of which is probably continuous replication of the surface with plastic tape. This procedure removes surface dirt, loosely adhering oxide scales, and some types of surface films. Other techniques, such as ultrasonic cleaning, inhibited-acid treatments, and oxide-removal processes, have been developed<sup>3</sup> and can be used when the plastic-tape replication procedure is not satisfactory.

There are several methods for replicating a fracture for electron fractography. These are described in detail in a later paper of this symposium<sup>3</sup> and therefore will only be mentioned here. The prime requirement of any replica is that it duplicates faithfully the finest features of the fracture. Numerous replication procedures have been developed; however, the three most common for electron fractography are the plastic tape, the direct carbon, and the oxide. Each of these has particular features which makes them suitable for certain applications. For example, the plastic tape, which is the most widely used, has the distinct advantage of being nondestructive to the specimen. Furthermore, replicas of this type can be made practically anywhere with a minimum of equipment. For example, if a failure should occur in a large part in the field, it is possible, without moving the part, to prepare a plastic replica of it. This replica can then be returned to the laboratory for shadowing, final preparation, and examination. Replicas of this type can be examined by both optical and electron microscopy, which provides an added advantage. Figure 3 shows a technician preparing a

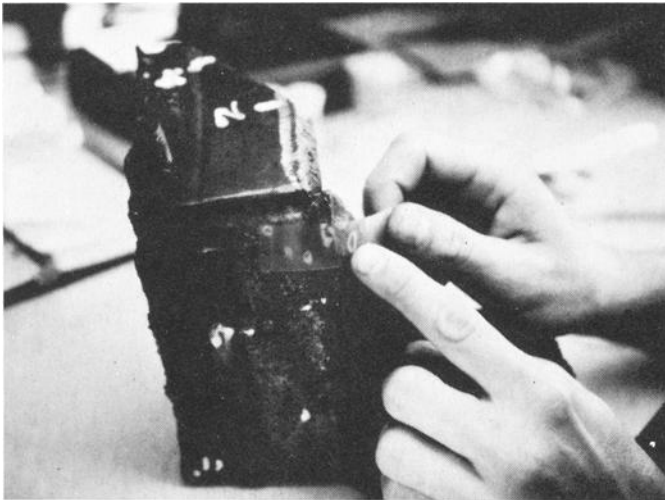


FIG. 3—Plastic-tape replication of a service failure.

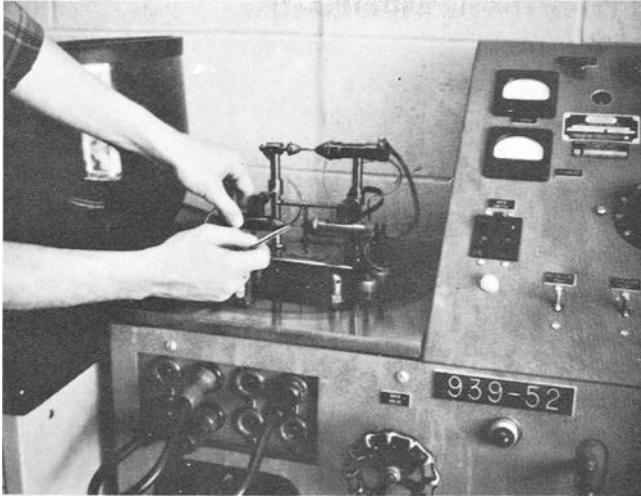


FIG. 4—*Shadowing a plastic-tape replica in a vacuum evaporator.*

plastic tape replica of the fracture of a rather large service failure. After the plastic replica is prepared, it is normally shadowed with some metal by vapor evaporation as shown in Fig. 4.

Direct carbon replicas have the advantage of better resolution than the plastic tape and can be particularly advantageous in research. Their greatest limitation is that only one replica can be made from a fracture since the specimen is destroyed during the removal of the replica. Therefore, the fracture is not available later for metallographic examination or other types of study. The oxide-replication technique, which has been developed for only a limited number of materials, provides other information which at times can be useful.

It should be recognized that introduction of the replica raises the possibility that the structure seen does not truly duplicate the features of the fracture. Features present on the replica but not the fracture are called artifacts. Several types of artifacts are encountered in the replicas, and these can originate either from the replica or from the specimen. Even when the most careful procedure is used by an experienced electron microscopist, artifacts still occur. Fortunately, the types of artifacts that are frequently encountered in electron fractographic work can be recognized readily and have been described [18,19].

In addition to normal examinations of replicas by electron microscopy, there are various specialized methods of examining replicas which have been developed and which can provide additional information. Foremost of these is stereoscopic viewing. This is accomplished by taking pairs of photographs of a single area of a replica at two



FIG. 5—Examination of stereo-pairs in a special viewer to observe the three-dimensional characteristics of a fracture.

slightly different angles in the electron microscope. When these pairs are viewed in a special stereo viewer, as shown in Fig. 5, the three-dimensional characteristics of a fracture can be observed and studied. This type of viewing is particularly useful for studies of fractures, since the true topographic appearance of the fracture can be seen readily. Furthermore, the topographic structure of a fracture can be quantitatively analyzed from the stereo pairs by use of a parallax bar. This type of information has proved useful in both theoretical and applied studies concerning the micromechanisms of certain types of fractures.

Other specialized methods of replications may be used for fractographic work, such as replication of a precise area in a fracture and replication and examination of identical areas of matching halves of a fracture. Many of these methods are described in a later paper of this symposium.<sup>3</sup>

### **Other Methods of Examination**

#### *The Electron Microprobe Analyzer*

Although optical and transmission electron microscopes are the principal tools of a fractographer, other instruments are presently being used to supplement these. The electron microprobe analyzer is probably the most widely developed and used so far. Since its development about 15 years ago [20], the microprobe has found wide application in all fields of materials research, including fractography. It has the unique capability of quantitatively analyzing areas as small as 1  $\mu\text{m}$  in diameter for their chemical composition. Figure 6 shows a

commercial electron microprobe instrument. The instrument makes use of a finely focused beam of high-energy electrons which impinge on a selected point of the specimen. When the electron beam is stopped by the specimen, a portion of its energy is converted to X-radiation having wave lengths characteristic of the elements contained in the analyzed area of the specimen. The wave lengths of the emitted X-rays can be analyzed by spectrometers, and, since the wave lengths of the X-rays from each element are peculiar to that element, the identity of the elements can be determined from measurement of the wave lengths. Quantitative measurements can be made by measuring the intensities of the emitted characteristic X-radiations and comparing them with intensities from standard specimens.

The instrument has been used in conjunction with fractographic work in a number of ways. For instance, quite often the path of fracture of a material is dictated by nonmetallic inclusions or other microstructural features of a material. This has been particularly demonstrated for fatigue fractures [17]. In many instances, these features are contained on the surface of the fracture, and their identification would be desirable. Also, many fractures are initiated on inclusions or other types of impurity defects. It has also been shown that each of the dimples of ductile fractures is initiated on inclusions. Since most of these inclusions are microscopic, identification of them *in situ* is possible only by electron-probe analysis.

Many electron microprobes are capable of performing beam-scanning types of analysis, where the beam is electronically deflected so that it scans a raster on the specimen. While the beam scans, the

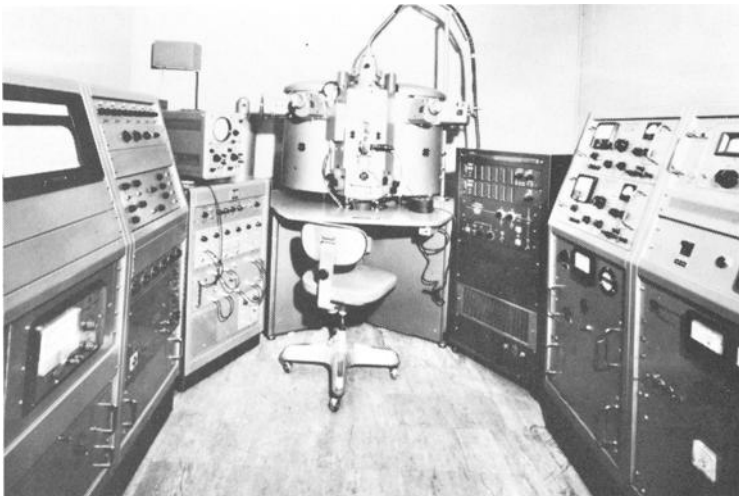


FIG. 6—Commercial electron microprobe analyzer.

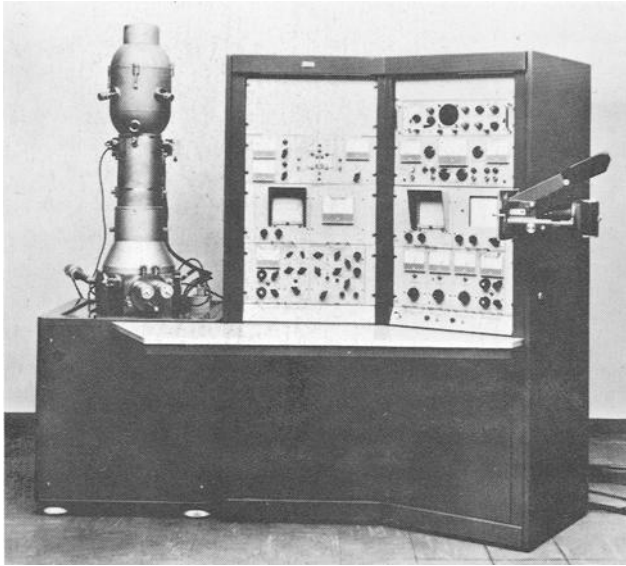


FIG. 7—Commercial scanning electron microscope.

signal from a spectrometer is fed into a cathode-ray tube that scans synchronously with the electron beam. The resultant image that forms on the cathode-ray tube shows the elemental distribution in the specimen. Banerjee [21] and Rice and Racus [22] have shown how this mode of electron-microprobe analysis can be used to view fractures and identify constituents.

### *The Scanning Electron Microscope*

Another instrument which is beginning to be employed for studies of fractures is the scanning electron microscope.<sup>4</sup> A commercial model of this instrument is shown in Fig. 7. This instrument makes use of a beam-scanning mode of operation similar to that in electron microprobe analysis. A fine electron beam scans the surface of the specimen in a two-dimensional raster. The back-scattered electrons are analyzed with a scintillation counter, and the signal from the counter is fed into a cathode-ray tube which is set to scan synchronously with the electron beam. As a result, a point-by-point image of the specimen is displayed on the cathode-ray tube. This instrument has an extremely large depth of focus and is therefore quite applicable to fracture studies. The resolution of this instrument depends on several factors, but resolutions of better than 300 Å have been achieved. Figures 8 and 9 are photographs of fractures taken with a scanning electron microscope. Figure 8<sup>4</sup> is a photograph of a fracture of magnesium oxide and Fig. 9<sup>5</sup>

<sup>4</sup> Cox, B., private communication.

<sup>5</sup> Whitcomb, P. B., private communication.

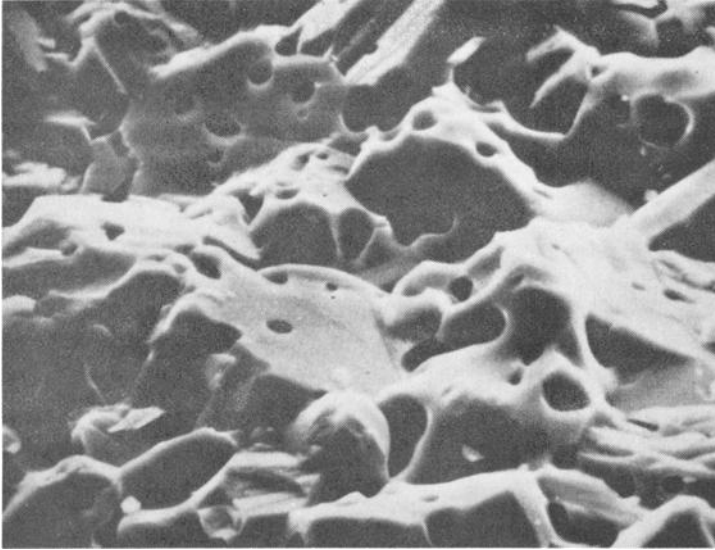


FIG. 8—Scanning electron micrograph of a fracture of magnesium oxide (see footnote 4) ( $\times 4000$ ).

is of a tensile fracture in a soft iron wire. These figures show the type of result that can be obtained with this instrument. As with transmission electron microscopy, stereo pairs of a fracture can be obtained and studied either qualitatively or quantitatively. To obtain the pairs, the fracture is tilted in the scanning electron microscope between photographs.

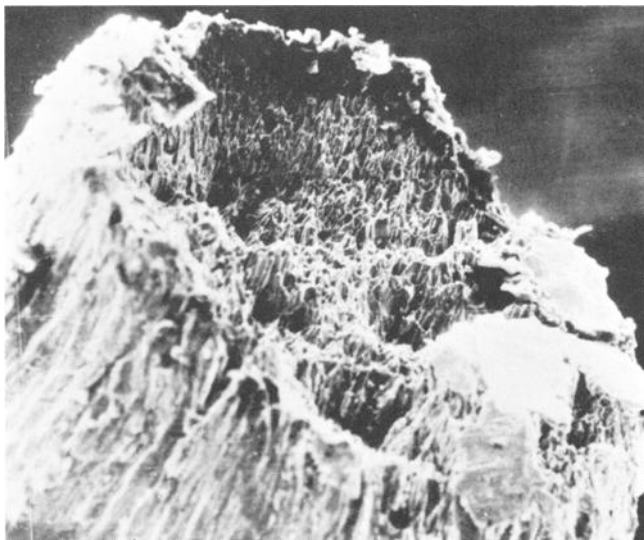


FIG. 9—Scanning electron micrograph of a ductile fracture in an iron wire (see footnote 5) ( $\times 260$ ).

### *Reflection Electron Microscopy*

Reflection electron microscopy has also been used as a method of studying fractures. It overcomes the large disadvantage of transmission electron microscopes in that a fracture can be examined directly; preparation of a replica step is unnecessary. This type of examination can be made on most commercial electron microscopes by the addition of certain accessories. The image obtained is similar in many respects to that seen with oblique illumination in the optical microscope. The image is formed by placing the specimen on the side of the electron beam in an electron-microscope column. The beam is focused so that it strikes the specimen at a glancing angle. The back-scattered electrons that are emitted are recorded on a fluorescent screen from the same low angle. Unfortunately, this leads to a severe foreshortening of the image, and normally only a small area of the specimen can be focused at any one time. The greatest disadvantage of the reflection technique is its low resolution. This is primarily due to inelastic scattering of the electron beam. For this reason, although it might seem like an ideal method for studying fractures, it has seen only limited application to date.

### **Information Obtained from Electron Fractography**

One might inquire what information electron fractographic research has provided in the relatively few years that it has been employed. The answer will be found in part by this symposium and is further demonstrated by the literature and widespread use of the technique. The micromechanisms of ductile fracture, that is, the initiation, growth, and coalescence of microvoids, has been confirmed by electron fractography, and correlations between void size and such things as stress and material cleanliness have been developed. Also, correlations between void shapes and state of stress have been developed. Several new models to explain the mechanisms of fatigue fracture have evolved, and correlations between fatigue striations, load cycles, striation spacing, and loading conditions have been developed. Also, rather conclusive experimental evidence regarding initiation mechanisms of fatigue fracture has been acquired from electron fractographic studies. In brittle fracture, an explanation has been offered for the cleavage patterns that occur on fractures, and the form of the patterns has been used successfully to determine such things as fracture directions and initiation points. The influence of the microstructure of a material on its fracture has been demonstrated for many different fracture modes.

In addition to a research tool, electron fractography also has developed into an extremely valuable tool for the analyses of service

failures. On many occasions, it has been shown by electron fractography that the interpretation of the cause of a failure based only on some of the more conventional techniques can be in error.

Other information regarding fracture processes that has been derived from electron fractographic examinations will be discussed in this symposium. It should be realized, however, that the use of electron microscopy as a tool for studying fracture is still essentially in its infancy and there are tremendous opportunities for performing significant research with it.

## References

- [1] Zappfe, C. A. and Clogg, M., "Fractography—A New Tool for Metallurgical Research," *Transactions, American Society for Metals*, Vol. 34, 1945, p. 71.
- [2] Martens, A., "The Microscopical Examination of Iron," *Z. Ver. dent. Ing.*, Vol. 21, 1878, p. 11.
- [3] Ewing, J. A. and Humfrey, J. C. W., "The Fracture of Metals Under Repeated Alternations of Stress," *Transactions, Royal Society, London*, Vol. 200A, 1902, pp. 241–250.
- [4] Ewing, J. A. and Rosenhein, W., "Experiments in Micro-Metallurgy: Effects of Strain Preliminary Notice," *Proceedings, Royal Society, London*, Vol. 65, 1899, pp. 85–90.
- [5] Ewing, J. A. and Rosenhein, W., "The Crystalline Structure of Metals," *Transactions, Royal Society, London*, Vol. 193A, 1899, pp. 353–375.
- [6] Ewing, J. A. and Rosenhein, W., "The Crystalline Structure of Metals," *Transactions, Royal Society, London*, Vol. 195A, 1900, pp. 279–302.
- [7] Howe, H. M., *Metallography of Steel and Cast Iron*, McGraw-Hill, New York, 1916.
- [8] Arpi, R., "The Fracture Test as Used for Tool Steel," *Metallurgia*, Vol. 11, 1935, p. 123.
- [9] Shepherd, B. F., "The P-F Characteristic of Steel," *Transactions, American Society for Metals*, Vol. 22 (1934), p. 979.
- [10] Plateau, J., Henry, G., and Crussard, C., "Quelques nouvelles applications de la microfractographie," *Revue de Metallurgie*, March 1957, pp. 200–216.
- [11] Crussard, C. et al., "A Study of Impact Tests and the Mechanism of Brittle Fracture," *Journal, Iron and Steel Institute*, Vol. 183, June 1956, p. 146.
- [12] Brandon, D. G., *Modern Techniques in Metallography*, Van Nostrand, London, 1966.
- [13] McLachlan, D., "Extreme Focal Depth in Microscopy," *Applied Optics*, Vol. 3, 1964, pp. 1009–1013.
- [14] Phillips, A., Kerlins, V., and Whiteson, B. V., "Electron Fractography Handbook," Technical Report ML-TDR-64-416, Air Force Materials Laboratory, Research and Technology Division, Air Force Systems Command, Wright-Patterson Air Force Base, Ohio, Jan. 1965.
- [15] Warke, W. R. and McCall, J. L., "Fractography Using the Electron Microscope," Technical Report No. W3-2-65, American Society for Metals, presented at the 1965 Western Metal Congress, 22–26 Feb. 1965, Los Angeles, Calif.
- [16] Beachem, C. D. and Pelloux, R. M. N., "Electron Fractography—A Tool for the Study of Micromechanisms of Fracturing Processes," *Fracture Toughness Testing and Its Applications, ASTM STP 381*, American Society for Testing and Materials, 1965.
- [17] Pelloux, R. M. N., "The Analysis of Fracture Surfaces by Electron Microscopy," *Metals Engineering Quarterly*, Vol. 5, Nov. 1965, p. 26.
- [18] Beachem, C. D., "The Interpretation of Electron Microscope Fractographics," Report 6360, Naval Research Laboratory, Jan. 1966.

- [19] Beachem, C. D. and Dahlberg, E. P., "Fractography Part XV. Some Artifacts Possible with the Two-Stage Plastic Carbon Replication Technique," Memorandum Report 1457, Naval Research Laboratory, Sept. 1963.
- [20] Castaing, R., thesis, University of Paris, 1951.
- [21] Banerjee, B. R., Bingle, W. D., and Blake, N. S., "Scanning Electron-Probe Microanalysis in the Metals Industry," *Journal of Metals*, Oct. 1963, pp. 769-773.
- [22] Rice, R. W. and Racus, R. G., "Electron-Probe Examinations of Fracture Surfaces," *Journal of Applied Physics*, Vol. 38, Jan. 1967, pp. 422-423.

W. A. Spitzig,<sup>1</sup> G. E. Pellissier,<sup>1</sup> C. D. Beachem,<sup>2</sup>  
A. J. Brothers,<sup>3</sup> M. Hill,<sup>4</sup> and W. R. Warke<sup>5</sup>

## A Fractographic Analysis of the Relationships Between Fracture Toughness and Surface Topography in Ultrahigh-Strength Steels

---

**REFERENCE:** Spitzig, W. A., Pellissier, G. E., Beachem, C. D., Brothers, A. J., Hill, M., and Warke, W. R., "A Fractographic Analysis of the Relationships Between Fracture Toughness and Surface Topography in Ultrahigh-Strength Steels," *Electron Fractography, ASTM STP 436*, American Society for Testing and Materials, 1968, pp. 17-31.

**ABSTRACT:** Fracture surfaces of fatigue precracked, notched tension test specimens of experimental oil quenched and tempered (800 F) 0.45C-Ni-Cr-Mo steels of different residual sulfur contents, and of two 18Ni maraging steels (250 and 300 grades) were investigated, using electron fractography, by a task group composed of various members of Subcommittee II on Fractography of ASTM Committee E-24 on Fracture Testing of Metals. Sulfur levels of 0.008, 0.016, 0.025, and 0.049 weight per cent in the 0.45C-Ni-Cr-Mo steels corresponded to fracture toughness values ( $K_{Ic}$ ) of 65.3, 55.6, 51.0, and 42.8 ksi  $\sqrt{\text{in.}}$ , respectively. The 250- and 300-grade maraging steels exhibited  $K_{Ic}$  values of 68 and 42 ksi  $\sqrt{\text{in.}}$ , respectively. The investigation was carried out to determine whether the differences in fracture toughness could be related to changes in fracture surface topography.

The differences in fracture toughness among the quenched-and-tempered 0.45 carbon alloy steels of different residual sulfur contents could be accounted for by differences in the frequency (or spacing) of the sulfide inclusions. These particles seemed to have nucleated microvoids in advance of the crack tip, which coalesced and resulted in dimple rupture. The particle spacing in each steel was equivalent to a process zone size based on the Krafft model. A similar correlation was not found for the two grades of 18Ni maraging steel having different toughness levels, possibly because the mechanism of fracture is more complex than for the 0.45 carbon alloy steels. Another fractographic feature,

<sup>1</sup> Senior research metallurgist and senior research consultant, respectively, Applied Research Laboratory, U.S. Steel Corp., Monroeville, Pa.

<sup>2</sup> Head, Micromechanical Metallurgy Section, Metallurgy Div., U.S. Naval Research Laboratory, Washington, D.C. Personal member ASTM.

<sup>3</sup> Research metallurgist, Metallurgy Applied Research, Materials and Processes Laboratory, Schenectady, N.Y.

<sup>4</sup> Research metallurgist, Research Center, Republic Steel Corp., Cleveland, Ohio.

<sup>5</sup> Instructor, Department of Metallurgy, Illinois Institute of Technology, Chicago, Ill.

namely, the extent of a "stretched" zone between the fatigue-cracked and overload regions of the fractures, did appear to show some correlation with the  $K_{Ic}$  levels for both classes of steels, and may be related to the size of the process or plastic zone at the crack tip. This feature, and its significance in terms of plane-strain fracture toughness, is being more extensively investigated by Subcommittee II of E-24.

**KEY WORDS:** fractography, fracture toughness, alloy steels, maraging steels, quenching (cooling), tempering

The important influence of microstructure and attendant strength level, and of certain impurity elements, on the fracture toughness of ultrahigh-strength steels has become generally recognized. For some medium-carbon, quenched-and-tempered alloy steels, it has been found that there is a strong dependence of plane-strain fracture toughness ( $G_{Ic}$  or  $K_{Ic}$ ) on the microstructure and strength developed by tempering at different temperatures [1].<sup>6</sup> Furthermore, for a given microstructure and strength level, the fracture toughness increased with a decrease in the combined amounts of the impurity elements, sulfur and phosphorus, in these steels [1]. Also, the sensitivity of fatigue-crack growth rates in such steels to changes in testing atmosphere appeared to be related to fracture toughness and microstructure [2,3]. On the other hand, for the ultrahigh-strength 18Ni maraging steels, the rather large difference in fracture toughness between the 250 ksi yield strength grade and the 300 ksi yield strength grade could not be readily related to differences in microstructure [4]. Nevertheless, the sensitivity of fatigue-crack growth rate in these steels to changes in testing atmosphere did appear to be related to differences in fracture toughness and fracture surface topography [3,5].

To gain further insight into the influence of impurities on the fracture toughness of ultrahigh-strength steels, and to ascertain the micro-mechanisms of fracture in relation to fracture toughness, a task group of Subcommittee II on Fractography, of ASTM Committee E-24, made a fractographic investigation of two types of ultrahigh-strength steels. The specific objective was to determine, on an interlaboratory basis, whether differences in fracture toughness among a series of medium-carbon, quenched-and-tempered, alloy steels having different sulfur contents, and between the 250-grade and the 300-grade 18Ni maraging steels, could be related to differences in fracture surface topography.

### Materials and Experimental Work

A series of 0.45C-2Ni-1.5Cr-0.4Mo steels (Table 1) having different levels of sulfur (0.008, 0.016, 0.025, and 0.049 per cent, re-

<sup>6</sup> The italic numbers in brackets refer to the list of references appended to this paper.

TABLE 1—Chemical compositions of the steels investigated.

0.45C-NI-CR-MO STEELS											
Steel	C	Mn	P	S	Si	Ni	Cr	Mo	Al	N	O
A.....	0.43	0.27	0.007	0.008	0.24	2.05	1.48	0.43	0.025	0.007	0.002
B.....	0.45	0.26	0.007	0.016	0.25	2.04	1.49	0.44	0.025	0.009	0.001
C.....	0.46	0.25	0.005	0.025	0.24	2.04	1.48	0.43	0.027	0.009	0.001
D.....	0.46	0.24	0.007	0.049	0.22	2.04	1.54	0.44	0.023	0.008	0.001

MARAGING STEELS											
Steel	C	Mn	P	S	Si	Ni	Mo	Co	Ti	Al	
250-grade.....	0.020	0.05	0.006	0.005	0.09	18.35	5.32	7.18	0.32	0.04	
300-grade.....	0.030	0.021	0.003	0.010	0.06	18.53	4.64	8.89	0.69	0.15	

NOTE—All compositions in weight per cent.

spectively) were especially prepared from electrolytically refined iron and high-purity alloying additions, by a combination of vacuum induction melting and vacuum consumable electrode remelting. The chemical compositions of the four steels were carefully controlled, so that they were nearly identical, except for sulfur content; these steels were remarkably free of nonmetallic inclusions other than sulfide particles. Selected-area electron diffraction analysis of particles extracted from fracture surfaces showed that the inclusions were manganese sulfide (MnS). The identification was confirmed by electron-beam X-ray microprobe analysis of the extracted particles. The specimens used for fractographic examination were the broken halves of fatigue-cracked, notched round tension test specimens (1.00 in. in diameter) which were convenient to test, and which provided valid plane-strain fracture toughness values ( $K_{Ic}$ ). The 1.00-in.-diameter notched round specimens were 6 in. long and contained a machined circumferential notch with a flank angle of 45 deg. The depth of the machined notch was 0.115 in. The heat treatment of the four steels consisted of normalizing at 1650 F for 45 min, austenitization at 1550 F for 45 min, oil quenching, and tempering at 800 F for 1 h. The tempering treatment was selected, on the basis of earlier work [7], to provide a microstructure in which considerable spheroidization of the grain boundary cementite ( $Fe_3C$ ), and recovery of the matrix, had taken place. The specimens were finish-machined and fatigue-cracked in rotating bending (to provide a fatigue crack of about 0.04 in. deep) after heat treatment, and tested at room temperature. The rate of loading corresponded to a rate of increase of the nominal net section stress of  $10^5$

psi/min. The  $K_{Ic}$  values were computed from the notch tensile strengths ( $\sigma_n$ ) using the relationship

$$K_{Ic} = 0.233\sigma_n\sqrt{\pi D}$$

where  $D$  = major specimen diameter. The values are given in Table 2, together with the smooth tensile properties. The  $K_{Ic}$  values are averages of three specimens for the 0.45C-Ni-Cr-Mo steels and of four specimens for the maraging steels. The deviation from the average value of  $K_{Ic}$  was less than  $\pm 2.5$  ksi $\sqrt{\text{in.}}$  for all the steels.

TABLE 2—Mechanical properties of steels investigated.

0.45C-NI-CR-MO STEELS						
Steel	Sulfur Level, weight %	Yield Strength (0.2% off-set), ksi	Tensile Strength, ksi	Elongation in 2 in., %	Reduction of Area, %	$K_{Ic}$ ksi $\sqrt{\text{in.}}$
A.....	0.008	211.0	237.6	11.8	48.2	65.3
B.....	0.016	211.5	237.8	10.0	40.1	55.6
C.....	0.025	214.2	237.7	11.5	44.4	51.0
D.....	0.049	217.8	236.0	10.0	41.7	42.8

MARAGING STEELS						
Steel	Yield Strength (0.2% off-set), ksi	Tensile Strength, ksi	Elongation in 2 in., %	Reduction of Area, %	$K_{Ic}$ ksi $\sqrt{\text{in.}}$	$K_{Ic}$ ksi $\sqrt{\text{in.}}$
250-grade.....	259	267	11.0	44.5	68 <sup>a</sup>	68 <sup>b</sup>
300-grade.....	285	293	6.5	31.5	52 <sup>a</sup>	42 <sup>b</sup>

<sup>a</sup> Notched bend tests (believed to be more accurate).

<sup>b</sup> Notched tension tests.

The two 18Ni maraging steels (250 grade and 300 grade) were commercial steels that were vacuum consumable electrode remelted. Their compositions are given in Table 1. The heat treatment of these steels consisted of solution annealing at 1600 F for 1 h, air cooling, and aging at 900 F for 3 h. The 1-in.-diameter notched round tension test specimens that were used to obtain  $K_{Ic}$  values, and for subsequent fractographic investigation, were finish-machined and fatigue-cracked in rotating bending after heat treatment. The  $K_{Ic}$  values, and smooth tensile properties are listed in Table 2. Additional  $K_{Ic}$  values were obtained for these same steels from fatigue-cracked notch bend test specimens, and these values also are given in Table 2. The values obtained for the 250-

grade steel by the two methods were identical, but the bend test value for the 300-grade steel was significantly higher than that obtained from the notch tension test; in the latter case, the bend test value is believed to be more accurate, because of possible nonaxiality of loading of this rather brittle material in the notch tension test. However, fractographic examinations were made only on the notch tension test specimens.

The replicas for electron fractographic examination of all steels were prepared by a two-stage plastic-carbon technique, using chromium as the replica shadowing material.

### Results and Discussion

The macroscopic appearance of the fracture surface of the 0.45C low-alloy steel containing 0.008 per cent sulfur is shown in Fig. 1. The fracture surfaces of the other steels of different sulfur contents looked

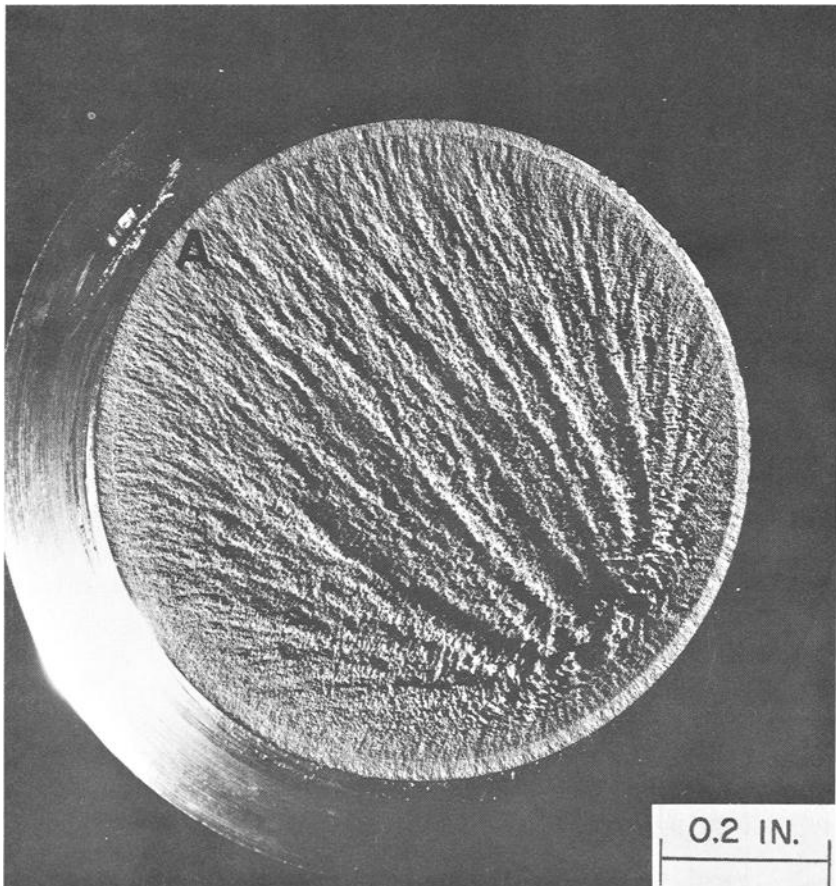


FIG. 1—Fracture surface of 0.45C-Ni-Cr-Mo steel with 0.008 weight per cent sulfur.

about the same. Figure 2 shows the macroscopic appearance of the fracture surface of the 18Ni(250) maraging steel notch tension test specimen; the appearance of the 18Ni(300) maraging steel fracture surface was very similar.

Although fractographs were prepared from many areas across the fracture surface of each steel specimen, only those taken from a region near the onset of plane-strain fracture instability (A in Figs. 1 and 2), immediately adjacent to the fatigue-crack, are discussed in this report. This region should be of most direct significance in any correlation of fracture surface topography with fracture toughness and microstructure.

In general, the results of fractographic examination of the series of 0.45C low-alloy steel specimens showed that all of the fracture surfaces were completely dimpled, and exhibited about the same degree of microscopic roughness, as evaluated by stereo-microscopic measure-

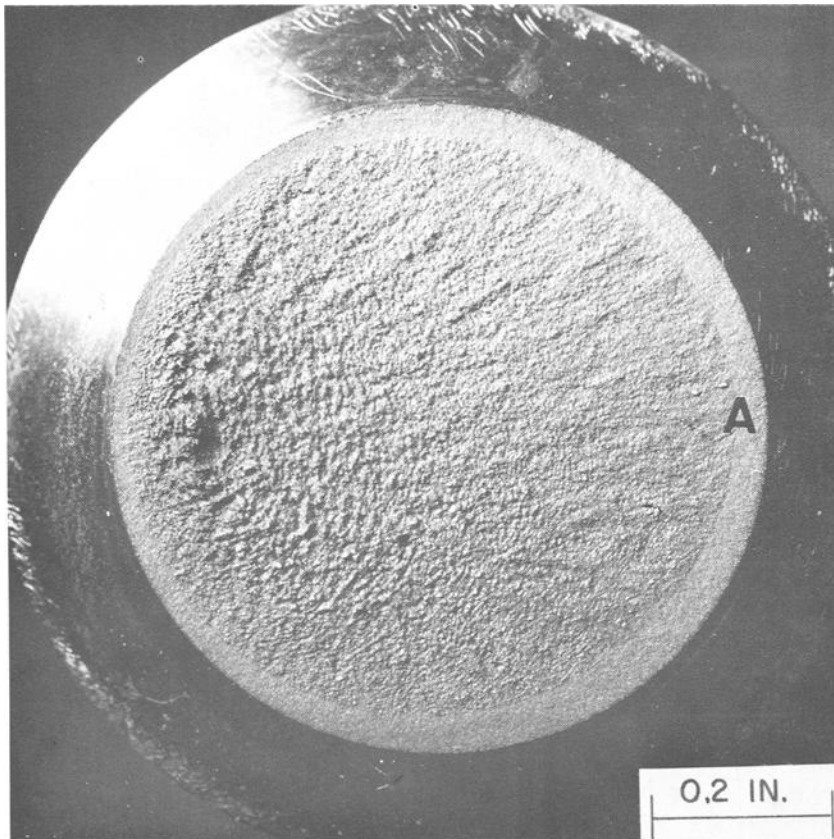


FIG. 2—Fracture surface of 250-grade maraging steel.



FIG. 3—Fracture surface of 0.45C-Ni-Cr-Mo steel with 0.008 per cent sulfur showing area adjacent to fatigue crack.

ments. Figures 3 and 4 are fractographs taken from regions adjacent to the fatigue starter crack of the steels containing 0.008 and 0.049 per cent sulfur, respectively. The fractographs of the other two steels of intermediate sulfur contents were very similar to these. The only difference observed among the fractographs of the four steels was an increase in number, and a corresponding decrease in spacing, of the rather large, sulfide-nucleated dimples (A in Fig. 4) with increasing sulfur content. The smaller dimples in Figs. 3 and 4 also appeared to have been nucleated by smaller particles, which resembled the cementite ( $\text{Fe}_3\text{C}$ ) particles in the tempered microstructure of these steels.

Recent work [6] has shown that the average spacing of the sulfide inclusions in these steels is equivalent to the process zone size predicted by the Krafft model for the onset of plane-strain fracture in-



FIG. 4—Fracture surface of 0.45C-Ni-Cr-Mo steel with 0.049 per cent sulfur showing area adjacent to fatigue crack.

stability [7]. According to this model, the plane-strain fracture toughness ( $K_{Ic}$ ) is related to the plastic flow properties of a material by

$$K_{Ic} = En\sqrt{2\pi d_T}$$

where  $E$  = Young's modulus,  $n$  = strain hardening exponent, and  $d_T$  = process zone size. The process zone is a region ahead of the crack in which tensile instability occurs, resulting in the onset of unstable fracturing; it has been shown to be invariant for a given material [7]. For these 0.45C low-alloy steels of different sulfur contents, it seems likely that the process zone size, and therefore  $K_{Ic}$ , may be controlled, in part, by the coalescence of voids that are nucleated by the sulfide particles.

However, another microscopic feature of the fracture surface was observed that might be related to the fracture toughness levels of these

steels, namely, a “stretched” region between the fatigue starter crack and the main overload fracture [8]. Such a region in the fracture surface of the steel containing 0.008 per cent sulfur is shown in Fig. 5. A region of this kind could not be found in the steel containing 0.049 per cent sulfur; either it did not exist or was too narrow to be detected. The fracture surfaces of the two steels of intermediate sulfur contents were not examined specifically for this feature. It is possible that this stretched zone corresponds to a region of crack extension through the plastic zone that existed at the tip of the fatigue crack just prior to the onset of the rapid, main fracturing process; the stretching might be involved in the separation process, or perhaps it represents localized plastic flow in the crack surfaces resulting from the bending that accompanies the crack opening. In either case, it is reasonable to think



FIG. 5—Fracture surface of 0.45C-Ni-Cr-Mo steel with 0.008 per cent sulfur showing area between fatigue crack and overload fracture regions.

that the extent of this stretched region may be related to plastic zone size, and that it increases with increase in plane-strain fracture toughness and plastic zone size. In this connection, it is interesting to note that the width of the stretched zone shown in Fig. 5 is about  $6 \mu\text{m}$ , which is the size of the process zone for this material computed from the Krafft model using values of  $2.9 \times 10^4$  ksi, 0.06 and  $65.3 \text{ ksi}\sqrt{\text{in.}}$  for  $E$ ,  $n$  and  $K_{Ic}$ , respectively [6]. The significance of this microscopic fracture surface feature is being explored more extensively by a newly formed Task Group of Subcommittee II on Fractography of ASTM Committee E-24.

The fracture surfaces of the 250-grade and of the 300-grade 18Ni maraging steels exhibited a wide range of dimple size throughout the fracture surfaces, as shown in the typical fractographs of Figs. 6 and 7, respectively. Although many inclusions appeared in the fracture sur-

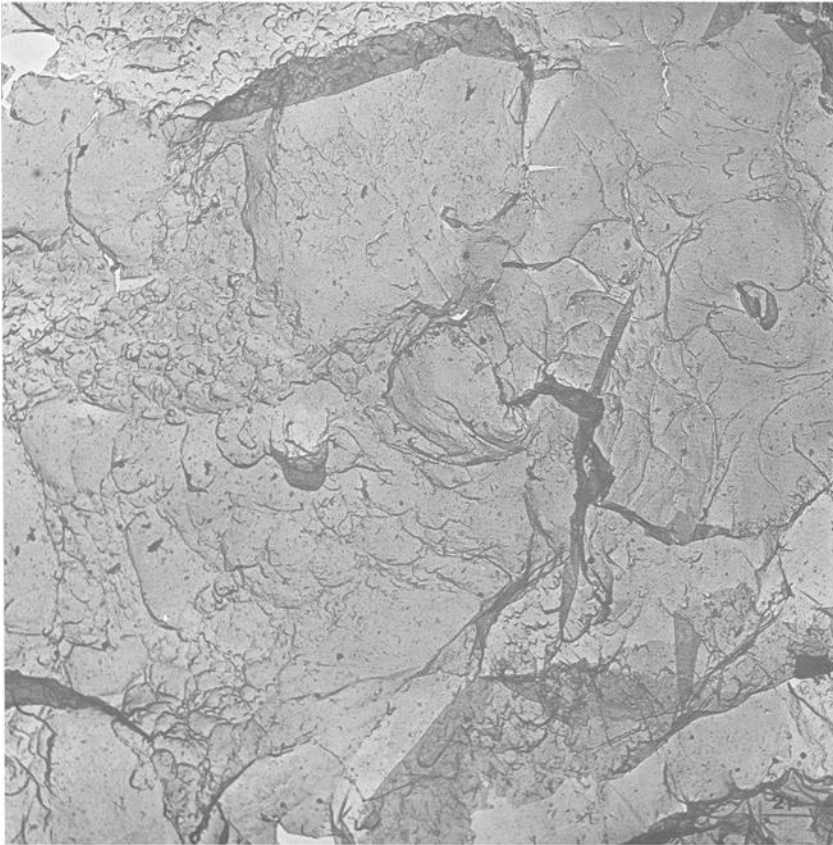


FIG. 6—Fracture surface of 250-grade maraging steel showing area adjacent to fatigue crack.

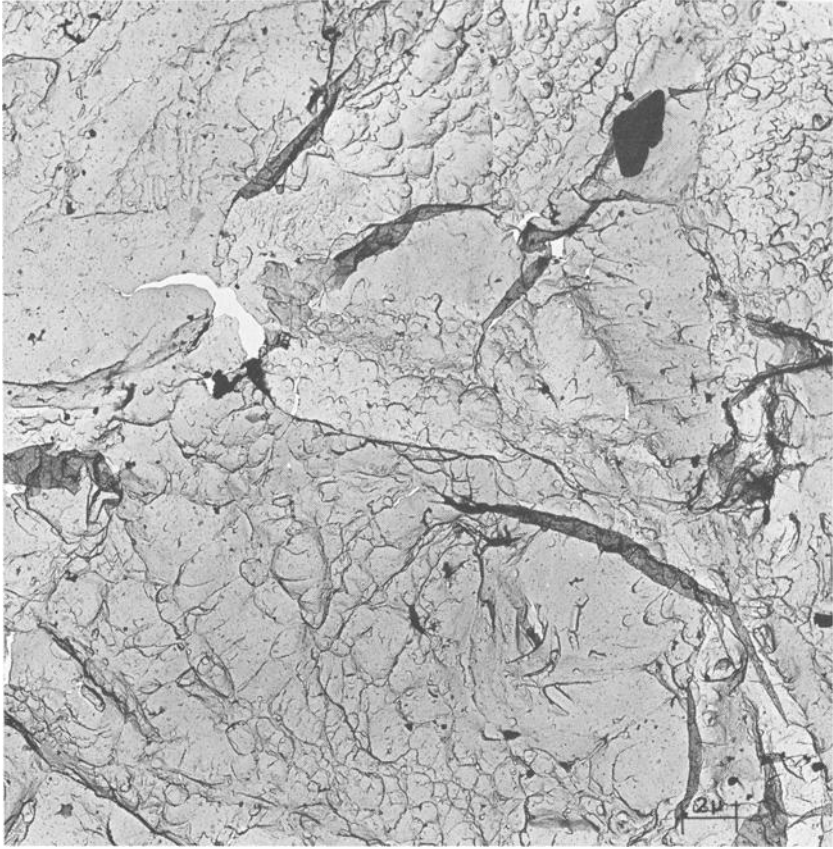


FIG. 7—Fracture surface of 300-grade maraging steel showing area adjacent to fatigue crack.

faces (for example, A in Fig. 9), there was no obvious correlation between the inclusion frequency or spacing, dimple size, and the measured values of plane-strain fracture toughness ( $K_{Ic}$ ). Stretched zones between fatigue cracked and overload fracture regions were observed in both steels, as shown in Figs. 8 and 9, and the width of the stretched zone was greater in the 250-grade steel having the greater plane-strain fracture toughness. However, for these steels, the measured widths of the stretched zones were more than an order of magnitude smaller than the process zone sizes calculated from mechanical property data for similar steels [3], on the basis of the present Krafft model [7]. Thus, the most readily measured microscopic features of the fracture surfaces of these two maraging steels (dimple size, or inclusion spacing, and width of stretched zone) have not provided a very satisfactory explanation for the measured differences in their plane-strain fracture



FIG. 8—Fracture surface of 250-grade maraging steel showing area between fatigue crack and overload fracture regions.

toughness ( $K_{Ic}$  values). Possibly, the microscopic fracture mechanism in these steels is more complex than for the medium-carbon quenched-and-tempered (800 F) alloy steels previously discussed, in that a tendency toward intergranular fracture in the maraging steels may reduce the importance of the role of microvoid formation and coalescence in the fracture process, and thus the significance of dimple size (or inclusion spacing) as the primary indicator of fracture toughness level. Likewise, the more complicated fracture mechanism may require some modification of the present Krafft model in order to permit calculation of a more realistic process zone size for this class of steels.

### Summary

This investigation revealed no differences in the type of fracture surface topography of the oil quenched and tempered (800 F) 0.45C-Ni-Cr-Mo steels of different residual sulfur levels. In general, all the frac-

ture surfaces were completely dimpled, and exhibited about the same level of surface roughness. There was, however, an increase in number, and decrease in spacing, of larger dimples with increasing sulfur content and decreasing plane-strain fracture toughness. This suggested that the larger dimples had been nucleated by sulfide particles, and that this mechanism was effective in reducing fracture toughness at the higher sulfur levels. For each steel of different sulfur content, the sulfide-particle spacing was equivalent to the process zone size calculated from the measured  $K_{Ic}$  values and strain hardening exponent ( $n$ ), using the Krafft model. Another fractographic feature of possible significance in relation to fracture toughness was noted, namely, a “stretched” zone between the fatigue cracked and overload regions of the fracture surface. The width of this stretched zone appeared to increase with increasing plane-strain fracture toughness.

A wide range of dimple size was observed throughout the fracture

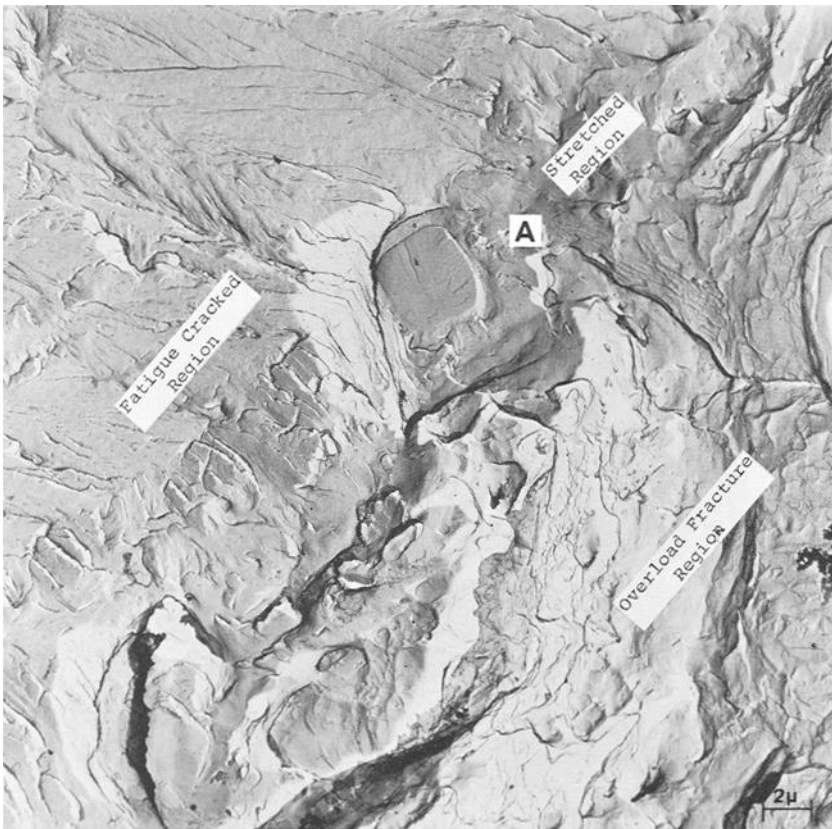


FIG. 9—Fracture surface of 300-grade maraging steel showing area between fatigue crack and overload fracture regions.

surfaces of the two 18Ni maraging steels. There was no obvious correlation between the inclusion frequency or spacing, dimple size, and the level of plane-strain fracture toughness of these steels. Although the extent of the stretched zone between fatigue cracked and overload fracture regions was greater in the 250-grade steel of greater toughness, its width was an order of magnitude smaller than the process zone size calculated from mechanical property data on similar steels, using the Krafft model. Thus, the fractographic findings did not account for the difference in fracture toughness of these steels very satisfactorily, possibly because of a more complex mechanism of microscopic rupture, involving both microvoid formation and coalescence and intergranular rupture, in the maraging steels.

## References

- [1] Baker, A. J., Lauta, F. J., and Wei, R. P., "Relationships Between Microstructure and Toughness in Quenched and Tempered Ultrahigh-Strength Steels," *Structure and Properties of Ultrahigh-Strength Steels, ASTM STP 370*, American Society for Testing and Materials, 1965, pp. 3-29.
- [2] Spitzig, W. A. and Wei, R. P., "A Fractographic Investigation of the Effect of Environment on Fatigue-Crack Propagation in an Ultrahigh-Strength Steel," *Transactions*, American Society for Metals, Vol. 60, 1967, pp. 279-288.
- [3] Wei, R. P., Talda, P. M., and Li, Che-Yu, "Fatigue-Crack Propagation in Some Ultrahigh-Strength Steels," *Fatigue Crack Propagation, ASTM STP 415*, American Society for Testing and Materials, 1967, pp. 460-485.
- [4] Baker, A. J. and Reisdorf, B. G., "Strengthening Mechanisms of the 18 Percent Nickel Maraging Steels," 4th Maraging Steel Project Review, Technical Documentary Report ML-TDR-64-225, Air Force Materials Laboratory, 1964.
- [5] Spitzig, W. A., Talda, P. M., and Wei, R. P., "Fatigue-Crack Propagation and Fractographic Analysis in 18Ni(250) Maraging Steel in Argon and Hydrogen Environments," presented at The National Symposium on Fracture Mechanics at Lehigh University, Bethlehem, Pa., June 1967, to be published in *Engineering Fracture Mechanics*, 1968.
- [6] Birkle, A. J., Wei, R. P., and Pellissier, G. E., "Analysis of Plane-Strain Fracture in a Series of 0.45C-Ni-Cr-Mo Steels with Different Sulfur Contents," *Transactions*, American Society for Metals, Vol. 59, 1966, pp. 981-990.
- [7] Krafft, J. M., "Correlation of Plane Strain Crack Toughness with Strain Hardening Characteristics of a Low, a Medium, and a High Strength Steel," *Applied Materials Research*, Vol. 3, 1964, pp. 88-101.
- [8] Beachem, C. D. and Meyn, D. A., "Illustrated Glossary of Fractographic Terms," Section 2, U.S. Naval Research Laboratory Memorandum Report 1547, June 1964.

## DISCUSSION

---

*W. R. Warke*<sup>1</sup> (written discussion)—In the report, the "stretched zone" is interpreted in terms of "crack extension through the plastic zone that existed at the tip of the fatigue crack just prior to the onset of the rapid, main fracturing process." My recollection of the examination

<sup>1</sup> Instructor, Illinois Institute of Technology, Chicago, Ill.

of these stretched zones by stereoscopic electron fractography is that the stretching involved blunting of the crack tip as well as extension. The extent of modification of the crack tip through stretching was approximately the same in the vertical direction (blunting) as in the horizontal direction (extension). This observation is in keeping with current views of deformation at the tip of a propagating fatigue crack during the increasing portion of the load cycle.<sup>2,3,4</sup> Loading of a fatigue precracked specimen to failure is basically the same as a quarter of a fatigue cycle so similarity of the crack tip deformation process would be expected. I wonder if Mr. Spitzig would care to comment on the influence the observed blunting would have on the fracture mechanics interpretation of the significance of the stretched zones.

*Author's closure* – Additional work<sup>5,6</sup> has shown that there definitely appears to be a correlation between the extent of the stretched zone and the process zone size. However, the actual physical significance of the stretched zone is not obvious at present, and, therefore, it is not possible to evaluate the effect of blunting or other plastic deformation processes on the significance of this region for fracture mechanics interpretation.

<sup>2</sup> Jacoby, G., "Application of Microfractography to the Study of Crack Propagation Under Fatigue Stresses," AGARD Report 541, 1966.

<sup>3</sup> Laird, C., "The Influence of Metallurgical Structures on the Mechanism of Fatigue Crack Propagation," *Fatigue Crack Propagation, ASTM STP 415*, American Society for Testing and Materials, 1967, pp. 131-180.

<sup>4</sup> McMillan, J. C. and Pelloux, R. M. N., "Fatigue Crack Propagation Under Programmed and Random Loads," Boeing Scientific Research Laboratories Document D1-82-0558, *Fatigue Crack Propagation, ASTM STP 415*, American Society for Testing and Materials, 1967, pp. 505-535.

<sup>5</sup> Spitzig, W. A., "Plane-Strain Fracture in 0.45C-Ni-Cr-Mo Steel," submitted to *Transactions*, American Society for Metals.

<sup>6</sup> Spitzig, W. A., "Correlation Between Microstructural Features and Plane-Strain Fracture Toughness in an Ultrahigh-Strength Steel," submitted for presentation at the 71st Annual Meeting of ASTM, San Francisco, Calif., June 1968.

## Cleavage Phenomena and Topographic Features

---

**REFERENCE:** Burghard, H. C., Jr., and Stoloff, N. S., "Cleavage Phenomena and Topographic Features," *Electron Fractography, ASTM STP 436*, American Society for Testing and Materials, 1968, pp. 32-58.

**ABSTRACT:** Cleavage fractures have been widely studied in body-centered-cubic and certain hexagonal-close-packed metals and alloys as well as ionic crystals. It is shown that the theoretical treatments due to Stroh, Cottrell, and Petch have successfully accounted for the effects of yield strength, grain size, and mode of deformation on crack nucleation and propagation. The results of these studies are summarized, and their application to the prediction of the ductile-to-brittle transition temperature is described. In addition, theoretical studies which have led to the prediction of cleavage planes and to an explanation of the influence of dispersed particles are reviewed.

Fractographic studies have established topographic features characteristic of cleavage fracture; namely, steps and river patterns, cleavage tongues, and herringbone patterns. Examples of these features are presented, and factors associated with their formation are described. It is shown that steps and river patterns are formed by secondary cleavage, slip, or plastic fracture and are influenced by crystallographic imperfections and microstructural discontinuities. Tongues and herringbone patterns are shown to be associated with deformation twins formed ahead of the advancing crack. In addition, a discussion of "cleavage-like" features observed in quenched and tempered steels, face-centered-cubic materials, and in certain environmentally induced fractures is presented.

**KEY WORDS:** cleavage (crystallographic), fracture, fractography, electron microscopy, brittle fracture, crack nucleation, crack propagation

Fracture of solids may occur by direct separation along low-index crystallographic planes by the process known as cleavage. Cleavage phenomena have been known and studied for many years; it is only in the past 10 to 15 years that the methods of dislocation theory have been applied to consideration of the mechanism of cleavage fracture. The past decade has also witnessed the wide application of fractographic techniques to reveal fine details of the fracture process which

<sup>1</sup> Senior research engineer, Department of Materials Engineering, Southwest Research Institute, San Antonio, Tex.

<sup>2</sup> Associate professor, Department of Materials Engineering, Rensselaer Polytechnic Institute, Troy, N.Y. Personal member ASTM.

may be used to develop realistic models of cleavage fracture. This paper discusses the mechanism of cleavage crack nucleation and propagation in solids, shows that fractographic observations are compatible with the proposed models, and finally discusses some characteristics of cleavage phenomena that only recently have been observed. In addition, attention will be directed to certain cases in which topographic features resembling those associated with cleavage have been observed in materials generally considered to be immune to cleavage.

The conditions under which the cleavage mechanism is operative vary with the particular material and the type of loading. In metals and metallic alloys, cleavage is generally limited to the body-centered-cubic (bcc) and hexagonal-close-packed (hcp) materials. In tension, cleavage may occur after significant amounts of plastic deformation (as measured over the entire specimen), while cleavage fracture induced by impact loading frequently occurs with little or no plastic deformation.

There are several materials which undergo a ductile-to-brittle transition in simple tension but do not fail by cleavage at low temperatures. Examples are cadmium [1]<sup>3</sup>, magnesium [2], and Ti-0.25O<sub>2</sub> alloys [3]. In addition, there are many examples of low-energy failures in high-strength steels and aluminum alloys in which there is no tendency to cleavage failure. These examples are listed here to emphasize the fact that cleavage and brittleness are not synonymous. Brittle failures can occur by mechanisms other than cleavage, and cleavage may be involved in the fracture of certain materials which exhibit relatively high ductility in simple tension. These factors and the recent advances in the understanding of fracture processes emphasize the importance of precise definitions of the terms used to describe and classify fracture. In this regard, Burghard and Davidson [4] have suggested that the specification of three characteristics is necessary for an unambiguous classification of fracture, that is, the basic mechanism involved (plastic fracture, cleavage, or fatigue), fracture mode (transgranular or intergranular), and the macroscopic aspects (ductile or brittle). With reference to the particular basic mechanism of interest here, cleavage may be defined as a low-energy, rapid fracture process producing a fracture surface coincident with low-index crystallographic planes.

## Theoretical Considerations

### *Mechanisms of Cleavage Crack Nucleation*

Cleavage cracks in nominally single-phase, polycrystalline metals and alloys originate at blocked slip or twin bands. The obstacle may be

<sup>3</sup> The italic numbers in brackets refer to the list of references appended to this paper.

a grain or subgrain boundary, another twin, or an inclusion particle. Cottrell [5] has proposed that intersecting slip bands also may constitute additional obstacles which form sites for crack nucleation. This model is generally referred to as the "double pileup model." Cracks originating at intersecting slip bands are frequently observed in Fe-3Si and in ionic crystals. A crack may form along the slip plane, as in zinc, or at some large angle to the slip plane, as in iron.

Direct observation of crack formation at blocked slip bands has been provided by experiments on ionic solids and certain metals. Ku and Johnston [6] have used birefringence of transmitted polarized light to reveal stress concentrations, and eventually crack nucleation, at blocked slip bands in magnesium oxide (MgO) bicrystals (see Fig. 1). Similarly, crack formation at blocked slip bands in silver chloride (AgCl) immersed in an aqueous sodium chloride (NaCl) solution has been noted by Westwood et al [7]. In the case of metals, Wronski and Fourdeux [8] have observed cracks to form along arrays of blocked dislocations on {110} slip planes in thin foils of polycrystalline tungsten.

Nucleation of cleavage cracks at twin intersections has been noted in many metals; a typical example for zinc is shown in Fig. 2. Cleavage crack formation along slip planes which are blocked by tilt boundaries is a common characteristic of hcp metals and alloys and is illustrated in Fig. 3. If the alloy is distinctly two-phase, an additional mode of crack formation is provided by the possibility of the second phase developing a crack which can extend into the matrix. Cleavage fractures originating at grain boundary inclusions as small as one micron in diameter have been observed in Fe-0.005C alloys [9] (see Fig. 4). In pearlitic steels, cracks originate in the cementite lamellae and then propagate into the adjacent ferrite. In more complex alloys, there may be a variety of possible nucleation sites, any of which could give rise to cleavage fracture.

The dislocation models of cleavage fracture at blocked slip or twin bands were developed for iron and steels, and have been applied to a variety of alloys with relatively simple microstructures. Perhaps the most successful model to date is that presented by Stroh [10], Cottrell [5], and Petch [11]. This model is based on the concept that a shear displacement arising from dislocation pileups gives rise to stress concentrations sufficient to nucleate a crack.

Cottrell [5] calculated the fracture stress,  $\sigma_F$ , of a perfect crystal in the presence of an isolated wedge of  $n$  coalesced dislocations of Burgers vector  $b$ :

$$\sigma_F = \frac{(2\gamma)}{(nb)} \dots \dots \dots (1)$$

where  $\gamma$  is the surface energy associated with the crack. The wedge may be formed, in the case of iron, by  $a/2\langle 111 \rangle$  dislocations gliding on

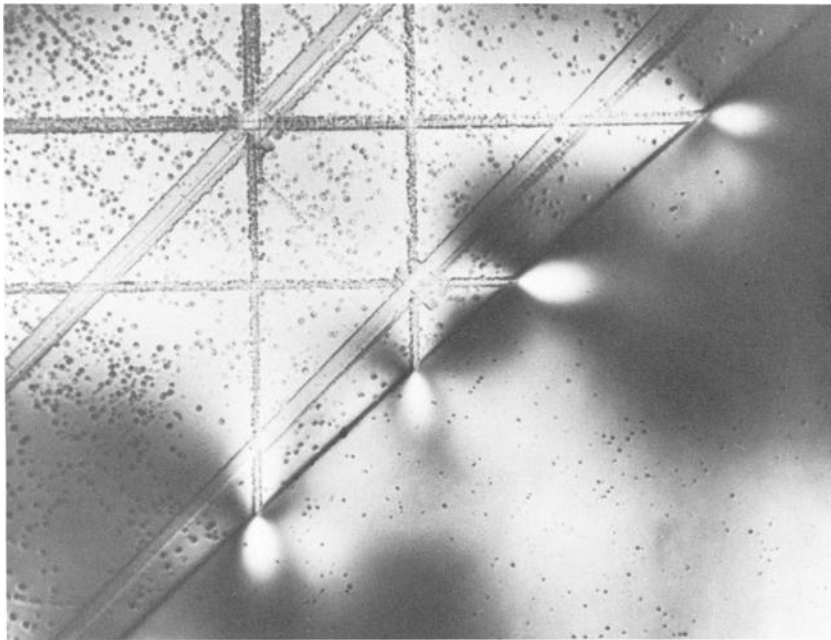


FIG. 1—Stress concentrations generated at the tips of blocked glide bands in magnesium oxide as revealed by birefringence. After Ku and Johnston [6]. ( $\times 78$ ).

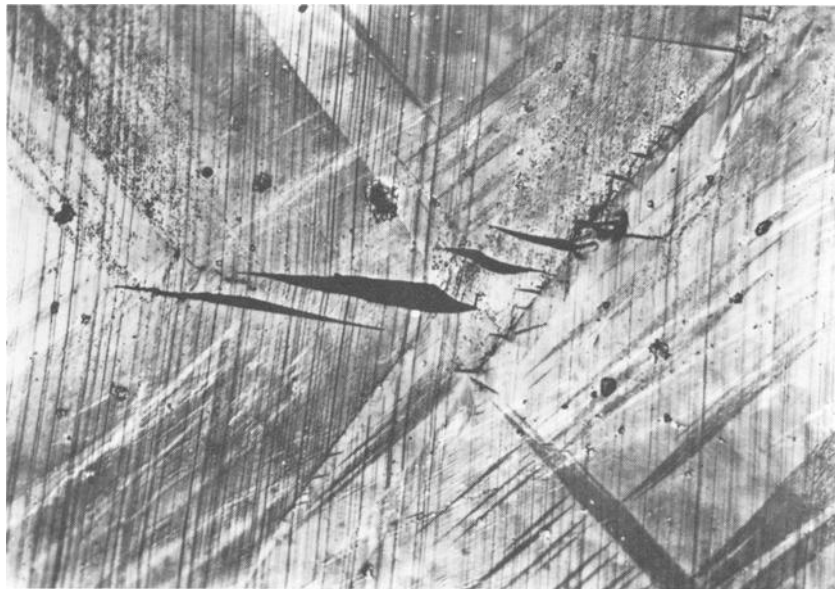


FIG. 2—Cleavage crack nucleated at the intersection of twin bands in a zinc single crystal compressed 9.6 per cent at  $-196\text{ C}$  ( $\times 200$ ).

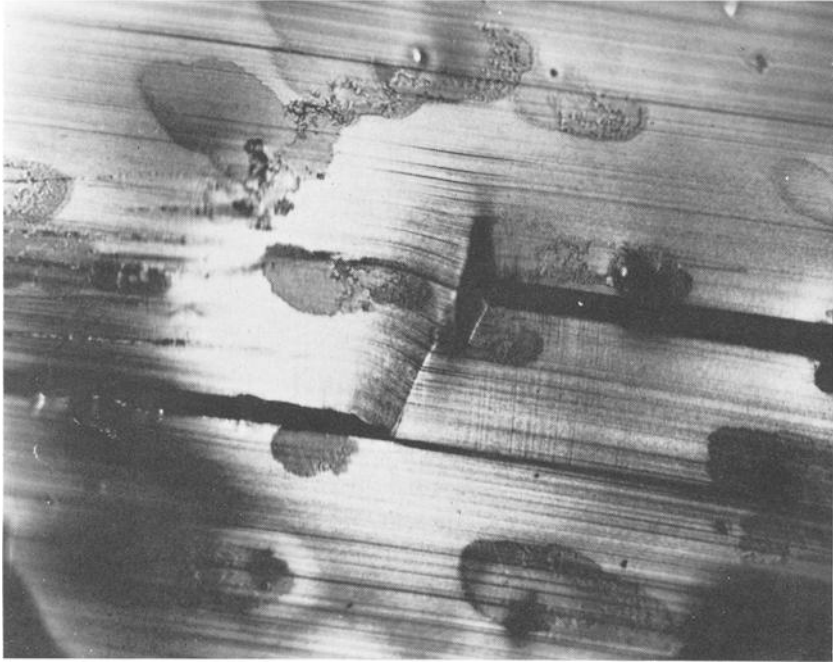


FIG. 3—Cleavage crack nucleated at a tilt boundary in Cd-3.7Mg alloy tested in compression at  $-196^{\circ}\text{C}$ . After Stoloff and Gensamer [1]. ( $\times 250$ ).

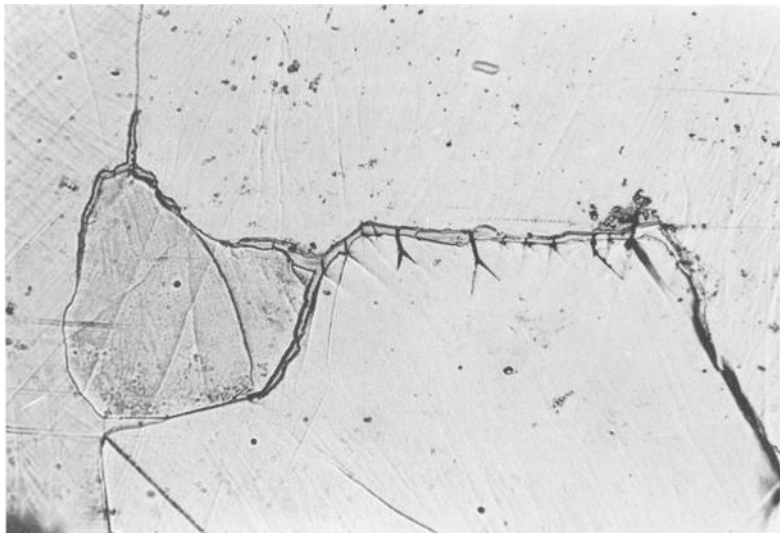


FIG. 4—Cleavage cracks nucleated at grain boundary carbide particles in Fe-0.005C. After McMahon and Cohen [9]. ( $\times 200$ ).

intersecting  $\{110\}$  planes, and interacting to form sessile  $\langle 100 \rangle$  dislocations through the reaction:

$$\frac{a}{2} [111] + \frac{a}{2} [\bar{1}\bar{1}1] = a[001] \dots \dots \dots (2)$$

Since this theory has been widely used for several years, and the details of the derivation are provided in many textbooks on mechanical behavior, we shall present only the final result of this model. It was calculated that cleavage fracture should occur at the yield stress,  $\sigma_y$ , when the following condition is satisfied:

$$\sigma_y k_y d^{1/2} \geq \beta G \gamma \dots \dots \dots (3)$$

The yield stress,  $\sigma_y$ , is related to the grain diameter,  $d$ , through the following relation:

$$\sigma_y = \sigma_i + k_y d^{-1/2} \dots \dots \dots (4)$$

Therefore,  $k_y$  is a measure of the contribution of grain boundaries to the strength of a polycrystal, and  $\beta$  is a constant expressing the ratio of shear to normal stress in the test specimens.  $G$  is the shear modulus. In Eq 4,  $\sigma_i$  is associated with the lattice friction which resists dislocation motion.

Substituting Eq 4 into Eq 3, an equivalent fracture criterion is obtained in terms of  $\sigma_i$  and  $k_y$ .

$$(\sigma_i d^{1/2} + k_y) k_y \geq \beta G \gamma \dots \dots \dots (5)$$

This equation correctly predicts that bcc and hcp materials with high friction stress, high grain boundary resistance to slip propagation, or large grain size tend to be susceptible to cleavage fracture.

#### *Ductile-to-Brittle Transition*

The analysis outlined in Eqs 1 through 5 also predicts a ductile-to-brittle transition at constant test temperature with increasing grain size. The transition occurs at a critical grain size  $d^*(T)$  which varies with test temperature,  $T$ . The more usually studied shear-to-cleavage transition occurring at low temperatures in steels also has been rationalized by identifying  $\sigma_i$  as the most temperature-dependent term in Eq 4. For example, Petch [12] has shown that, if:

$$\sigma_i = B e^{-CT} \dots \dots \dots (6)$$

where  $B$  and  $C$  are numerical constants established by experiment, then the relation between transition temperature,  $T_c$ , and metallurgical variables, obtained by substituting Eq 6 into Eq 5 is

$$T_c = \frac{1}{C} \ln [(B k_y d^{*1/2}) / (\beta G \gamma - k_y^2)] \dots \dots \dots (7)$$

The relation between transition temperature and grain size reduces to:

$$T_c = D \ln (d^{*1/2}) \dots \dots \dots (8)$$

where  $D$  is a constant.

This equation has been experimentally verified for several materials, and data obtained for an iron-base alloy are shown in Fig. 5 [13].

Johnston et al [14] have recently suggested that hcp materials which exhibit few slip systems (for example, zinc), as well as bcc metals which slip on several systems but in which cross-slip is difficult, will tend to have a high value of  $k_y$ , and will therefore be more susceptible to cleavage fracture than materials with many degrees of freedom to slip. Therefore, iron-silicon alloys, which deform primarily by  $\{110\}$  slip, with little cross-slip onto other planes, tend to be more brittle than unalloyed iron, which slips also on  $\{112\}$  and  $\{123\}$  planes, with copious cross-slip among the planes. Moreover, in many alloys, the number of active slip systems and ease of cross-slip tend to decrease with decreasing temperature, constituting an additional reason for an increase in the tendency for cleavage with decreasing temperature. As a result of these factors, one may expect a more complex relation between transition temperature and microstructural parameters than is suggested by Eq 8.

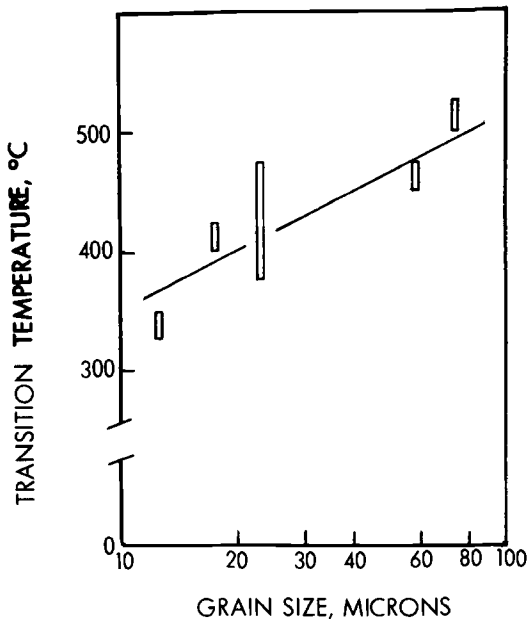


FIG. 5—Effect of grain size on the ductile-to-brittle transition temperature in Fe-49Co-2V. After Jordan [13].

### *Crack Propagation*

The question of whether or not a cleavage crack, once nucleated, can grow catastrophically has been the subject of much analysis. Clearly, in certain steels, crack propagation requires a *higher* stress than crack nucleation. In such cases, Hahn et al [15] have noted stable microcracks of a length corresponding to one grain diameter. These cracks are nucleated at the yield stress, propagate through a single grain, and then are held up by grain boundaries. On the other hand, for pure single-phase solids tested over a wide range of temperature, crack nucleation was noted to be the critical event, and no microcracks are observed [14].

The Cottrell-Petch model does not explicitly take into account the fact that cleavage crack growth will be more difficult than nucleation only if the effective fracture surface energy,  $\gamma_e$  (which includes the work of plastic deformation), is increased appreciably above the true elastic energy,  $\gamma_s$ , appropriate to the nucleation stage. Neither Cottrell nor Petch has taken into account the possibility of increase in surface energy with crack length. Rather, the surface energy has been treated as a disposable parameter which generally is calculated from Eqs 3 and 5 to be at least an order of magnitude greater than the true elastic surface energy. Another disadvantage of the Cottrell-Petch approach is concerned with the lack of means to take into account the role of precipitates in crack nucleation. Finally, there is quantitative disagreement between fracture surface energies calculated from the theory and directly measured true surface energies. Hahn and Rosenfield [16] have suggested that the excessively large calculated surface energy is not a consequence of plastic relaxation due to cross-slip, as suggested by Johnston et al [14], but rather originated from an incorrect estimate of the number of coalesced dislocations and the effective shear stress appropriate to the Cottrell double-pileup model. In spite of these reservations, this theory stands as the only framework with which to discuss the influence of metallurgical variables on cleavage fracture.

### *Influence of Dispersed Particles*

When cleavage in low-carbon iron is initiated within carbide particles located at grain boundaries, the probable cause is pileup of dislocations in the adjacent ferrite grains. If the particle-matrix interface is weak, the interface tends to crack first, but the size of the crack is limited by the size of the particle. The crack can propagate into the matrix only if the Griffith criterion (for plane strain) is satisfied:

$$\sigma_F \geq \{(2E\gamma)/[\pi c(1 - \nu^2)]\}^{1/2} \dots\dots\dots(9)$$

where  $c$ , the crack length, is proportional to the particle radius. This

condition predicts a critical particle size for propagation of a crack through the matrix. The double pileup model of Hahn and Rosenfield [16] predicts that fine, uniform dispersions of hard particles can strengthen without impairing ductility and can even lower the ductile-to-brittle transition temperature. This prediction is based on the premise that the particles decrease the maximum pileup length from the grain diameter to the order of the interparticle spacing, and therefore the stress concentration is reduced.

Examples of instances where fine, hard particles have enhanced strength without increasing the tendency towards cleavage are as follows: AgCl-Al<sub>2</sub>O<sub>3</sub> [17], 4340 steel (200 Å cementite particles) [18], and W-ThO<sub>2</sub> alloys [19]. However, in the discussion of the work on W-ThO<sub>2</sub> alloys, Rosenfield and Hahn point out that there is no unambiguous experimental evidence that the improved ductility arises from smaller dislocation arrays. Since coherent precipitates, which can be cut by dislocations, strengthen the matrix without decreasing pileup length, alloys containing this type of particle should be no more resistant to cleavage than the matrix.

#### *Prediction of Cleavage Planes*

Since one of the most fundamental characteristics of cleavage fracture is that the crack propagates on a low-index crystallographic plane, it is of interest to predict the cleavage plane from atomic binding principles. Gilman [20] has examined the problem, basing his calculations on the concept that the cleavage plane is the plane of minimum surface energy. By assuming a sinusoidal attractive stress field between two atomic surfaces, and equating the surface energy to the work done in separating the two surfaces, Gilman developed the following relation between surface energy  $\gamma$  and lattice constants:

$$\gamma_{hkl} = (E/y_0)(a_0/\pi)^2 \dots \dots \dots (10)$$

where  $E$  is the elastic stiffness perpendicular to the designated plane  $hkl$ ,  $y_0$  is the separation between these planes, and  $a_0$  is the diameter of atoms in the cleavage surface, measured parallel to the surface. This calculation correctly predicted the cleavage plane (plane of lowest energy) in 16 crystalline solids but failed to predict the primary cleavage plane of beryllium, iron, and tungsten. The latter two elements were predicted to cleave on {110} planes, in contrast to the {100} cleavage generally observed. The reason for the discrepancy may lie in the energy density of broken bonds, which is greater for {110} than {100} cleavage. It is interesting to note, however, that fracture along {110} slip planes has been observed in molybdenum [21], Fe-3Si [22], tungsten [8] and other bcc metals, suggesting that there is a greater tendency for {110} cleavage in the bcc structure than

has been generally recognized. The specific cleavage planes for various classes of solids are listed in Table 1.

TABLE 1—*Cleavage planes in solids.*

Crystal Structure	Material	Primary Cleavage Plane	Secondary Cleavage Plane
bcc .....	Fe	001	.....
	Cb	001	110
	W	001	110
	Mo	001	110
	Fe-3Si	001	110
hcp .....	Zn	0001	.....
	Cd	0001	.....
	Mg	10 $\bar{1}$ 1	11 $\bar{2}$ 4
	$\alpha$ Ti-0.5O <sub>2</sub>	12 $\bar{3}$ 2	10 $\bar{1}$ 0, 12 $\bar{3}$ 0
Diamond .....	Si	111	.....
	Ge	111	.....
Ionic solids .....	NaCl	100	110
	KCl	100	110
	LiF	100	110
Zinc blende.....	ZnS	110	.....
Fluorite .....	CuF <sub>2</sub>	111	.....
	UO <sub>2</sub>	111	.....
	ThO <sub>2</sub>	111	.....

### Topography of Cleavage Fracture

Consideration of the factors discussed in the previous section emphasizes that the unique, distinguishing feature of cleavage fracture is the definite association of the fracture path with particular, low-index crystallographic planes. This crystallographic dependence results in characteristic topographic features, both on a macro- and microscopic scale. The fracture surfaces created by cleavage in polycrystalline materials are generally made up of a multitude of flat facets, each representing the particular cleavage plane for a given grain. It is these flat facets, and their contribution to the high reflectivity of cleavage fracture surfaces, that have long served as a basis for classification of fracture from macroscopic examinations.

Based on the single factor of a definite crystallographic dependence, cleavage fracture would be expected to produce perfectly flat, featureless facets. Real materials, however, exhibit a high degree of sub-microscopic imperfections, and metallic crystals are subject to a definite, though limited, amount of plastic deformation in the immediate vicinity of a cleavage crack. The latter point is confirmed by observations of regions of high dislocation density ahead of the tip of a cleavage crack [23], Fig. 6, and in certain cases by the presence

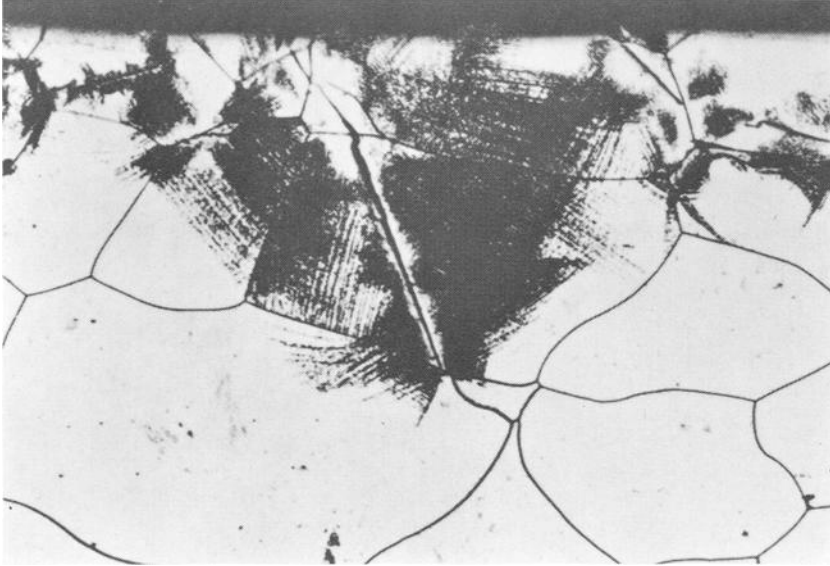


FIG. 6—Plastic deformation in immediate vicinity of stopped cleavage crack in Fe-3Si. After Tetelman [23]. ( $\times 150$ ).

of slip markings on cleaved surfaces [24]. These factors, coupled with microstructural features such as second-phase particles, inclusions, grain boundaries and subgrain boundaries, influence the propagation of a cleavage crack and result in the formation of characteristic fine-scale surface features within individual cleavage facets.

#### *Cleavage Steps in River Patterns*

As a cleavage crack propagates through a crystal, it is most often broken into a set of parallel cracks by interaction with imperfections and microstructural features. Thus, gross crack propagation may be the net result of the simultaneous propagation of individual crack segments on sets of parallel planes. As the individual segments approach one another (and possibly overlap), the segments join by fracture of the connecting ligament, producing steps in the fracture surface. These steps are generally observed to converge in the direction of local crack propagation, either cancelling or reinforcing each other to produce the familiar river patterns on individual facets.

Comprehensive investigations of the nature of steps observed in cleavage fractures have been carried out by Berry [25] and Low [26]. These investigations established that the steps within a single cleavage facet may be attributed to one or more of the following factors: intersection of screw dislocations with the cleavage plane, secondary cleavage, shear, secondary fracture on a twin-matrix interface or, in

the case where considerable overlap of two crack segments occurs, deformation and necking-down of the interconnecting ligament. Since a number of processes may be involved in the formation of cleavage steps, facets exhibiting wide variations in the appearance of steps and river patterns are observed. Examples illustrating the extremes in appearance of steps and river patterns are given in Fig. 7.<sup>4</sup> Steps formed by secondary cleavage, shear, or twin-interface separation may be expected to appear as distinctly resolvable subfacets (Fig. 7*a*), while those associated with the formation of flaps or extensive local deformation would appear as heavy lines with less resolvable detail (Fig. 7*b*).

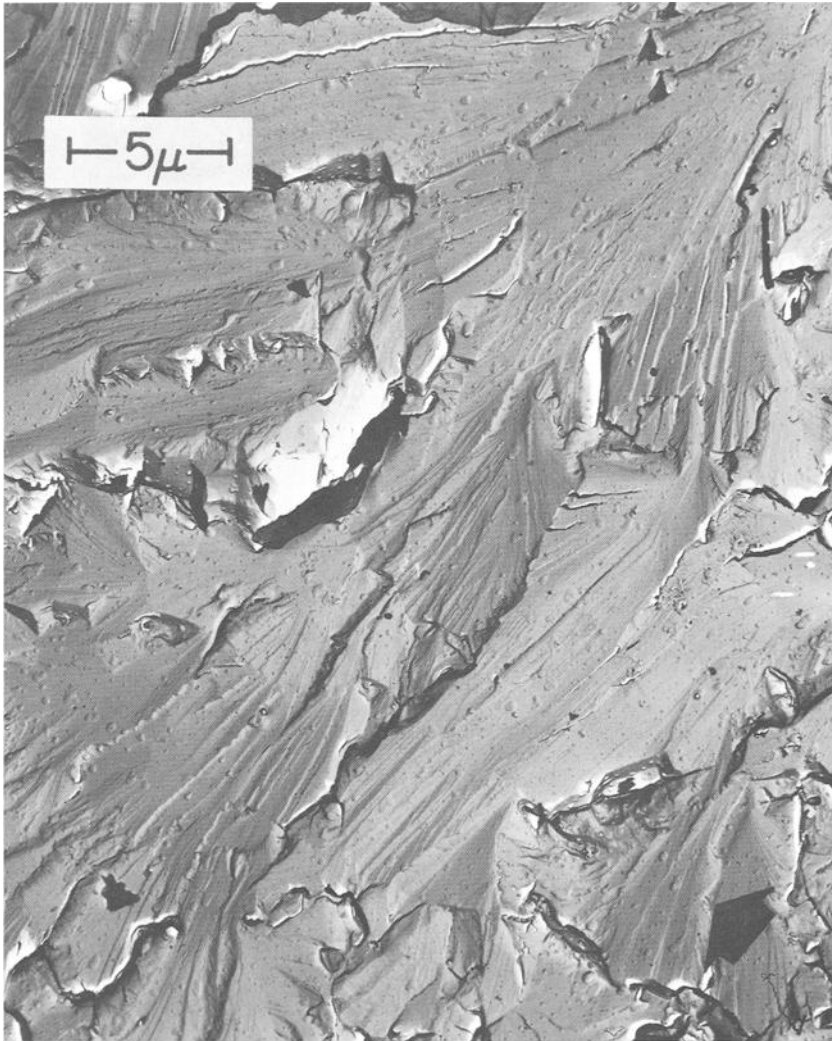
Since steps and river patterns result from the division of a crack into parallel segments, they may be expected to originate at regions of mismatch (grain boundaries or subboundaries). Figure 8 illustrates a case where new river patterns initiated at the point where the crack crossed a boundary. In cases where the crack crosses a low-angle boundary, an increase in step density occurs. Propagation of a cleavage crack across a high-angle grain boundary usually requires the initiation of a new crack in the second grain, resulting in the formation of new sets of rivers or steps.

The microstructure of the material also exerts a marked influence on the appearance of steps and river patterns formed in cleavage fracture. Low [26] has reported that in a 0.5 per cent carbon steel with a pearlitic or upper bainitic structure, the fracture path follows the cleavage plane of the ferrite through several pearlite or bainite colonies. For the same steel with a tempered lower bainitic or tempered martensitic structure, many small cleavage facets were noted. In the latter case, the facets were reported to be related to the bainite or martensite needle size. Irvine and Pickering [27] have studied the topography of impact fractures in low-carbon bainitic steels heat treated to various strength levels. In this study, it was noted that, at the higher strength levels, the fracture surfaces exhibited smaller river patterns and more irregular tearing than in the structures corresponding to the lower strength levels. Some alteration of the direction of crack propagation at bainitic boundaries was noted, and more marked changes were observed at prior austenite boundaries.

Recent studies utilizing electron fractographic techniques have provided numerous additional examples of steps and river patterns in cleavage fractures [28–30]. These examples have shown that, while differences in fine-scale features may exist, steps and river patterns are a characteristic feature of cleavage fracture, and specific information related to this mechanism may be gained from such features.

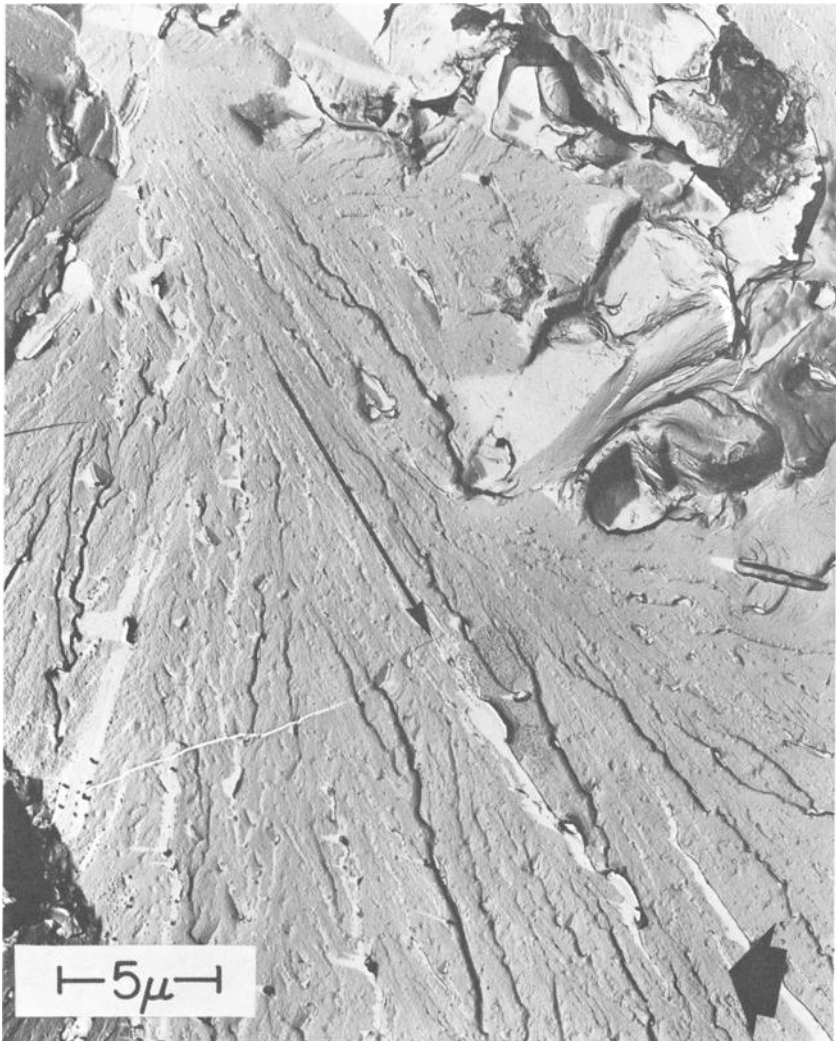
As mentioned earlier, steps and river patterns converge in the direc-

<sup>4</sup> In Figs. 7, 9, 10, and 12, the block arrow in one corner indicates the macroscopic crack propagation direction.



(a) Molybdenum:  $-320$  F. Two-stage plastic-carbon replica ( $\times 5000$ ).

FIG. 7—*Cleavage facets observed in low-temperature impact fractures of molybdenum and steel.*



(b) A 302B Steel:  $-98$  F. Long arrow indicates local direction of crack propagation. After Burghard and Davidson [4]. Two-stage plastic-carbon replica ( $\times 5000$ ).

FIG. 7—Continued



FIG. 8—River patterns on cleavage surface of ordered Fe-49Co-2V. After Johnston *et al* [14]. ( $\times 30,000$ ).

tion of crack propagation within individual facets. Thus, these markings serve as a reliable indication of the local or microscopic direction of crack propagation. In numerous studies, it has been observed that the microscopic direction of crack propagation does not necessarily correspond to the macroscopic direction. Individual cleavage facets may show directions of propagation markedly different from the macroscopic direction as illustrated in Fig. 9. These observations indicate that the propagation of a cleavage crack in a polycrystalline aggregate occurs by simultaneous or near simultaneous fracture of several

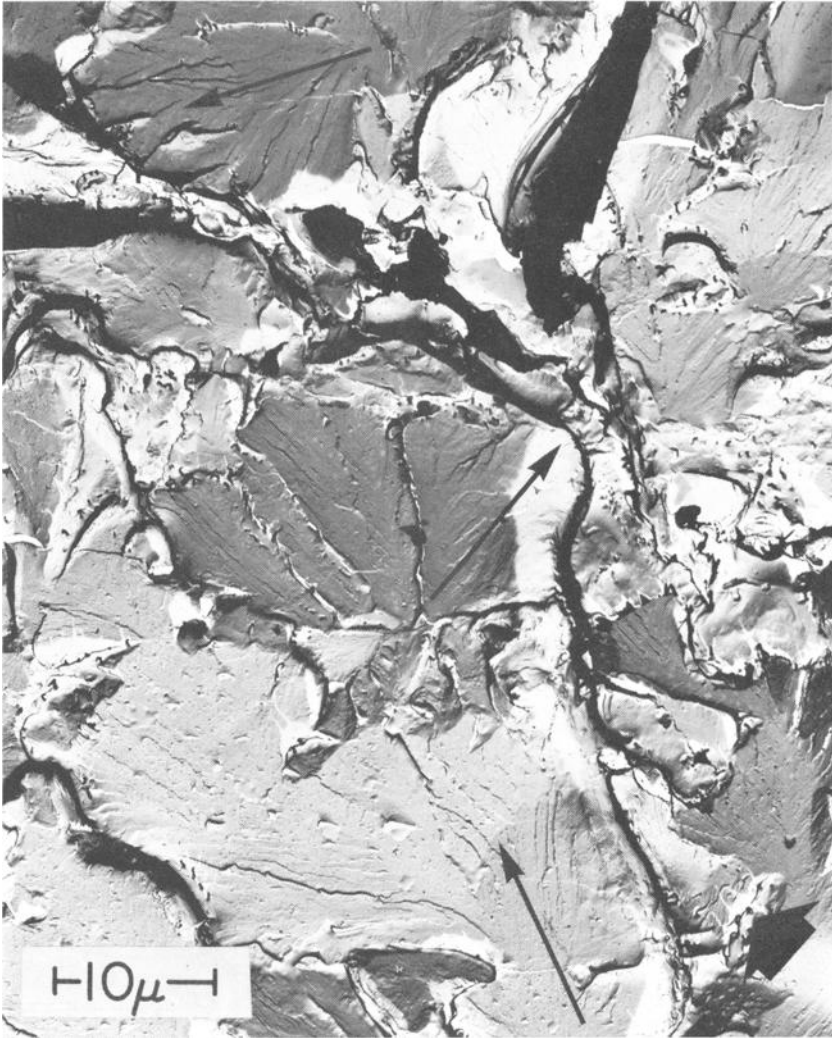


FIG. 9—Fracture surface topography of A 302B steel impact specimens broken at  $-98^{\circ}\text{F}$ . Arrows indicate local direction of crack propagation in individual facets. After Burghard and Davidson [4]. Two-stage plastic-carbon replica ( $\times 2500$ ).

individual grains, each with an independent direction of propagation, and a joining of the individual cracks to form a general, macroscopic crack front.

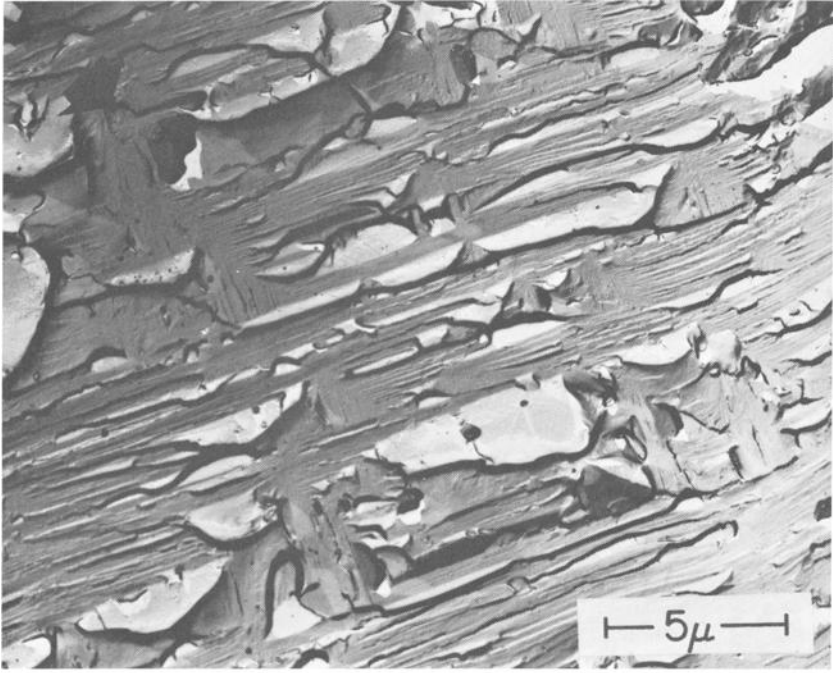
#### *Tongues and Herringbone Patterns*

In certain metals and alloys, fine-scale fracture surface features generally described as “tongues” have been observed to be uniquely associated with cleavage fracture. These features consist of protrusions

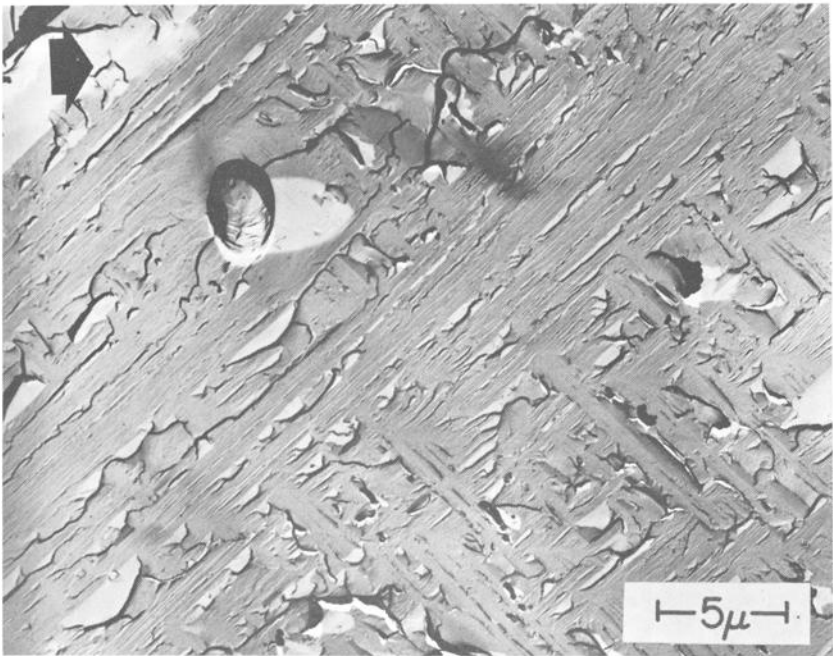
from or intrusions into the general fracture plane and are made up of flat facets inclined to the cleavage plane and terminating at a sharp step. Cleavage tongues were observed in impact fractures of a pearlite-free steel as early as 1956 [31]. Examples of cleavage tongues, observed in an impact fracture of a ferritic stainless steel, are shown in Fig. 10. It should be noted that these two examples represent observations on fractures occurring at widely different temperatures (70 and 264 F). In this case, the occurrence of tongues was more predominant in the 70 F fracture than in the specimen broken at 264 F. Berry [25] suggested that the inclined facets of tongues represented fracture along  $\{112\}$  planes corresponding to the interface between the matrix and the deformation formed ahead of the advancing crack. In a written discussion of Berry's work, Crussard et al also presented examples of well-defined cleavage tongues in Fe-3Si crystals and concluded, from observations of shadowing effects, that these features were associated with the twin-matrix interface [25]. Cleavage on twin-matrix interfaces has also been observed in cadmium tested in liquid gallium [32],<sup>5</sup> magnesium [33], and Fe-3Si [22]. More recently, Beachem [34] has observed distinct tongues in cleaved iron and has established that on two mating fracture surfaces, protruding tongues on one surface are matched by corresponding depressions on the opposite surface. In addition, the orientation of individual tongues relative to crystallographic directions was established by etch-pitting fracture surfaces [35]. These observations provide definite evidence that tongues are formed when a cleavage crack (propagating along an  $\{100\}$  plane) is diverted along the  $\{112\}$  twin-matrix interface of an intersecting twin while the main crack propagates around the twin. The step bounding the tongue on three sides is formed by deformation and fracture of the ligament between the two local cracks. This final stage results in the rejoining of the diverted crack segment with the main crack which continues to propagate on the main cleavage plane. To date, observations of well-defined cleavage tongues have been reported in the fracture of Fe-3Si [25], iron [34], low-carbon steel [31], chromium-base alloys [36], and in Type 430 stainless steel (see Fig. 10).

In certain particular cases of cleavage fracture, topographic features referred to as "herringbone patterns" have been observed. These features are characterized by two groups of lines and narrow inclined facets (sometimes including a few well-defined, isolated tongues) oriented at 90 deg to one another and separated by a narrow, flat strip bisecting the 90-deg angle. Cleavage herringbones, nearly identical in appearance, have been observed in tungsten [37], chromium-base alloys [36], Fe-25Cr-3Al alloy [38], and in Type 430 stainless steels. A

<sup>5</sup> Cadmium does not cleave when tested in air, but liquid metal environments induce cleavage on slip planes and twin interfaces.



(a) Test temperature 70 F. Two-stage plastic-carbon replica ( $\times 7000$ ).



(b) Test temperature 264 F. Two-stage plastic-carbon replica ( $\times 5000$ ).

FIG. 10—Cleavage tongues in impact fractures of Type 430 stainless steel.

typical cleavage herringbone, observed in the last case cited above, is shown in Fig. 11. The relative orientation of the various components in herringbone patterns has led Beachem to conclude that the narrow central strip corresponds to cleavage crack propagation on one of the  $\{100\}$  planes in one of the  $\langle 100 \rangle$  directions and that the fracture on each side is formed by  $\{100\}\langle 110 \rangle$  and  $\{112\}\langle 110 \rangle$  twin interface cleavage mixed with considerable plastic fracture [38].

The cleavage tongues and herringbone patterns described above constitute closely related topographic features in that both are attributed to the interaction of an advancing cleavage crack with deformation twins. As such, these particular features serve as evidence of the nature of plastic deformation accompanying cleavage fracture in certain materials. Because of their dependence on the presence of deformation twins, it is reasonable to expect that both features would be observed in fractures in a single metal or alloy. This expectation is borne out in the observations of impact fractures of Type 430 stainless steel, see Figs. 10 and 11. However, no cases of herringbone patterns in cleaved iron or well-defined tongues in tungsten have been published to date.

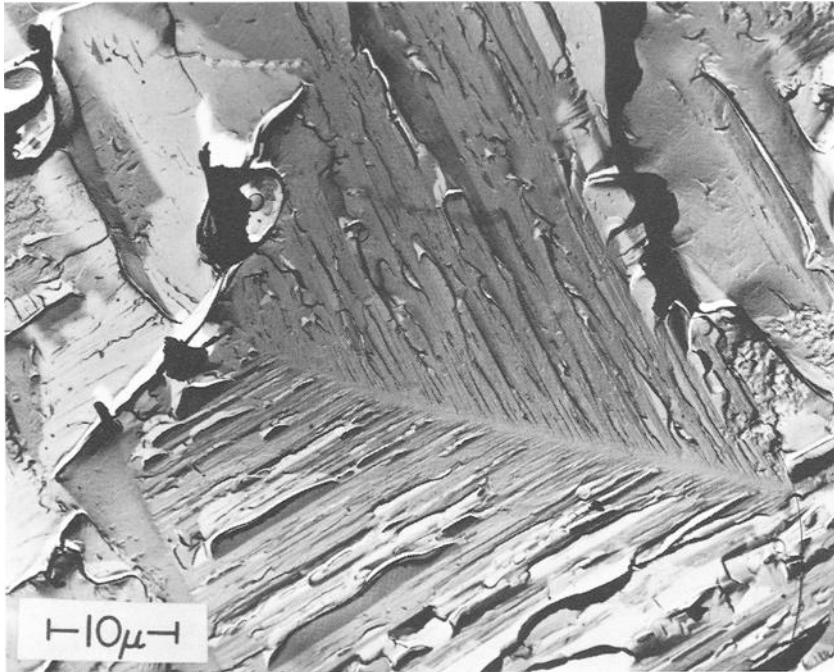
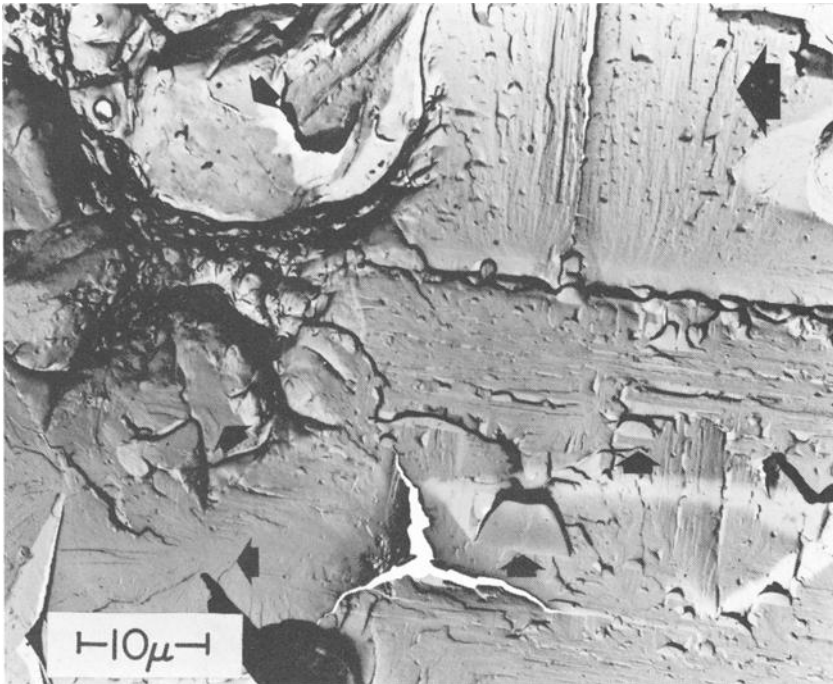


FIG. 11—Herringbone pattern in impact fracture of Type 430 stainless steel. Two-stage plastic-carbon replica ( $\times 2500$ ).

### Mixed Fracture

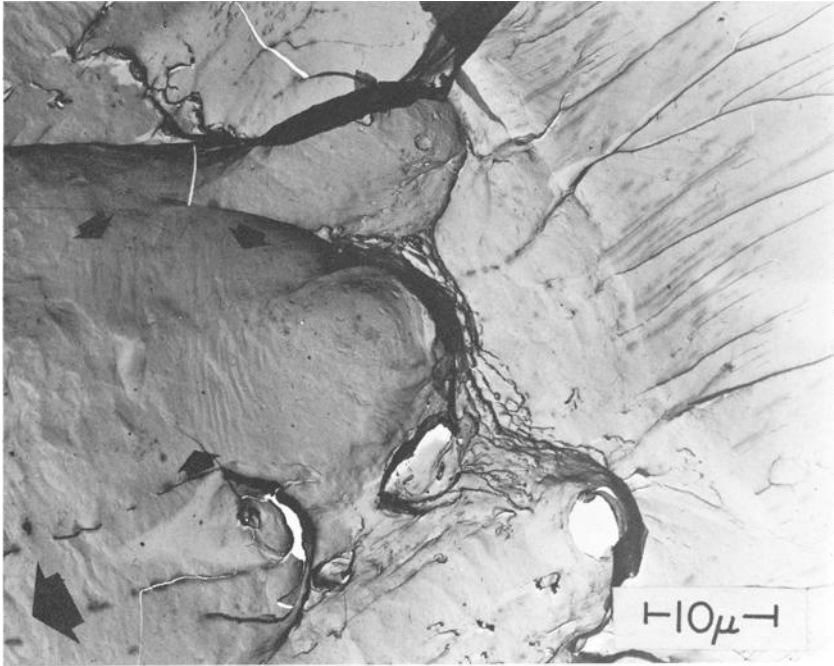
The foregoing discussion has considered cleavage fracture independently without regard to the possibility of simultaneous involvement of two distinct fracture mechanisms in a single fracture. Although there are cases in which fracture occurs completely by cleavage, intimate mixtures of plastic fracture and cleavage are frequently observed. This latter situation is particularly true of fractures in materials exhibiting a ductile-brittle transition. In impact fractures of low-alloy steels, tested in the transition temperature range, topographic features associated with both cleavage and plastic fracture have been observed in the central, flat portion of the fracture surfaces [27,31,39].

In each case, the degree of plastic fracture, as indicated by the relative area of dimpled structure, increased with increasing temperature. Similar observations have been made on impact fractures in Type 430 stainless steel, two examples of which are shown in Fig. 12. This fractographic evidence of the simultaneous involvement of the two dis-



(a) Test temperature 72 F. Note patch of dimples (oblique arrows), facet with river pattern (horizontal arrows) and cleavage tongues (vertical arrows). Two-stage plastic-carbon replica ( $\times 2500$ ).

FIG. 12—Regions of mixed fracture in Type 430 stainless steel impact specimens.



(b) Test temperature 90 F. Note large dimples and stretched surface (arrows) adjacent to cleavage facet with river patterns. Two-stage plastic-carbon replica ( $\times 2500$ ).

FIG. 12—Continued

tinct fracture mechanisms supports the conclusion drawn earlier that the interdependence of transition temperature and microstructural parameters in polycrystalline materials may be expected to be more complex than the relations derived from simplified models (see Eqs 7 and 8).

### *Quasi-Cleavage*

The fracture surfaces of quenched and tempered steels often exhibit flat facets resembling those observed in cleavage. These facets are considerably larger than the microstructural features of tempered martensite and are generally transgranular with respect to prior austenite grains. Because of the highly complex microstructure involved in these cases, no definite relationship has been established between the orientation of these facets and any specific crystallographic planes. As a result, the fracture process producing these particular topographic features cannot be considered as true cleavage. In view of the above factors, the term "quasi-cleavage" was coined to describe this particular class of topography in quenched and tempered steels until such

time as the mechanisms involved in their formation were definitely established. A general definition for quasi-cleavage has been given by Phillips et al [30] as: "A fracture mode resembling cleavage in that it produces planar or nearly planar facets but differing from cleavage in that the facets are not known to be parallel to cleavage planes."

Beachem [40] has noted that quasi-cleavage facets in quenched and tempered steels usually exhibit river patterns and tongues similar to those observed in true cleavage but that, in contrast to true cleavage, the fracture origin is usually located within the boundaries of the facet. In addition, these facets often exhibit tear ridges intermixed with the river patterns and tongues. These latter features are not observed in true cleavage and serve to distinguish the two classes of fracture surface topography.

Beachem has also suggested that the growth and coalescence of completely submerged cracks (in or near the same plane) could result in features corresponding to those observed in quenched and tempered steels (see Ref 40). No further work related to the nature of the mechanisms involved in this fracture process has been published to date. Thus, it seems that, until further investigations are carried out, the formation of quasi-cleavage facets in quenched and tempered steels should be considered to result from an undefined modification of the cleavage mechanism associated with the complex microstructural characteristics of these materials.

In general, cleavage cracks are not observed in single phase face-centered-cubic (fcc) alloys, presumably because of the multiplicity of slip systems, high dislocation mobility and ease of cross-slip. However, in certain cases, flat facets with fine-scale features resembling those of cleavage facets have been observed. Similar features have also been noted in certain hcp materials normally considered immune to cleavage. Although these facets exhibit steps and partial river patterns, and are frequently feather-shaped, no characteristic appearance common to a particular material or to particular fracture conditions has been established. The only specific aspects of these observations are that the facets are definitely transgranular, are not associated with any significant degree of plastic fracture, and are observed both in static and fatigue fractures.

This particular type of fracture surface topography has been observed most frequently in cases involving environmentally induced (or enhanced) fracture. Vennett and Ansell [41] have cited examples in tensile fractures of Type 304 stainless steel tested in high-pressure hydrogen, Fig. 13. Similar features have also been observed in stress-corrosion failure of titanium alloys tested in aqueous environments [42]. In the latter case, X-ray diffraction measurements established that the facets were oriented at a small angle (varying from 8 to 20



FIG. 13—Fracture surface topography of Type 304 smooth-bar tension specimen exposed 24 h and pulled to fracture in 10,000 psi hydrogen. After Vennett and Ansell [41]. Two-stage plastic-carbon replica ( $\times 5300$ ).

deg) to the basal plane. Other examples of “cleavage-like” features have been noted in stress corrosion failures of Ti-6Al-4V alloys tested in methyl alcohol [43] and in titanium-aluminum alloys fractured by low-cycle fatigue crack propagation followed by tensile overload [44].

Because of the uncertainty in the identification of the crystallographic orientation of the facets exhibiting cleavage-like features in fcc materials and in other particular cases where cleavage fracture is unexpected, the observed features cannot be associated with true cleavage fracture. As a result, the term quasi-cleavage has also been employed in the description of these features. The use of this term in these cases is justified only in the sense of the general definition and meaning of quasi-cleavage (that is, “quasi” meaning seemingly or “as if”). It should be emphasized that all fracture surface regions described as quasi-cleavage do not exhibit the specific features categorized for the particular case of fracture in quenched and tempered steels. In view of origin and definition of quasi-cleavage, particular care should be exercised in the use of the term, and every effort should be made to restrict its use to cases where the meaning is clear. Certainly the term should not be used, *in any case*, to suggest or imply a specific fracture mechanism.

## Summary

Cleavage fracture of solids has been the subject of considerable study over the past 10 to 15 years. Significant advances in the theoretical aspects of this fracture mechanism have been made through the application of dislocation theory to cleavage crack nucleation and propagation. In addition, a more complete description of the micro-mechanical aspects of cleavage has resulted from observations of the fine-scale topographic features of fracture surfaces.

Theoretical considerations of cleavage fracture have been based on models which attribute crack nucleation to blocked slip bands. The common obstacles to slip include grain boundaries, other slip bands or twins, and second-phase particles. In general, the theoretical models consider these microstructural features as barriers to dislocation motion which lead to dislocation pileups. Cleavage crack initiation is considered to occur as the result of stress concentrations associated with these dislocation pileups. Consideration of these models has led to the statement of an equivalent fracture criterion expressed in terms of the friction stresses resisting dislocation motion and the contribution of grain boundaries and other microstructural discontinuities to the strength of polycrystals. This fracture criterion correctly predicts the susceptibility of certain bcc and hcp materials to cleavage fracture. Applications of this fracture criterion to materials exhibiting a ductile-to-brittle transition also led to a relationship between transition temperature and grain size consistent with experimental observations. In addition, current fracture theories predict effects of variables such as grain size, size and distribution of precipitate particles, and yield stress on the susceptibility of a material to cleavage fracture.

The theoretical models of cleavage fracture have not explicitly taken into account the fact that, under certain conditions, crack growth may be more difficult than crack nucleation. It appears that the principal problem associated with a theoretical description of crack propagation is that of accurately accounting for the energy associated with plastic deformation in the vicinity of the crack tip.

In addition to considerations of cleavage crack nucleation and propagation, some attention has been directed toward the prediction of characteristic cleavage planes from atomic binding principles. Calculations based on the concept that a cleavage plane is the plane of minimum surface energy have correctly predicted the cleavage planes in the majority of cases to which the theory has been applied.

Fractographic studies have established three classes of fine-scale topographic features characteristic of cleavage fracture, that is, river patterns, cleavage tongues, and herringbone patterns. Each of these features has been studied in detail, and the factors affecting their for-

mation are fairly well understood. These topographic features provide direct information related to the nucleation and propagation of cleavage cracks. Specifically, the fine-scale topography frequently provides direct information as to the origin of fracture within a facet, the local direction of crack propagation, and the general influence of microstructural features on the fracture process.

Cleavage tongues and herringbone patterns have been shown to be associated with deformation twins formed ahead of an advancing crack, and certain aspects of river patterns have been attributed to plastic deformation occurring during fracture. Thus, topographic features provide a qualitative indication of the amount of plastic deformation associated with cleavage fracture. Fractographic studies have also shown fracture can occur by simultaneous involvement of cleavage and microvoid coalescence.

Topographic features resembling those of cleavage have been observed in numerous cases where a definite relationship between the fracture surface and low-index crystallographic planes cannot be established. The term quasi-cleavage has been introduced as a temporary description of this particular class of topography in quenched and tempered steels. Cleavage-like features have also been observed in the fracture of certain fcc materials and in other cases where cleavage fracture is unexpected. These observations are usually associated with fractures induced or enhanced by environmental conditions (for example, stress corrosion and environmentally enhanced fatigue). Because of the uncertainty in the identification of the crystallographic orientation of facets in this latter group of fractures, the term quasi-cleavage has also been employed in the description of these features. It is emphasized that the term quasi-cleavage was introduced strictly for the purpose of describing certain topographic features which are not fully understood and that the term should not be used to imply a specific fracture mechanism.

It may be concluded that certain basic aspects of cleavage fracture have been thoroughly described from a theoretical point of view and that fractographic analysis has established definite characteristics associated with true cleavage. The observation of fine-scale topographic features associated with plastic deformation suggests that further application of fractographic techniques may provide more specific information related to the role of plastic deformation in cleavage fracture. Additional systematic studies directed toward correlation of cleavage fracture topography with microstructural features are necessary for a more complete understanding of the cleavage mechanism. It is also evident that additional work is necessary to establish the mechanisms involved in the formation of topographic features described as quasi-cleavage.

## References

- [1] Stoloff, N. S. and Gensamer, M., "Deformation and Fracture of Polycrystalline Cadmium," *Transactions*, American Institute of Mining, Metallurgical, and Petroleum Engineers, Vol. 227, 1963, p. 70.
- [2] Toaz, M. W. and Ripling, E. J., "Flow and Fracture Characteristics of Binary Wrought Magnesium-Lithium Alloys," *Journal*, Institute of Metals, Vol. 85, 1956, p. 137.
- [3] Amateau, M. F., Burrier, H. I., Jr., and Ebert, L. J., "Brittle Fracture in Alpha-Titanium," *Transactions*, American Society for Metals, Vol. 59, 1966, p. 921.
- [4] Burghard, H. C. and Davidson, D. L., "Fracture Mechanisms and Fracture Surface Topography," *Proceedings of the First International Conference on Fracture*, Japanese Society for Strength and Fracture of Materials, 1966, Vol. 2, p. 571.
- [5] Cottrell, A. H., "Theory of Brittle Fracture in Steel and Similar Metals," *Transactions*, American Institute of Mining, Metallurgical, and Petroleum Engineers, Vol. 212, 1958, p. 192.
- [6] Ku, R. C. and Johnston, T. L., "Fracture Strength of MgO Bicrystals," *Philosophical Magazine*, Vol. 9, 1964, p. 231.
- [7] Westwood, A. R. C., Goldheim, D. L., and Pugh, E. N., "Fracture Behavior of AgCl in Aqueous NaCl," *Acta Metallurgica*, Vol. 13, 1965, p. 695.
- [8] Wronski, A. and Fourdeux, A., "Slip-Induced Cleavage in Polycrystalline Tungsten," *Journal of Less Common Metals*, Vol. 6, 1964, p. 413.
- [9] McMahon, C. J., Jr., and Cohen, M., "Initiation of Cleavage in Polycrystalline Iron," *Acta Metallurgica*, Vol. 13, 1965, p. 591.
- [10] Stroh, A. N., "The Formation of Cracks as a Result of Plastic Flow," *Proceedings*, The Royal Society, Vol. 223A, 1954, p. 404.
- [11] Petch, N. J., "The Ductile to Brittle Transition in the Fracture of Alpha-Iron," *Philosophical Magazine*, Vol. 3, 1958, p. 1089.
- [12] Petch, N. J., "The Ductile-Cleavage Transition in Alpha Iron," *Fracture*, Wiley, New York, 1959, p. 54.
- [13] Jordan, K. R., Ph.D. thesis, Rensselaer Polytechnic Institute, 1967.
- [14] Johnston, T. L., Davies, R. G., and Stoloff, N. S., "Slip Character and the Ductile to Brittle Transition of Single Phase Solids," *Philosophical Magazine*, Vol. 12, 1965, p. 305.
- [15] Hahn, G. T. et al., "Initiation of Cleavage Microcracks in Iron and Steel," *Fracture*, Wiley, New York, 1959, p. 91.
- [16] Hahn, G. T. and Rosenfield, A. R., "A Modified Double Pile-Up Treatment of the Influence of Grain Size and Dispersed Particles on Brittle Fracture," *Acta Metallurgica*, Vol. 14, 1966, p. 1815.
- [17] Johnston, T. L., Stokes, R. J., and Li, C. H., "The Fracture Behavior of Silver Chloride-Alumina Composites," *Transactions*, American Institute of Mining, Metallurgical, and Petroleum Engineers, Vol. 221, 1961, p. 792.
- [18] Keh, A. S., Leslie, W. C., and Sponseller, D., "Interactions of Dislocations and Precipitates in Some Iron-Base Alloys," *Precipitation in Iron Base Alloys*, Gordon and Breach, New York, 1966, p. 281.
- [19] Rosenfield, A. R. and Hahn, G. T., "Effects of Second Phase Particles on Ductility," *Proceedings of Conference on Physical Basis of Yield and Fracture*, Institute of Physics and Physical Society, Conference Series No. 1, 1966, p. 47.
- [20] Gilman, J. J., "Cleavage, Ductility and Tenacity in Crystals," *Fracture*, Wiley, New York, 1959, p. 193.
- [21] Guiu, F., "Twinning and Cleavage Fracture in Molybdenum Single Crystals," *Journal of Less Common Metals*, Vol. 12, 1965, p. 77.
- [22] Hull, D., "Twinning and Fracture of Single Crystals of 3% Silicon Iron," *Acta Metallurgica*, Vol. 8, 1960, p. 11.
- [23] Tetelman, A. S., "The Ductile-Brittle Transition in Iron-3% Silicon Monocrystals," *Acta Metallurgica*, Vol. 12, 1964, p. 324.
- [24] Rosenbaum, H. S., "Non-Basal Slip and Twin Accommodation in Zinc Crystals," *Acta Metallurgica*, Vol. 9, 1961, p. 742.

- [25] Berry, J. M., "Cleavage Step Formation in Brittle Fracture Propagation," *Transactions, American Society for Metals*, Vol. 51, 1959, p. 556.
- [26] Low, J. R., "A Review of the Microstructural Aspects of Cleavage Fracture," *Fracture*, Wiley, New York, 1959, p. 68.
- [27] Irvine, K. J. and Pickering, F. B., "The Impact Properties of Low Carbon Bainitic Steels," *Journal, Iron and Steel Institute*, Vol. 20, 1963, p. 518.
- [28] Beachem, C. D. and Pelloux, R. M. N., "Electron Fractography - A Tool for the Study of Micromechanisms of Fracturing Processes," *Fracture Toughness Testing and Its Applications, ASTM STP 381*, American Society for Testing and Materials, 1965, p. 210.
- [29] Pelloux, R. M. N. and McMillan, J. C., "The Analysis of Fracture Surfaces by Electron Microscopy," *Proceedings of the First International Conference on Fracture*, Japanese Society for Strength and Fracture of Materials, Vol. 2, 1966, p. 547.
- [30] Phillips, A., Kerlins, V., and Whiteson, B. V., "Electron Fractography Handbook," ML-TDR-64-416, Air Force Materials Laboratory, Wright-Patterson Air Force Base, Ohio, 1965.
- [31] Crussard, C. et al, "A Study of Impact Tests and the Mechanism of Brittle Fracture," *Journal, Iron and Steel Institute*, Vol. 183, June 1956, p. 146.
- [32] Stoloff, N. S. and Johnston, T. L., "Crack Propagation in a Liquid Metal Environment," *Acta Metallurgica*, Vol. 11, 1963, p. 251.
- [33] Reed-Hill, R. E. and Robertson, W. D., "The Crystallographic Characteristics of Fracture in Magnesium Single Crystals," *Acta Metallurgica*, Vol. 5, 1957, p. 728.
- [34] Beachem, C. D., "The Formation of Cleavage Tongues in Iron," Report of NRL Progress, Naval Research Laboratory, Feb. 1966, p. 19.
- [35] Beachem, C. D., "1966 ASTM Photographic Exhibit," *Materials Research and Standards*, Vol. 6, 1966, p. 519.
- [36] Gilbert, A., "Influence of Alloying Elements on Mechanisms of Fracture in Chromium," Second Annual Report (to Pratt & Whitney Aircraft Corp.).
- [37] Dahlberg, E. P., "Characteristics of Twinning on Fracture Surfaces of Single and Polycrystalline Tungsten," *Proceedings of Fifth International Congress for Electron Microscopy*, Academic Press, 1962, Paper J-5.
- [38] Beachem, C. D., "The Crystallography of Herringbone Fractures in an Iron-Chromium-Aluminum Alloy," Report of NRL Progress, Naval Research Laboratory, Jan. 1967, p. 28.
- [39] Burghard, H. C., Jr., and Norris, E. B., "The Effect of Neutron Irradiation on the Fracture Characteristics of Pressure-Vessel Steels," ASME Paper No. 67-MET-1, American Society of Mechanical Engineers, 1967.
- [40] Beachem, C. D., "Electron Fractographic Studies of Mechanical Processes in Metals," *Transactions, American Society of Mechanical Engineers, Series D*, Vol. 87, 1965, p. 299.
- [41] Vennett, R. M. and Ansell, G. S., "Effect of High-Pressure Hydrogen upon Tensile Properties and Fracture Behavior of 304L Stainless Steel," *Transactions, American Society for Metals*, Vol. 60, 1967 (to be published).
- [42] Meyn, D. A., "A Study of the Crystallographic Orientation of Cleavage Facets Produced by Stress-Corrosion Cracking of Ti-7 Al-2 Nb-1 Ta in Water," Report of NRL Progress, Naval Research Laboratory, Aug. 1965, p. 21.
- [43] Meyn, D. A., Dahlberg, E. P., and Beachem, C. D., "Analysis of Stress-Corrosion Cracking of Ti-6 Al-4 V Fuel Tank Material in Methyl Alcohol," NRL Memorandum Report 1744, Naval Research Laboratory, Jan. 1967.
- [44] Judy, R. W., Jr., et al, "Low Cycle Fatigue-Crack Propagation and Fractographic Investigation of Ti-7 Al-2 Nb-1 Ta and Ti-6 Al-4 V in Air and Aqueous Environments," *Transactions, American Society for Metals*, Vol. 59, 1966, p. 195.

## Fracture by Microscopic Plastic Deformation Processes

---

**REFERENCE:** Beachem, C. D. and Meyn, D. A., "Fracture by Microscopic Plastic Deformation Processes," *Electron Fractography, ASTM STP 436*, American Society for Testing and Materials, 1968, pp. 59-88.

**ABSTRACT:** The various fracture surface features formed by fine-scale plastic flow processes are discussed, and the mechanisms by which they are formed are discussed where they are known.

Glide plane decohesion, as it has been used in the literature, is shown to be misleading, and a more descriptive term, "stretching," is used in its place. The use of "ductile cleavage" to describe the same process is also misleading.

Since brief, descriptive, nonmisleading terminology is necessary for immediate communication, several terms have evolved to describe the surfaces created by unknown processes. Glide plane decohesion, serpentine glide, ripples, stretching, and three kinds of microvoid coalescence are shown to be parts of a spectrum of plastic rupture.

**KEY WORDS:** electron microscopy, fractography, surface features, plastic flow, metals, fracture mechanisms

The metals and alloys which are tough owe this property to their ability to deform plastically and absorb energy before or during fracturing. The present paper describes the mechanisms responsible for several fracture modes involving extensive plastic deformation, insofar as these mechanisms have been worked out. All of these modes involve the same fundamental process, glide on one or more sets of crystallographic planes, but the resulting fracture topography is different, and therefore different names are used for the various fracture appearances even though the basic process in each is the same.

The naming of fracture topographic features often reflects the current concepts of the manner in which the features are generated. The features observed at the magnifications used in electron microscopy are produced by local stresses which, because of inclusions, voids,

<sup>1</sup> Head, Micro-Mechanical Metallurgy Section, Physical Metallurgy Branch, Metallurgy Div., Naval Research Laboratory, Washington, D.C. Personal member ASTM.

<sup>2</sup> Physical metallurgist, Micro-Mechanical Metallurgy Section, Physical Metallurgy Branch, Metallurgy Div., Naval Research Laboratory, Washington, D.C.

anisotropic grains in polycrystalline metals, etc., may be very different from the macro stresses imposed on the specimen. One is often forced, therefore, to infer not only the microfracture process but also the local state of stress which produced the observed feature.

### **Fine Scale Mechanisms**

#### *Glide Plane Decohesion*

Single crystals of pure metal may, when plastically deformed, glide apart along slip planes. When these crystals are large, slip along these planes is readily visible to the unaided eye. This process, if continued on the same plane, leads eventually to the specimen parting along a glide plane. This mode of separation, whether on a macroscopic or microscopic scale, and whether or not carried to completion, is appropriately called glide plane decohesion when the glide surfaces can be identified as such. It is an important process in the fracturing of many alloys of practical usefulness.

If a metal specimen separates by glide plane decohesion, particularly if this is along only a few members of one set of crystallographic planes, the fracture surface consists largely of facets of one or at most a few specific lattice planes, and in this respect the fracture surface might be considered akin to cleavage, which also occurs on only one or at most a few crystallographic planes. It is understandable then why the process has been called "ductile cleavage" (ductile because extensive glide precedes fracture). This is considered a less suitable term than glide plane decohesion.

The term "ductile rupture" has been used in the past for the process which, in this paper, has been termed microvoid coalescence. Although some of the most ductile metals and alloys fracture by this mode, so do some of the alloys having very low engineering ductility. The term ductile rupture might suggest to the mechanical metallurgist greater toughness than a given alloy may possess, and, accordingly, ductile rupture might best be used to describe macroscopic ductile fracture, such as occurs in pure gold or ultra-pure aluminum.

The use of the term glide plane decohesion is misleading in cases where the featureless surfaces under consideration are created by unidentified processes of extreme plastic deformation operating on a scale much smaller than the size of the smooth surface. The term stretching is now being widely used to specify this type of process, as discussed in the next section.

#### *Serpentine Glide*

Particularly in polycrystalline metals where the deformation of a given grain must accommodate to the deformation of its neighboring

grains, gliding may occur on many sets of intersecting planes and in an irregular manner giving rise to a pattern which has come to be known as serpentine glide. Serpentine glide surfaces, then, are formed by (partial) glide plane decohesion on several sets of planes by unspecified mechanisms, giving a particular interwoven or plaited appearance on the fracture surface. This will be illustrated in several subsequent electron fractographs.

The sketch in Fig. 1 shows the idealized stress pattern at a free surface at the root of a notch or crack (or any other free surface) in a stressed specimen. Figure 2 is a further consideration of the stresses at a free surface. Here we are viewing the stressed element along the intersection of the local planes of maximum shear stress, that is, along the direction of  $\sigma_2$ . Though glide need not occur on planes of maximum shear stress, localized glide is shown here along one family of planes parallel to the planes of maximum shear stress producing steps which may also be seen in an actual case in Fig. 3a. This specimen was an ingot iron wire,  $\frac{1}{8}$  in. diameter, notched with a file perpendicular to the axis of the wire. The root of the notch was caused to open by bending the wire as shown in the sketch in Fig. 3b. The features indicated at A and B in Fig. 3a are serpentine glide, and such surfaces may be seen in stereo viewing to be stepped as in Fig. 2. The light surfaces marked

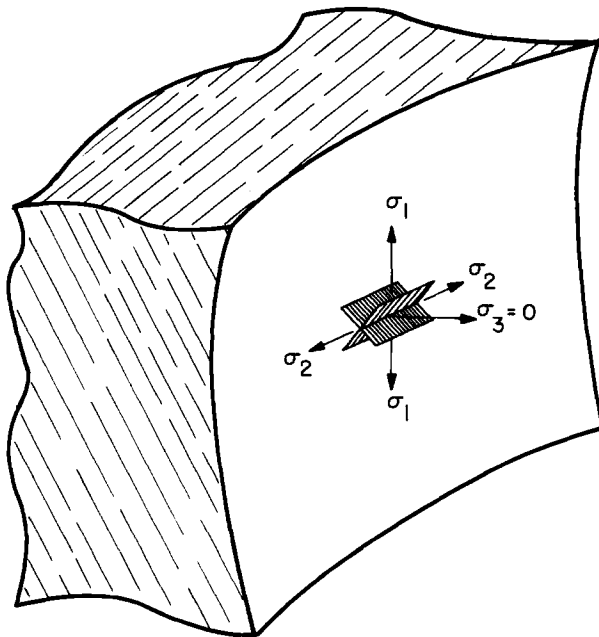
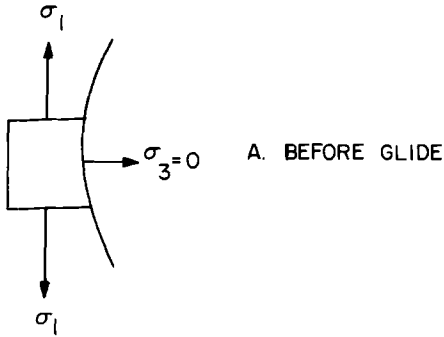


FIG. 1—Stress configuration at a free surface where the local maximum principal stress is vertical. The shaded planes are the local planes of maximum shear stress.



A. BEFORE GLIDE

B. AFTER GLIDE ON A SERIES OF  
PARALLEL PLANES THAT ARE  
FAVORABLY ORIENTED FOR GLIDE

FIG. 2—Simplified general model for the creation of a rupture or fracture surface by a simple glide process. Though glide by a slip process is shown, glide by twinning may also produce new free surfaces. Arrows indicate the new (rupture, fracture) surfaces, created by glide plane decohesion.

by B's (Fig. 3a) are the new free surfaces created by plastic flow on glide planes—glide plane decohesion. If further glide takes place either on other planes in the same set or on planes in other sets, the markings tend to be smoothed out, becoming first ripples [1]<sup>3</sup> (as seen at C in Fig. 3a) and then featureless as the glide steps become too small to be shown by the fidelity of present-day replicas. These events are sketched in Fig. 4 and are apparent in Fig. 3a when one realizes that the sharp step-like markings of serpentine glide are at the bottom of the trough where plastic flow is not extensive and that the ripples are smoother near the file marks where additional glide has taken place.

Such glide markings as are visible in Fig. 3a, and others throughout this report, can in general be formed by a combination of such elementary slip mechanisms as pencil or wavy slip [2-4], irregular slip, cross slip, and multiple slip. Two of these are illustrated in Fig. 5. It is likely that multiple slip will operate independently of the other mechanisms and increase the general complexity of the surface appearance.

<sup>3</sup> The italic numbers in brackets refer to the list of references appended to this paper.

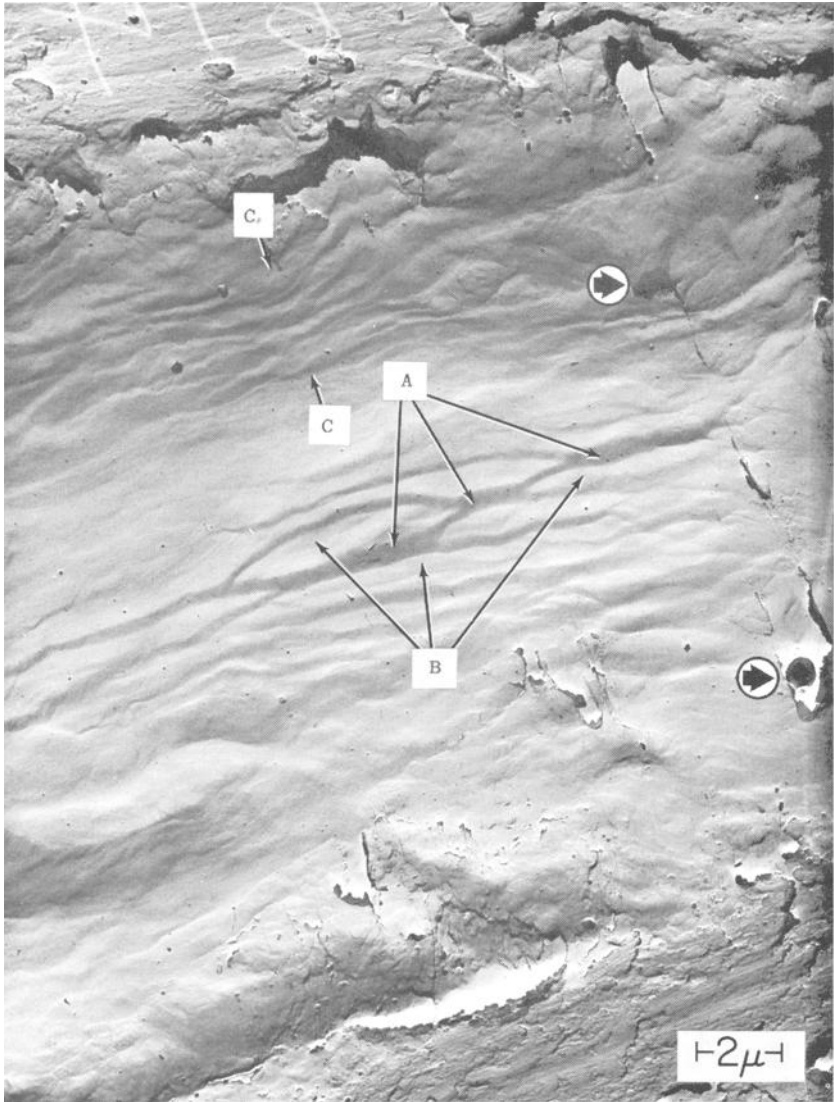


FIG. 3a—Serpentine glide surface in annealed Armco iron. This glide was produced by slip when the root of a notch in this wire specimen was opened up by bending at room temperature. The dark surfaces (A) apparently were a single surface before slip on a second series of parallel planes produced the light parallel surfaces (B). Examples of ripples may be seen between the arrows (C). Palladium-shadowed direct-carbon replica ( $\times 9000$ ).

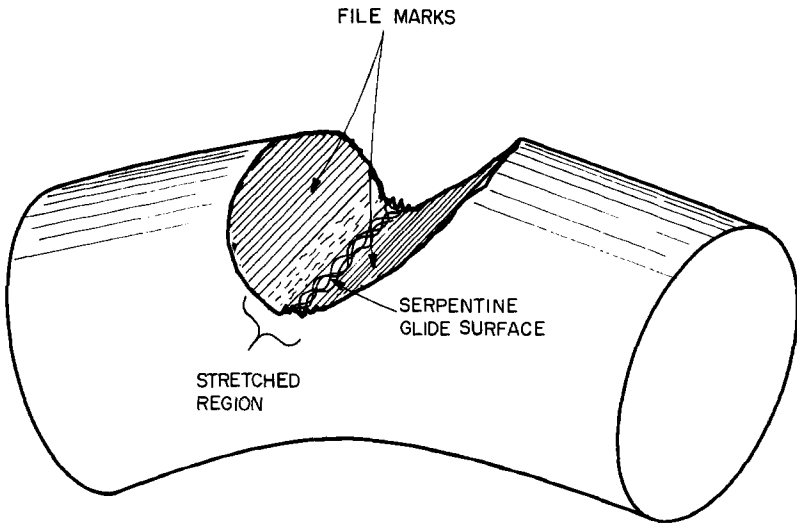


FIG. 3b—Sketch of wire specimen from which replica shown in Fig. 3a was taken.

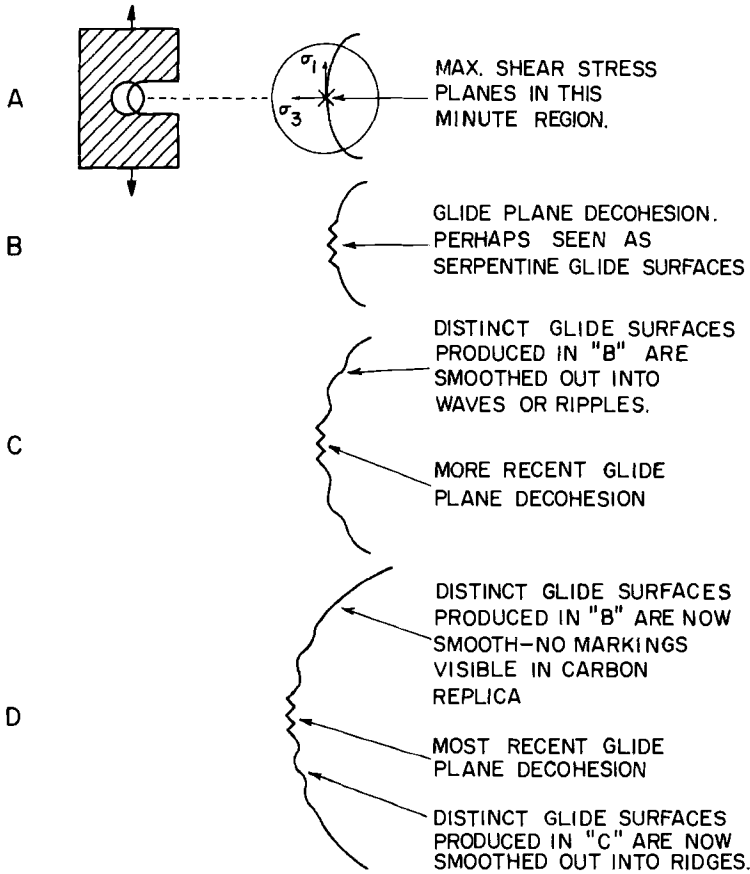


FIG. 4—The production of smooth surfaces by plastic flow. Surfaces definitely produced by glide plane decohesion are smoothed by severe plastic deformation—stretching—until no markings are visible on ordinary replicas. Elongation is vertical, and increases from top to bottom. Crack propagation direction is from right to left.

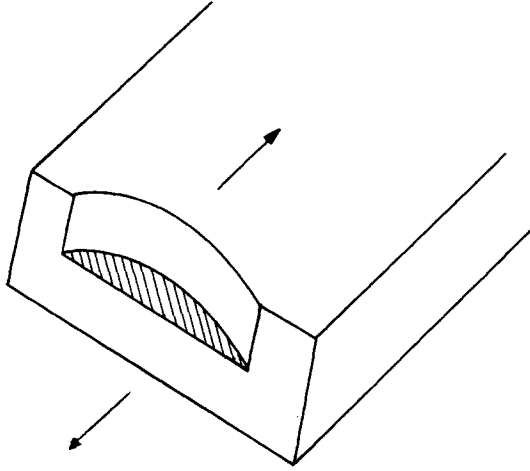


FIG. 5a—Irregular slip. Slip intersects the surface in irregular fashion, producing irregular slip steps (cross-hatched). This is very similar to some features actually seen in Fig. 3a.

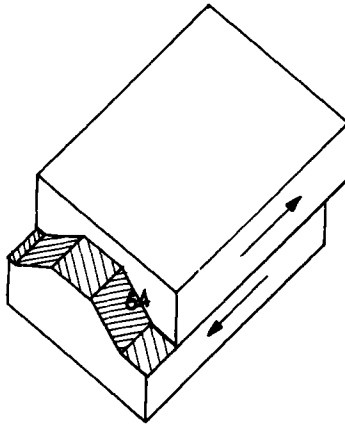


FIG. 5b—Pencil slip, also called wavy slip or wavy glide in  $\alpha$ -iron by Barrett [2]. Cross-slipping screw or multiplanar edge dislocations can create this appearance. Resulting slip step is cross-hatched. From Cottrell [3].

### Stretching

When glide produces new surfaces in heavily cold-worked metal, the glide planes are poorly defined and the glide steps may be so poorly delineated (at least in replication processes now available for fracture surfaces) that the new surface may appear featureless. The term which has been used for the processes which generate such surface areas is stretching, which is then glide plane decohesion on a scale so fine that the glide marks are no longer seen.

An experiment which illustrates the fact that these smooth featureless surfaces are formed by stretching rather than by glide plane decohesion or ductile cleavage is illustrated in Figs. 6 and 7. A piece of

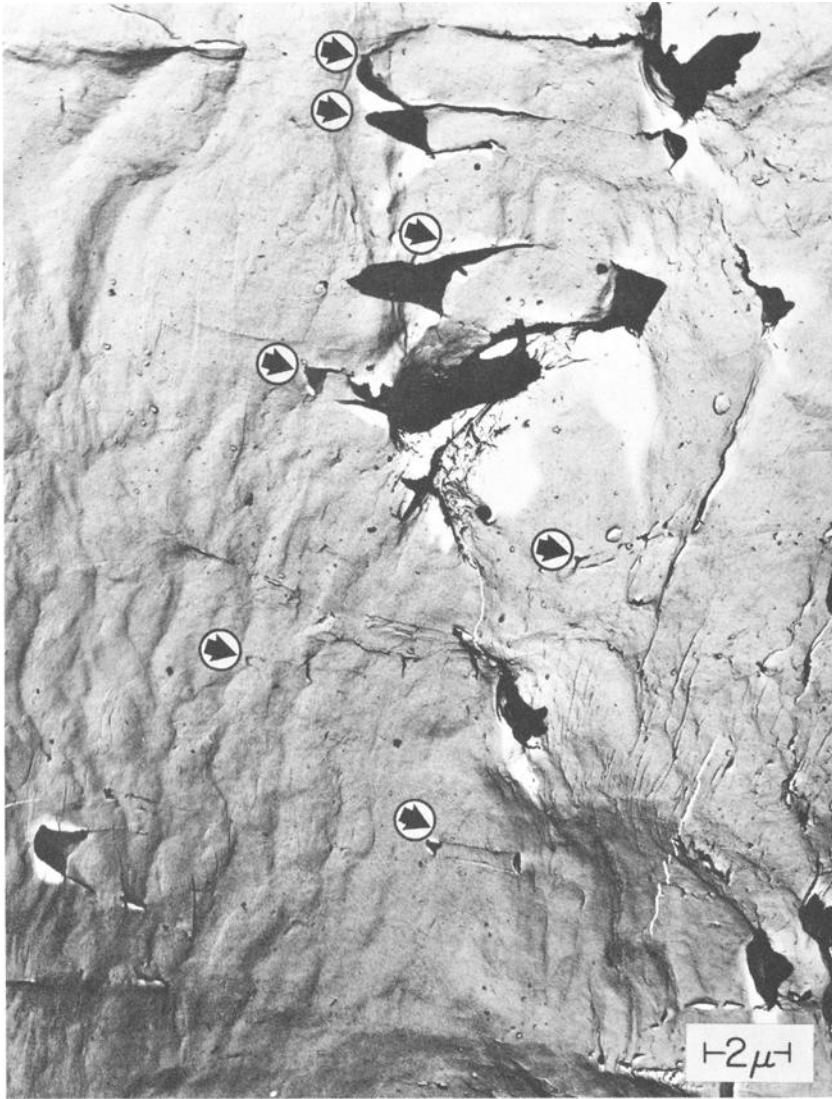


FIG. 6—Stretching at the root of a notch in a 99.999 per cent pure copper wire specimen. Stretching occurred in directions of the arrows after the palladium was deposited, and before the carbon was deposited. Dark areas are palladium, light areas are newly stretched. Direct-carbon replica ( $\times 6000$ ).

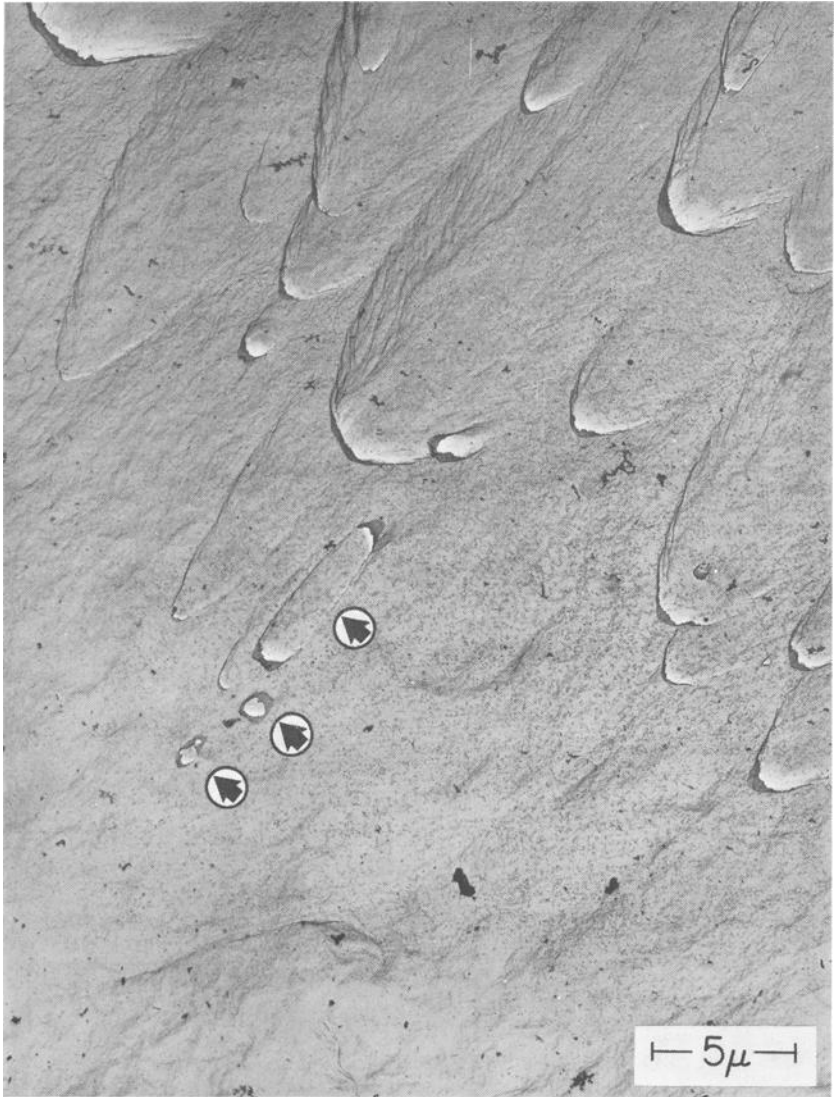


FIG. 7—Extensive stretching in 99.999 per cent copper after the deposition of palladium. Direct-carbon replica ( $\times 9000$ ).

annealed 99.999 per cent pure copper wire was notched, and the wire was bent to open the root of the notch thus introducing severe cold work into the material at the notch root. After palladium was evaporated into the notch, the wire was bent further, and carbon was evaporated into the notch. This direct carbon replica was then freed from the specimen and studied. Figure 6 shows a portion of the root of the notch which was only slightly stretched in the direction of the arrows after the palladium was evaporated. Figure 7 shows a region where additional stretching was more extensive on one side than on the other. The right-hand side of the picture shows such extreme stretching that one cannot tell in which direction it was stretched.

Another example of the stretching process is shown in Fig. 8. In this as-cast Ti-2Al-2Zr-2V-1Mo alloy, a sheet of an unknown constituent is seen to be broken up into segments which have moved apart by stretching of the bulk material in the directions shown by the arrows.

Stretching is defined as the production of smooth featureless free surfaces by extremely complex plastic flow mechanisms acting on too fine a scale to produce characteristic surface traces in present-day replicas. Thus stretching, which is by no means an accurate description of the basic plastic flow mechanisms, is a much more descriptive and much less misleading term than glide plane decohesion or ductile cleavage for this form of deformation.

### *Microvoid Coalescence*

Small precipitate particles, undissolved carbides, sulfides, silicates, oxides, or other brittle or weak constituent particles are generally present in large numbers in all but the purest of metals. When the metal around them is plastically deformed these particles often create internal free surfaces by either cleaving or separating from the adjacent metal along their interfaces.

Under plastic strain such free surfaces nucleate voids which grow by plastic rupture processes similar to those at the root of the opening notch in Fig. 3. With extreme plastic growth of voids, which frequently grow one or two orders of magnitude larger than the free surfaces that initiate them, steps or ripples are visible only rarely in present-day replicas. This is particularly true in the high-strength alloys that have complex fine-scale microstructures. The spherical or rounded shape of the voids prohibits simple deformation: glide must occur in a highly complex manner in the severely worked material at the surface of the void during the growth of a spherical or rounded internal void (hundreds or thousands of per cent elongation — if one cares to visualize plastic deformation on this scale in this manner).

The voids which are nucleated at these metallurgical singularities

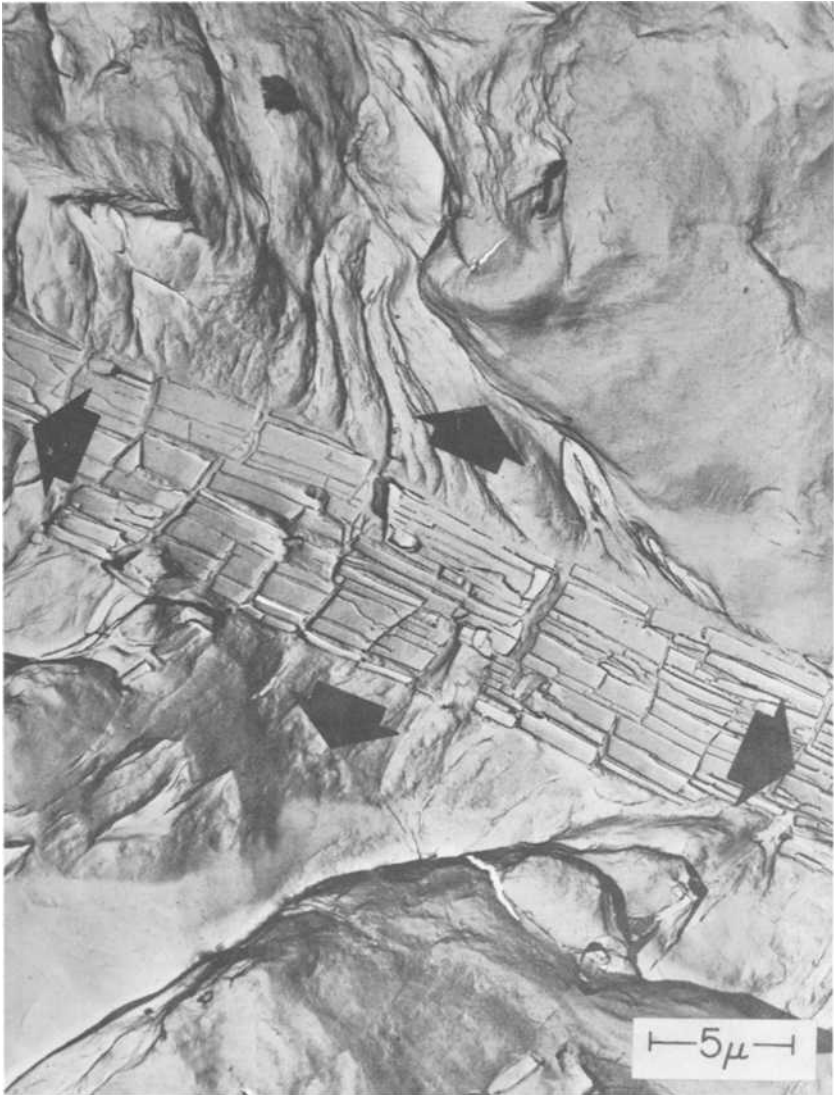


FIG. 8—Stretching in as-cast Ti-2Al-2Zr-2V-1Mo. The flat constituent particles have been expanded in two directions (arrows) on a relatively flat area as a result of stretching of the underlying metal. Surrounding metal is much more severely stretched. Two-stage carbon replica ( $\times 6000$ ).

grow under plastic strain by the glide processes which have been termed "stretching" above. (Growth by diffusion of vacancies is too slow a process.) A void may grow until it impinges on a neighboring void under one of three stress configurations as depicted in Fig. 9. When voids impinge and the last remaining metal separates under normal stress, the newly opened surface can be shown to consist of a cup-like depression on both fracture faces which has come to be called an equiaxed dimple (or sometimes a cupule), and the process has come to be called normal dimpled rupture.

If, however, the voids grow and coalesce under shear stresses, as in the second series of Fig. 9, they are elongated in the shearing direction. The surface of the shear fracture shows the elongated

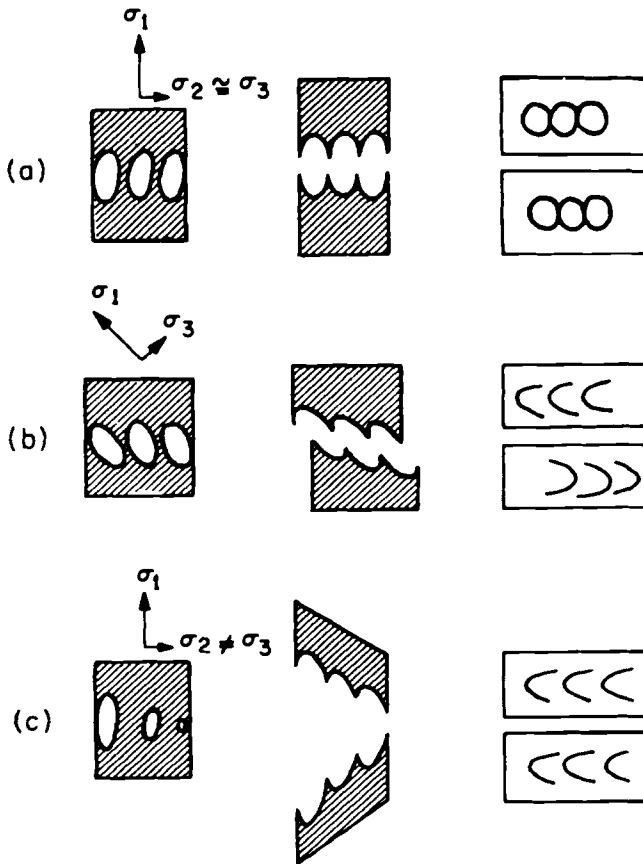


FIG. 9—Three observed basic modes for the coalescence of microvoids. For each mode the sketches show from left to right: material stressed almost to the point of local rupture; local rupture; and the directional sense of dimples on the rupture surfaces. The three coalescence modes are called (a) normal dimpled rupture; (b) shear rupture; and (c) tearing.

dimples with one end continuous and the other end stretched out until that end appears open. Observations on precisely matched fracture sites have confirmed that one set of shear dimples, as these are called, points toward the origin of the shear fracture, and the set on the other fracture surface points in the opposite direction.

If voids grow and coalesce under a strain gradient, as in the third sequence of Fig. 9, they are also elongated, and when observed on only one fracture surface they are presently indistinguishable from shear dimples. But the dimples on the matching surface in this case are "pointing" in the same direction as on the other half, and on both fracture surfaces the dimples point toward the fracture origin. These have been termed tear dimples since they have been generated by a tearing action.

It will be seen that these three forms of surfaces created by microvoid coalescence—equiaxed, shear, and tear dimples—may sometimes appear close together in what appears macroscopically to be a surface of a single fracture mode. This is attributed to the metallurgical heterogeneities mentioned earlier or to transients in the stress pattern.

#### *Fractographs Further Illustrating Plastic Rupture Surfaces*

Metals that are soft and sufficiently free from precipitate particles, inclusions, etc., tend to favor failure by glide plane decohesion and its extensions, serpentine glide and stretching. Figures 3a, 6, 7, and 10 show fracture surfaces created by this mode. The serpentine glide surfaces might be mistaken for fatigue fracture surface markings by the unwary doing a failure analysis. The occasional crossing of the glide markings, however, may often be used to identify these as serpentine glide surfaces rather than fatigue fracture surfaces.

Figure 3a (arrows) also shows isolated dimples which nucleated near the stretching surface, grew to the surface, opened, and stretched out in the surface. In Fig. 3a the stretching of the dimple in the surface is so extensive that its two separated ends are not easily recognized as mates. Figures 10 and 11 show increasing numbers of dimples in stretched surfaces, while Figs. 12 and 13 are composed entirely of dimples. Thus a full spectrum is seen, ranging from no dimples to all dimples on a stretched surface. Figure 12 clearly shows serpentine glide in many of the dimples.

Surfaces formed by the tearing mode of microvoid coalescence are illustrated in Figs. 12 and 13. (Figures 10, 11, and 13 show both ends of oval dimples in a stretch surface where it is obvious that the dimples grow by an "opening" mode and are therefore by definition tear dimples.) Most of the tear dimples in Fig. 13 could be identified only by checking the directional sense of the dimples on the matching fracture surface.

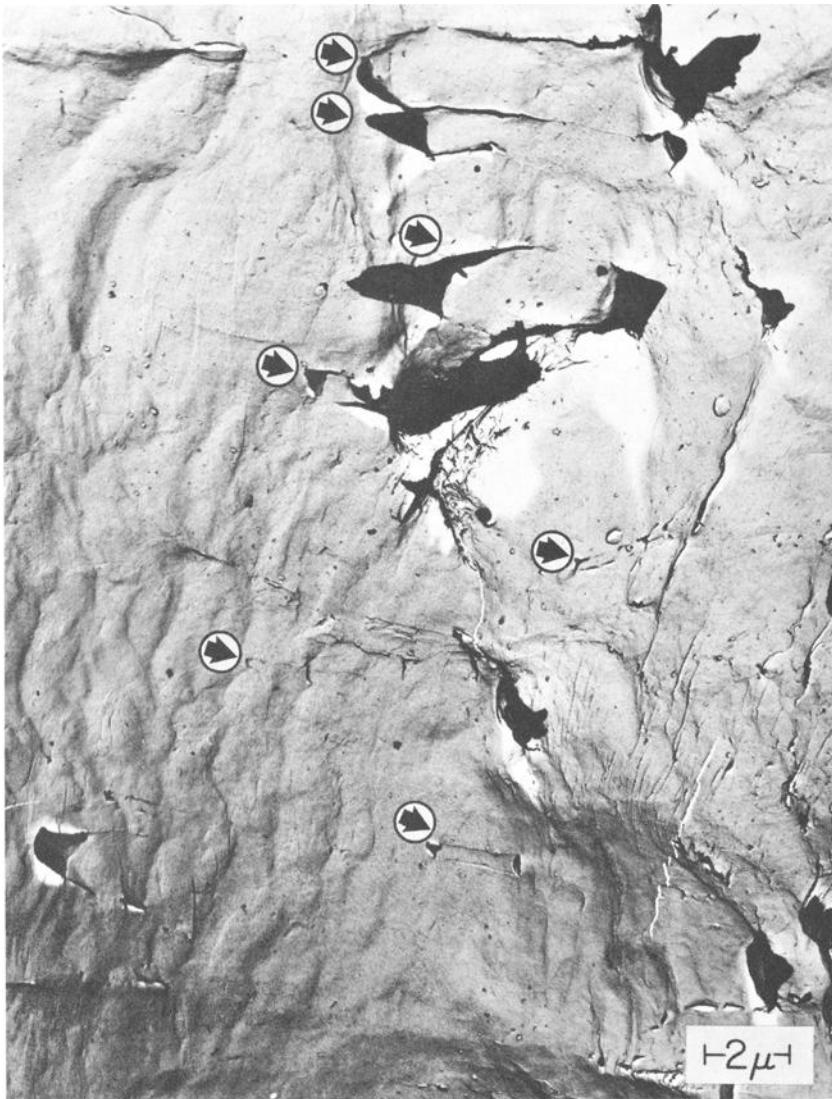


FIG. 10—Ripples (lower left quarter of fractograph), stretching, and oval tear dimples (arrows) in Armco iron. Two-stage palladium-shadowed carbon replica ( $\times 9000$ ).

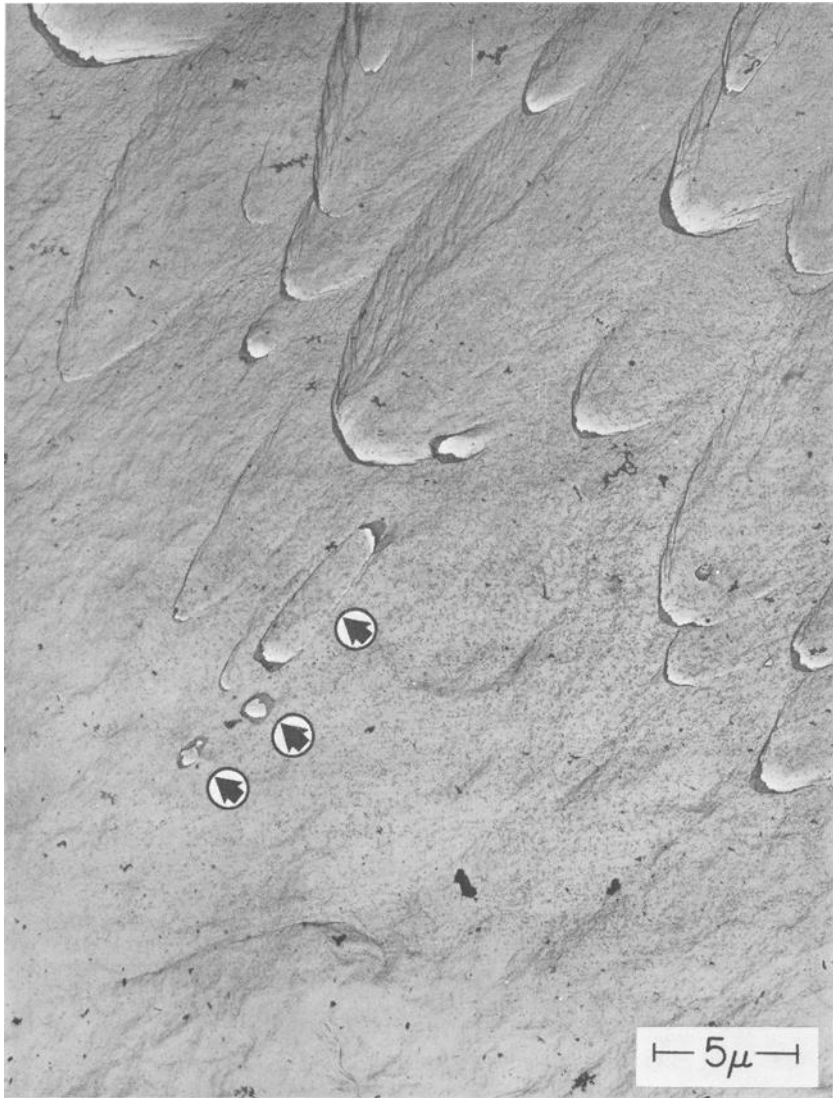


FIG. 11—Stretched regions, shear dimples, and oval tear dimples (arrows) in AISI 304 stainless steel. Palladium-shadowed direct-carbon replica ( $\times 6000$ ).



FIG. 12—Examples of serpentine glide in dimples in tough pitch copper. Specimen alligatored due to residual stresses from rolling. An equiaxed dimple is shown by the horizontal arrow. Tear dimples are shown between slanted arrows. Palladium-shadowed direct-carbon replica ( $\times 5000$ ).

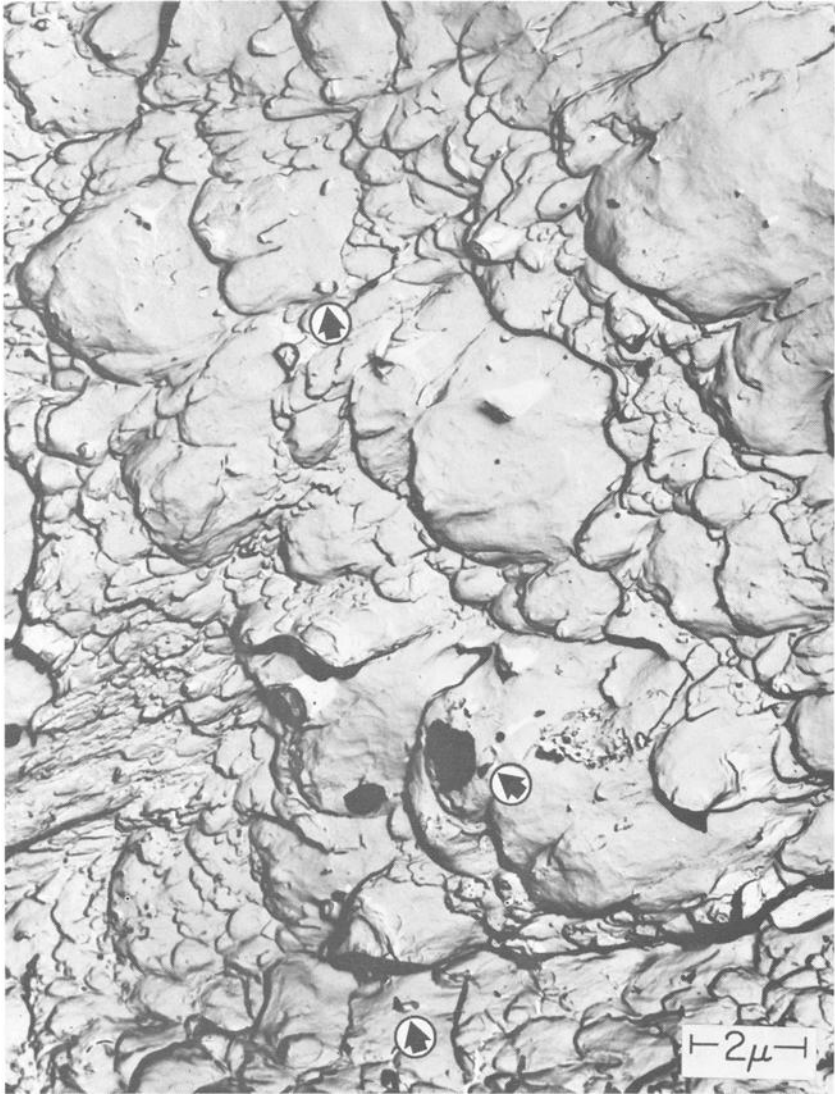


FIG. 13—Tear dimples formed during the early stages of internal fracture of a hardened and tempered AISI 4340 smooth tension test specimen broken in tension. Oval tear dimples are shown by arrows. Palladium-shadowed two-stage carbon replica ( $\times 12,000$ ).

The tear dimples shown in Fig. 13 were observed in a replica from the center of a cup-and-cone tensile failure surface in a 282,000 UTS AISI 4340 smooth bar specimen. The two halves of the specimen are shown in Fig. 14 while the fracture initiation region is shown in Fig. 15 at a high magnification. The fracture started at a small diameter (but deep) "pinhole" by radial tearing. Tearing proceeded about one tenth the specimen diameter before it changed to mixed tearing, shear rupture, and normal dimpled rupture.

Examples of surfaces formed by normal dimpled rupture are seen in Figs. 16 and 17. Normal dimpled rupture is a mode often operative in running "brittle fractures" of high-strength steels and aluminum alloys. This fracture mode is almost always accompanied by shearing or tearing in neighboring microscopic regions.

Examples of surfaces formed by shear rupture are seen in Figs. 18 to 20. Precisely matched shear dimples are shown in Figs. 19 and 20 with



FIG. 14—Macroscopic view of AISI 4340 cup-and-cone fracture surface from which the fractograph in Fig. 13 was made. Fracture initiation region may be seen just above the center of the fracture surface ( $\times 4$ ).

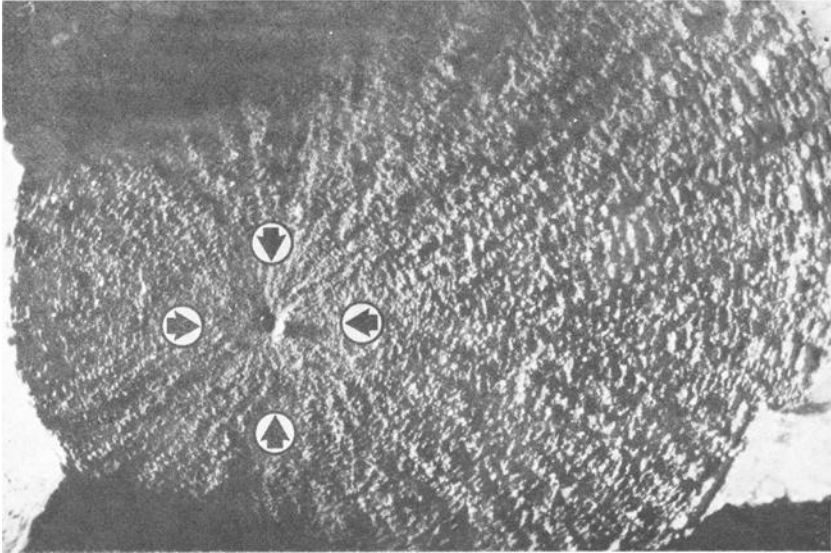


FIG. 15—Closer view of “pinhole” fracture initiation region. Tearing was found in the central region bounded by the arrows ( $\times 35$ ).

the matching dimples marked with arrows. In the shear dimple area of Figs. 19 and 20 there is an area of quasi-cleavage [5], and it may be noted that matching shear dimples adjacent to the quasi-cleavage are not of the same size or length. This effect extends for several microns up the shear lips. The sketch in Fig. 21 explains why the matching dimples are not of equal length. This effect has been observed also in AISI 4340 steel fracture toughness specimens, where the boundary between the flat fracture and the shear lips was well delineated. The effect is difficult to recognize in fracture faces of smooth tensile specimens and in fracture toughness specimens when the flat fracture is composed of dimples. Both test conditions give rise to large plastic flow, producing less sharply defined boundaries.

Tear dimples form frequently when voids coalesce with larger free surfaces. Low magnification photographs of a rubber-band model are shown in Fig. 22 for comparison with the oval tear dimples in Figs. 10, 11, and 13, and an explanatory sketch of the process is shown in Fig. 23. The model is shown only to indicate, in a simple manner, the stretching of this type dimple after the void has coalesced with the surface. Successive replicas from progressively stretched dimples at the bottom of notches in iron wire have confirmed this process in metal.

Another repeatedly observed feature of void coalescence and stretching is shown in Fig. 24. Sharp fatigue cracks are frequently used as stress raisers in crack propagation fracture toughness evaluations.



FIG. 16—Equiaxed dimples in the AMS 6434. Two-stage palladium-shadowed carbon replica ( $\times 6000$ ).



FIG. 17—Equiaxed dimples in a hardened-and-tempered low-alloy steel specimen. Palladium-shadowed two-stage carbon replica ( $\times 6000$ ).

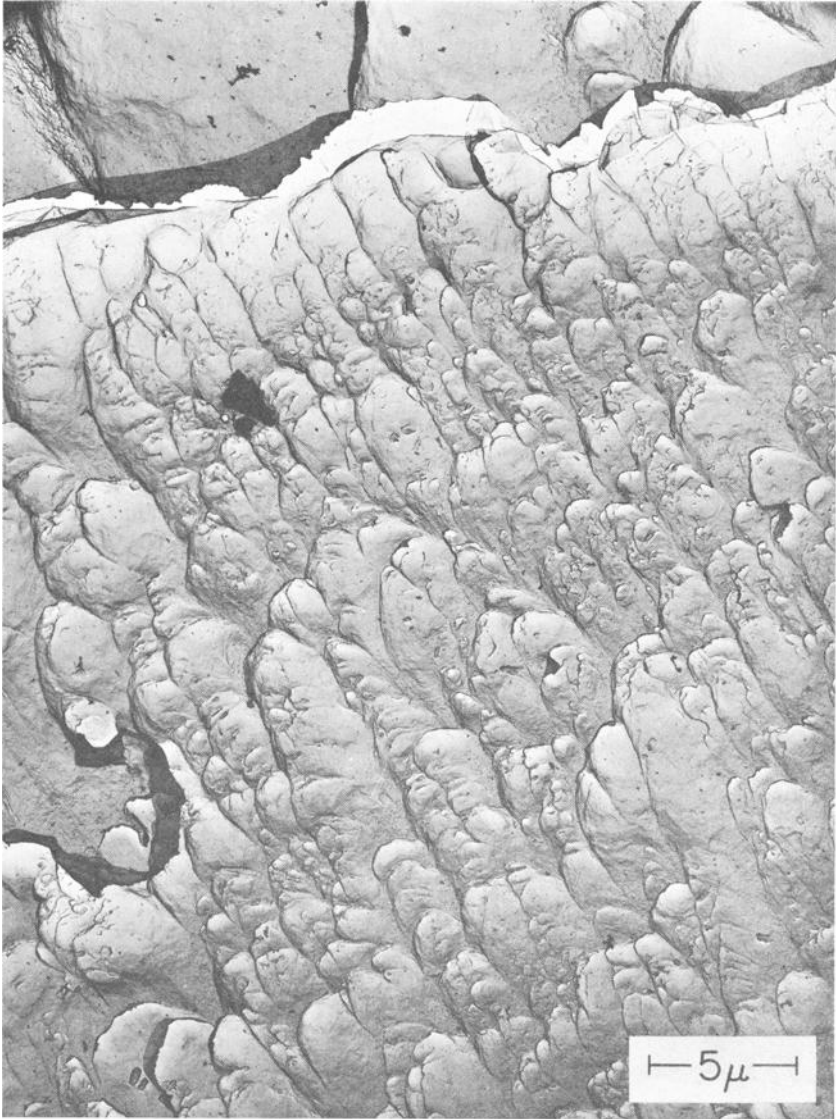


FIG. 18—*Shear rupture dimples in AISI 304 stainless steel "scab" formed by hypervelocity impact. Palladium-shadowed direct-carbon replica ( $\times 6000$ ).*

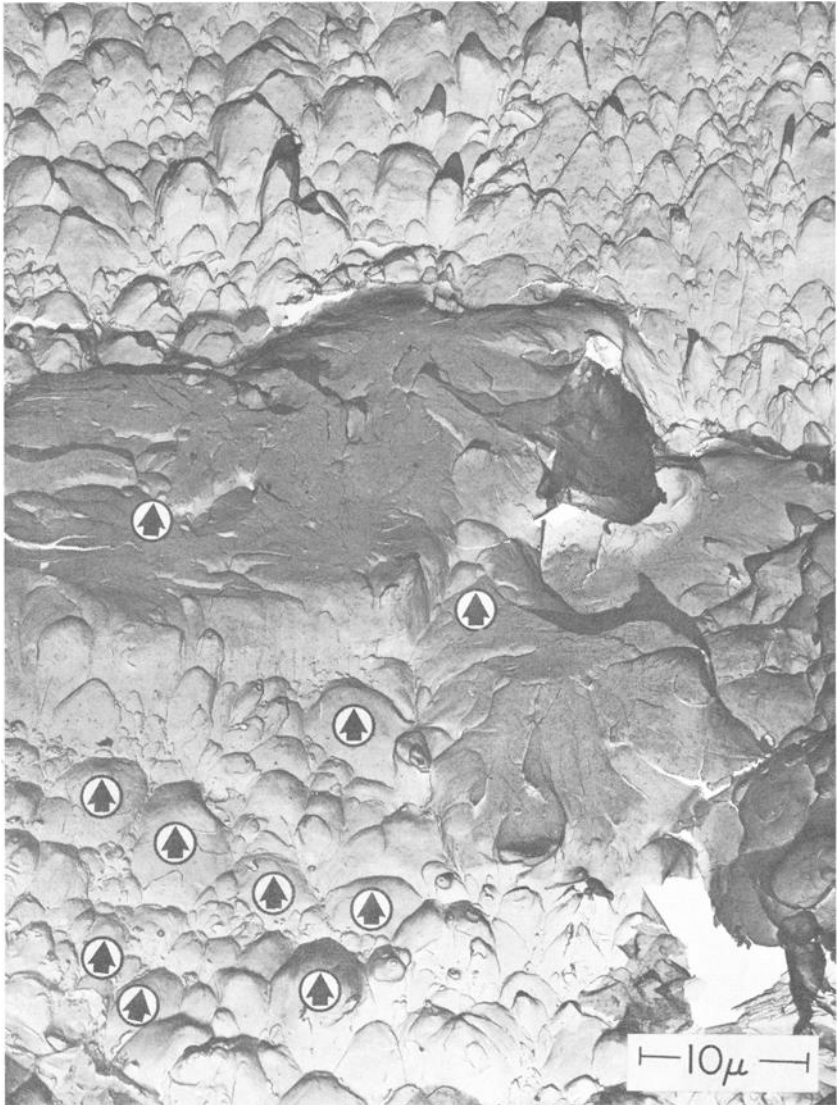


FIG. 19—Shear rupture dimples on two sides of a quasi-cleavage facet. The arrows indicate shear dimples that have mates in Fig. 20. Material is hardened-and-tempered 410 stainless steel. Palladium-shadowed two-stage carbon replica ( $\times 3500$ ).

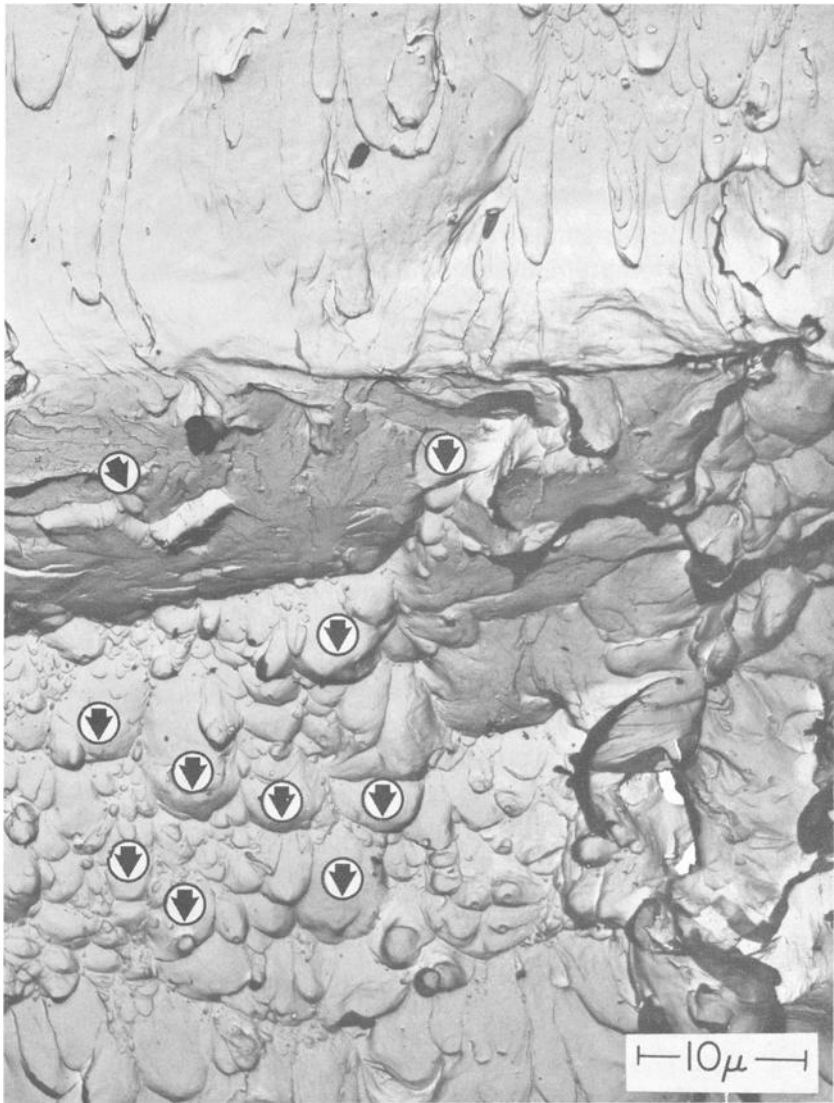


FIG. 20—Fracture surface which matches that shown in Fig. 19. Same replicating conditions ( $\times 3500$ ).

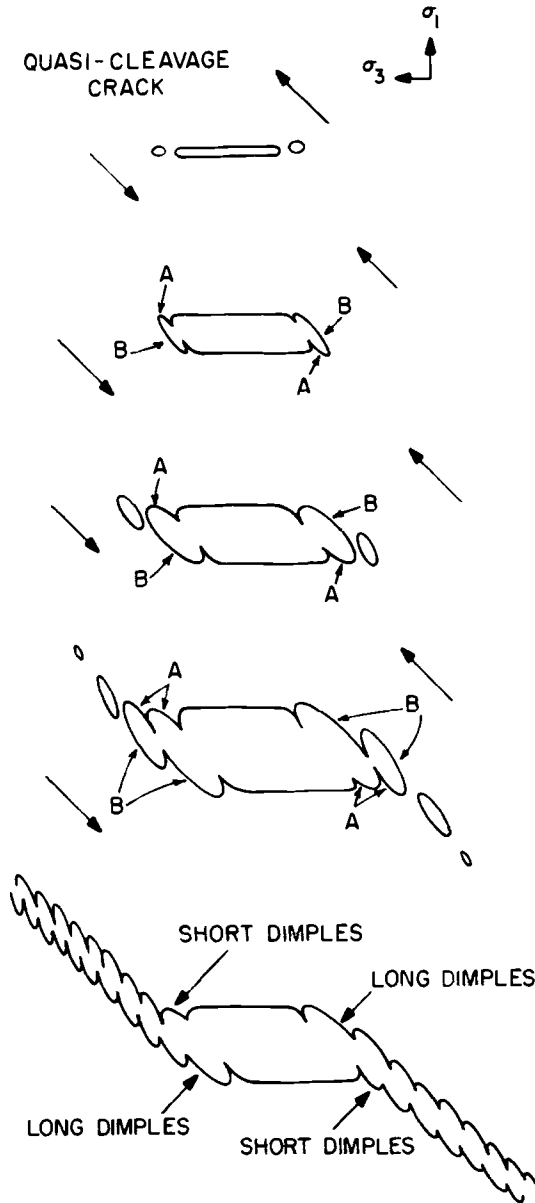


FIG. 21—A simplified model of the formation of the shear rupture dimples shown in Figs. 19 and 20. A slightly opened quasi-cleavage crack is shown at top, and successive stages of shear rupture are illustrated in the lower sketches. The macroscopic principal stresses are shown at the top. Arrows on either side of the crack indicate shear directions. Dimples are stretched more at points B than at points A, particularly after the voids have started to coalesce with the advancing shear rupture crack.

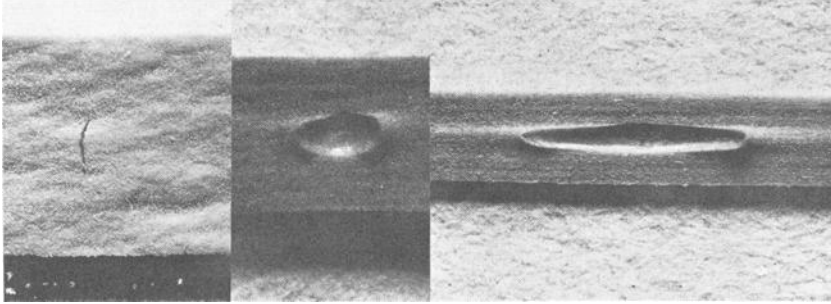


FIG. 22—A rubber model demonstrating how a tear dimple stretches into an oval shape after the void coalesces with another free surface. The model is a rubber band, sliced part-way through the thickness with a razor blade, and then stretched.

Invariably, if the specimen does not cleave, stretching will occur at the tip of the crack when it is opened up in testing, as indicated by Fig. 24. Initial failure by void coalescence cannot occur because (1) a third stress component at the free surface is lacking, or (2) the material at the tip of the crack is not sufficiently deformed to grow voids. After a finite amount of growth by stretching, the crack usually intersects increasing numbers of voids as it grows through increasingly strained material, and tear dimples are formed as in Fig. 24. As the crack grows further—through material contained in an increasingly larger plastic zone—patches of voids open up and coalesce ahead of the crack, and the fracture is seen to increasingly consist of random mixtures of tear dimples, shear dimples, and equiaxed dimples, as seen in Fig. 24.

As shown in Ref 6 the length of shear dimples depends upon the value of the ratio of normal (perpendicular to the shear plane) strain to shear strain in the material surrounding the voids during growth and coalescence of the voids. As the value of the ratio decreases, the

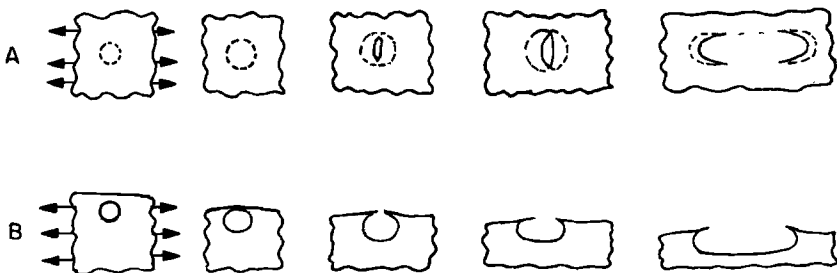


FIG. 23—Sketch of the coalescence of a void with a larger free surface. The arrows indicate the direction of principal strain. The fracture surface is seen in (A) and the corresponding cross sections of the void are seen in (B). Plastic deformation increases from left to right.

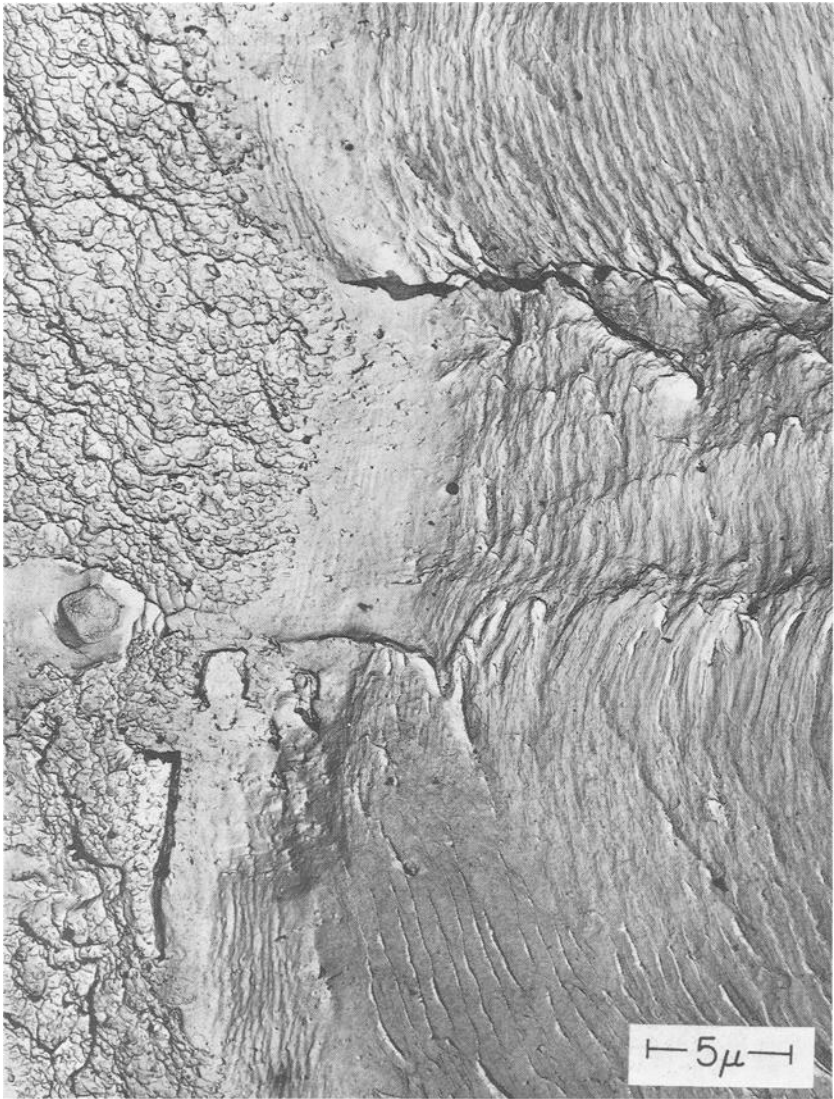


FIG. 24—Stretching, glide plane decohesion and tearing at the tip of a fatigue crack. The fatigue crack was introduced into this 7075-T6 aluminum alloy specimen as a stress raiser from the monotonic test which later produced the plastic rupture. Palladium-shadowed two-stage carbon replica ( $\times 6000$ ).

dimples are observed to become very long—five to ten times as long as they are wide (Fig. 25). Another effect of reducing the ratio of normal strain to shear strain is that when the specimen does shear apart at tiny local points, the two rupture surfaces may rub against one another as they separate. Where void coalescence markings end and burnishing markings begin has not yet been established, but both will consist mainly of long parallel lines; neither of the markings indicates glide



FIG. 25—Long shear rupture dimples in an OFHC copper torsion rupture surface. Two-stage palladium-shadowed carbon replica ( $\times 9000$ ).

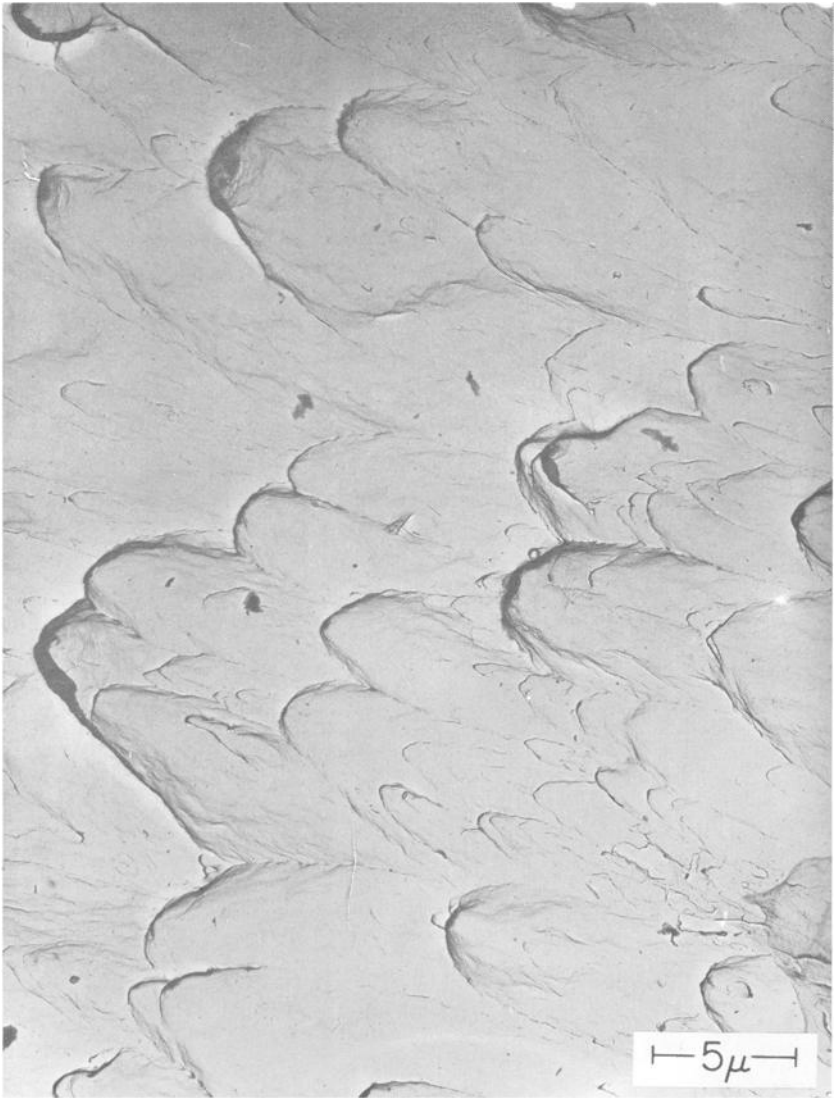


FIG. 26—Shear rupture dimples in 99.999 per cent copper. These dimples were formed by lightly rubbing two mechanically polished surfaces together, causing friction welding and subsequent rupture. Two-stage palladium-shadowed carbon replica ( $\times 6000$ ).

plane decohesion. To illustrate the complexity of distinguishing between initial rupture surfaces and burnishing markings, Fig. 26 shows rupture dimples where two mechanically polished pure copper surfaces were lightly rubbed together. These dimples were formed during rupture after local friction-welding occurred.

## Summary

Fine-scale plastic flow processes are seen to be basically the same regardless of the features produced. Early stages of plastic deformation in soft crystals produce stepped free surfaces by glide plane decohesion. If these steps form an interwoven pattern, the process is called serpentine glide. If the steps are further smoothed out, the surface features are called ripples. If the process is carried far enough, smooth featureless surfaces are formed. These featureless surfaces grow under further deformation by an unidentified mechanism (or mechanisms) called stretching.

Depending upon whether or not internal microvoids are opened, and upon their number, the stretched surfaces may or may not contain dimples, and the number of dimples will depend upon the number of microvoids intersected by the stretching surface. If a large number of closely spaced microvoids is present, the fracture may progress by the microvoid coalescence process, rather than by stretching. Three distinctly different types of microvoid coalescence mechanisms have been observed—normal dimpled rupture, shear rupture, and tearing. Tearing dimples are found usually at the beginnings of fracture where fracture initiates at a sharp crack or internal flaw. A macroscopically flat “brittle” fracture surface may contain scattered patches of the three different types of fracture.

The mechanisms of stretching operate on a scale usually much smaller than the dimple size, and no difference is suspected between the mechanisms underlying the growth of dimples and stretched surfaces.

## Acknowledgments

The authors extend their thanks to B. F. Brown and E. P. Dahlberg of the Naval Research Laboratory and to several members of ASTM Subcommittee II of Committee E-24 for their interest, help, and constructive criticism during the preparation of this paper.

## References

- [1] Rogers, H. C., “Tensile Fracture of Ductile Metals,” *Transactions, American Institute of Mining, Metallurgical, and Petroleum Engineers*, Vol. 218, July 1960, p. 498.
- [2] Barrett, C. S., *Structure of Metals*, McGraw-Hill, New York, 1952, p. 340.
- [3] Crussard, C. et al, “A Comparison Between Ductile and Fatigue Fractures,” *Swampscott Conference on Fracture*, Wiley, New York, 1959, pp. 19–21.
- [4] Cottrell, A. H., *Dislocations and Plastic Flow in Crystals*, Oxford University Press, London, 1953, p. 4.
- [5] Beachem, C. D., “Electron Fractographic Studies of Mechanical Fracture Processes in Metals,” *Transactions, American Society of Mechanical Engineers, Journal of Basic Engineering*, Vol. 87, Series D, No. 2, June 1965, p. 299.
- [6] Beachem, C. D., “An Electron Fractographic Study of the Influence of Plastic Strain Conditions Upon Ductile Rupture Processes in Metals,” *Transactions, American Society for Metals*, Vol. 56, No. 3, Sept. 1963, pp. 318–326.

## Application of Electron Fractography to Fatigue Studies

---

**REFERENCE:** McMillan, J. C. and Hertzberg, R. W., "Application of Electron Fractography to Fatigue Studies," *Electron Fractography, ASTM STP 436*, American Society for Testing and Materials, 1968, pp. 89-123.

**ABSTRACT:** A review of the application of fractography to fatigue studies is presented that covers fatigue fracture appearance, the occurrence of striations, and qualitative and quantitative aspects of the fracture surface micro-details. Recent experimental results in three areas are also discussed: (1) the effect of prior loading history on subsequent crack propagation, (2) the smallest observable crack growth increments, and (3) the effect of environment on fatigue crack growth.

**KEY WORDS:** electron microscopy, fractography, fatigue (materials), aluminum alloys, corrosion fatigue, fracture mechanics

Fatigue crack extension occurs in either three or four stages, depending on the applied stress conditions, specimen geometry, and the mechanical properties of the material. Stage one, the initiation stage, usually extends only over a small percentage of the fracture surface. If no nucleation site is readily available, reverse slip of dislocations on a slip plane subjected to a high resolved shear stress will lead to crack formation on a slip plane at an angle to the applied stress direction. After a relatively short distance, this crack will shift into a position leading to the plane strain (stage two) and plane stress (stage three) propagation stages. With a low relative stress level, the initiation stage may represent a significant portion of the total fatigue life of the component, but the total percentage of the fracture surface in stage one will usually be much smaller. In most engineering structures and components there are a sufficient number of nucleation sites to cause a fatigue-nucleated crack to enter the propagation stages after relatively few loading cycles. At the other extreme, stage four represents final fracture in the last quarter cycle. Since this stage is beyond the scope

<sup>1</sup> Research engineer, Commercial Airplane Div., The Boeing Co., Renton, Wash.

<sup>2</sup> Assistant professor, Department of Metallurgy and Materials Science, Lehigh University, Bethlehem, Pa.

of interest of this paper, attention will be focused on stages two and three, the propagation stages. Therefore, succeeding remarks will draw attention to the surface characteristics of the propagation stages in fatigue.

### *Macroscopic Fracture Surface Appearance*

A macroscopic examination of service and laboratory failures by fatigue loading reveals distinct fracture surface characteristics. The fracture surface is generally flat, indicating the absence of any appreciable amount of gross plastic deformation in the overall component. The surface can be either normal or inclined at 45 deg to the applied stress direction; the latter condition is more prevalent in thin plates and sheet material. The gross orientation of the fracture surface depends on the specimen geometry, material properties, and the stress conditions during the crack propagation sequence. This is readily seen by consideration of the concepts of fracture mechanics [1-3].<sup>3</sup> When the stress-intensity factor, a measure of the stress amplification at the crack tip of the advancing crack front, is small, the resulting plastic zone at the crack tip is also small. When the thickness of a component or test panel is large compared with the size of the crack-tip plastic zone, the fracture will propagate on a plane normal to the stress direction under plane strain conditions. When the size of the plastic zone becomes large compared with sheet thickness before the incidence of stage four (final fracture), the fracture surface will shift to a plane at 45 deg to the sheet thickness and stress direction, and stage three propagation will occur, reflecting plane stress conditions. When the initial size of the plastic zone is very large compared with sheet thickness, stage three propagation will begin immediately and preclude stage two growth.

In the case of service failures occurring over long periods of time, the fracture surface contains lines referred to in the literature as "clam shell" markings, arrest lines, and "beach markings." These markings have been attributed to periods of crack extension followed by crack arrest. During the arrest periods, the fracture surface is presumed to be oxidized or corroded; consequently, the alternate periods of crack growth and arrest result in the formation of a fracture surface containing concentric rings of varying colors, thereby indicating the intermittent nature of the fatigue cracking process. In a recent review article, Jacoby [4] cited examples of clam shell markings and associated color changes on the fracture surfaces of specimens subjected to programmed loading. The explanation for these markings is not clear at the moment, but it does indicate that the arrest markings generally reveal perturbations in the loading pattern during the

<sup>3</sup>The italic numbers in brackets refer to the list of references appended to this paper.

life of the component. By contrast, when simple sinusoidal loading patterns are imposed on laboratory specimens, no evidence of such markings is found.

#### *Microscopic Fracture Surface Appearance*

A detailed examination of the clam shell markings on service fractures and the fracture surfaces of laboratory specimens subjected to simple loading patterns has revealed that they are composed of many smaller parallel lines referred to as fatigue striations (Fig. 1). (In all



FIG. 1—*Optical fractograph of fatigue striations in an aluminum alloy.*

the photographs the large arrow indicates the general direction of crack propagation.) Observation of this fine structure, often orders of magnitude smaller than the clam shell markings, has prompted extensive examination of fatigue specimens by several fractographic techniques.

Zappfe and Worden were the first to report patches of parallel markings on the fractured surfaces of fatigue specimens [5]. During the early 1960's, work continued to establish more clearly the details of these striations and to determine the extent to which they were found in many classes of engineering materials. It was during this period that the techniques of electron fractography were perfected and employed in this investigation. Under Forsyth and Ryder [6-9] and Crussard and co-workers [10,11] much progress was made. It was found that fatigue striations appeared on the fracture surfaces of face-centered-cubic, body-centered-cubic and hexagonally-closely-packed metals and even in amorphous polymer materials [12]. Of extreme importance was the determination of a possible correlation between the number of fatigue striations found on the fracture surface and the number of loading cycles. It was not until Forsyth and Ryder [6] performed their critical experiment that this point was clarified. They proved that each load excursion was responsible for one striation and that the size (that is, distance between markings) depended strongly on the stress amplitude. Thus, it is appropriate to emphasize that there is a clear distinction between the macroscopically observed clam shell markings, which represent periods of growth during which thousands of loading cycles may have occurred, and the striations, which represent the extension of the crack front during one load excursion. There may be thousands or even tens of thousands of striations within a single clam shell marking.

#### *Qualitative Aspects of Fracture Surface Microdetails*

As discussed earlier, the propagation of a fatigue crack can occur either as stage two plane strain propagation or as stage three plane stress propagation. An examination of the fracture surfaces resulting from these two modes reveals that the two fracture processes are somewhat different. In the plane strain region, the fracture surface contains many areas of fatigue striations. In some of these the striations are well defined, while in others they are only roughly outlined. Two general observations about fracture surfaces in the plane strain region in metals are that adjacent packets of striations are often at large angles to each other (Fig. 2) and that there are regions where no striations are observed. The significance and interpretation of these observations will be discussed later. In the plane stress region, the fracture surface contains areas of elongated dimples resulting from the resolved shear

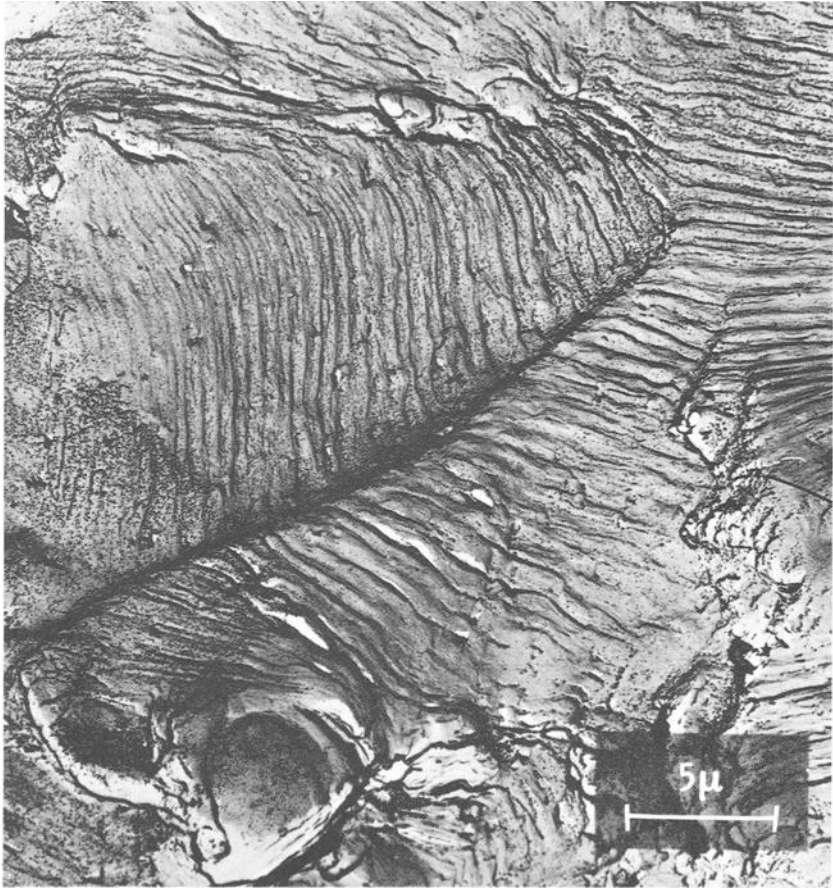
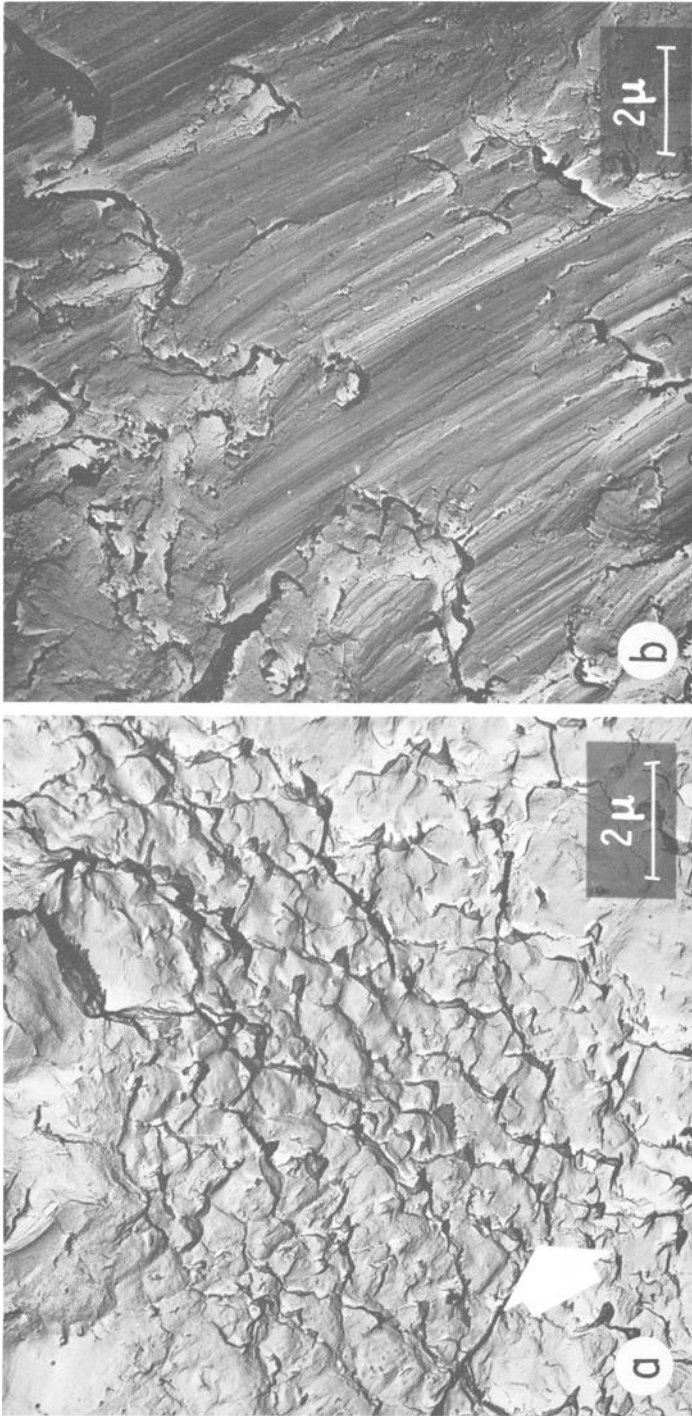


FIG. 2—Large angle between adjacent packets of fatigue striations in an aluminum alloy.

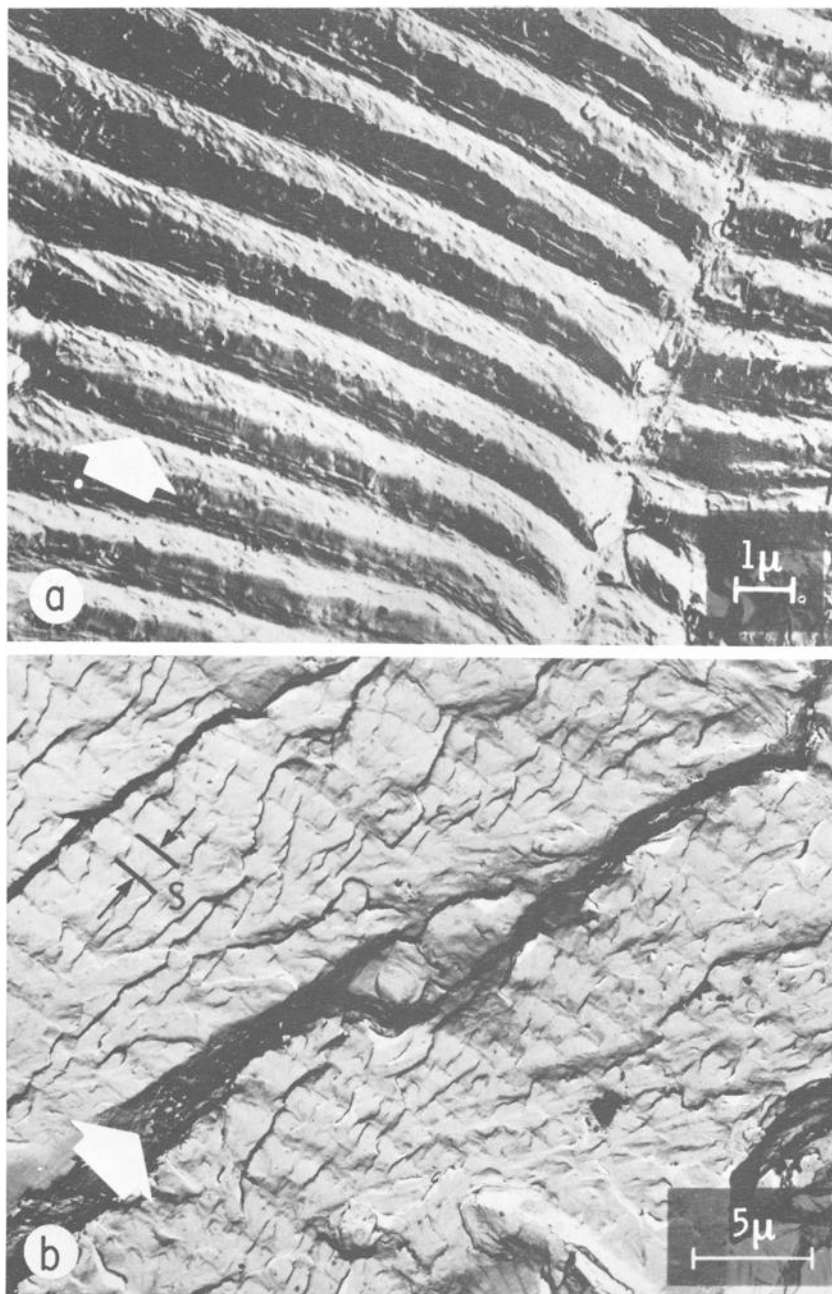
stresses on the 45-deg fracture planes, far fewer indications of fatigue striations, and abraded or rubbed areas that obliterate many of the details of the fracture surface (Fig. 3).

#### *Striation Morphology*

Fatigue striations can take many forms. They may be clearly or poorly delineated, as described earlier, and may take on many shapes. Forsyth, for example, has made a distinction between ductile and brittle striations [8,9]. Examples are shown in Fig. 4. It is not absolutely clear why these morphologies are different, but they are often associated with the test environment during crack propagation. Fatigue striations tend to be much flatter and take on a brittle appearance when formed in an aggressive environment, but tend to be generally more



(a) Elongated dimple formation.  
(b) Rubbing marks.  
FIG. 3—Fractographs of plane stress fatigue fracture surface of 2024-T3 aluminum alloy.



(a) Ductile fatigue striations.  
(b) Brittle fatigue striations.

FIG. 4—Electron fractographs of fatigue striations in an aluminum alloy.

ductile when formed in an inert environment. The effects of environments and alloy composition on fatigue crack propagation rates and striation morphology will be discussed in a later section. While striation formation may be affected by environment, drastic changes have been observed in the appearance of fatigue striations after exposure to oxidizing or corroding atmospheres. Thompson and Mulhearn [13] observed that fatigue striations were completely obliterated as a result of exposure to a high-temperature, oxidizing environment. Striations have also been noted to be both continuous and noncontinuous, clearly and poorly defined, and straight and smoothly curved in different materials.

From metallographic sections and electron fractographic examination, three basic interpretations of the morphology of fatigue striations have evolved. The striations are considered to be undulations on the fracture surface with (1) peak-to-peak and valley-to-valley matching of the two mating surfaces, (2) matching crevices separating flat facets, or (3) peak-to-valley matching. Based on these interpretations of striation morphology, different mechanisms have been proposed for striation formation. These mechanisms have recently been reviewed [14], so a detailed discussion will not be given at this time. One aspect of the models will be reviewed, however. The earlier models, proposed by Forsyth and Ryder [7] and Laird and Smith [15], did not relate striation formation with crystallographic considerations, but this was proposed by Stubbington [16], Jacoby [4], and Hertzberg [17]. More recently, Laird [14] considered some of the details of the deformation process at the crack tip and the role of crystallographic effects on striation morphology. He argued that striation morphology would be more symmetrical if the individual grains were favorably oriented with respect to the stress pattern at the tip of the crack. This evaluation reflects agreement with Stubbington, Jacoby, and Hertzberg as to the importance of crystallographic considerations, although not with their proposed mechanisms for striation formation.

The effect of crystallography on striation formation can be supported by much circumstantial evidence. For example, if the slip planes are favorably oriented with respect to the stress pattern at the advancing crack front, then a clearly defined striation could be formed. A similar argument relating to slip plane orientation could explain the formation of poorly defined striations or none at all. Large angle differences found between adjacent packets of striations could be explained in terms of the misorientation of adjacent grains, or the crystallographic orientation change associated with a twin boundary. McEvily and Boettner [18] have explained the difference in the curvature of striations observed in several alloys in terms of the stacking-fault energy of the material, a crystal structure property: striations become straighter

and the crack growth rate decreases with decreasing stacking-fault energy [18,19].

It has been argued that it is not correct to base striation formation mechanisms on crystallographic considerations, since striations are clearly observed in amorphous polymer materials [12]. There is no inconsistency in this approach, however. A striation will form as a result of the stress pattern at the crack tip. Because a polymer material is amorphous, there is no restriction on the manner in which the polymer may deform. Thus, it will deform in accordance with the prevailing stress pattern. In metals, where there are a restricted number of possible slip planes and directions, a striation will be formed when the slip systems are favorably oriented with respect to the stress pattern at the crack tip. If the slip systems are not favorably oriented, a poorly defined striation or no striation will result. The observation of striation-free regions on the fatigue fracture surfaces of metals and of 100 per cent striation formation on polymer fatigue fracture surfaces supports the aforementioned argument.

#### *Quantitative Aspects of Fracture Surface Microdetails*

More quantitative information has been obtained from the measurement of fatigue striations than from any other fracture surface detail. Since the striation represents the position of the crack front at the end of every loading cycle, it can be used to measure the fatigue crack propagation rate at a given position along the fracture surface. The usefulness of this observation depends on the correlation of the growth rate measurements with some quantity or quantities that reflect the prevailing stress conditions at the tip of the advancing crack front. Pelloux [20], Schijve [3], and Hoepfner et al [21] have found that striation spacing increases with increasing crack length under constant-load range conditions. As mentioned earlier, the experiment by Forsyth and Ryder [6] showed that striation spacing was a function of the load amplitude. Since the stress-intensity factor reflects both stress level and crack length in the description of the stress conditions at the crack tip, it was logical to determine whether this factor could more completely correlate striation spacings. Paris and Erdogan [22,23] clearly showed that the macroscopically measured crack propagation rates were strongly related to the stress-intensity factor range at the crack tip. Extending this approach to fractographic observations, Hertzberg and Paris [2], Carmen and Shuler [24] and McMillan [25] showed that as the stress-intensity factor increased, the spacing of the fatigue striations also increased. Furthermore, there was a general correlation between the macroscopically determined growth rate as measured with a traveling microscope and the microscopic growth rate as measured by the striation spacings. More recently, McMillan and

Pelloux [26] have demonstrated that striation spacing is affected by both maximum and range values of the stress-intensity factor.

In an attempt to determine the rate of crack propagation by measuring elongated dimple widths during stage three propagation, Hertzberg [15] found that the width of the dimples was a constant value even though the stress-intensity factor increased. Since the macroscopic growth rate increased by over two orders of magnitude while the dimple width remained constant, it was assumed that microscopic growth was produced by an increasing number of dimples being formed during each loading cycle.

Though the stress-intensity factor has been proved to affect crack growth rates, there are many factors that also must be considered, for example, the roles of mean and maximum stress level, cyclic frequency, and test environment on crack propagation rates. Once these roles are fully understood, it will become possible to determine by postfracture analysis the stress conditions in a fatigue-fractured component by measurement of the fatigue striations.

#### *Effect of Loading History*

It has been known for some time that load history can affect subsequent fatigue behavior. With respect to crack propagation studies, Hudson and Hardrath [27] and Schijve [28] have observed that the macroscopic crack growth rate appears to decrease with the imposition of peak loads in the loading sequence. This retardation of crack velocity has been associated with a favorable residual stress pattern at the crack tip. However, it has been reported by Jacoby [4], Hertzberg [17], and McMillan and Pelloux [26] that striations formed immediately after the peak loads were larger than those formed prior to the peak loads, even though the applied stress-intensity conditions were the same (Fig. 5). This behavior tended to decrease with increasing distance from the crack position where the peak loads were applied [15]. It is thought that this behavior might be related to strain hardening or to some kind of conditioning of the material ahead of the crack front. The observed macroscopic crack arrest and microscopic crack acceleration is significant and shall be considered in a later section in the light of new experimental observations.

#### **Recent Experimental Observations**

In this section, quantitative and qualitative electron fractography results from three recent fatigue crack propagation studies are discussed: (1) the effect of prior loading history on subsequent crack propagation, (2) the smallest observable growth increments, and (3) the effect of environment on fatigue crack growth.

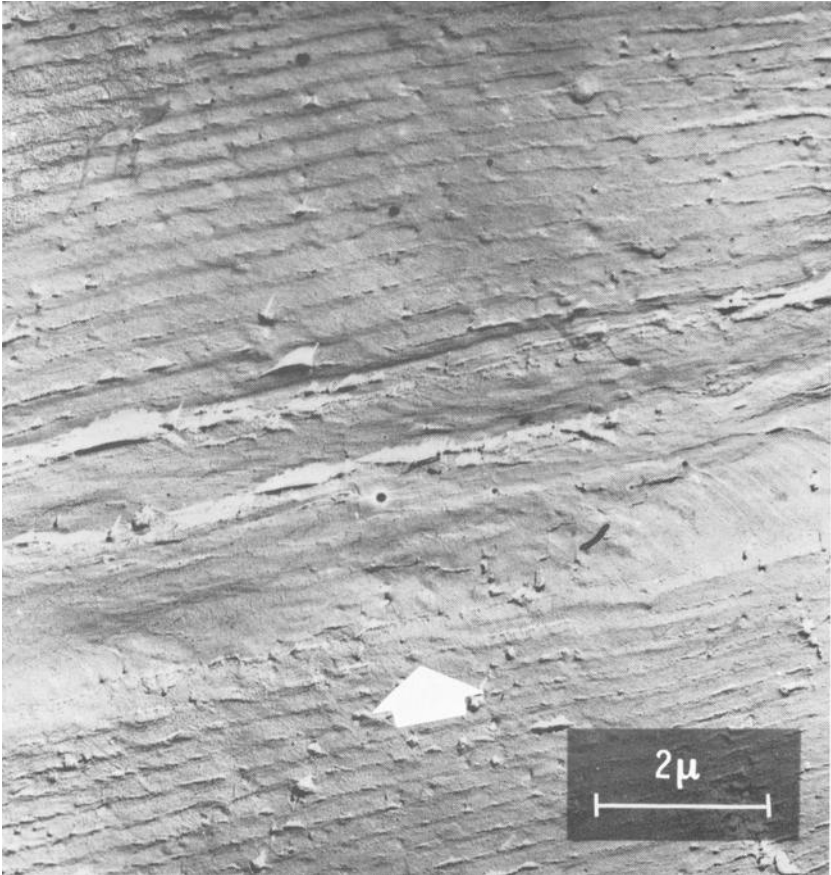


FIG. 5—Fractograph of 7075-T6 aluminum alloy revealing increased striation spacing after peak load cycles.

#### *Effect of Prior Loads on Subsequent Crack Propagation*

These experiments were designed to investigate the effect on subsequent crack growth rates of superimposing periodic peak loads on uniform cyclic loads. The peak loads are termed positive when the superimposed load is greater than the maximum load of the uniform cyclic loads and negative when the superimposed load is less than the minimum load of the uniform cyclic loads. Schijve et al [29] previously examined similar load histories and observed that the introduction of a positive peak load can have a very favorable influence on the fatigue life because crack extension following the peak load is arrested or severely retarded. The retardation was attributed to the development of compressive residual stresses in the plastic zone ahead of

the crack that resulted from the peak tensile load. If the positive peak load was followed by a negative peak, the retardation, while still apparent, was significantly reduced. In that instance, the effect of the negative peak presumably was to remove part of the residual compressive stress field.

Hardrath [30], in a related series of tests, showed that under uniform cyclic loading a change in maximum stress from  $\sigma_1$  to  $\sigma_2$  resulted in acceleration of crack growth when  $\sigma_1 < \sigma_2$ , and arrest or retardation when  $\sigma_1 > \sigma_2$ . Hardrath also suggested that compressive residual stresses near the crack tip accounted for this behavior. Rice [31] considered several models and argued that blunting of the crack tip by large deformations was a more plausible explanation for the retardation of growth.

We felt that electron fractography could provide additional information concerning crack arrest or retardation, and specimens from two test programs with peak loads were examined. In the first set of tests, a positive and a negative peak were introduced after every 200 uniform load cycles. In one loading program, designated P 14, the negative peak preceded the positive peak and in the other, designated P 15, the order was reversed. The loading sequences are shown in Fig. 6. (Programs P 1 through P 12 were discussed in a previous paper [26].) The test specimens were 9 by 24 by 0.160-in. center-notched aluminum 2024-T3 fracture panels with an initial crack length ( $2a$ ) of approximately  $3/4$  in. The mechanical properties of the materials tested with these program loads are listed in Table 1. The program loads were introduced by punched tape digital programming, and crack lengths versus crack growth rates are shown in Fig. 7.

The macroscopically observed growth rate was faster when the neg-

TABLE 1—Mechanical properties of materials in test programs  
(transverse grain direction).

Test Program	Material	$F_{tu}$ , psi	$F_{ty}$ , psi	Elongation, Reduction	
				%	of Area, %
P 14 and P 15.....	2024-T3	70 100	45 600	20	27
(peak loads).....	2024-T3	70 400	45 700	20	...
Environmental tests.....	2024-T3	71 200	49 400	21	28
	2024-T6	70 000	60 600	10	26
	7075-T6	88 000	81 000	14	22
	7178-T6	90 200	85 300	12	22
(from Ref 40) .....	7000 series 0Cu	55 200	48 000	14.2	...
	7000 series 0.9Cu	58 400	46 600	16.5	...

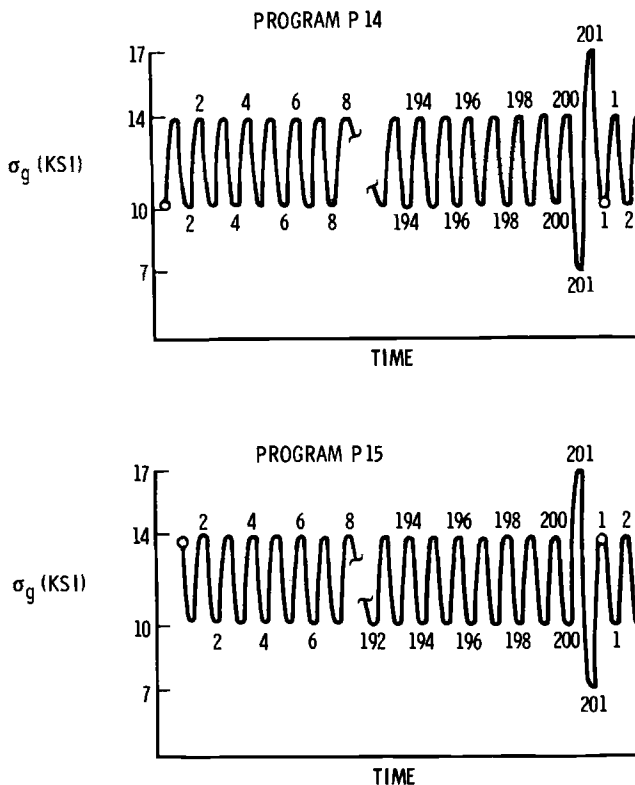


FIG. 6—Oscillograph recordings for the applied loads of programs P 14 and P 15.

ative peak followed the positive peak (program P 15). On the premise that crack extension occurs only on the load rise portion of the load cycle, we expected that one larger-than-normal growth increment, corresponding to the half cycle 201-201, would be associated with the peak load in program P 14, while two larger growth increments, corresponding to the half cycles 200-201 and 201-1, would be observed in program P 15. Characteristic electron fractographs of the fracture topographies resulting from these two programs are shown in Figs. 8 and 9. As expected, program P 14 shows one large growth increment, designated *A* in Fig. 8, while program P 15 shows two large growth increments, designated *B* and *C* in Fig. 9. The magnitude of the stress rise ( $\Delta K$ ) is the same for 200-201 and 201-1 in program P 15. The growth increment is not only controlled by the magnitude of the load excursions, but is also affected by the mean stress, as evidenced by the difference in striation size of *B* and *C* in program P 15. The uniform load cycles in each program caused growth, since it was possible to count 201 separate growth increments for each program.

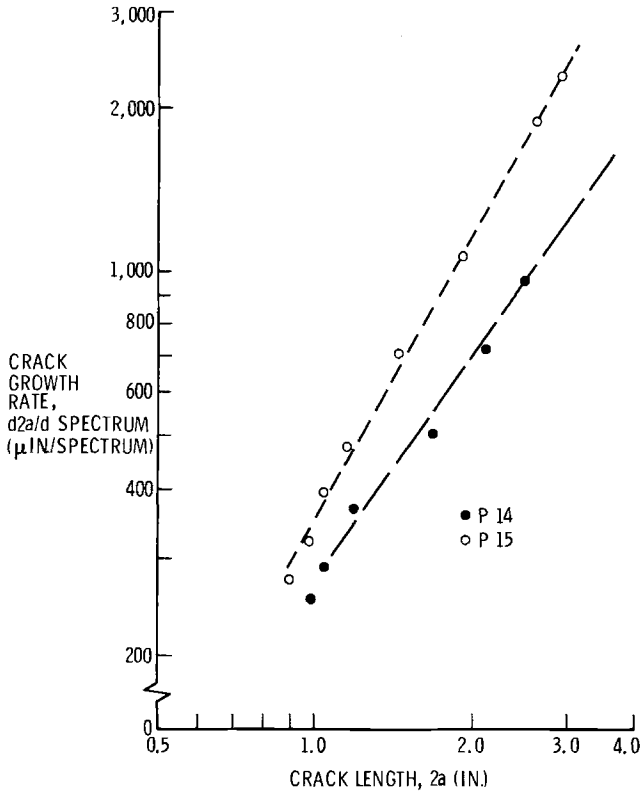


FIG. 7—Crack growth rates for programs P 14 and P 15.

The two fractographs (Figs. 8 and 9) are of the same magnification and were obtained at the same crack lengths. The growth increments associated with the peaks are approximately the same size; that is, increment  $A$  is approximately equal to  $B$  plus  $C$ , and cannot account for the observed difference in macroscopic growth rates. The major portion of the growth rate difference is due to the difference in propagation rate resulting from the uniform load cycles. This difference does not appear to be related to crack-tip blunting, since the growth increments due to the uniform load cycles for both programs are larger immediately following the peaks than they are immediately preceding the peaks. This suggests that programs P 14 and P 15 introduce different amounts of plastic damage or different states of residual compressive stress in the material so as to alter crack growth rate. A complete analysis of these observations is presently impossible, since the peak load plastic zones overlap, and the effects of this interaction are not understood.

In the second set of tests to determine the effect of prior load history, 9 by 24 by 0.160-in. center-notched aluminum 2024-T3 fracture



FIG. 8—Fracture topography resulting from application of program P 14.



FIG. 9—Fracture topography resulting from application of program P 15.

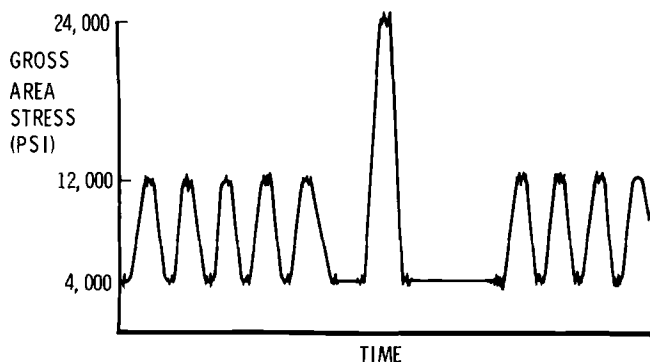


FIG. 10—Oscillograph recording of load-time history for application of a single peak load.

panels with an initial crack length ( $2a$ ) of approximately  $\frac{1}{2}$  in. were subjected to a sinusoidal loading pattern with positive peak loads introduced at specific crack lengths. A fixed-range load controller was used to introduce the uniform loads, while the peak overload was introduced by changing the load limits for one cycle. An oscillograph recording is shown in Fig. 10. The time delays before and after the peak were necessary for setting and resetting load limits. Only three peaks per specimen were introduced at crack lengths ( $2a$ ) of approximately 0.6, 1.2, and 2.4 in. to ensure that no interaction occurred between the plastic zones for each peak. Estimates of the plane stress plastic zone size based on Irwin's analysis [32] are tabulated in Table 2.

TABLE 2—Estimates of plastic zone size.

$2a$	$\sigma_o$ (max), ksi	$\sigma_o$ (min), ksi	$K,^a$ ksi $\sqrt{\text{in.}}$	Plane Stress, $2r_y,^b$ (in.)
0.6.....	12	4	11.6	0.02
0.6.....	18	4	17.4	0.046
0.6.....	24	4	23.2	0.08
1.2.....	12	4	16.4	0.04
1.2.....	18	4	24.6	0.09
1.2.....	24	4	32.7	0.16
2.4.....	12	4	23.3	0.08
2.4.....	18	4	35.0	0.18
2.4.....	24	4	46.6	0.32

<sup>a</sup>  $K = \sigma_o$  (max)  $\sqrt{\pi a}$ .

<sup>b</sup>  $2r_y = \frac{1}{\pi} \left( \frac{K}{\sigma_{ys}} \right)^2$  plane stress.

The crack length versus cycles data are shown in Fig. 11. The data are from the baseline case (maximum gross area stress of 12 ksi but with no peak loads) and from tests where peak loads of 18 and 24 ksi were introduced. Very pronounced crack retardation occurred with the 24-ksi peaks. It was not possible to tell by macroscopic measurement whether complete arrest had occurred (particularly over the whole crack front) or whether growth from the 12-ksi uniform loadings was still occurring, but at a much slower rate. At the end of each retardation period, crack growth again progressed at about the same rate as in the baseline specimen. With the 18-ksi peak loads, the retardation effects were substantially reduced.

The magnitude of the retardation depended on the magnitude of the peak loads. When the peak loads were  $1\frac{1}{2}$  times the uniform maximum cyclic load, each retardation period was less than 10 per cent of the baseline life. However, when the peak loads were twice the uniform maximum cyclic load, each retardation period was equivalent to the total life of the baseline case.

These specimens were examined fractographically in the region of the peak load application to assess the magnitude and type of crack growth associated with the maximum load and its effect on subsequent growth at lower loads. In Fig. 12, the effect of the 18-ksi peak load at  $2a = 1.2$  in. is shown. The characteristic striation spacing 0.003 in. before the peak application is shown in Fig. 12a, and the extent of the growth due to the 18-ksi peak, designated  $P$ , is shown in Fig. 12b.

There is little or no difference in striation spacings before and immediately after the peak load application. However, as the crack propagates away from the peak, the striation spacings become progressively

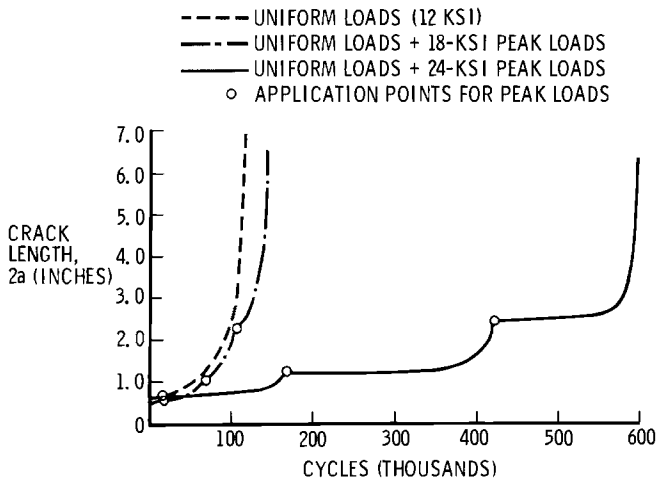
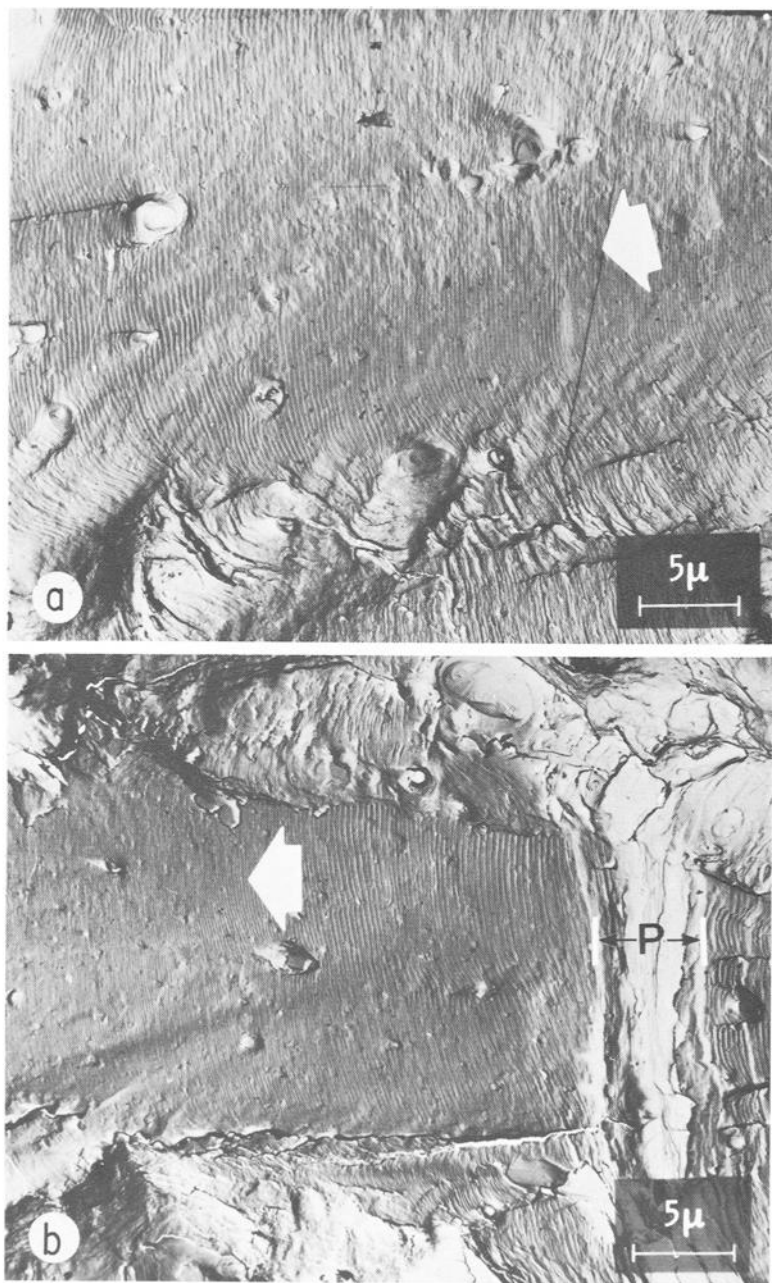
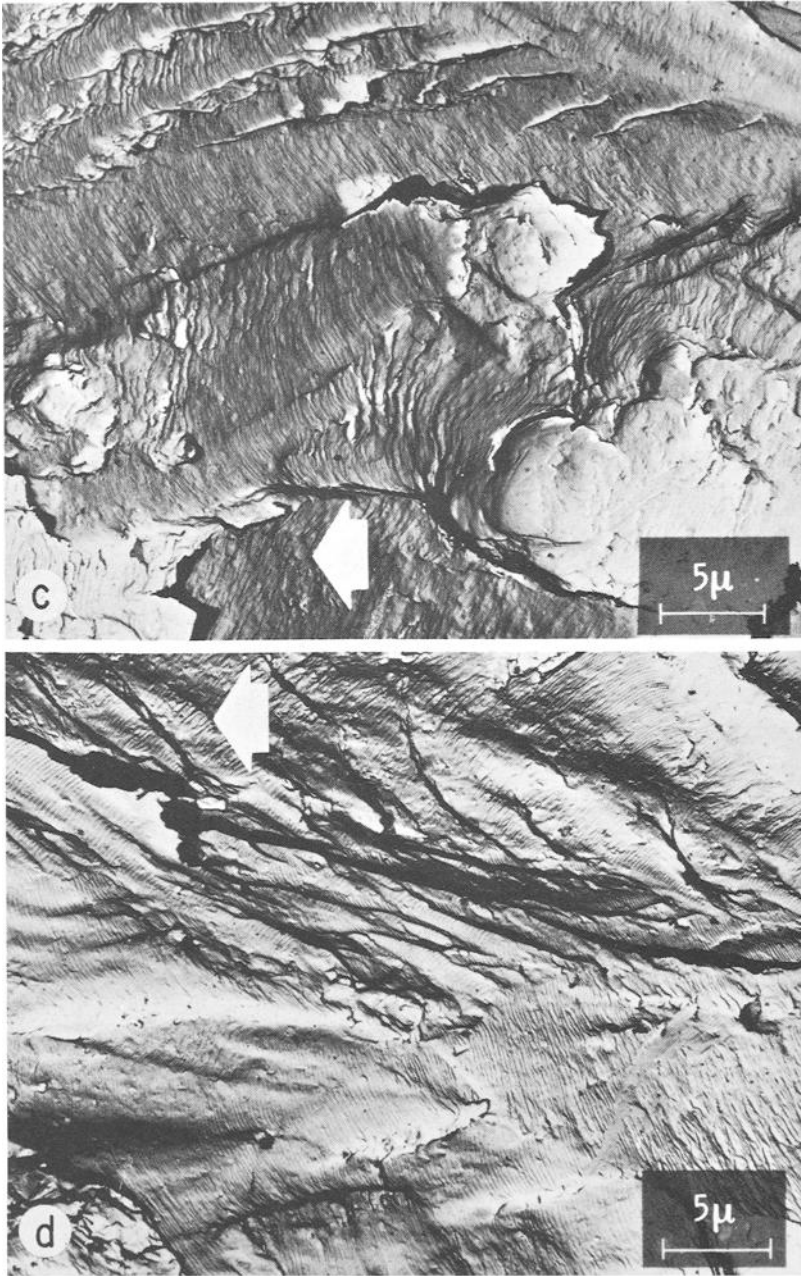


FIG. 11—Crack retardation due to application of peak loads.



(a) Area 0.003 in. before application of peak load.  
 (b) Crack growth due to peak load application is designated  $P$ . Striation spacing is the same before and immediately after peak.

FIG. 12—Effect of 18-ksi peak load at  $2a = 1.2$  in.



(c) Area 0.007 in. after peak.  
(d) Area 0.034 in. after peak.

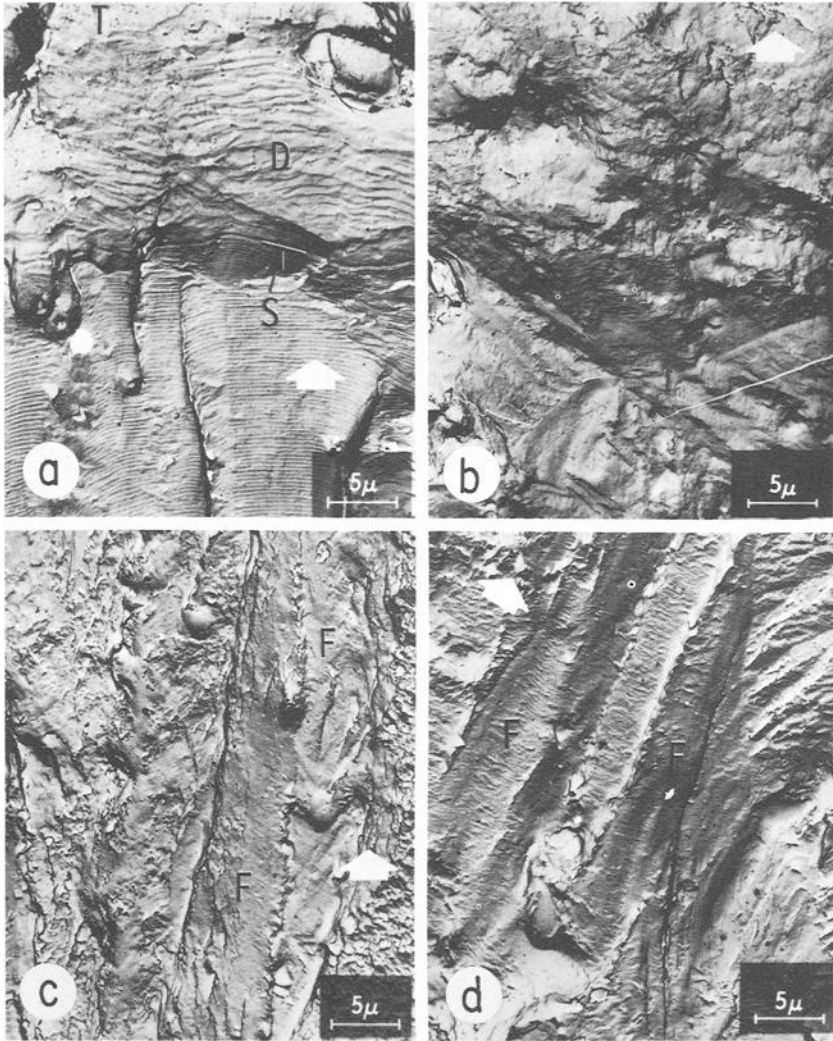
FIG. 12—Continued

smaller, reach a minimum, and then become progressively larger until they are approximately the same size as those in the area preceding the peak (Figs. 12*b*, *c*, and *d*). The significant finding is that the maximum retardation occurs not at the peak load application point, but later, as the crack propagates through the peak load plastic zone.

The clear definition of the peak load and subsequent striations implies that there was no microscopic crack arrest. Propagation continued with the next smaller load-amplitude cycle and the macroscopically observed effects were due to a retardation of growth rates. However, this situation was not as clear-cut when the peak stress intensity was higher, as shown in Fig. 13. Again, in Fig. 13*a*, the point of application of the peak load, designated *S*, is readily apparent. However, the total extent of the peak load growth increment is not clearly defined and is probably beyond the boundary of this photomicrograph. Extensive deformation, as evidenced by the deformation bands, designated *D*, and some tearing of the matrix, designated *T*, accompanied these peak load applications. Moreover, the fracture surface immediately following the peak load was badly damaged by fretting and abrasion (Figs. 13*b*, *c*, and *d*), indicating contact between the two fracture halves. Owing to the damage, striations are not readily visible in the areas immediately following the peak, Fig. 13*b*. However, as the crack propagates away from the peak, the extent of the surface damage decreases and striations are observed in protected regions, designated *F*, in Figs. 13*c* and *d*. These striations are extremely fine and not yet well defined even 0.050 in. past the peak.

In analyzing the results of the peak load tests, three factors should be considered: (1) mechanical factors, (2) plastic zone conditions, and (3) residual stress distributions. It is obvious in Figs. 12 and 13 that large plastic deformations accompany the application of the positive peak loads and that the extent of the deformations is a function of their magnitude. Blunting of the crack tip would be expected. However, when the load is lowered, reversed plastic flow occurs that resharpens the crack tip. The crack extension model discussed by Schijve [33] demonstrates how crack-tip resharpening may occur. The fact that striation spacings immediately following the peak load are the same as those immediately preceding the peak (Fig. 12) suggests the effectiveness of this resharpening process.

When the peak load is applied, a large volume of material yields plastically; the remainder of the specimen cross section is strained elastically. As the load falls, a smaller volume of material yields through reversed flow. At the same time, the remainder of the monotonic plastic zone experiences elastic compressive stresses due to the relaxation of elastic tensile strains in the surrounding material. The magnitude of these compressive stresses is a function of the plastic



(a) Peak load application line is designated *S*, deformation bands *D*, and matrix tearing *T*.

(b) Fracture appearance 0.003 in. after peak.

(c) Area 0.014 in. after peak. Regions of fine striations are designated *F*.

(d) Area 0.050 in. after peak. Regions of fine striations are designated *F*.

**FIG. 13**—Effect of 24-ksi peak load at  $2a = 1.2$  in. The photomicrographs are arranged to show the actual spatial relationships.

volume and the extent of the elastic strain recovery. Subsequent positive excursions of smaller amplitude will be insufficient to completely offset the surrounding compressive stress field established by the peak load. Based on the fractographic evidence, the macroscopically observed crack arrest due to occasional peak loads can be attributed to the microscopic crack retardation due to the compressive residual stress zone in front of the crack.

#### *Smallest Observable Growth Increments*

Acknowledging the importance of quantitative measurements of fatigue striations, the Electron Fractography Subcommittee has begun a study of the lower limit of striation size. In this program, it is proposed to determine, within the limits of replication technique, how slow fatigue cracks can propagate by the striation-formation growth mechanism. Based on the strong relation of striation spacings to the stress-intensity conditions at the tip of the moving crack, these studies would determine the tentative lower limits of stress-intensity conditions below which striation-type growth might not occur. Such information would be valuable in design considerations and would be useful in numerical integration procedures of total fatigue life by furnishing carefully measured, lower limit growth rate values. These studies have thus far shown that striations spaced approximately 100 Å apart have been found on the fracture surfaces of aluminum alloys. Based on the unit slip distance for aluminum, this suggests a dislocation motion of 30 to 40 Burgers vector units of translation. If it is assumed that the striation formation process is related to some multiple of dislocation translation, the minimum striation spacing would be expected to be not much less than 50 to 100 Å. In this connection, Linder [34] has reported macroscopically determined crack growth rates in 7075-T6 aluminum alloy of the order of  $2 \times 10^{-10}$  in./cycle. Since this rate is an extension of only hundredths of an angstrom per cycle, not possible for dislocation processes, it implies that the growth rate was discontinuous across the crack front.

The experimental difficulties inherent in the direct measurement of striation spacings less than 100 Å are formidable, and the measurements themselves are subject to some controversy. It would seem desirable to investigate indirect measurement to determine these values.

The introduction of periodic peak loads offers one possible technique for indirect measurement. In programs P 14 and P 15, we observed that every load cycle produced a growth increment at the larger crack lengths. There is reason to assume that each uniform load cycle would also produce growth at progressively shorter crack lengths until growth was mechanically impossible. A fractograph at crack length  $2a = 0.81$  in. (very near the origin) for program P 14 is shown in Fig.

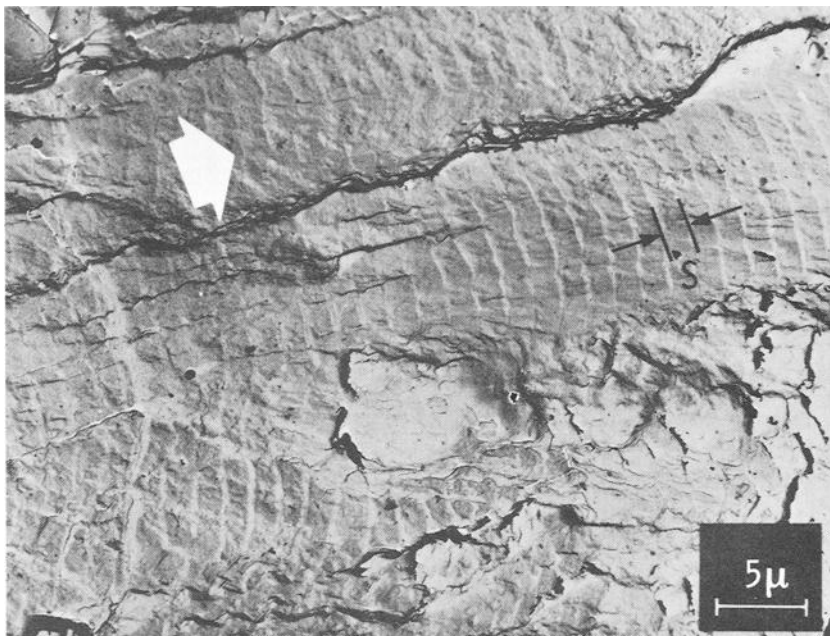


FIG. 14—*Spectrum spacing for P 14 at  $2a = 0.81$  in. is  $54 \mu\text{in.}$  One spectrum is designated S.*

14. The periodic repetition is readily apparent, with the peak loads separated by growth bands attributed to the 200 uniform load cycles. The crack extension per spectrum is measured at  $54 \mu\text{in./spectrum}$  and the 200 uniform load cycles account for approximately  $45 \mu\text{in.}$  of this growth. The growth increment per uniform load cycle, then, is less than  $60 \text{ \AA}$ . Attempts at direct observation of striations within these bands have so far been unsuccessful.

#### *Environmental Effects*

Haigh [35] established 50 years ago that the choice of test environment could have an appreciable effect on the fatigue lives of certain brasses and bronzes. Since this pioneering work, corrosion fatigue studies have been extended to include many materials and many test environments. Environmental effects were reported initially in terms of total fatigue life. However, fatigue life can be divided into at least four parts: (1) precrack initiation damage and crack initiation, (2) plane strain stable crack propagation, (3) plane stress stable crack propagation, and (4) final fracture. More recently, workers have investigated these life periods separately, and it appears that a major portion of the effect occurs in the stable crack propagation stages. The exact mechanisms by which the environment influences crack growth have not been

firmly established, but the total effect appears to be a function of frequency, stress range, and stress intensity.

It has been established that water vapor and various aqueous environments [36-38] can reduce the fatigue life and accelerate the crack growth rate of certain aluminum alloys. In one of the few fractographic examinations of corrosion fatigue specimens, Stubbington and Forsyth [39] compared the fracture appearances of specimens of an Al-7.5Zn-2.5Mg alloy tested in air and in an aqueous 3 per cent sodium chloride (NaCl) solution. They observed that the specimen tested in air had the longer life and exhibited only ductile type striations on the fracture surface, whereas the specimen tested in the salt solution exhibited brittle type striations.

The purpose of our test program was to determine the influence of various environments on the fatigue crack propagation behavior of several high-strength aluminum alloys. A fractographic analysis was conducted in support of this program to determine whether observed growth rate differences could be correlated with fracture surface features. The specimens, 9 by 24-in. center-notched crack growth panels, were tested in sinusoidal tension-tension loading at 120 cpm. The standard material thickness was 0.160 in., but 0.040 and 0.50-in. materials were also tested.

The initial phase of the program was conducted to determine the relative effects of five environments on 7178-T6 aluminum alloy. Desiccated air was chosen as the standard environment. The remaining environments were: (1) high humidity air (relative humidity 90 per cent at 70 F), (2) distilled water, (3) aqueous 3.5 per cent NaCl solution, and (4) hydraulic fluid (Skydrol).

The results of this series of tests are shown in Fig. 15. The slowest fatigue crack growth rate occurred in the standard dry air environment. The fastest growth rates occurred in wet air and distilled water; the growth rate was slightly slower in the salt solution. The growth rates in Skydrol were lower than those in water-containing environments.

The environmental effect was greatest at the shortest crack length (smallest stress intensities) and appeared divergent for extrapolations to lower stress-intensity values. The growth rates in the initial stages differed by as much as a factor of five. This information has particular significance when it is realized that the major portion of crack growth life is expended in the area where crack extension per cycle is extremely small, that is, less than 10  $\mu\text{in./cycle}$ . If these extrapolated rates are truly divergent, then life changes of one order of magnitude or greater could be expected. At the higher stress-intensity factor end of the curve, the rates in all environments tended to converge, indicating that the mechanical aspects of fatigue crack growth were overshadowing any environmental effects.

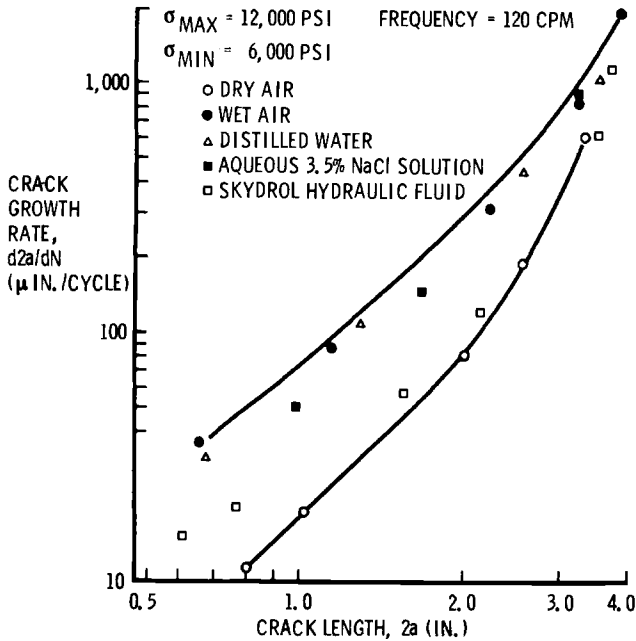
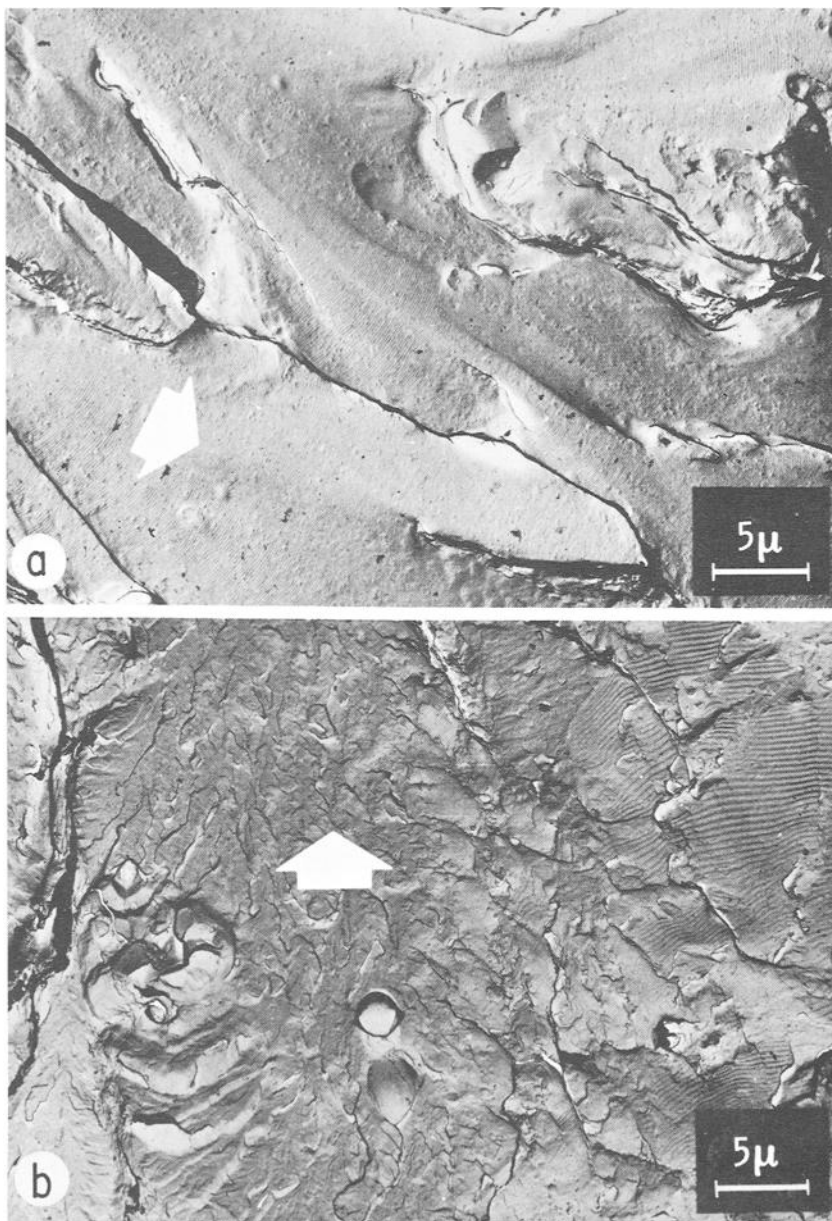


FIG. 15—Effects of environments on crack growth rate of 7178-T6 aluminum alloy.

To shed some light on the environmental effects, the fracture surfaces of these specimens were examined by electron fractographic techniques. Topographies typical of specimens tested in dry air and wet air are shown in Fig. 16. In the dry-air specimen, finely spaced ductile striations cover nearly 100 per cent of the fracture surface. In contrast, the wet-air specimen (and the distilled water specimen) exhibits only isolated patches of ductile striations, while the remainder of the surface has a brittle, cleavage-like appearance. However, crack arrest markings are sometimes observed; this appears to be a form of the brittle striations described by Forsyth [8]. Corrosion product or corrosion damage is not apparent on these surfaces. On the other hand, the fracture surfaces of the specimens tested in salt solution and Skydrol both showed corrosion damage, but it was apparent that ductile and brittle striations were present. However, we observed that the proportion of ductile striations was significantly larger on the specimens tested in Skydrol.

The gross changes in crack growth rates in dry air and wet air are associated with the change in fracture mode from ductile to brittle striation formation. This implies that, for the same stress conditions, brittle striation growth is more rapid than ductile striation growth. It is not clear at this time what differences exist in the mechanism of formation of ductile and brittle striations. It should be noted



(a) Dry air.  
(b) Wet air.

FIG. 16—Typical fracture topographies of 7178-T6 aluminum alloy specimens tested at  $2a = 0.6$  in. in wet and dry air.

that fatigue specimens tested in laboratory air and specimens with service-induced fatigue cracks mainly show brittle striations in 7178-T6 aluminum alloy.

The second phase of the test program compared the fatigue crack propagation behavior of several commonly used high-strength aluminum alloys in two environmental test conditions. Again, dry air was chosen as the standard environment, and wet air was used for comparison. The materials compared were 7178-T6, 7075-T6, 2024-T3, and 2024-T6. The mechanical properties of these materials are tabulated in Table 1. The results of the environmental tests are summarized in Fig. 17.

The two 7000 series aluminum alloys showed a significant difference in crack growth rates in the two test conditions. Both alloys had essentially the same rate in dry air, but 7178-T6 was noticeably more affected by wet air. The 2024 alloy in both the room temperature and artificially aged conditions showed no difference in growth rate as a function of humidity.

Significant differences in fracture surface appearance were also noted. In dry air, all four materials showed extensive ductile striation development. Brittle striations predominated in the two 7000 series

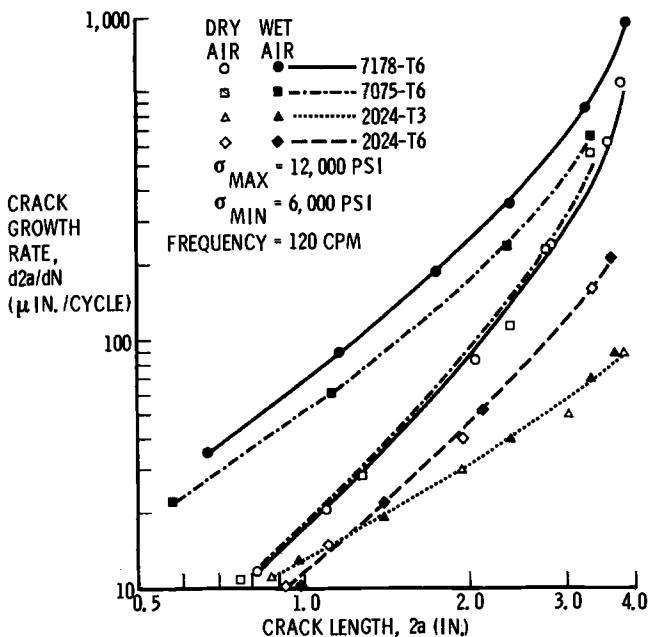


FIG. 17—Crack growth rate of several aluminum alloys as a function of environment.

alloys when tested in wet air. In the 2024 alloy, however, brittle striations were not observed for either aging treatment in wet air.

Again, the pronounced changes in crack growth rates with environment are related to the change in fracture mode. However, it should be noted that the rate may change without a concurrent change in fracture mode. This was observed by Hyatt and Quist [40] while testing two 7000 series experimental alloys in dry and wet air. The chemistry of the two alloys differed only in that one contained 0.9 per cent copper, while the other contained no copper. The change in copper content exerted only a small effect on the mechanical properties of these alloys as shown by the mechanical properties given in Table 1. The crack growth rate data are shown in Fig. 18. The addition of 0.9 per cent

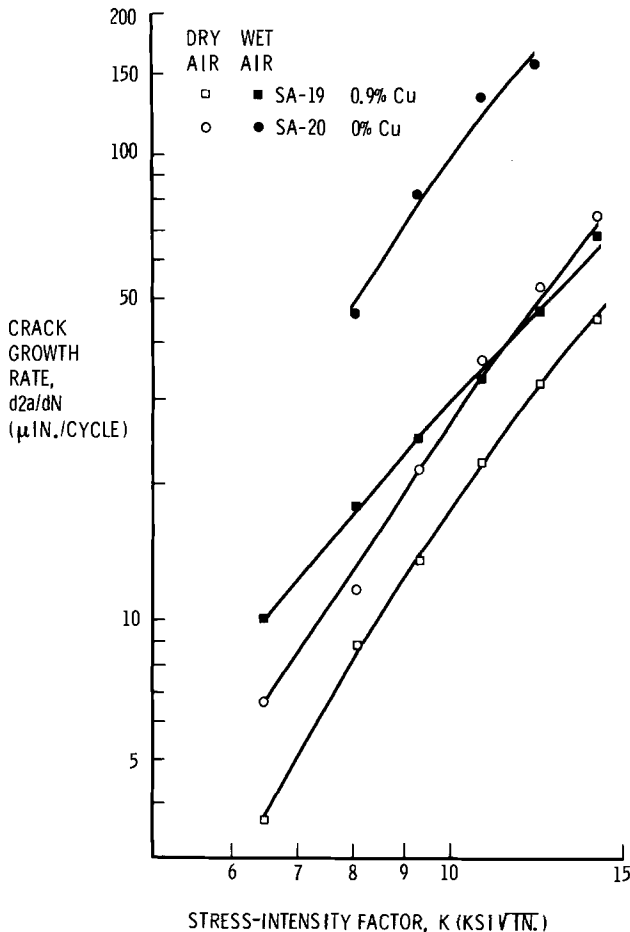
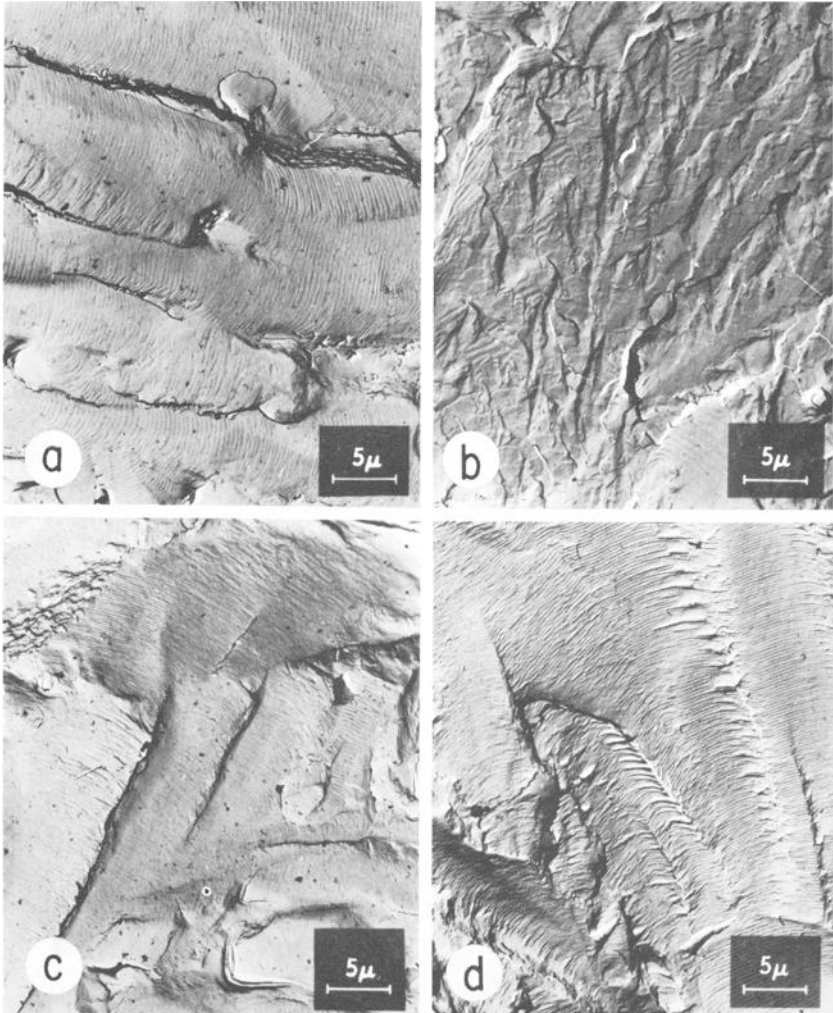


FIG. 18—Effect of environment on crack growth rate of two experimental 7000 series aluminum alloys as a function of copper content (from Ref 40).

copper slows the growth rate and, while not eliminating the environmental effect, substantially reduces its severity.

In the subsequent fractographic examination, Fig. 19, the material without copper exhibited the expected topography, that is, ductile striations in dry air and brittle striations in wet air. The surprising result was that the specimen containing copper exhibited duc-



- (a) 0Cu—dry air.
- (b) 0Cu—wet air.
- (c) 0.9Cu—dry air.
- (d) 0.9Cu—wet air.

FIG. 19—Typical fracture topographies of two experimental 7000 series aluminum alloys tested in wet and in dry air (from Ref 40).

tile striations in both environments, even though a positive environmental effect was observed in the crack growth rate data. On the basis of this observation it is not possible to make a general statement concerning the relation between a positive environmental effect and a transition in striation morphology from ductile-to-brittle type.

When the fracture surfaces of the aluminum specimens tested in different environments are examined optically, the fracture mode changes are readily apparent. The brittle striations occur typically on flat, highly reflective facets whose orientations are nearly normal to the tensile axis. Around these flat facets are patches of ductile striations on the inclines. When 100 per cent ductile striations are observed, the flat reflective facets do not occur, and flat fracture planes normal to the tensile axis are not common. It is also observed that when brittle and ductile striations are present in adjacent areas, the crack front leads and the striation spacing is larger in the brittle striation area. The ductile striations trail behind, as shown in Fig. 20.

Changes in fracture appearance as a function of environment are not limited to aluminum alloys or to aqueous environments. Spitzig [41] reported in acceleration of fatigue crack growth in an 18Ni (250) maraging steel tested in a dry hydrogen atmosphere. The cracking mode was transgranular, with the resulting structure appearing

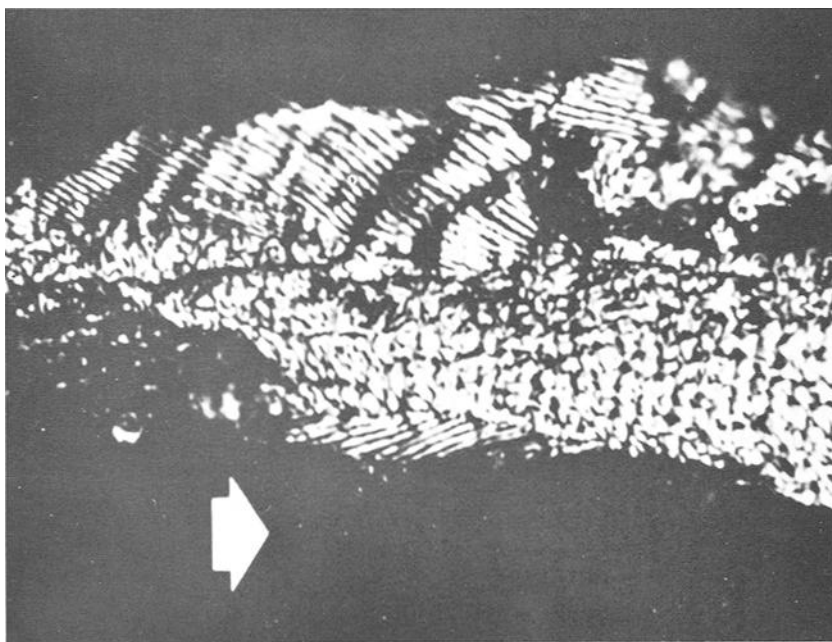


FIG. 20—Optical fractograph of brittle and ductile striations in adjacent areas of an aluminum alloy.

very similar to the brittle striations in aluminum alloys. When this same material was tested in dry or humid argon or humid hydrogen, the cracking mode was characterized by ductile striations.

Another case where the fracture appearance changed as a function of environment was reported by Dahlberg [42]. The material tested was AISI 4340 steel, heat treated to very high strengths (approximately 260 to 280 ksi ultimate tensile strength). The environments chosen were dry and wet air. The crack growth rate in dry air was significantly slower than in wet air. The fracture path in dry air was transgranular, with some striations visible, whereas in wet air the fracture path was intergranular, along the prior austenite grain boundaries.

### Summary

The resolution and depth of field of the electron microscope allow us to examine fatigue fracture surfaces in minute detail. Concurrent with improvements in the interpretation of fractographic observations, electron fractography has evolved from producing purely qualitative results to the point where quantitative information may be derived.

Different surface characteristics of fatigue fracture surfaces may be observed, depending on the level of magnification. With little visual enlargement, many service failure fatigue surfaces show "clam shell" markings that indicate that fatigue crack propagation occurred in finite stages separated by crack arrests. Electron fractographic examination at high magnification reveals the clam shell markings to be composed of many fine striations representing crack growth increments for each loading cycle. By careful measurement of these striations, it has been possible to relate fatigue crack propagation rates with crack-tip stress-intensity conditions. Changes in striation appearance and orientation on the fracture surface have been associated with crystallographic considerations.

The principal findings with respect to the recent experimental results are as follows:

1. When periodic positive and negative peaks are superimposed on a uniform loading history, the sequence of applying the peak load has a pronounced effect on the subsequent crack growth rate.

2. When occasional peak loads are superimposed on a uniform loading history so that the peak load plastic zones do not overlap:

- (a) Crack retardation results.

- (b) Crack-tip blunting occurs, but the crack resharpenes on the load decrease portion of the peak load cycle and crack propagation continues with the next load cycle.

- (c) The cracking rate immediately before and immediately after the peak load application point is approximately equal.

- (d) Crack retardation occurs in the plastic zone ahead of the crack

and the extent of the retardation is governed by the magnitude of the peak load.

3. The effects of environment on crack growth rate in several commercial aluminum alloys are:

(a) In 7178-T6, crack growth rate is slowest in dry air and progressively faster in Skydrol, aqueous 3.5 per cent NaCl solution, distilled water, and wet air. The growth rates differed by as much as a factor of five.

(b) In both 7178-T6 and 7075-T6 when tested in dry and wet air, a pronounced acceleration of growth rate was observed in wet air. Alloys 2024-T3 and 2024-T6 showed no difference in growth rate in these two environments.

(c) The effect of environment was most pronounced at the lowest stress-intensity values.

(d) Changes in cracking rate at a constant stress intensity were usually associated with changes in fracture mode, with the faster rates favoring a more brittle mode.

#### *Acknowledgments*

The authors wish to thank W. E. Anderson, C. S. Carter, and R. M. N. Pelloux for their helpful suggestions and comments concerning the text. One of the authors (R. W. Hertzberg) is grateful for support from the National Science Foundation under Grant GK-1225. The assistance of T. E. Kane in performing the fatigue tests and R. R. Boyer in conducting the fractographic analyses is gratefully acknowledged.

#### **References**

- [1] Irwin, G. R., "Fracture Mode Transition for a Crack Traversing a Plate," *Journal of Basic Engineering, Transactions, American Society of Mechanical Engineers, Series D*, Vol. 82, No. 2, June 1960, p. 417.
- [2] Hertzberg, R. W. and Paris, P. C., "Application of Electron Fractography and Fracture Mechanics to Fatigue Crack Propagation," presented at International Conference on Fracture, Sendai, Japan, Sept. 1965.
- [3] Schijve, J., "Analysis of the Fatigue Phenomenon in Aluminum Alloys," NLR Technical Report M2122, Amsterdam, The Netherlands, July 1964.
- [4] Jacoby, G., "Fractographic Methods in Fatigue Research," *Experimental Mechanics*, Vol. 5, No. 3, March 1965, p. 65.
- [5] Zappfe, C. A. and Worden, C., "Fractographic Registrations of Fatigue," *Transactions, American Society for Metals*, Vol. 43, 1951, p. 958.
- [6] Forsyth, P. J. E. and Ryder, D. A., "Fatigue Fracture," *Aircraft Engineering*, Vol. 32, No. 374, 1960, p. 96.
- [7] Forsyth, P. J. E. and Ryder, D. A., "Some Results of the Examination of Aluminum Alloy Specimen Fracture Surfaces," *Metallurgia*, Vol. 63, 1961, p. 117.
- [8] Forsyth, P. J. E., "A Two Stage Process of Fatigue Crack Growth," *Proceedings of the Crack Propagation Symposium*, The College of Aeronautics, Cranfield, England, Vol. I, Sept. 1961, p. 76.
- [9] Forsyth, P. J. E., "Fatigue Damage and Crack Growth in Aluminum Alloys," *Acta Metallurgica*, Vol. 11, July 1963, p. 703.

- [10] Crussard, C., "A Study of Impact Tests and the Mechanism of Brittle Fracture," *Journal of the Iron and Steel Institute*, Vol. 183, June 1956, p. 146.
- [11] Crussard, C. et al, "A Comparison of Ductile and Fatigue Fractures," *Fracture* (Swampscott Conference), Wiley, New York, 1959.
- [12] McEvily, A. J., Jr., Boëttner, R. C., and Johnston, T. L., "On the Formation and Growth of Fatigue Cracks in Polymers," *Fatigue—An Interdisciplinary Approach*, Syracuse University Press, Syracuse, N.Y., 1964, p. 95.
- [13] Thompson, K. R. L. and Mulhearn, T. O., "The Obliteration of Fatigue Fracture Striations by Corrosion," *The Journal of the Australian Institute of Metals*, Vol. 10, No. 3, Aug. 1965, p. 303.
- [14] Laird, C., "The Influence of Metallurgical Structures on the Mechanism of Fatigue Crack Propagation," *Fatigue Crack Propagation, ASTM STP 415*, American Society for Testing and Materials, 1967, pp. 131–180.
- [15] Laird, C. and Smith, G. C., "Crack Propagation in High Stress Fatigue," *Philosophical Magazine*, Vol. 7, 1962, p. 847.
- [16] Stubbington, C. A., "Some Observations on Air and Corrosion Fatigue of an Aluminum-7.5% Zinc-2.5% Magnesium Alloy," *Metallurgia*, Vol. 68, 1963, p. 109.
- [17] Hertzberg, R. W., "Fatigue Fracture Surface Appearance," *Fatigue Crack Propagation, ASTM STP 415*, American Society for Testing and Materials, 1967, pp. 205–225.
- [18] McEvily, A. J., Jr., and Boettner, R. C., "On Fatigue Crack Propagation in F. C. C. Metals," *Acta Metallurgica*, Vol. 11, No. 7, 1963, p. 703.
- [19] Miller, G. A., "Fatigue Crack Growth in Some Copper Base Alloys," Ph.D. dissertation, Massachusetts Institute of Technology, 1965.
- [20] Pelloux, R. M. N., "Fractographic Analysis of the Influence of Constituent Particles on Fatigue Crack Propagation in Aluminum Alloys," *Transactions, American Society for Metals*, Vol. 57, No. 2, 1964, p. 511.
- [21] Hoepfner, D. W., et al, "Fatigue Behavior of Materials for the SST Electron Fractographic Studies," Battelle Report for Contract NAS 1-4460, 30 July 1965.
- [22] Paris, P. C., "The Growth of Cracks Due to Variations in Load," Ph.D. dissertation, Lehigh University, Sept. 1962.
- [23] Paris, P. C. and Erdogan, F., "A Critical Analysis of Crack Propagation Laws," *Journal of Basic Engineering, Transactions, American Society of Mechanical Engineers, Series D*, Vol. 85, No. 4, Dec. 1963, p. 528.
- [24] Carmen, C. and Schuler, M., "Low Cycle Fatigue Properties of 18 Ni-Co-Mo250 Maraging Steel," presented at American Society for Testing and Materials Subcommittee Meeting on Electron Fractography, Schenectady, N.Y., Sept. 1964.
- [25] McMillan, J. C., "Fractographic Analysis of Fatigue Crack Propagation," presented at American Society for Testing and Materials Subcommittee Meeting on Electron Fractography, Lehigh University, Oct. 1965.
- [26] McMillan, J. C. and Pelloux, R. M. N., "Fatigue Crack Propagation Under Programmed and Random Loads," *Fatigue Crack Propagation, ASTM STP 415*, American Society for Testing and Materials, 1967, pp. 505–535.
- [27] Hudson, C. M. and Hardrath, H. F., "Investigation of the Effects of Variable-Amplitude Loadings on Fatigue Crack Propagation Patterns," NASA Technical Note D-1803, National Aeronautics and Space Administration, Aug. 1963.
- [28] Schijve, J., "The Significance of Fatigue Cracks in the Micro-Range and Macro-Range," *Fatigue Crack Propagation, ASTM STP 415*, American Society for Testing and Materials, 1967, pp. 415–459.
- [29] Schijve, J., Broek, D., and de Rijk, P., "Fatigue Crack Propagation Under Variable-Amplitude Loading," NLR Report NLS-RN-M. 2094, Naval Research Laboratory, 1961.
- [30] Hardrath, H. F., "Cumulative Damage," *Fatigue—An Interdisciplinary Approach*, Syracuse University Press, Syracuse, N.Y., 1964, p. 345.
- [31] Rice, J. R., "The Mechanics of Crack Tip Deformation and Extension by Fatigue," *Fatigue Crack Propagation, ASTM STP 415*, American Society for Testing and Materials, 1967, pp. 247–311.

- [32] Irwin, G. R., "Plastic Zone Near a Crack and Fracture Toughness," Seventh Sagamore Ordnance Materials Research Conference, Aug. 1960.
- [33] Schijve, J., discussion of "Fatigue Crack Propagation Under Programmed and Random Loads" (see Ref 26).
- [34] Linder, B., "Extremely Slow Fatigue Crack Growth Rates in 7075-T6 Aluminum Alloy," M.S. thesis, Lehigh University, Bethlehem, Pa., June 1965.
- [35] Haigh, B. P., "Experiments on the Fatigue of Brasses," *Journal of the Institute of Metals*, Vol. 18, 1917, p. 55.
- [36] Broom, T. and Nicholson, A., "Atmospheric Corrosion-Fatigue of Age-Hardened Aluminum Alloys," *Journal of the Institute of Metals*, Vol. 89, Feb. 1961, p. 183.
- [37] Bennett, J. A., "Changes in the Influence of Atmospheric Humidity During Fatigue of an Aluminum Alloy," *Journal of Research*, National Bureau of Standards, Vol. 68C, 1964, p. 91.
- [38] Bradshaw, F. J. and Wheeler, C., "The Effect of Environment on Fatigue and Crack Growth in Aluminum and Some Aluminum Alloys," *Applied Materials Research*, April 1966.
- [39] Stubbington, C. A. and Forsyth, P. J. E., "Some Corrosion Fatigue Observations on a High-Purity Aluminum-Zinc-Magnesium Alloy and Commercial D.T.D. 683 Alloy," *Journal of the Institute of Metals*, Vol. 90, 1961-62, p. 347.
- [40] Hyatt, M. V. and Quist, W. E., "The Influence of Heat Treatment and Composition on the Stress Corrosion, Fatigue, and Fracture Properties of 7075 Aluminum Alloys," presented at the AFML Fiftieth Anniversary Corrosion of Military and Aerospace Equipment Technical Conference, 23-25 May 1967.
- [41] Spitzig, W. A., "Effect of Hydrogen Environment on Fatigue Crack Propagation in 18 Ni(250) Maraging Steel," presented at the Electron Fractography Subcommittee Meeting, Westinghouse Research and Development Center, Pittsburgh, Pa., March 1967.
- [42] Dahlberg, E. P., "Fatigue Crack Propagation in High-Strength 4340 Steel in Humid Air," *Transactions*, American Society for Metals, Vol. 58, 1965, p. 46.

## Environmental Effects on Fracture Morphology

---

**REFERENCE:** Nielsen, N. A., "Environmental Effects on Fracture Morphology," *Electron Fractography, ASTM STP 436*, American Society for Testing and Materials, 1968, pp. 124–150.

**ABSTRACT:** The utility of fractography can be greatly increased if the technique can be applied on a broader basis to provide unambiguous interpretation of fracture surface morphology (and thereby, identification of the fracture mode) resulting from specific environmental exposure of stressed metals and alloys.

This paper reviews the present status of electron fractography in this area of expanded application. High-strength steels, martensitic and austenitic alloys, and titanium and zirconium alloys are considered with respect to the effects chemical environment, including high energy irradiation, induces in the fracture characteristics of the alloys.

**KEY WORDS:** embrittlement, fractography, electron microscopy, fracture, stress corrosion, radiation effects, stainless steel, ferritic alloys, titanium, zirconium

With the acceptance of electron fractography as a unique and important tool in the observation and analysis of the micromechanisms of "simple" fracture processes in metals, new extensions and applications of the techniques are now being found in more complex fracture processes where special environmental conditions have a controlling effect. Environmental conditions are here arbitrarily defined as the "chemical" environment (gaseous or liquid) as well as exposure to high energy radiation. When fracture occurs in these environments, it is because the specific environmental conditions often act synergistically with the applied or residual stresses to produce failure which, in the absence of the specific environment, would not occur. Examples of this can be found in the phenomena of stress-corrosion cracking, stress-accelerated intergranular corrosion, hydrogen embrittlement, liquid metal embrittlement, corrosion fatigue, etc.

<sup>1</sup> Research fellow, Engineering Materials Laboratory, Engineering Department, E. I. du Pont de Nemours & Co., Inc., Wilmington, Del.

Because the application of electron fractography to all of these areas is relatively recent, interpretation of the information in the fractographs is difficult and often incomplete and problematical. The effects of corrosion, the solution of gases, or the effects of irradiation damage superposed with a static or dynamic stress state on the metal or alloy generally produce fractures of complex and varying surface morphologies. This is particularly true for stress-corrosion fractures where fractography provides more information than can yet be reliably interpreted and agreed upon.

The purpose of this paper is not to provide a comprehensive "state-of-the-art" review of the subject but to indicate by chosen examples how electron fractography is being used in several of the previously mentioned areas in the attempt to provide new information on environment-induced fracture processes in alloys. The writer's primary utilization of the technique has been in the subject of stress-corrosion cracking of stainless steels, and this application will be emphasized. When other systems are mentioned, the contributions of other individuals will be acknowledged.

## **Stress Corrosion and Hydrogen Embrittlement**

### *High Strength Steels*

Premature failure often occurs in these materials through the embrittling effect of hydrogen or by a stress-corrosion mechanism in which hydrogen evolution may or may not play a secondary role. Because the fractures in both types of failure are primarily intergranular, one of the earliest hopes for electron fractography has been that this technique will be able to provide microtopographical information which can reliably and uniquely distinguish a failure caused purely by hydrogen embrittlement from one in which corrosion is involved. Specific research on this subject has been carried out by Phillips et al and is summarized in Section Six of the *Electron Fractography Handbook [1]*.<sup>2</sup> They conclude that in AISI 4340, 4330M, and D64C steels "no exclusive single feature precisely identified either fracture type." It appears, however, that stress-corrosion fractures show a combination of features differing in degree from those observed in hydrogen embrittlement which may allow a differentiation to be made. On the basis of their work, to which it is recommended the reader refer, it is obvious that careful technique and observation must be employed in this particular application of fractography. Knowledge of the exposure and service history of the steel is also necessary to make a considered judgment of the cause of failure.

Intergranular fracture can be produced by other mechanisms in high

<sup>2</sup> The italic numbers in brackets refer to the list of references appended to this paper.

strength steels as Warke and Elsea [2] have pointed out. Quench cracks, for example, are quite similar in their fracture surfaces to those produced by hydrogen embrittlement and stress corrosion. More information than the fractographic data are presently needed to differentiate these.

Tiner and Gilpin [3] have used tritiated water solutions in a study of the microprocesses in stress corrosion of Type 4340 steel to elucidate the role of hydrogen in the failure mechanism.

### *Martensitic Stainless Steels*

The martensitic stainless steels when heat treated to very high strength levels are subject to failure by stress corrosion in relatively mild corrosive environments. For example, a USS 12MoV stainless steel (12 per cent chromium, 1 per cent molybdenum with nickel and vanadium) was reported by Phelps and Mears [4] to fail intergranularly in 10 min when exposed as a stressed U-bend specimen to 1.0 *M* neutral sodium chloride (NaCl). The standard commercial martensitic alloys do not exhibit this extreme susceptibility, but nevertheless their behavior is similar. Inasmuch as they can also be made to fail by hydrogen embrittlement when cathodically polarized (with applied cathodic currents sufficiently high to stop all corrosion attack), the martensitic alloys constitute another class of steels on which electron fractography may cast further light in differentiating these two fracture mechanisms.

### *Austenitic Stainless Steels*

Another potentially fruitful material for this specific study is cold-worked AISI 301 and 302 stainless steels. Phelps and Mears [4] demonstrated that Type 302 stainless, cold-worked 75 per cent could be made to fail either by stress-corrosion cracking (with applied anodic current) or by hydrogen embrittlement (with applied cathodic current) in a 3 per cent NaCl solution saturated with hydrogen sulfide (H<sub>2</sub>S).

Matsushima et al [5] have discussed the stress corrosion and hydrogen cracking of 17-7 stainless steel (Type 301). They concluded that "contrary to reactions observed in pure phase alloys, stainless steels containing mixtures of austenite and ferrite may fail either by hydrogen cracking or by stress corrosion, depending on the environment."

The writer has also confirmed that severely cold-rolled Type 301 stainless can be made to fail by either mechanism. Tested as stressed U-bend specimens Type 301 sheet cold-reduced 70 per cent fails rapidly by stress-corrosion cracking in boiling 42 per cent magnesium chloride (MgCl<sub>2</sub>) (in less than 1 h). Failures occurred overnight at room temperature in 10 per cent ferric chloride (FeCl<sub>3</sub>) as well as in a MgCl<sub>2</sub>-Na<sub>2</sub>S slurry. When exposed to the latter environment and

simultaneously polarized with a strong cathodic current ( $0.1 \text{ A cm}^{-2}$ ), the stressed Type 301 stainless steel will crack as a result of hydrogen embrittlement.

Examples of electron fractographs made of these specimens appear in Figs. 1-4. It is obvious from these that the environment in which fracture occurred had an important influence on the resulting fracture-surface morphology. These fractographs were selected to illustrate what the main points of typical difference appear to be. (However, it must also be pointed out that in each set of micrographs made for each fracture system, there is enough variation in topographical structure that the examination of many areas is required for complete appreciation of the range of fracture morphology that can form in one system.)

Cold-rolling of Type 301 stainless steel develops a banded ferritic-austenitic structure. The stress-corrosion fracture produced in boiling 42 per cent  $\text{MgCl}_2$  shows both elongated "blocky" strata and the irregular topography more typical of stress corrosion in austenite (Fig. 1). Further observations, including the use of oxide replicas are re-

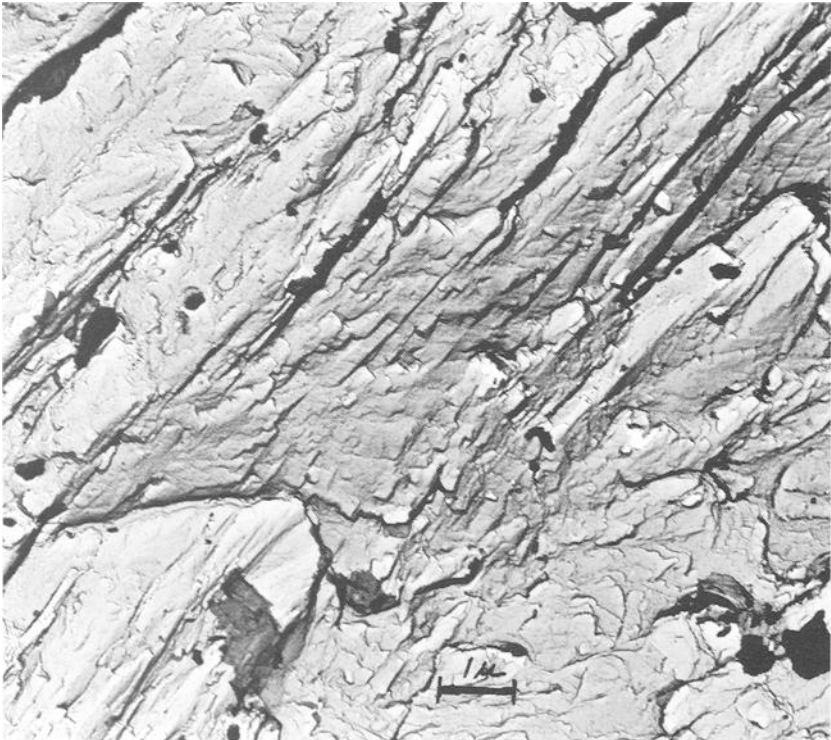


FIG. 1—Stress-corrosion fracture of Type 301 stainless steel in boiling 42 per cent  $\text{MgCl}_2$  ( $\times 9200$ ).



FIG. 2—Stress-corrosion fracture of Type 301 stainless steel in 10 per cent  $\text{FeCl}_3$ , room temperature ( $\times 11,600$ ).

quired to classify the fracture features characterizing each phase in this alloy. (It is noted that Douglass et al [6] have made fractographs of Type 310 stainless steel cold rolled 50 per cent and tested to failure in boiling 42 per cent  $\text{MgCl}_2$ . They reported that the austenite-martensite interface appeared to be the preferential fracture path and indicated that their work was the first observation of stress-induced martensite in Type 310 stainless steel.)

The stress-corrosion fracture produced in 10 per cent  $\text{FeCl}_3$  shows considerable etching and surface roughening which is to be expected of  $\text{FeCl}_3$ , an acidic pitting corrodent (Fig. 2). (The alteration of fracture surfaces by subsequent reaction with their chemical environment occurs in many other systems as well. It must be considered and evaluated for each fractographic analysis of an environmentally induced alloy failure.) The fractures, however, which developed on ex-

posure of the cold-worked and stressed Type 301 alloy to  $MgCl_2-Na_2S$ , were entirely different in character. The path of cracking was partially intergranular; the fracture surfaces showed elongated tear dimples, the size of which varied with change in direction of the fracture in following a local intergranular path. Again the ferrite and austenite cannot be reliably differentiated in their topography (Fig. 3).

Lastly, failure induced in stressed Type 301 stainless steel by cathodic charging of hydrogen develops more of a dual-structured topography (Fig. 4). Areas of quasi-cleavage containing ridges of small equi-axed rupture dimples were observed. Local areas of large equi-axed dimples were also present (in what is believed to be austenite) indicating that differentiation of austenitic and ferritic (martensitic) areas by electron fractography may be accomplished in this or other duplex  $\alpha-\gamma$  alloys when failure occurs by a hydrogen embrittlement mechanism.

In summary, it appears from these preliminary studies that electron fractography will provide further information on the several fracture

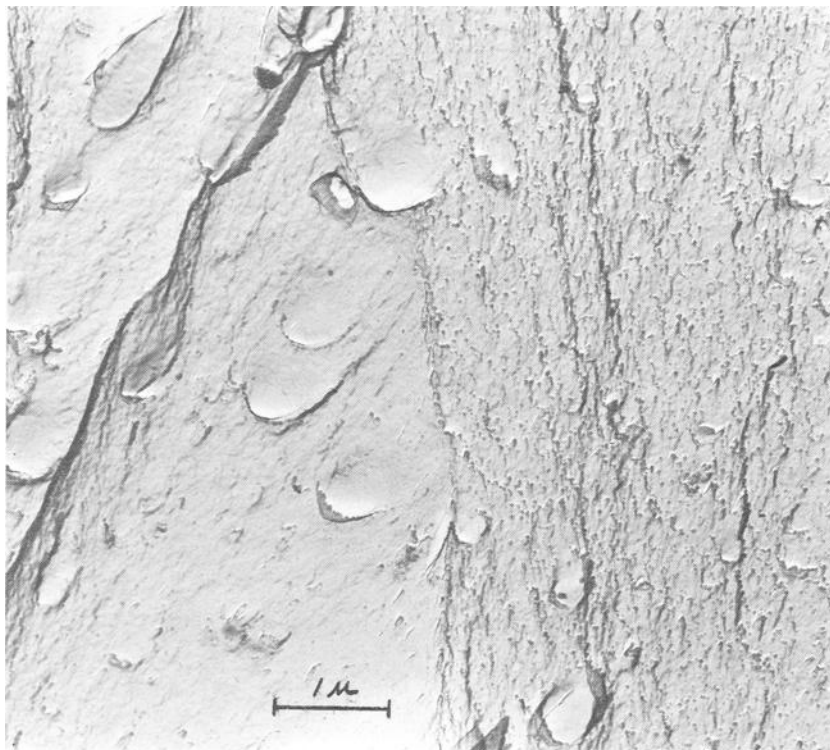


FIG. 3—Stress-corrosion fracture of Type 301 stainless steel in  $MgCl_2 + Na_2S$ , room temperature ( $\times 15,200$ ).

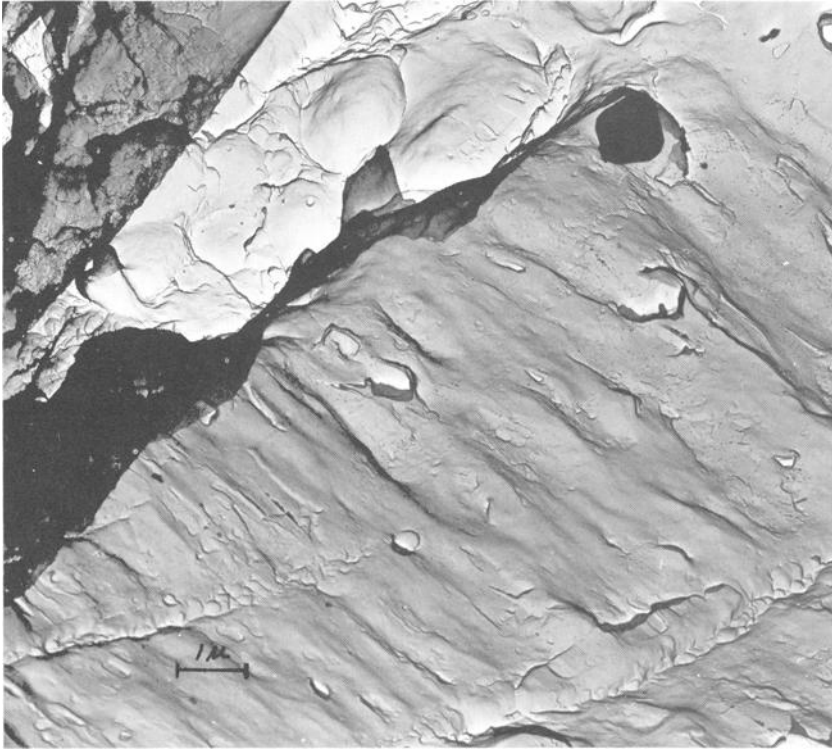


FIG. 4—Hydrogen-embrittlement fracture of Type 301 stainless steel ( $\times 9200$ ).

mechanisms which can cause failure of the hardenable (by heat treatment or cold rolling) grades of ferritic and austenitic stainless steel. The differentiation and classification of fractographic features which characterize failures in various stress-corrosion cracking environments, however, will require a more intensive and organized research study than anyone has yet made in this field.

#### *Stress-Corrosion Cracking of Austenitic Stainless Steels*

The susceptibility of this class of steels to transgranular stress-corrosion cracking (SCC) in solutions containing chloride ions has engendered corrosion research on a world-wide basis. The objective of the work in many laboratories is to determine the mechanism of this form of "brittle" fracture in the normally, inherently ductile austenitic structure.

Stress-corrosion cracking takes the form of a low strain failure. There is often little surface appearance of corrosion having taken place. A failed specimen does not show evidence of plastic deformation. There are no macroscopic dimensional changes measurable, and

the path of cracking is mostly transcrystalline, hence, the designation "brittle fracture."

In the 1959 Pittsburgh Conference on Physical Metallurgy of Stress-Corrosion Fracture, the present author [7] described an application of fractography in research on the micromechanisms of SCC in austenitic stainless steels. In restatement of the advantages of fractography in this case, it can provide information on: (1) the ductile-brittle characteristics of the topography, (2) fracture-face corrosion and precipitated corrosion products in the crack system, and (3) the role of metallic or nonmetallic phases which may embrittle the alloys by providing preferential paths for fracture.

That study and a later one (Nielsen [8]) in which electron metallography was employed to examine the early stages of corrosion attack by chloride ions on stressed stainless steel surfaces, along with their transition into recognizable microcracks which lead to ultimate brittle fracture, have confirmed the utility and value of fractography in stress-corrosion research. If there is a weakness or limitation in the practice of fractography, it exists in the present inability to interpret completely, and with 100 per cent confidence, all of the information which the fractograph (particularly the electron fractograph) presents. It is the writer's conviction that inherent in the proper interpretation of electron fractographs are many of the answers to the now puzzling questions of crack propagation mechanism in SCC of austenitic stainless steels.

Figure 5 is a photomicrograph of an SCC fracture in Type 316 stainless steel. It shows surface morphology that is commonly observed in these cases, namely, a feathery, dendrite-like surface topography. Figure 6 is a second example of this taken from a failed section of Type 316 stainless tubing. In this case the photomicrograph has been made from the carbon replica of the fracture. It is included here to illustrate a minor problem in applying electron fractography to fracture surface analysis. The difficulty is that of correlating surface topography observable by light microscopy with the same surface features, in replica form, examined in the electron microscope. The dendritic-like structure in Fig. 6 shows up clearly because it is all within the depth of field of the metallograph and properly oriented to reflect light back to the observer. It stands out from the rest of the fracture surface for these reasons. When the same area is examined in the electron microscope, all of the fracture surface is now within the depth of field of the microscope, and the outlines of the "dendrite" are lost. Many of the features seen in the photomicrograph are no longer readily identifiable in the electron micrograph. Examination based solely on electron fractography would characterize the surfaces shown in Fig. 7 as cleavage faces or perhaps quasi-cleavage. What this indicates, of course, is that the actual metallurgical surface, or if not convenient, the replica of

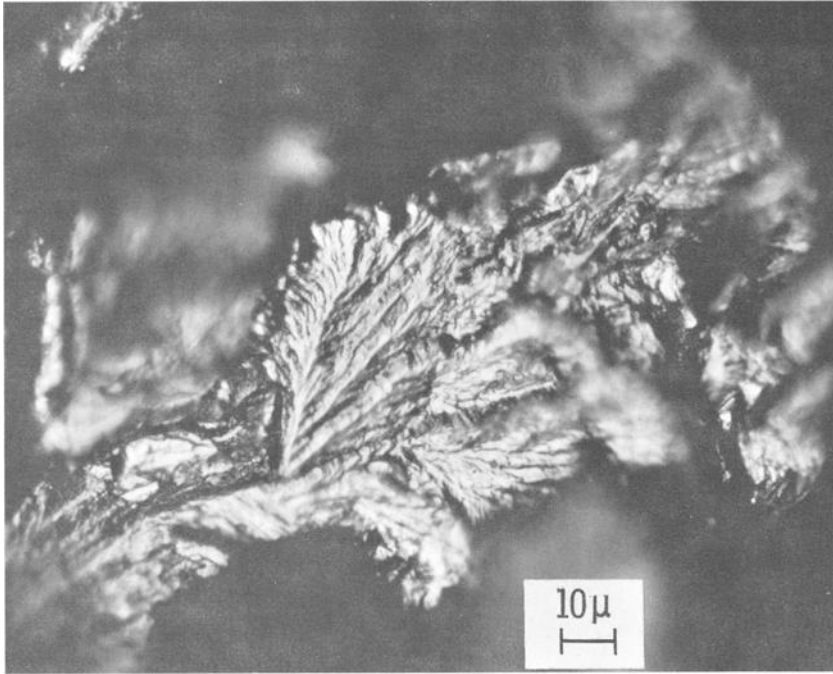


FIG. 5—"Feather" morphology in fracture by SCC of Type 316 stainless steel tube ( $\times 750$ ).

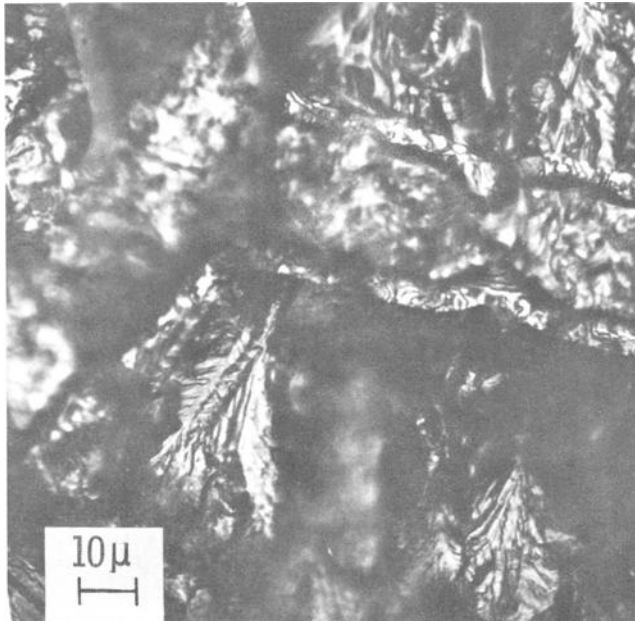


FIG. 6—"Feather" morphology in carbon replica of fracture by SCC of Type 316 stainless steel tube ( $\times 750$ ).



FIG. 7—Electron micrograph of “feather” area of Fig. 7 ( $\times 4000$ ).

the fracture should also be examined on a metallograph in order to develop a maximum of descriptive information on the fracture surface morphology.

In other SCC failures of austenitic stainless steels (particularly tubing in which residual tensile stresses from the forming operation are present), the fracture mode is not always entirely transcrystalline cracking. A small percentage of the fracture surface shows reflective facets which represent grain surfaces exposed by an intergranular corrosion cracking. However, some highly reflective surfaces may be true cleavage surfaces which formed when fracture followed a preferential path along a pseudo-martensite-austenite interface in Type 304 steel. The exact mechanistic interpretation for the formation of fracture areas such as shown in Fig. 8 is uncertain. These photomicrographs are of matching areas in the two fracture surfaces. They possess surface features (“cleavage steps”) suggesting that their mode

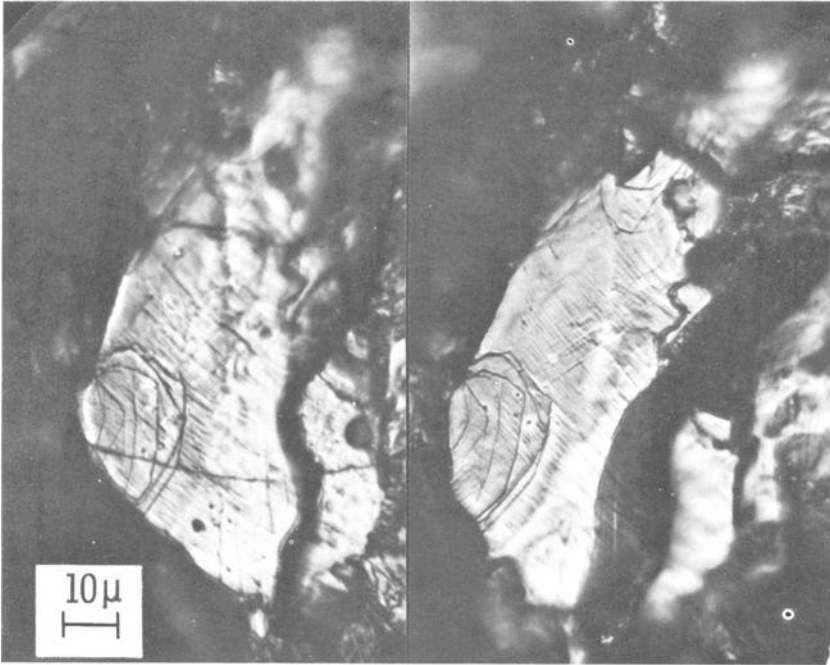


FIG. 8—Matching “cleavage facets” in fracture surfaces of Type 304 steel failed in boiling 42 per cent  $MgCl_2$  ( $\times 750$ ).

of formation was mechanical rather than electrochemical—yet electrochemical corrosion must necessarily occur in SCC of these alloys. The surface detail at  $\times 750$  does not indicate, however, any corrosion attack sufficiently intense to have altered or obscured the matching topography. In this case and in future work precise electron fractographs must be examined to determine the true degree of matching detail and whether superficial corrosion has in fact occurred on these surfaces. Such a study remains to be made to answer the point.

The stainless steels and refractory metals and alloys in general are particularly amenable to electron fractographic study through the use of oxide replicas. These possess the best dimensional stability of all surface replicas. Being the actual specimen surface thermally converted to a thin oxide film, this form of replica can provide the truest topographical information (Mahla and Nielsen [9]). Figure 9 is an example of oxide replication of a Type 304 stainless steel SCC fracture in which mixed modes of crack propagation are present. The central area shows a region of intergranular decohesion surrounded by areas of transgranular fracture. The smooth topography of the grain surface contrasts sharply with the topographic structure of the transgranular fracture. The latter frequently shows “river markings” similar to

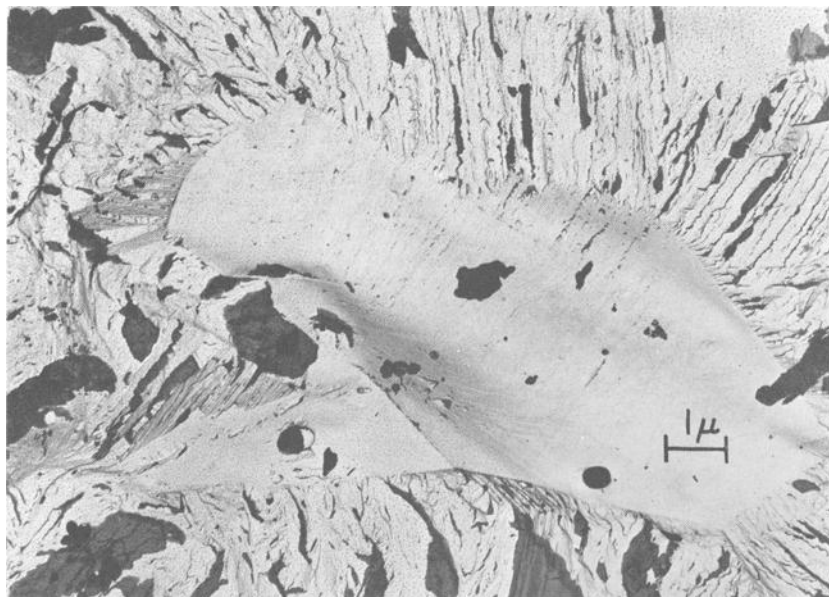


FIG. 9—Mixed modes of fracture produced by SCC of Type 304 steel (oxide replica) ( $\times 10,000$ ).

cleavage structure commonly found in brittle fractures where the environment has had no effect on the fracture process. The striations that are also present in the electron fractograph are best interpreted as crack-arrest lines. Another example of these is shown in Fig. 10.

Striations of this nature have been observed in other low strain SCC systems. They have been reported to occur in stress-corrosion cracked aluminum alloys and copper alloys. They will probably be found in other systems when electron fractography is applied to the study of stress-corrosion failures.

If the striations are crack-arrest lines, SCC cannot be considered as a confirmed form of purely electrochemical corrosion. The evidence points to their origin in a two-stage crack propagation process where short steps of corrosion alternate with steps of crack propagation by mechanical fracture. This periodic process, which appears to be crystallographically oriented, produces striations having a sawtooth profile and running at right angles to the direction of crack propagation.

The dark patches present in the electron fractographs of Figs. 9 and 10 are corrosion-product films randomly extracted with the oxide replica from the original fracture surfaces. That such corrosion products play a role in the SCC mechanism has been theorized by Nielsen [7] and Pickering et al [10].

The observation of striations in stress-corrosion fracture and their

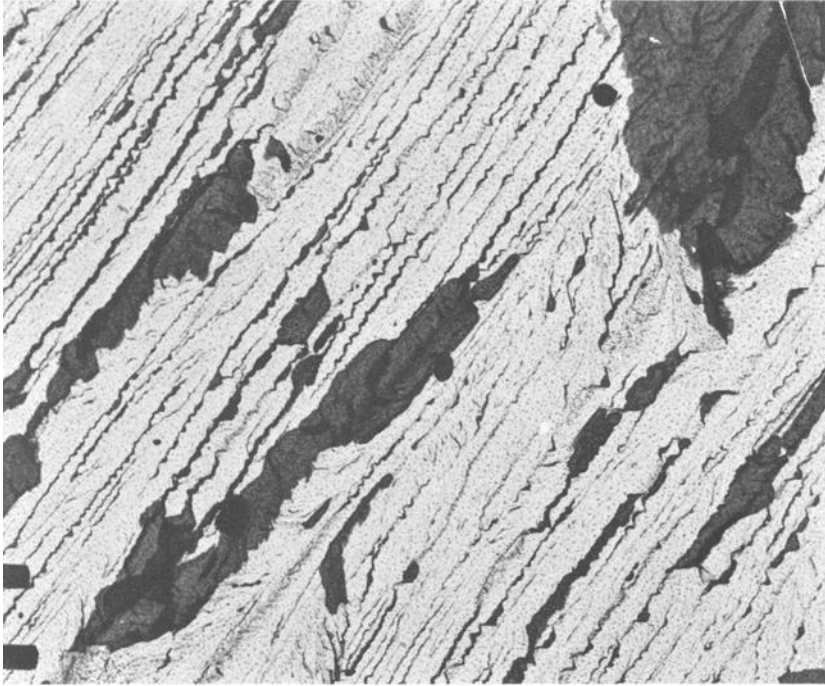


FIG. 10—*Striated fracture surface produced by SCC of Type 304 steel (oxide replica) ( $\times 10,000$ ).*

significance in terms of failure mechanism is being given increased attention. Nielsen [7] and Logan [11] have commented on striations markings in SCC of stainless steel. McEvily and Bond [12] have discussed striation formation in alpha brass and Al-5.5Zn-2.5Mg alloys during SCC. Their interpretation is in terms of a mechanism of periodic rupture of anodic films or tarnish layers. The common conclusion that investigation of these striation markings has developed is that SCC is not solely an electrochemical mechanism but does involve steps of mechanical fracture separating the stages of crack advance by electrochemical corrosion.

#### *Stress-Corrosion Cracking of Titanium Alloys*

Most titanium alloys are now known to be susceptible to hot salt stress-corrosion cracking or to accelerated failure or both when exposed under stress in a fatigue precracked condition to a variety of environments at ambient temperature. These environments include water, methanol, nitrogen tetroxide, and many aqueous and non-aqueous solutions and liquids. The mushrooming interest and activity stems from 1965 when Brown [13] reported at the national ASTM

meeting that titanium will crack when exposed as a stressed and pre-cracked cantilever beam to 3 per cent sodium chloride solution.

Hot salt stress-corrosion cracking has been known since 1957 [14] and was discussed in a symposium held at the ASTM Pacific Area National Meeting in Seattle, Wash., in 1965 [15]. Several of the studies reported at this Symposium utilized electron fractography to provide information on stress-corrosion crack propagation. Avery and Turley [16] identified both intergranular and transgranular propagation in 5Al-2.5Sn alloy. This alloy was much less resistant to SCC than 4Al-3Mo-1V alloy which cracked primarily along an intergranular path. The sites of crack initiation were grain boundaries and slip planes emergent in the surface exposed to the hot (600 to 800 F) synthetic sea salt.

One problem with replication of hot salt SCC fractures is the presence of corrosion products and adherent oxide films on the fracture surfaces. Martin [17], Hatch et al [18], and Rideout et al [19] mention this point. Even so, distinguishing intergranular fracture from transgranular fracture does not present special difficulty.

As examples of stress-corrosion cracking of titanium alloys at room temperature, two examples are given in this paper, both through the courtesy of C. D. Beachem of the U.S. Naval Research Laboratory. Figure 11 is an electron fractograph of a 6Al-4V titanium alloy which in test under sustained load in methanol (the specimen was not pre-cracked) developed a stress-corrosion crack along a machining mark. The fracture surface is characterized by elongated areas of cleavage showing shallow river-pattern markings. Alternating and interspersed bands and regions of dimpled rupture are also present. Meyn et al [20] suggested that the latter areas which are characteristic of microvoid coalescence may correspond to the ductile failure of ligaments remaining between the cleavage areas. Similar features, but with somewhat less cleavage, were observed in a similar specimen broken in distilled water. The respective  $K_I$  values for these stress-corrosion failures were 15 ksi  $\sqrt{\text{in.}}$  and 30 ksi  $\sqrt{\text{in.}}$ .

Another example of stress-corrosion cracking of a titanium alloy (7Al-2Cb-1Ta) in distilled water was reported by Meyn [21]. In this all martensitic,  $\alpha$ -phase alloy, the cleavage surfaces were sufficiently large (alloy grain size was  $\frac{1}{16}$  in. diameter) to permit the use of Laue back reflection X-ray diffraction techniques to determine the crystallographic orientation of the cleavage planes. The cleavage facets shown in Fig. 12 are inclined at an angle of  $16 \text{ deg} \pm 2 \text{ deg}$  from the  $(0001)\alpha$  plane. They are high index planes, contrary to the normal expectation of a low index cleavage plane, but there are two (or more) similar crystal planes along which the crack can propagate in a given grain.



FIG. 11—SCC in Ti-6A-4V alloy exposed to methanol [21] (crack initiated at machining mark on right) ( $\times 6000$ ).



FIG. 12—SCC in Ti-7Al-2Cb-1Ta alloy exposed to distilled water [21] ( $\times 4000$ ).

The reader interested in the subject of ambient temperature stress-corrosion cracking of titanium alloys is referred to the bibliography by Dahlberg [22] and to the DMIC Technical Note, 1 Feb. 1966 [23], which contains a summary of the whole subject of accelerated crack propagation of precracked titanium alloys. (The program of the 1967 Symposium at Battelle Memorial Institute is not known to the writer at the time of this writing.)

### Fractography in the Study of Radiation Effects

ASTM Committee E-10 on Radioisotopes and Radiation Effects has published four special technical publication volumes which discuss the effects of radiation on engineering materials and on flow and frac-

ture behavior [24-27]. Two ASM-AEC monographs have been published which also consider radiation effects on cladding, structural materials, and ferritic steels [28,29].

Although there are marked effects of neutron irradiation on the tensile and impact properties of steel as Trudeau [28] has detailed, there appears to be few reported applications of electron fractography on ferritic, irradiated steels. Wilson and Berggren (see bibliography, Chapter 3 in Ref 28) found that an ASTM A106 steel irradiated at 300 C broke after 6 per cent elongation with no necking down. The fracture surface showed about 50 per cent cleavage and 50 per cent intergranular fracture.

Bush [29] has summarized the effects on neutron irradiation on the mechanical properties of stainless steels. Marked increases in the yield strength occur with less pronounced increases in tensile strength. Decreases in elongation and reduction of area are observed. These effects, however, are decreased in magnitude when post-irradiation annealing and testing is carried out at or above 350 C. There is a nominal effect of irradiation on the impact strength of austenitic stainless steels; in ferritic stainless it is more marked.

In considering the loss of ductility phenomena which austenitic steels exhibit following exposure to nuclear reactor environments, one must distinguish between the water-cooled reactors operating in the 300 C temperature range and the gas-cooled (superheat) reactors operating at about 600 C.

In the former case fracture is intergranular and apparently the result of preferential grain boundary corrosion by the reactor coolant with  $\text{Cr}^{+6}$  ions accelerating attack (in the absence of carbide precipitation in the grain boundaries). The role of stress is one of acceleration of grain boundary dissolution and of the rate of intergranular fracture. The importance of the role of radiation is not clearly established. Figures 13, 14, and 15, all of Type 304 stainless steel cladding, illustrate this type of failure. It should be pointed out that the "dimple-like" areas in Fig. 14 contrast with the smooth intergranular separation shown in Fig. 13. That the features are not dimples was shown by stereoexamination of this area of the fracture. They are small hills and not to be confused with the equi-axed dimples characteristic of ductile rupture. Figure 15 is considered to be a faceted intergranular fracture (corrosion) surface on which crystallographic etching has occurred [30].

When austenitic stainless steels and high-nickel alloys are exposed to irradiation under superheat conditions, the temperatures,  $\sim 600$  C, result in intergranular carbide precipitation. Very long exposures (2000 h) cause matrix strengthening which in turn promotes intergranular fracture in room temperature tension tests. Figures 16 and 17 compare

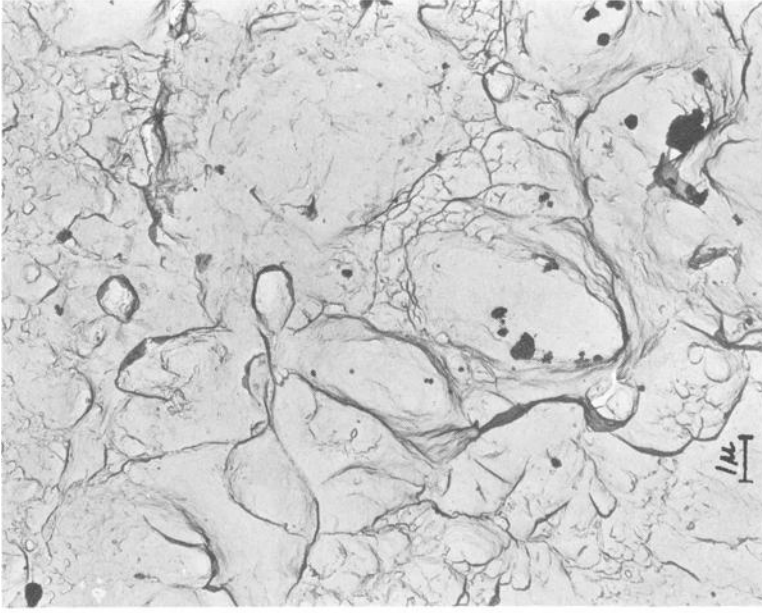


FIG. 14 – Nodular intergranular fracture in Type 304 stainless steel cladding [30] ( $\times 6000$ ).

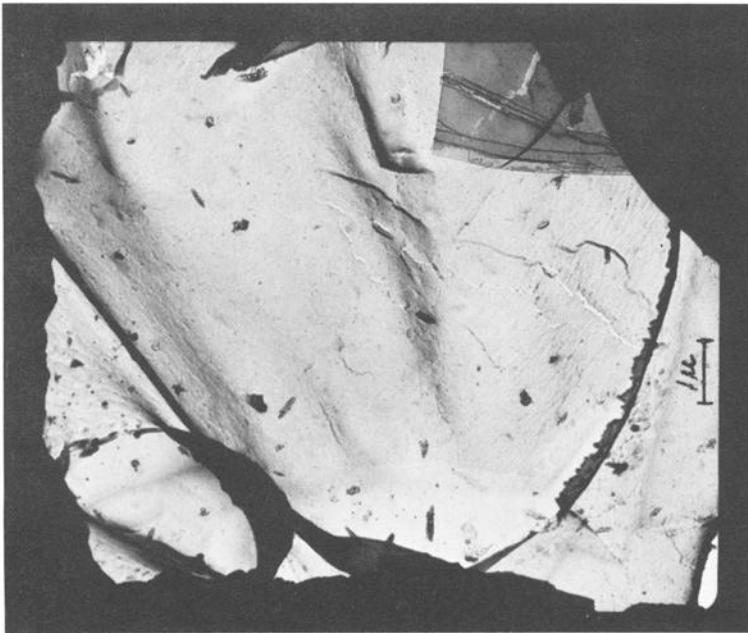


FIG. 13 – Grain boundary separation in failed Type 304 stainless steel cladding [30] ( $\times 9000$ ).

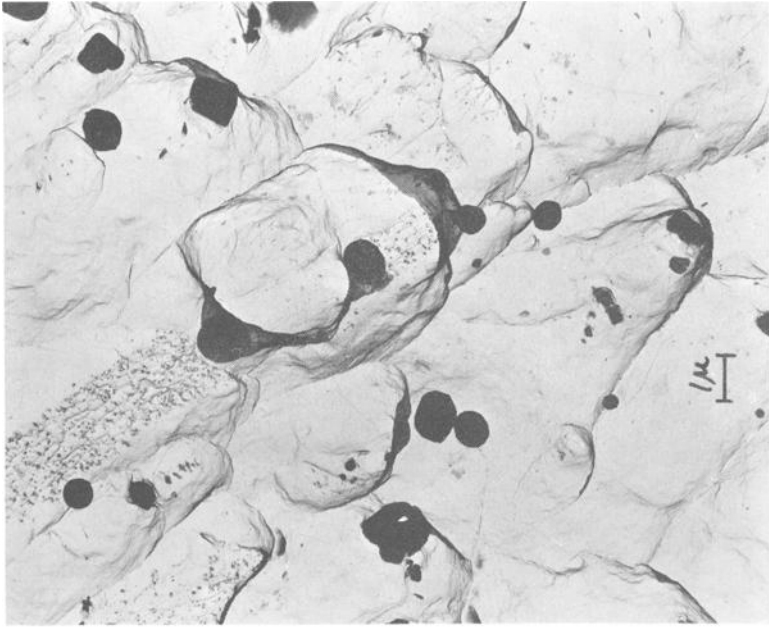


FIG. 16—Tensile fracture in as-received Hastelloy-X [31] ( $\times 6000$ ).

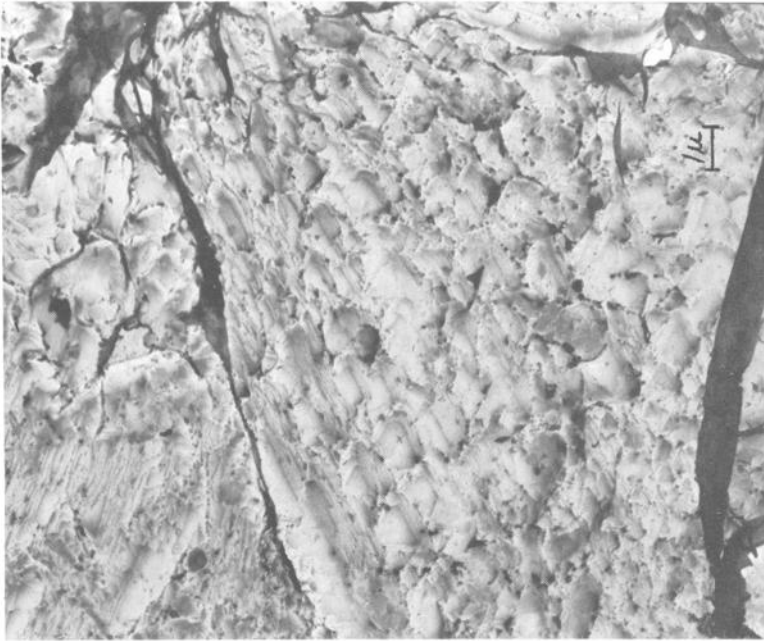


FIG. 15—Faceted fracture surface in Type 304 stainless steel cladding [30] ( $\times 6000$ ).

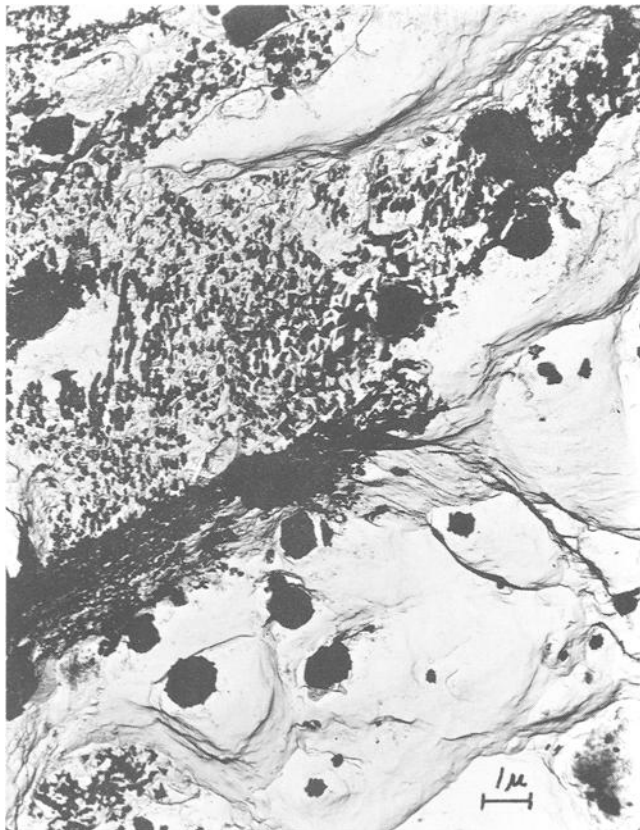


FIG. 17—Extraction replica of mixed ductile-brittle fracture in Hastelloy-X after exposure of 2000 h at 565 C [31] ( $\times 6000$ ).

the ductile fracture characteristics of Hastelloy X (22 per cent chromium, 19 per cent iron, 9 per cent molybdenum, balance nickel plus cobalt) in the as-received condition with those developed in the same alloy after 2000 h at 565 C. In the latter case the fracture is partially intergranular (brittle). Separation occurs along the interface of an austenite grain and a continuous grain boundary network of precipitated carbide. When a grain boundary is not conveniently oriented relative to the axis of the applied tensile load, ductile transgranular rupture occurs [31].

The effects of irradiation show up only in tension tests at 600 or 700 C. Irradiated specimens fracture in a brittle intergranular mode. Unirradiated specimens are ductile. The research investigations at the General Electric Vallecitos Nuclear Center indicate that irradiation enhances matrix strengthening and matrix-carbide precipitation which in turn would result in the increased high temperature brittleness ob-

served in the irradiated austenitic alloys. Electron fractographs of irradiated Type 304 stainless steel, Incoloy 800, and Inconel 600 appear in Figs. 18 through 21. Carbides of several different morphological forms are shown in the carbon-extraction replicas of Figs. 18 and 19. These fractographs were made at the failure region of Type 304 superheat fuel cladding [32]. Inconel 600 alloy cladding exhibited a completely intergranular fracture when tensile tested at 700 C (Fig. 20). Incoloy 800 showed a partly intergranular, partly ductile fracture on tensile testing at 600 C (Fig. 21) [33].

Zircaloy-2 (1.2 to 1.7 per cent tin, 0.07 to 0.20 per cent iron, 0.05 to 0.15 per cent chromium, 0.03 to 0.18 per cent nickel, <100-ppm nitrogen, balance zirconium) and other zirconium alloys are discussed by Bush [29] as materials of construction for water-cooled nuclear reactors. The effect of irradiation is perhaps best reflected in the notch



FIG. 18—Fracture of irradiated fuel cladding (Type 304 steel) at 600 C superheat. Extraction replica [32] ( $\times 3750$ ).

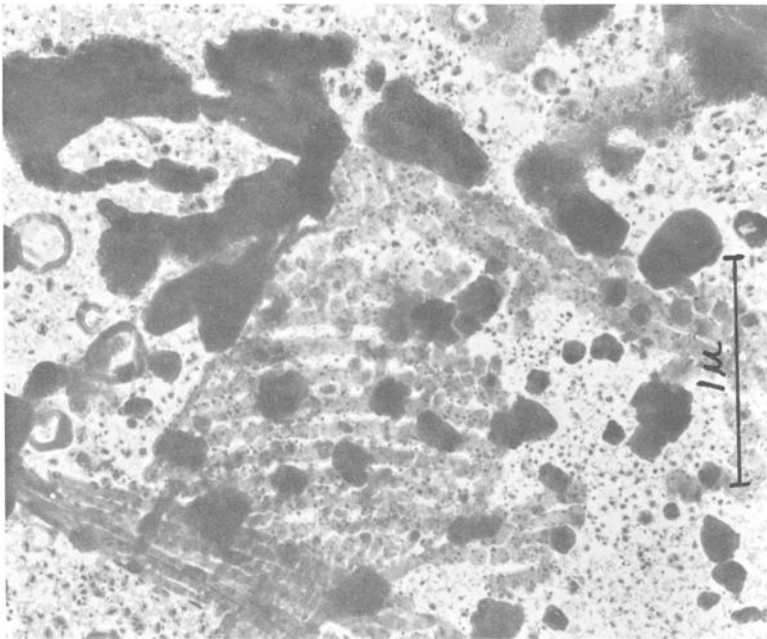


FIG. 19—Fracture of irradiated Type 304 steel fuel cladding at 600 C superheat. Extraction replica [32] ( $\times 30,000$ ).

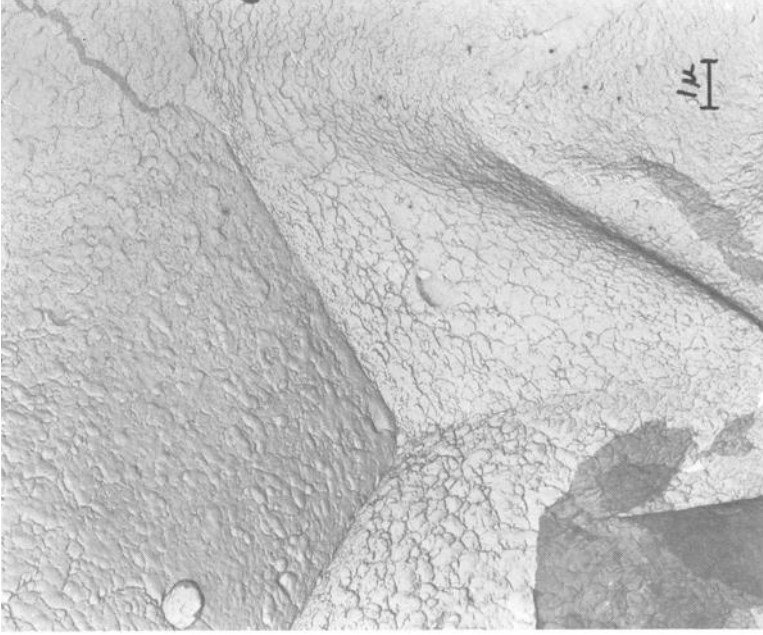


FIG. 20—Intergranular fracture at 700 C in irradiated Inconel 600 fuel cladding [33] ( $\times 6000$ ).

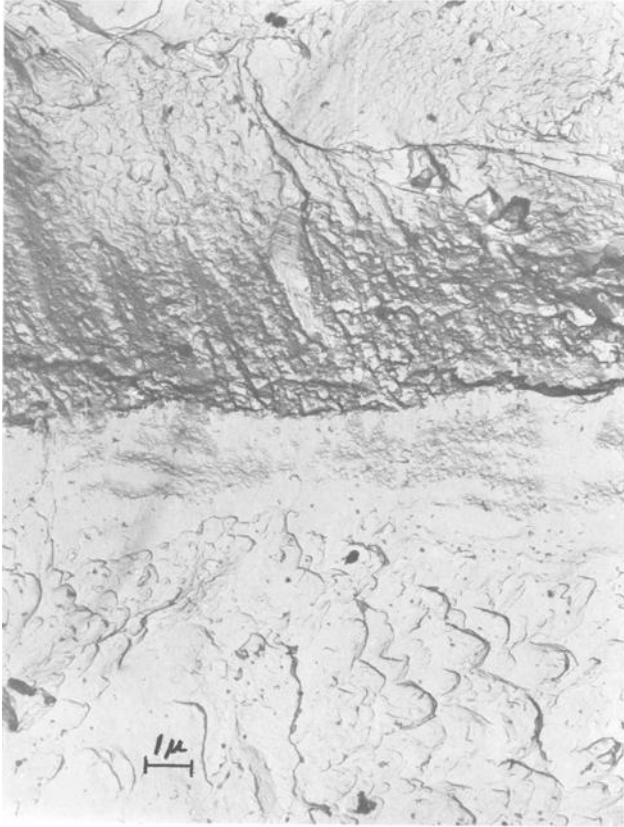


FIG. 21—Mixed ductile-brittle fracture at 600 C in irradiated Incoloy-800 fuel cladding [34] ( $\times 6000$ ).

tensile properties as a function of cold work, temperature of irradiation, integrated flux, and direction. Above about 40 per cent cold work notch strength and ductility decrease very sharply at high flux densities. The effects of irradiation on the fractographic characteristics of Zircaloy-2, however, are somewhat confusing. Figures 22 and 23 are included to show the comparison of ductile fracture in unirradiated Zircaloy-2 cladding for fuel rods with the partially brittle fracture of irradiated alloy. Figure 23 shows cleavage and intergranular separation, as well as ductile rupture [34].

Electron fractographic studies have also been made at Battelle Memorial Institute of fission-fragment effects<sup>3</sup> in Type 304 stainless steel and Zircaloy-2 for short time exposures at 150 C. The effect of neutron irradiation<sup>3</sup> was also examined on these alloys whose stress-

<sup>3</sup>The neutron exposure was about  $9.2 \times 10^{16}$  nvt; the fission-recoil exposure was about  $2.1 \times 10^{14}$  fragments  $\text{cm}^{-2}$ .

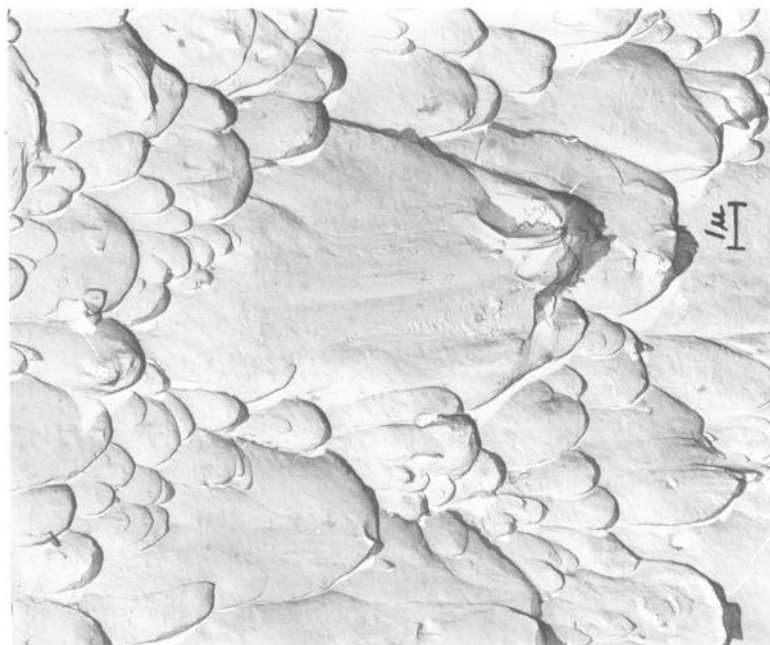


FIG. 22—Fracture in unirradiated burst specimen of Zircaloy-2 [34] ( $\times 6000$ ).

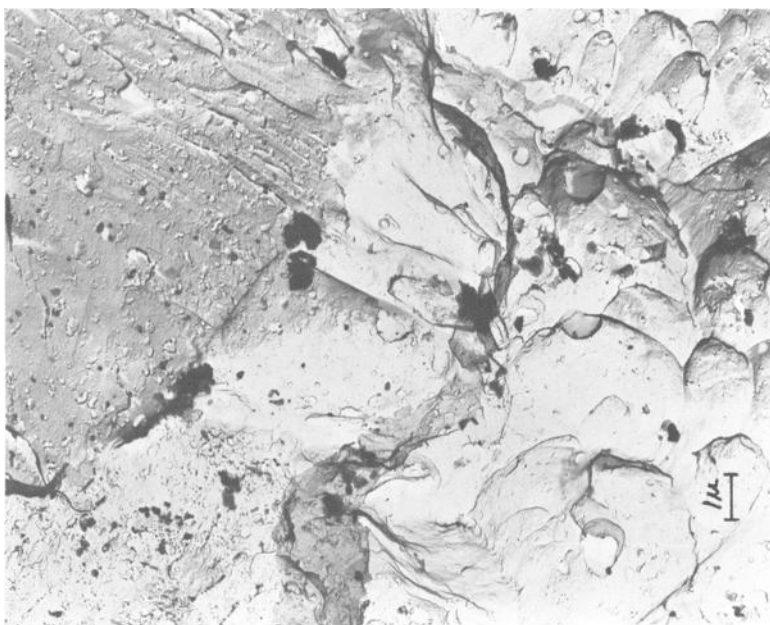


FIG. 23—Fracture in irradiated burst specimen of Zircaloy-2 [34] ( $\times 6000$ ).

strain behavior was determined by bend tests. The electron fractography did not reveal any changes in the fracture mode of either the Type 304 stainless steel or the Zircaloy-2 alloy as a result of exposure to neutron irradiation or fission-fragments. In all specimens fracture occurred by a dimpled rupture mechanism [35]. Other work in which fission-fragment damage in irradiated Type 304 stainless steel resulted in intergranular cracking and microstructural effects at grain boundaries has been reported by Rosenbaum et al [36].

### Summary

The examples of application of electron fractography to environmental effects (chemical and radiation) on fracture presented in this paper are only a brief sampling of past and present research areas in which this technique has demonstrated its value. Its utility is growing in a wide spectrum of service failure analyses. Concurrent research is developing new applications and an increased facility and confidence in the interpretation of fractographic features. Hopefully, electron fractography will ultimately provide reliable differentiation and explanation of many of the presently puzzling fracture phenomena metals and alloys exhibit in their stress-strain-environmental relationships.

### Acknowledgment

The author wishes to acknowledge gratefully the contributions of several others to this paper. C. D. Beachem (Naval Research Laboratory) provided the electron fractographs of the titanium alloys. H. S. Rosenbaum and U. E. Wolff (General Electric Co.) contributed all of the figures and pertinent references to the section on Fractography in the Study of Radiation Effects. J. L. McCall contributed the report of the Battelle study on fission-fragment effects.

### References

- [1] Phillips, A. et al, "Specific Applications of Electron Fractography," Section 6, *Electron Fractography Handbook*, AFML-TR-64-416, 31 Jan. 1965.
- [2] Elsea, A. R. and Warke, W. R., "Electron Microscopic Fractography," DMIC Memorandum 161, 21 Dec. 1962.
- [3] Tiner, N. A. and Gilpin, C. B., "Microprocesses in Stress Corrosion of Martensitic Steels," *Corrosion*, Vol. 22, No. 10, Oct. 1966, pp. 271-279.
- [4] Phelps, E. H. and Mears, R. B., "The Effect of Composition and Structure of Stainless Steels Upon Resistance to Stress-Corrosion Cracking," First International Congress on Metallic Corrosion, London, 10-15 April 1961, Butterworths, 1962, pp. 319-327.
- [5] Matsushima, I., Deegan, D., and Uhlig, H. H., "Stress Corrosion and Hydrogen Cracking of 17-7 Stainless Steel," *Corrosion*, Vol. 22, No. 1, Jan. 1966, pp. 23-27.
- [6] Douglass, D. L., Thomas, G., and Roser, W. R., "Ordering, Stacking Faults, and Stress-Corrosion Cracking in Austenitic Alloys," 2nd International Congress on Metallic Corrosion, New York, 11-15 March 1963, National Association of Corrosion Engineers, 1966, pp. 66-79.
- [7] Nielsen, N. A., "The Role of Corrosion Products in Crack Propagation in

- Austenitic Stainless Steel. Electron Microscopic Studies," *Physical Metallurgy of Stress Corrosion Fracture*, Metallurgical Society Conferences, Vol. 4, Interscience, New York, 1959, pp. 121-154.
- [8] Nielsen, N. A., "Nature of Initial Corrosion of Stressed Austenitic Stainless Steel by Chloride Ions," *2nd International Congress on Metallic Corrosion*, New York, 11-15 March 1963, National Association of Corrosion Engineers, 1966, pp. 116-123.
  - [9] Mahla, E. M. and Nielsen, N. A., "An Oxide Replication Procedure for Stainless Steels and High Nickel Alloys," *Journal of Applied Physics*, Vol. 19, 1948, p. 378.
  - [10] Pickering, H. W., Beck, F. H., and Fontana, M. G., "Wedging Action of Solid Corrosion Product During Stress Corrosion of Austenitic Stainless Steels," *Corrosion*, Vol. 18, No. 6, June 1962, pp. 230t-239t.
  - [11] Logan, H. L., McBee, M. J., and Kahan, D. J., "Evidence for an Electrochemical-Mechanical Stress Corrosion Fracture in a Stainless Steel," *Corrosion Science*, Vol. 5, 1965, pp. 729-730.
  - [12] McEvily, A. J. and Bond, A. P., "On Film Rupture and Stress-Corrosion Cracking," *Environment-Sensitive Mechanical Behavior*, Gordon and Breach, New York, 1966, pp. 421-443.
  - [13] Brown, B. F., "A New Stress-Corrosion Cracking Test Procedure for High Strength Alloys," *Materials Research & Standards*, Vol. 6, No. 3, March 1966.
  - [14] Stough, D. W., Fink, F. W., and Peoples, R. S., "The Stress Corrosion and Pyrophoric Behavior of Titanium and Titanium Alloys," TML Report No. 84, DMIC, Battelle Memorial Institute, Columbus, Ohio, 15 Sept. 1967.
  - [15] *Stress-Corrosion Cracking of Titanium*, ASTM STP 397, American Society for Testing and Materials, 1966.
  - [16] Turley, R. V. and Avery, C. H., "Elevated-Temperature Static and Dynamic Sea-Salt Stress Cracking of Titanium Alloys," *Stress-Corrosion Cracking of Titanium*, ASTM STP 397, American Society for Testing and Materials, 1966, pp. 1-30.
  - [17] Martin, G., "Investigation of Long-Term Exposure Effects Under Stress of Two Titanium Structural Alloys," *Stress-Corrosion Cracking of Titanium*, ASTM STP 397, American Society for Testing and Materials, 1966, pp. 95-121.
  - [18] Hatch, A. J., Rosenberg, H. W., and Erbin, E. F., "Effects of Environment on Cracking in Titanium Alloys," *Stress-Corrosion Cracking of Titanium*, ASTM STP 397, American Society for Testing and Materials, 1966, pp. 122-136.
  - [19] Rideout, S. P., Louthan, M. R., Jr., and Selby, C. L., "Basic Mechanisms of Stress-Corrosion Cracking of Titanium," *Stress-Corrosion Cracking of Titanium*, ASTM STP 397, American Society for Testing and Materials, 1966, pp. 137-151.
  - [20] Meyn, D. A., Dahlberg, E. P., and Beachem, C. D., "Analysis of Stress-Corrosion Cracking of Ti-6Al-4V Fuel Tank Material in Methyl Alcohol," NRL Memorandum Report 1744, Jan. 1967, Naval Research Laboratory, Washington, D.C.
  - [21] Meyn, D. A., "Micromechanical Metallurgy (A study of the Crystallographic Orientation of Cleavage Facets Produced by Stress-Corrosion Cracking of Ti-7Al-2Nb-1Ta in Water)," Report of NRL Progress, Naval Research Laboratory, Aug. 1965, pp. 21-23.
  - [22] Dahlberg, E. P., "An Annotated Bibliography of Recent Papers and Reports on the Subject of Ambient Temperature Aqueous Stress-Corrosion Cracking of Titanium and Titanium Alloys," AD 642128 Oct. 1966, Naval Research Laboratory, Washington, D.C.
  - [23] Jackson, J. D. and Boyd, W. K., "The Stress-Corrosion and Accelerated Crack-Propagation Behavior of Titanium and Titanium Alloys," DMIC Technical Note, 1 Feb. 1966, DMIC Battelle Memorial Institute, Columbus, Ohio.
  - [24] *Radiation Effects on Materials*, ASTM STP 233, American Society for Testing and Materials, 1959.
  - [25] *Reactor Structural Materials: Engineering Properties as Affected by Nuclear Reactor Service*, ASTM STP 314, American Society for Testing and Materials, 1962.
  - [26] *Radiation Effects on Metals and Neutron Dosimetry*, ASTM STP 341, American Society for Testing and Materials, 1963.
  - [27] *Flow and Fracture of Metals and Alloys in Nuclear Environments*, ASTM STP 380, American Society for Testing and Materials, 1965.

- [28] Trudeau, L. P., *Radiation Effects on Toughness of Ferritic Steels for Reactor Vessels*, Rowman and Littlefield, New York, 1964.
- [29] Bush, S. H., *Irradiation Effects in Cladding and Structural Materials*, Rowman and Littlefield, New York, 1965.
- [30] Low, J. R., Jr., Wolff, U. E., and Cowden, W. C., "Electron Microscopic Examination of Failed Stainless Steel Fuel Cladding—Dresden Advanced Fuel Assembly PF-1 and PF-4," General Electric Company Report, APED-4242, March 1966.
- [31] Comprelli, F. A. and Wolff, U. E., "Stability of High-Nickel Alloys in Superheated Steam," AEC Research and Development Report, GEAP-4745, Atomic Energy Commission, Nov. 1964.
- [32] Hazel, V. E. et al, "Fuel Irradiations in the ESADE-VBWR Nuclear Superheat Loop," AEC Research and Development Report, GEAP-4775, Atomic Energy Commission, March 1965.
- [33] Beaudreau, B. C. et al, "Tensile Properties of Fuel Clad Materials Irradiated in Superheat Environments," AEC Research and Development Report, GEAP-4754, Atomic Energy Commission, April 1965.
- [34] Williamson, H. E. et al, "AEC Fuel Cycle Program Examination of Zircaloy Clad  $UO_2$  Fuel Rods Operated in the VWBR to 10,000 MWD/TU," AEC Research and Development Report, GEAP-4597, Atomic Energy Commission, March 1965.
- [35] DeMastry, J. A. et al, "Fission-Fragment Effects in Structural Materials," Report No. BMI-1766, 22 March 1966, Battelle Memorial Institute, Columbus, Ohio.
- [36] Rosenbaum, H. S., Armijo, J. S., and Wolff, U. E., "Fission-Fragment Damage to Type 304 Stainless Steel Fuel Cladding," AEC Research and Development Report, GEAP-5002, Atomic Energy Commission, 1966.

B. V. Whiteson,<sup>1</sup> A. Phillips,<sup>1</sup> V. Kerlins,<sup>1</sup>  
and R. A. Rawe<sup>1</sup>

## Special Fractographic Techniques for Failure Analysis

---

**REFERENCE:** Whiteson, B. V., Phillips, A., Kerlins, V., and Rawe, R. A., "Special Fractographic Techniques for Failure Analysis," *Electron Fractography, ASTM STP 436*, American Society for Testing and Materials, 1968, pp. 151-178.

**ABSTRACT:** In order to assist the investigator of service failures, work was performed using electron fractographic methods to resolve three separate problems that have not been solvable using the more conventional macro- or light microscopic techniques. Three independent problems were examined, and solutions were achieved. These were: (1) determination of fracture direction in thin sheet metal components, (2) differentiating between hydrogen embrittlement and stress corrosion in high-strength steels, and (3) determination of applied cyclic stress as a function of fatigue striation spacing.

The results of the investigation indicated that:

1. Fracture direction in thin sheet-metal components can be determined by replicating the acute angle shear lip. The direction of open dimples with respect to the fracture edge indicated the fracture direction in the plane of fracture.

2. There is reasonable evidence that stress corrosion and hydrogen embrittlement fractures in high-strength steel can be separated by the following: (a) Hydrogen embrittlement fractures initiated subsurface, while stress corrosion fractures initiated at the free surface. (b) The corrosion attack in hydrogen embrittlement fractures, if present, was random while in stress corrosion the oxidation products were more concentrated at the nucleus. (c) Stress corrosion fractures had stronger indications of secondary cracking than hydrogen embrittlement failures. (d) The fracture features on the hydrogen embrittled specimens were more clearly defined than those on the stress corrosion fractures.

3. A correlation was established between cyclic stress and fatigue striation spacing for several aluminum alloys over a wide range of alternating and mean stresses in thicknesses of 0.050 and 0.500 in. The correlation was empirically derived.

**KEY WORDS:** electron microscope, fractography, failure analysis, fracture, replication methods, hydrogen embrittlement, stress corrosion, fatigue (materials), crack propagation rates, fracture toughness, aluminum, steel, sustained load testing, intergranular fracture, cadmium plating, high-strength materials

<sup>1</sup> Chief, Metallurgy Development Section; group leader, Electron Microscope Laboratory; research and development engineer, Electron Microscope Laboratory; and group leader, Development Metallurgy, respectively, Metals-Ceramics Branch, Materials Research and Production Methods Dept., Missiles and Space Systems Div., Douglas Aircraft Co., Santa Monica, Calif. Mr. Rawe is a personal member of ASTM.

Although service failure analysis has many aspects, its final objective is structural improvement. Since it is essential to examine the fracture origin, a technique must be developed for the determination of fracture direction in sheet materials which exhibit none of the usual macroscopic features associated with fracture direction. If the mode of fracture at the origin is hydrogen embrittlement or stress corrosion, distinguishing between these two modes is a difficult task since the fracture appearances are quite similar. In case of fatigue, it would be advantageous to be able to calculate propagation stresses by observing the variation in striation spacings. The following three sections of this paper present the results of work directed towards solving these specific problems:

1. Determination of fracture direction in thin sheet-metal components.
2. Differentiation between hydrogen embrittlement and stress corrosion in high strength steel.
3. Determination of applied cyclic stress as a function of fatigue striation spacing.

### **Problem 1 – Determination of Fracture Direction in Thin Sheet-Metal Components**

In service failure analysis, an extremely important aspect of the investigation usually centers around locating the origin or nucleus of the fracture. Generally, the fracture origin holds the key to the reason for failure and also paves the way for corrective action. If the origin is not clearly identifiable visually, the most common method of locating it is to trace the fracture direction on the failed components back to a common intersection point. The ability to trace fracture direction on the failed components generally depends on macroscopic features such as chevron marks, localized zones of plane strain, hackle marks [1],<sup>2</sup> etc. This task becomes difficult, if not impossible, when all of the fracture is oblique shear, which is usually the case with relatively thin, ductile materials that are used in the skins of aircraft and the fuel tanks of missiles and launch vehicles. In this case there are no macroscopic features that are clearly identifiable with fracture direction, much to the frustration of the investigator.

The purpose of this work was to find out if the electron microscope could provide a method to determine fracture direction in thin sheet-metal components.

### **Experimental Procedure**

The materials investigated for the determination of fracture direction were several high-strength steels, aluminum alloys, and a nickel base superalloy. Two thicknesses, 0.050 and 0.125 in., were employed for

<sup>2</sup> The italic numbers in brackets refer to the list of references appended to this paper.

each alloy. Two types of specimens were tested in order to obtain a tensile tear (Fig. 1a) and a combined shear and tear fracture (Fig. 1b). All materials failed with fractures that had 100 per cent oblique shear, Fig. 2, with no areas of plane strain that provided any macroscopic indication of fracture direction.

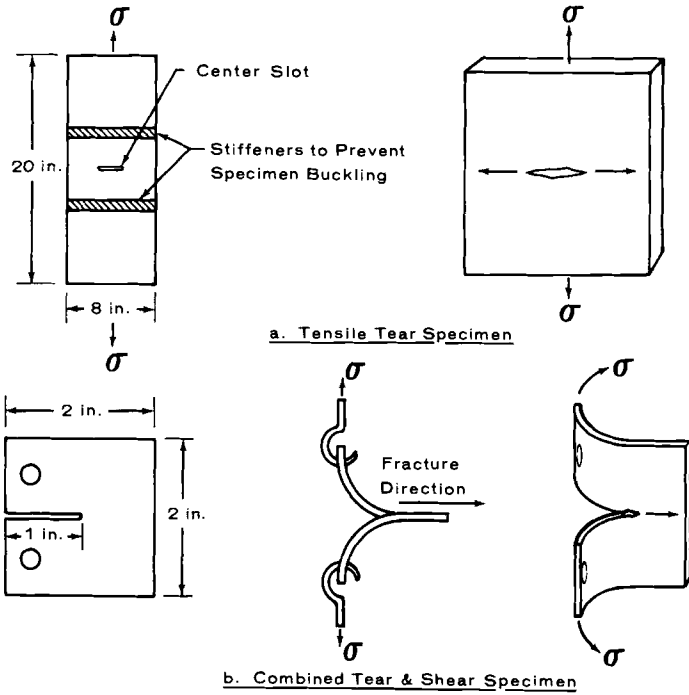


FIG. 1—Configuration of test specimens.

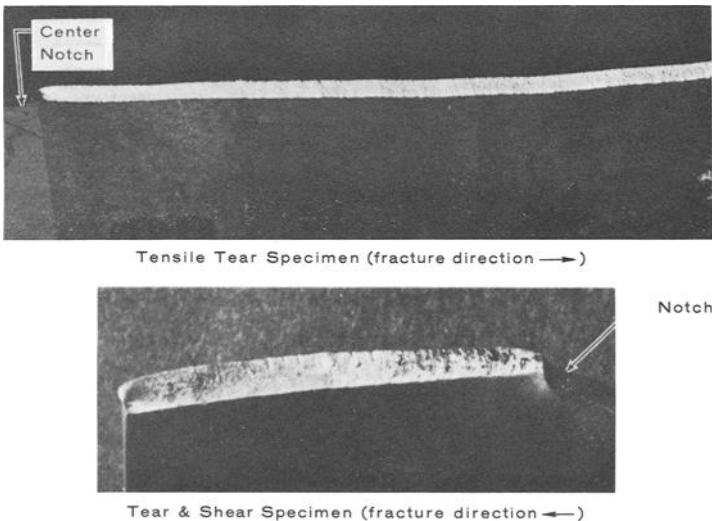


FIG. 2—The appearance of the fracture surface of tensile tear and shear specimens.

**Results**

In all specimens, fracture direction was discernible using the electron microscope, and it is believed that the technique for determining fracture direction is applicable to all materials that fail by dimple rupture [2]. For simplicity, none of the individual materials tested are delineated in the illustrations, since the fractographic features analyzed are identical, except for the relative size and abundance of the observed dimples.

The basic concept of determining fracture direction that applies to all materials which fail by dimple rupture is illustrated in Fig. 3. For all

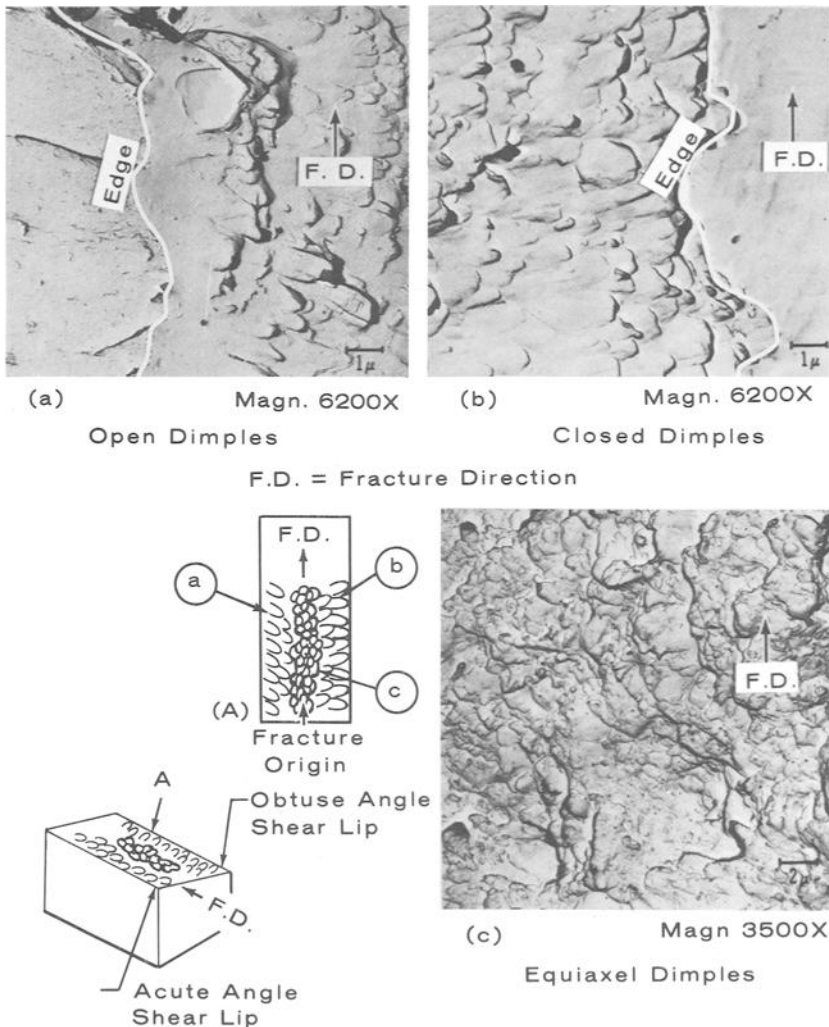


FIG. 3—Relationship between orientation of open dimples along fracture edge and fracture direction.

specimens tested, the open elongated dimples (dimples with the open end of their parabolas toward the fracture edge) along the edge of the rupture point back to the fracture origin (Fig. 3a). The open dimples occur exclusively on the acute angle shear lip. The closed elongated dimples (dimples with the closed ends of their parabolas toward the fracture edge) along the obtuse angle shear lip and those found in the center of the fracture were usually randomly oriented and could not be used for fracture direction determination (Fig. 3b and c).

The acute angle shear lip was replicated by the plastic-carbon technique [2] in such a way as to overlap the edge of the fracture. In order to orient the replica with respect to the fractured specimen, one or both corners of a rectangular replica were cut so as to indicate the desired orientation. The replica was then placed in the electron microscope so that the replica orientation with respect to the fracture could be maintained in the electron fractograph. The fracture direction was then related back to the actual specimen. The complete technique is illustrated in Fig. 4.

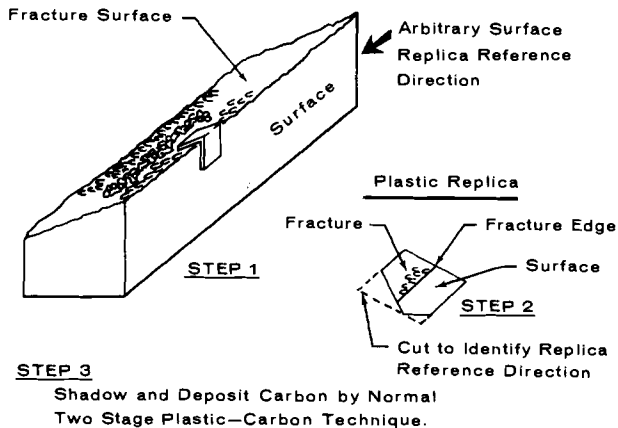


FIG. 4—Fracture direction replication technique.

It was very important to obtain a good replica of the fracture edge and the open dimples immediately adjacent to it. This was essential because the orientation of the open dimples had to be determined locally with respect to the edge. In obtaining an accurate indication of the edge line, low magnification (approximately  $\times 500$ ) electron microscopy techniques were used instead of optical microscopy because of resolution and depth of field requirements. A series of overlapping electron fractographs were taken along the edge region in order to obtain an accurate sense of the dimple direction. A typical low magnification electron fractograph showing open dimples along a fractured edge is shown in Fig. 5.

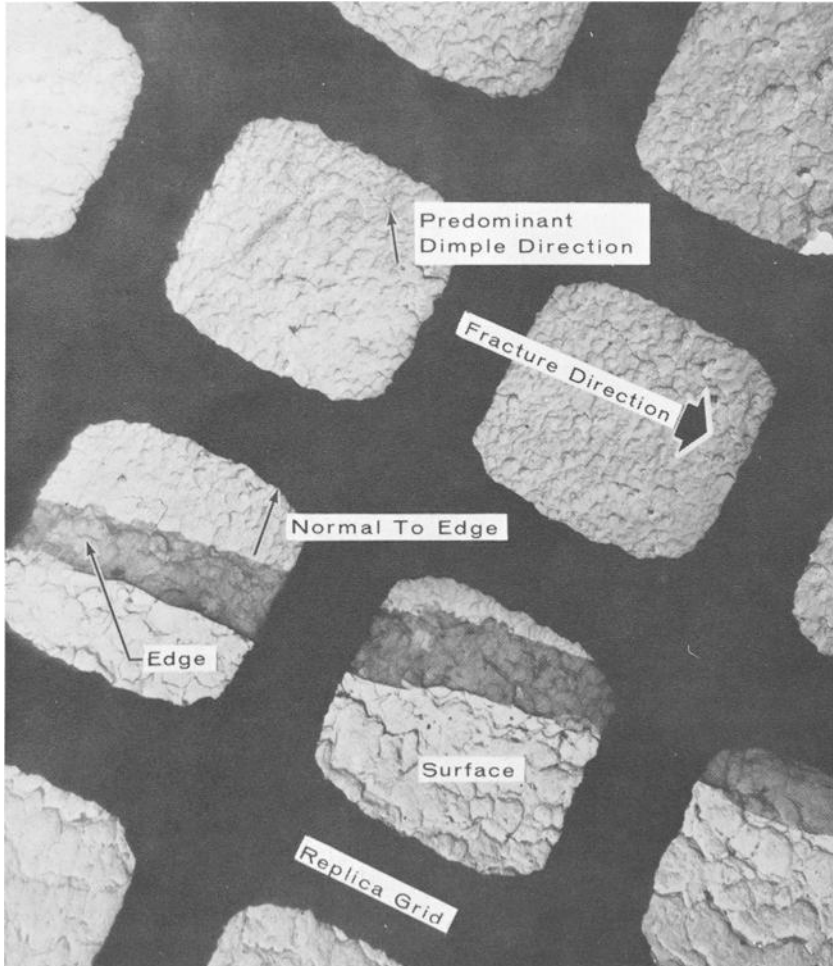


FIG. 5—Open dimples along fracture edge indicate fracture direction ( $\times 400$ ).

## Discussion

The sensitivity of dimples to fracture direction can be explained by considering the basic difference between shear and tear dimples. In case of a “pure” shear fracture, the dimples point in opposite directions on mating fracture surfaces [2]. In case of a “pure” tear, the dimples point in the same direction (back to the fracture origin) on both mating fracture surfaces. Since from a practical standpoint no fracture occurs by pure shear alone, that is, some tearing always accompanies a running fracture in thin sheet material, the resulting elongated dimples observed on a fracture surface are the end product of a combined shear and tear type of fracture. If a fracture propagates predominantly by a tear mechanism, the elongated dimples would point more strongly in

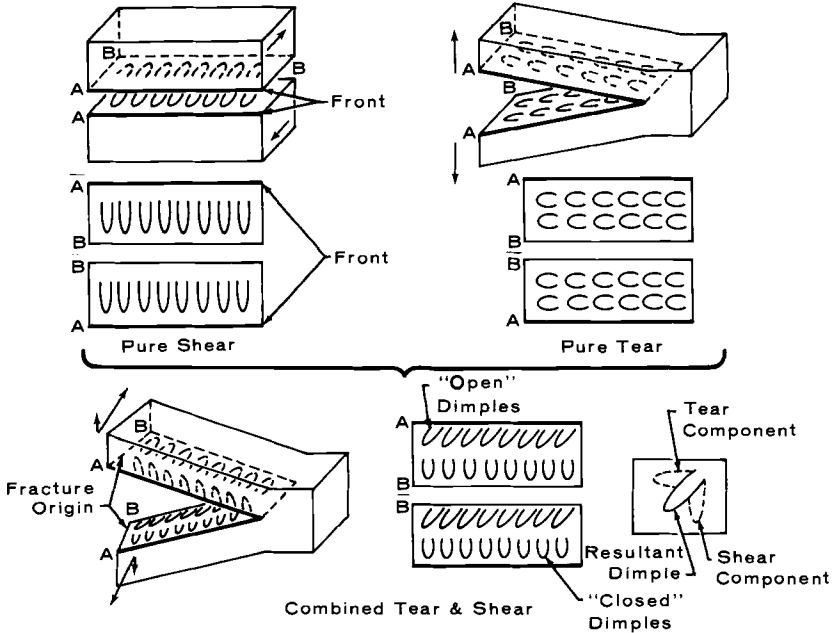


FIG. 6—Relationship between open dimple orientation and fracture origin.

the direction of fracture origin than if it propagated primarily by a shear mechanism. This concept of resultant combined dimples is illustrated in Fig. 6.

It is not clear, however, why open dimples are consistent in their orientation with respect to fracture direction while closed dimples have shown inconsistency. Assuming that a fracture separation can be non-symmetrical, it is difficult to explain why this nonsymmetry should only affect closed dimples since their apparent "twin" is an open dimple which is oriented in a systematic and orderly fashion. Perhaps discontinuous propagation at the center of the fracture (voids occurring ahead of the crack front) could account for the lack of orderly dimple orientation in this region.

### Conclusions

1. It is possible to determine fracture direction in thin sheet-metal that fails in an oblique shear mode, and by dimpled rupture, by observing the orientation of open dimples along the fracture edge at the acute angle shear lip.
2. Replicas must be made so that they overlap the fracture surface and the sheet-metal face, coupled with low magnification microscopy, in order to obtain an accurate assessment of the open dimple orientation with respect to the fracture edge.
3. The type of material examined is not important, as long as dimples are visible on the fracture surface.

## Problem 2—Electron Fractographic Technique for Distinguishing Stress Corrosion from Hydrogen Embrittlement in High-Strength Steels

Stress corrosion and hydrogen embrittlement have been a common and exceptionally perplexing source of service failures in the high-strength, medium-carbon, low-alloy steels. These fractures most commonly occur on components that have long life spans and exist under some level of sustained stress even when the component is not in use. There have been attempts to distinguish between the appearances of the fractures caused by stress corrosion and hydrogen embrittlement without substantial success because the two failure types exhibit a remarkably similar fracture appearance [2]. It would be of great importance in failure analysis to have the ability to recognize differences in the fracture appearances of the two failure mechanisms so that appropriate corrective action can be taken.

### Experimental Procedure

Sustained load tests were conducted to produce failures due to stress corrosion or hydrogen embrittlement. The alloys selected were forged 4340, 4330M, and D6AC. The mechanical properties are shown in Table 1. The sustained load specimen configuration is shown in Fig. 7.

TABLE 1—Mechanical properties of steels used for hydrogen embrittlement and stress corrosion tests.

Material	Thickness, in. <sup>a</sup>	Strength	
		$F_{tu}$	$F_{1v}$
4340 .....	0.050	277.2	240.9
4330M .....	0.050	224.4	193.8
D6AC .....	0.050	289.6	243.2

<sup>a</sup> Cut from 4½-in. billet in the transverse grain direction.

To evaluate hydrogen embrittlement, three distinct cadmium plating processes were used to provide qualitative differences in the hydrogen levels in the test specimens:

1. Acid pickle plus cadmium fluoborate plating.
2. Bright cadmium cyanide plating.
3. Cadmium fluoborate plating.

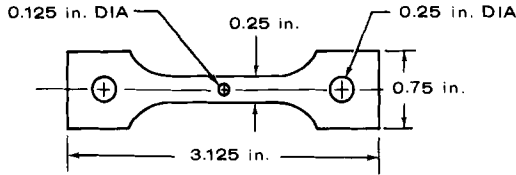


FIG. 7—Configuration of hydrogen embrittlement and stress corrosion specimens.

All plating conformed to the requirements of QQ-P-416, except that specimens were not embrittlement relief baked after plating. This was done to ensure specimen failure. The stress corrosion specimens were tested in the bare and vacuum cadmium plated condition (MIL-L-3387). Both hydrogen embrittlement and stress corrosion tests were conducted at 50, 75, and 90 per cent of yield strength. Specimens were axially loaded in single spring jigs. The hydrogen embrittlement tests were conducted in plastic bags containing silica gel desiccant. The stress corrosion tests were conducted by alternate immersion in deionized water (10 min in water, 50 min in air).

## Results

The electron fractographic examination of known stress corrosion and hydrogen embrittlement fractures revealed similar characteristics for the steels examined, and it appeared that no exclusive single feature precisely identifies either fracture mechanism. However, a combination of features could be used to distinguish between the two types of failure. The features associated with stress corrosion fracture were:

1. Predominantly surface nucleation of intergranular fracture.
2. Intergranular regions show pronounced secondary cracking or deep crevices.
3. A relatively greater amount of oxidation or corrosion attack at the nucleus and slow growth region than in the rapid fracture area.
4. Less pronounced hairline indications on the intergranular surfaces of stress corrosion fractures in comparison to intergranular surfaces of hydrogen embrittlement fractures.

The fractures associated with hydrogen embrittlement were:

1. Predominantly subsurface nucleation of intergranular fracture.
2. Both the nucleus and the rapid fracture areas exhibit equal degrees of (postfracture) oxidation or corrosion products.
3. Evidence of partial dimples and distinct hairline indications in the intergranular regions.

In order to determine whether a fracture nucleus was surface or subsurface, a two-stage plastic-carbon replication technique was used. The suspected nucleus region was marked by placing a fine scribe line on the free surface next to the nucleus area. The plastic replica was

allowed to overlap the edge so as to include the scribe line on the free surface. This line was then used as a guide to locate the nucleus area. The differences between the nucleus regions of stress corrosion and hydrogen embrittlement fractures are shown in Fig. 8. In the case of stress corrosion, the intergranular nucleus area followed the surface and extended straight back from the surface. In the case of hydrogen embrittlement, the intergranular nucleus region formed predominantly subsurface.

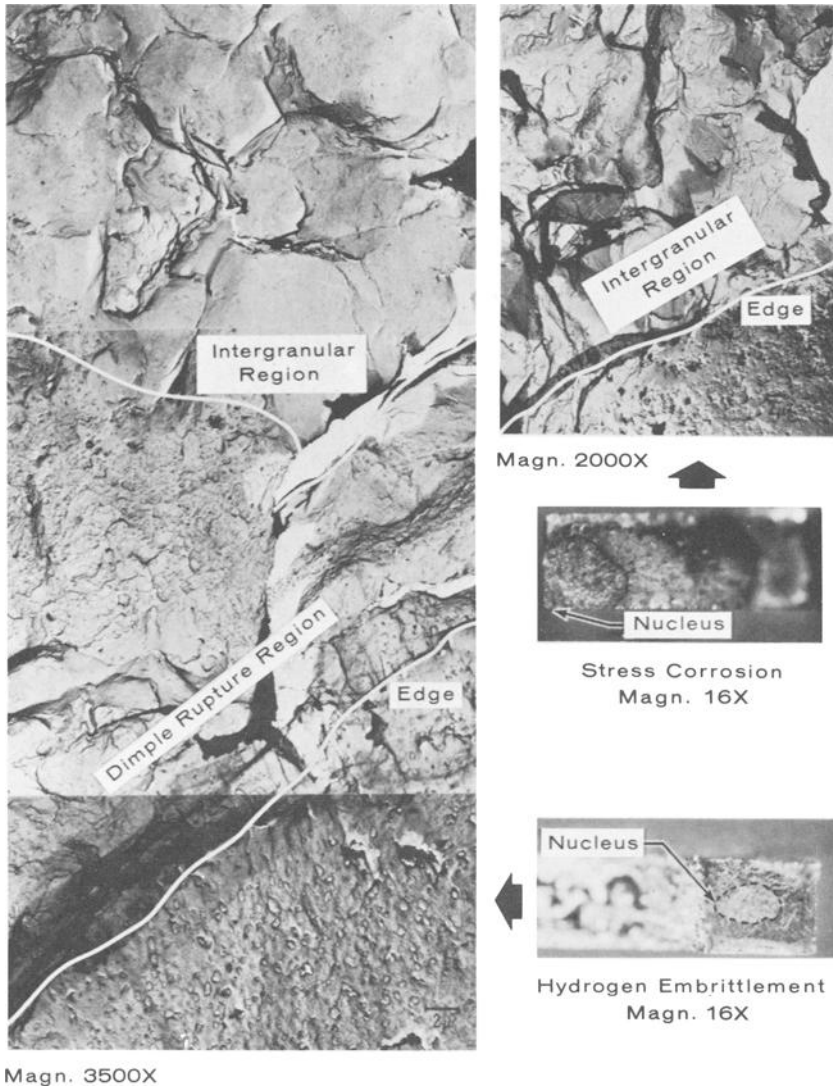
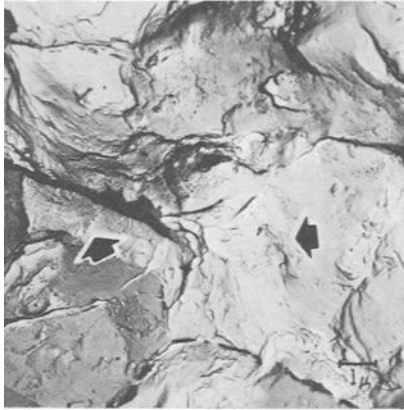
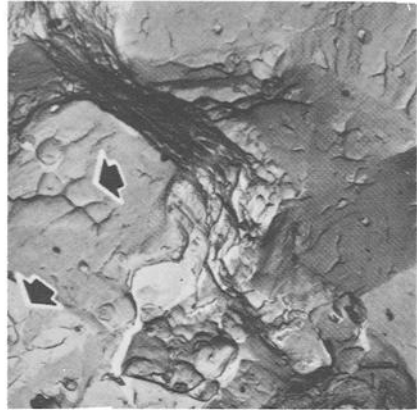


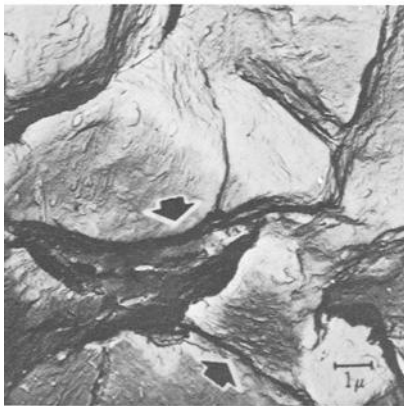
FIG. 8—The nature of nucleus region for stress corrosion and hydrogen embrittlement fractures.



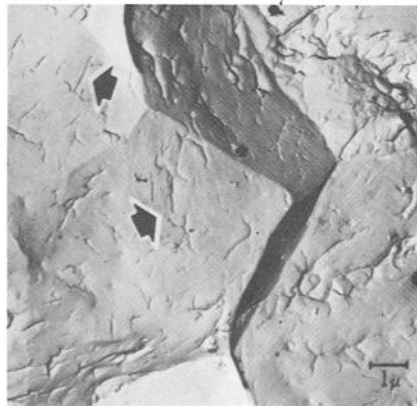
Stress Corrosion — Corrosion Products (Arrows)



Hydrogen Embrittlement — Partial Dimples (Arrows)



Stress Corrosion — Secondary Cracks and Crevices (Arrows)



Hydrogen Embrittlement - Hairline Indications (Arrows)

FIG. 9—Typical electron fractographs showing the distinguishing features of stress corrosion and hydrogen embrittlement ( $\times 6500$ ).

Other features associated with each type of fracture are shown in Fig. 9. Stress corrosion usually showed evidence of secondary cracking and corrosion products in the nucleus region. The hairline indications in the intergranular regions and partial dimples which are thought to be associated with the fracturing process are somewhat more distinct in hydrogen embrittlement than in stress corrosion fractures. These subtle differences are illustrated in Fig. 10.

By using a microautoradiographic technique [3], it was shown that hydrogen was associated only with the intergranular portion of the fracture. Due to the relatively low resolution of the technique, it was not possible to relate hydrogen accumulation at specific structural details such as partial dimples or hairline indications.

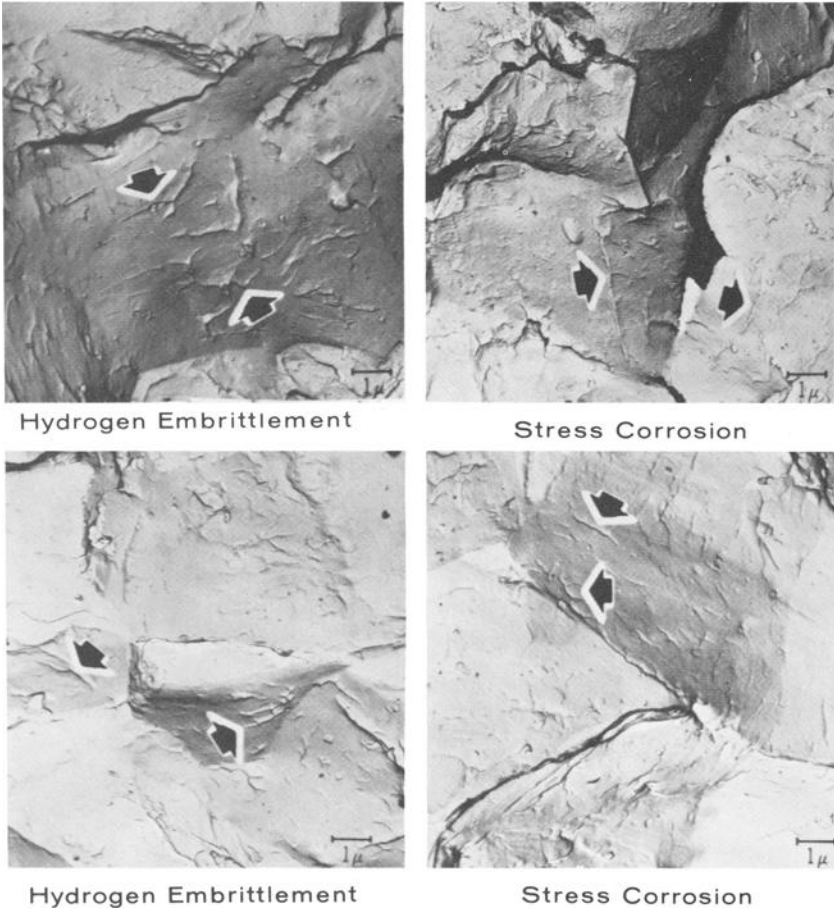


FIG. 10—Illustration of subtle differences between hairline indications (arrows) of stress corrosion and hydrogen embrittlement fractures in 4340, 260/280 steel ( $\times 6500$ ).

### Discussion

It has been shown that the accumulation of hydrogen with accompanying crack nucleation occurs at a region of high triaxial state of stress [3,4]. This triaxial state of stress exists subsurface at the root of a notch; therefore, it is not unexpected to find evidence of subsurface nucleation in hydrogen embrittlement fractures. In stress corrosion fractures, however, surface nucleation occurs because corrosion initiates from the surface and progresses into the material.

Intergranular fracture is associated with both stress corrosion and hydrogen embrittlement failures, and is generally confined to the nucleus region. Hydrogen embrittlement intergranular fracture showed a preponderance of partial dimples and hairline indications on the

grain boundary surfaces. This suggests that a mechanical separation has been involved, whereas in stress corrosion fractures, disregarding corrosion products with their accompanying surface attack, show smoother intergranular surfaces, thereby suggesting a smaller degree of mechanical separation (dissolution).

When attempting to distinguish stress corrosion from hydrogen embrittlement fractures it was important to obtain a good overall impression of the nucleus area. Often, the differences between these two failure types were subtle and examining only a few isolated areas might have led to incorrect analysis.

In addition, because of the subtlety between these two sustained load failure appearances, we must make use of all the facts available. This includes knowledge of the part processing practices, service history, and prior service failures of the same type. The electron microscope should be used primarily to supplement knowledge rather than be the only source of information when analyzing this type of failure.

## Conclusions

The features associated with stress corrosion fracture are:

1. Predominantly surface nucleation of intergranular fracture.
2. Intergranular regions show pronounced secondary cracking or deep crevices.
3. A relatively greater amount of oxidation or corrosion attack at the nucleus and slow growth region than in the rapid fracture area.
4. Less pronounced hairline indications on the intergranular surfaces than observed on hydrogen embrittlement fractures.

The features associated with hydrogen embrittlement are:

1. Predominantly subsurface nucleation of intergranular fracture.
2. Both the nucleus and the rapid fracture areas exhibit relatively equal degrees of oxidation or corrosion products.
3. Evidence of partial dimples and pronounced hairline indications in the intergranular regions.

### **Problem 3 – Relationship Between Cyclic Stress and Fatigue Striation Spacing**

Fatigue cracking in metal alloys is one of the most commonly observed modes of structural failure in the aerospace industry. It occurs as a result of the repeated application of loads well below the ultimate strength of the material. When the fracture surface of a fatigue crack is examined at high magnification by means of electron microscopy, periodic markings, known as striations, are observed. The spacing

between striations is characteristic of the microscopic progression of the crack front during one loading cycle.

The major objective of this program was to develop a correlation between the striation spacings and the cyclic load history of through-the-thickness fatigue cracks in various sheet and plate aluminum alloys. Such a correlation would then be useful in the analysis of fatigue failures of structures fabricated from these alloys.

### Experimental Procedure

The aluminum alloys studied included 2024-T3, 7075-T6, 7075-T73, 7079-T6, and 6061-T6 (Table 2). For the purpose of detecting an ef-

TABLE 2—*Mechanical properties of aluminum alloys used for crack propagation tests.*

Material	Thickness, in.	Strength	
		$F_{tu}$ , ksi	$F_{tu}$ , ksi
2024-T3.....	0.050	51.2	69.5
		51.0	69.4
		52.4	69.6
2024-T3.....	0.500	56.0	66.0
		56.6	66.6
		56.4	66.6
7075-T6.....	0.050	75.6	83.5
		76.1	84.3
		76.1	84.1
7075-T6.....	0.500	75.6	82.4
		74.7	82.0
		78.2	84.3
7075-T73.....	0.050	66.9	77.7
		67.8	78.5
		65.8	76.6
7075-T73.....	0.500	63.8	73.7
		64.1	74.2
		62.0	73.0
7079-T6.....	0.050	65.7	71.8
		64.6	72.0
		64.4	72.0
6061-T6.....	0.050	42.1	47.4
		42.0	47.4
		42.3	47.6

fect of material thickness on the properties to be studied, both 0.050-in. sheet and 0.500-in. plate of 2024-T3, 7075-T6, and 7075-T73 were used. The remaining alloys were tested in the 0.050 in. thickness only.

Fatigue cracks were developed in 8-in.-wide by 18-in.-long specimens, centrally slotted and fatigue-precracked. Growth of the fatigue crack was monitored visually and by means of 2-in.-long crack propagation gages bonded on one specimen surface in the path of the growing crack, Fig. 11. Each gage consisted of 20 elements, equally spaced at 0.10-in. intervals. Sequential rupture of gage elements by the propagating crack was recorded by an oscillograph simultaneously with the output from the load cell. The oscillographic trace provided a detailed loading and cracking history of each specimen.

The cyclic stresses which were employed were selected to represent loading environments encountered in military aircraft and to provide evidence of the effect on striation spacing of mean stress, alternating stress, and frequency of loading.

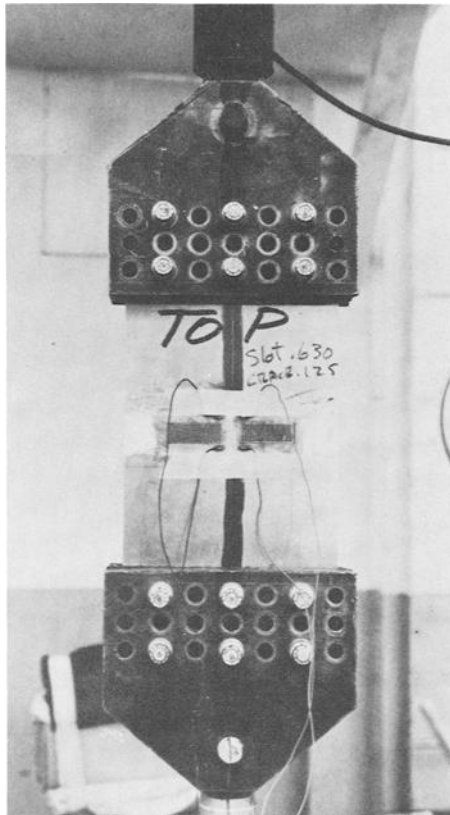


FIG. 11—Location of crack propagation gages on a fatigue specimen.

The cyclic stresses for fatigue crack propagation tests are presented in Table 3. Standard fatigue crack propagation (Table 3a) was established in tests with constant mean and alternating stresses. In each of these tests one of the four scheduled mean stresses and one of the five scheduled alternating stresses characterized the cyclic stress for that test. The loading frequency for these tests was 1000 cpm. In several tests, a frequency of 10 cpm was employed.

TABLE 3—Fatigue cracking test conditions.  
(a) STANDARD FATIGUE CRACK PROPAGATION

Alloy	Thick- ness, in.	Fre- quency, cpm	$\sigma_m$ , ksi <sup>a,b</sup> $\sigma_a$ , $\pm$ ksi <sup>c</sup>	8.25		13.75		16.5	22.5
				6.75	2.5	7.5	11.25	13.5	6.75
2024-T3 .....	0.050	1000		X	X	X	X	X	X
		10		...	...	X	X	...	...
	0.500	1000		...	X	X	X	...	...
7075-T6 .....	0.050	1000		X	X	X	X	X	X
		10		...	...	X	X	...	...
	0.500	1000		...	X	X	X	...	...
7075-T73 .....	0.050	1000		X	X	X	X	X	X
		10		...	...	X	X	...	...
	0.500	1000		...	X	X	X	...	...
7079-T6 .....	0.050	1000		X	X	X	X	X	X
6061-T6 .....	0.050	1000		X	X	X	X	X	X

(b) SPECTRUM-LOAD FATIGUE CRACK PROPAGATION

Alloy	Thick- ness, in.	Fre- quency, cpm	$\sigma_m$ , ksi $\sigma_a$ , $\pm$ ksi	13.75		8.25	13.75	22.5
				2.5	7.5	11.25	6.75	
2024-T3 .....	0.050	600			X			X
7075-T6 .....	0.050	600			X			X
7075-T73 .....	0.050	600			X			X
7079-T6 .....	0.050	600			X			X
6061-T6 .....	0.050	600			X			X
6061-T6 .....	0.050	600			X			X

<sup>a</sup> All stresses based on gross area.

<sup>b</sup>  $\sigma_m$  = mean stress.

<sup>c</sup>  $\sigma_a$  = alternating stress =  $\frac{\sigma_{max} - \sigma_{min}}{2}$

Spectrum-load fatigue crack propagation tests (Table 3b) were also performed in order to simulate service conditions and duplicate single mean or alternating cyclic loads. In one series of these tests the mean stress was held constant while the alternating stress varied every ten cycles. In the second series, the alternating stress was held constant

and the mean stress was varied every ten cycles. These tests were performed at a frequency of 600 cpm.

The standard two-stage plastic-carbon technique was used in preparing replicas of the fatigue crack surfaces for examination in the electron microscope. A corner was cut off on each replica in order to orient it with respect to the macroscopic crack propagation direction. Striation spacings were measured from electron fractograph negatives taken at a standard magnification of  $\times 5300$ . Calibration of this magnification was accomplished using a replica of a diffraction grating containing 28,800 lines/in.

The fatigue cracks examined ranged from approximately a total length of 0.7 to 4.3 in. The selection of areas to be replicated on individual specimens was based on the number of cycles used to propagate the left or right crack front 0.10 in. Since it was difficult to observe distinct fatigue striations in areas where less than about 200 cycles were used to grow the fatigue crack 0.10 in., these areas were not replicated. For 0.10-in. increments containing more than 200 cycles of stress, replicas were taken at significant intervals (usually 3 to 4) along the fracture path.

The fatigue striation spacing data were obtained by examining a specific 0.10-in. area to gain an impression of representative striation spacings in this area. Generally, a fatigue striation spacing for a specific area represents an average of four readings, depending on the definition and number of striations present. Where possible, measurements were taken from relatively flat regions that exhibited the largest uniform striation spacings over an appreciable distance. Striations that were influenced by second phase particles, or occurred on steep slopes, were not considered. It was found that distinct fatigue striations could be observed on both the normal and oblique mode of the macroscopic fracture profile in the fatigue region.

## Results

Completely detailed data from all the tests may be found in Ref 5. Because of its tabular bulk, only representative results will be given in this paper.

When comparing the macroscopic fatigue crack growth rate (obtained by dividing the observed 0.10-in. incremental crack growth by the number of cycles used to propagate the crack through that increment) to the microscopic growth rate (striation spacing), the behavior observed is illustrated in Fig. 12. At relatively low crack growth rates, the macroscopic rate was less than the microscopic rate. This difference in growth rates may be due to crack arrest periods during fatigue cycling. At higher crack growth rates, the macroscopic rate was greater than the microscopic rate. This can be explained by the presence of

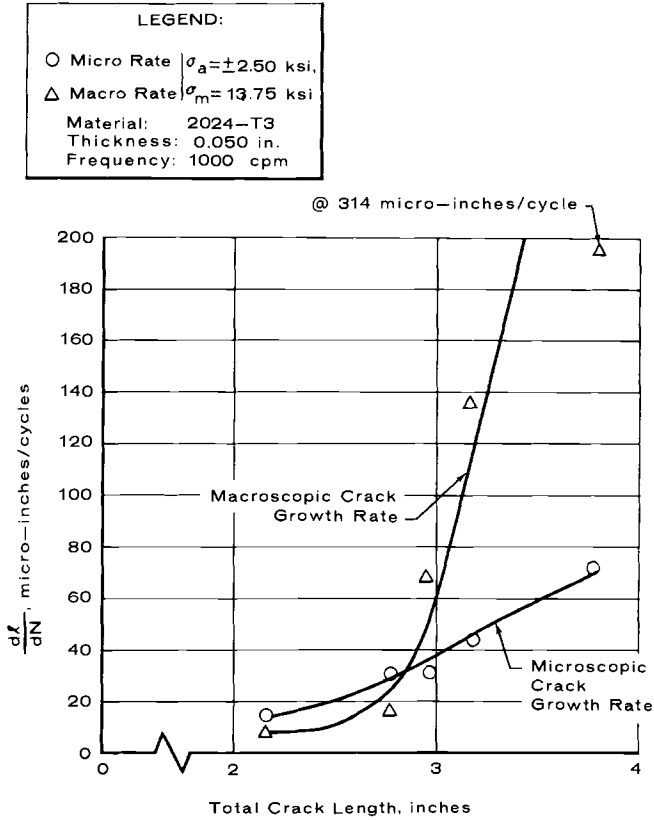


FIG. 12—Relationship between fatigue microscopic and macroscopic crack growth rate.

dimple rupture regions along with the striation-producing fatigue propagation. In calculating macroscopic growth rate, it is assumed that the crack propagation over a measured increment of length was due entirely to fatigue. However, in reality, regions of dimple rupture have contributed substantially to the progression of the crack front as revealed by fractographic examination.

Electron fractograph analysis of spectrum loaded specimens indicates that when a fatigue striation is produced, it is the result of one cycle of stress. However, it has been observed that for both varying alternating and varying mean stresses, when the applied mean or alternating stress range changes abruptly from a high to a low level, there is a period (at least 10 cycles) during which the fatigue crack apparently does not propagate, Fig. 13. On the other hand, when the low level is not immediately preceded by high levels of stress, fatigue crack propagation is observed. Since this paper is only concerned with the striation producing portion of fatigue crack propagation, the arrest phenomena

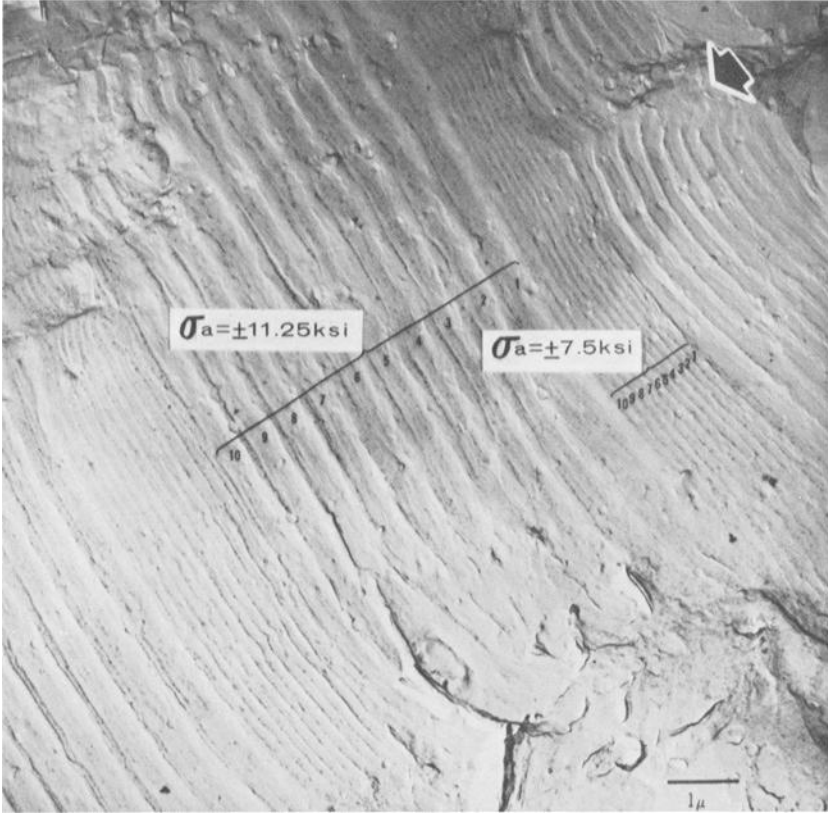


FIG. 13—Characteristics of spectrum loading. Mean stress = 13.75 ksi, three alternating stresses (2.5, 7.5, and 11.25 ksi) applied in 10 cycle intervals. Note lack of striations for lowest alternating stress (2.5 ksi). Arrow indicates fracture direction ( $\times 13,800$ ).

are relevant to calculation of number of stress cycles, not to calculation of stress intensity.

The striation spacings were examined in terms of a parameter  $K$  [6] which describes the local intensity of stress in the vicinity of the crack tip, as:

$$K = \sigma \left[ w \tan \left\{ \frac{\pi}{2w} \left( \ell + \frac{K^2}{\pi \sigma_y^2} \right) \right\} \right]^{1/2} \dots\dots\dots(1)$$

where:

- $\sigma$  = gross section stress,
- $w$  = panel width,
- $\ell$  = total crack length, and
- $\sigma_y$  = tensile yield strength.

A representative plot of fatigue striation spacing,  $d\ell/dN$ , as a function of  $\Delta K$ , ( $K_{\max} - K_{\min}$ ), is shown in Fig. 14. The dashed lines in the

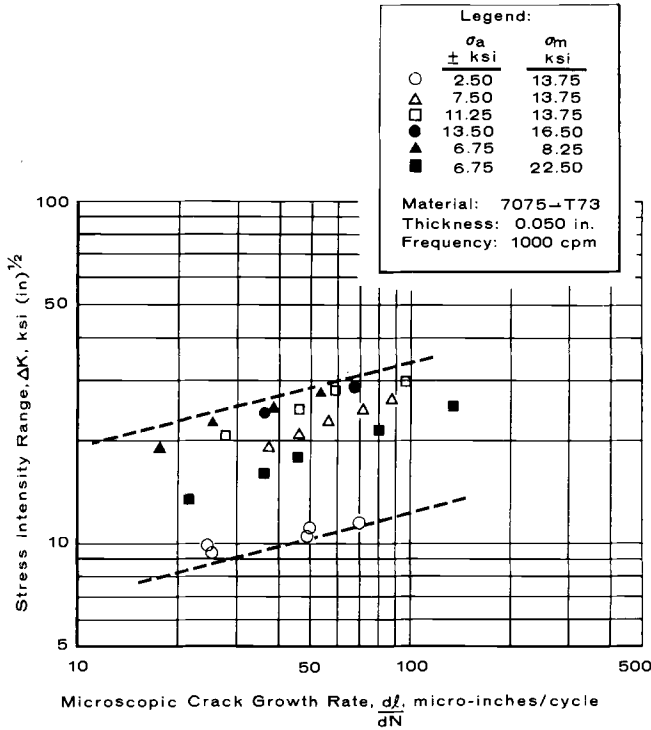


FIG. 14—Relationship between striation spacing and stress intensity range parameter,  $\Delta K$ .

figure encompass the range of data points and suggest a relationship of the type:

$$\frac{dl}{dN} = \frac{(\Delta K)^4}{M} \dots\dots\dots(2)$$

This relationship is somewhat in agreement with previously published analyses [7-9]. However, examination of the figure reveals that the proportionality constant,  $M$ , is some complex function of the stress environment. For example, knowledge of  $dl/dN$  alone from fractographic analysis will not define  $\Delta K$  with satisfactory precision. A further relationship between  $M$  and the stress environment must be known to make Eq 2 useful as a correlation between striation spacing and stress environment.

When the range of the cyclic stresses under investigation is small, Eq 2 will appear to define a correlation between  $\Delta K$  and striations spacing (and between  $\Delta K$  and macroscopic growth rate) and the proportionality constant,  $M$ , will have a discrete value.

When the range of cyclic stresses is expanded, however, as was true in this program as well as in Ref 10, based on macro-rate,  $M$  is revealed as a multivalued function of the stress.

For most aircraft structures the average mean stress is known (1-g load) and is generally constant for a given aircraft gross weight. Alternating stress, on the other hand, will vary and for many extreme operating conditions the magnitude of the alternating stress is not known. For this reason, striation spacings were examined with the objective of developing a correlation between alternating stress and the distance between fatigue striations.

Logarithmic plots of striation spacing,  $s$ , versus total crack length,  $\ell$ , revealed that striation spacings increase with distance from the origin ( $\ell/2$ ) as:

$$s = S_w \left( \frac{\ell}{W} \right)^m \dots\dots\dots(3)$$

where:

- $S_w$  = a constant depending on material, frequency and thickness,
- $m$  = a constant depending on the stress environment, and
- $W$  = panel width.

As shown in Fig. 15 the slope,  $m$ , of the curves varies with the cyclic stress in such a manner that all curves intersect at a common point,

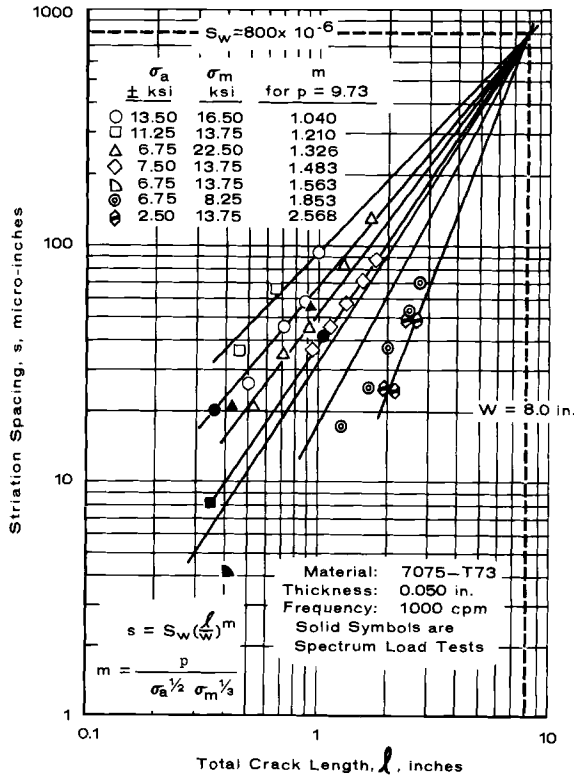


FIG. 15—Striation spacings versus crack length for 7075-T73, 0.050-in.-thick panels.

( $S_w, W$ ). From this plot, however, the exact manner in which the cyclic stress influences the slope is not immediately obvious.

Further plots of the slope as a function of alternating stress at equal mean stresses, Fig. 16, and as a function of mean stress at equal alternating stresses, Fig. 17, indicated that the slope,  $m$ , can be described as:

$$m = p\sigma_a^{-1/2}\sigma_m^{-1/3} \dots\dots\dots(4)$$

where  $p$  is a constant nearly equal to 10, as shown in Fig. 18. Solving for alternating stress,

$$\sigma_a = \left(\frac{p}{m\sigma_m^{1/3}}\right)^2 \dots\dots\dots(5)$$

From Eq 3,

$$m = \frac{\log s/S_w}{\log \ell/W} \dots\dots\dots(6)$$

Substituting in Eq 5,

$$\sigma_a = \left[\frac{p}{\sigma_m^{1/3}} \left(\frac{\log \ell/W}{\log s/S_w}\right)\right]^2 \dots\dots\dots(7)$$

Equation 7 relates alternating stress to striation spacing by means of two constants,  $p$  and  $S_w$ , which can be determined by test. Values for

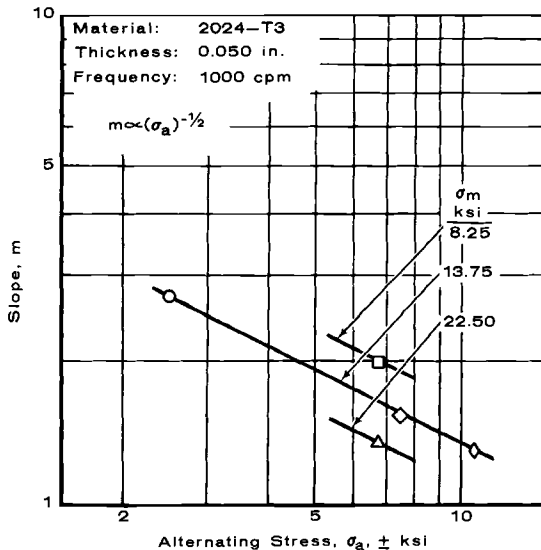


FIG. 16—Effect of alternating stress on slope,  $m$ .

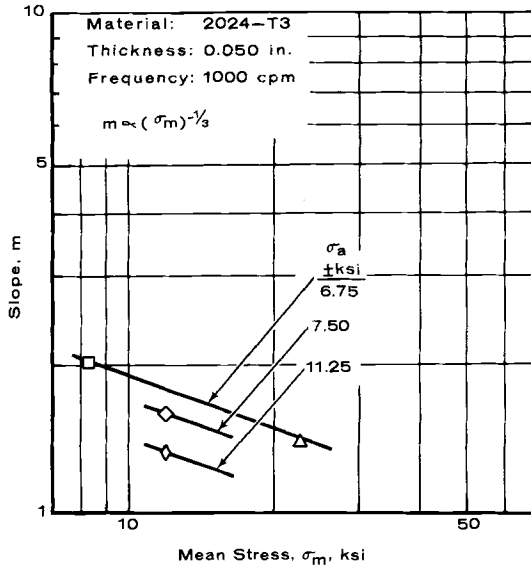


FIG. 17—Effect of mean stress on slope,  $m$ .

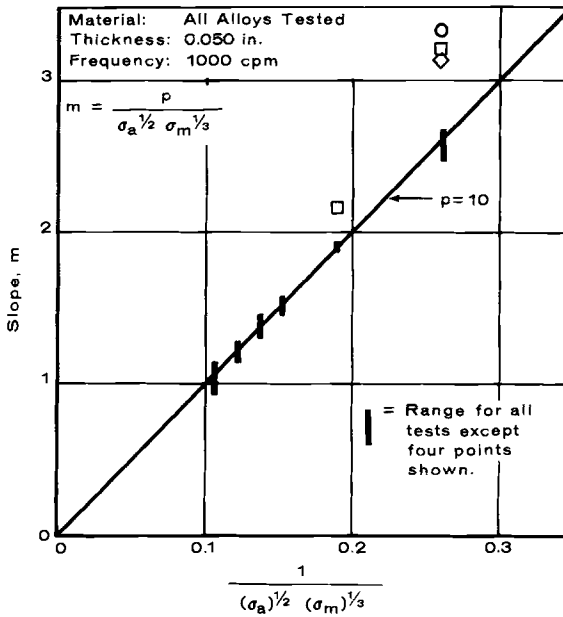


FIG. 18—Determination of the value of the constant,  $p$ , in Eq 3.

the aluminum alloys tested in this program are given in Table 4. The value of the constant,  $p$ , varies only slightly from alloy to alloy and does not appear to be affected by cyclic frequency. The constant,  $S_w$ , varies more from alloy to alloy and shows a definite trend to increase with decreasing frequency and increasing thickness. An increase in  $S_w$  reflects larger striation spacing (higher crack growth rate).

The ability of Eq 7 to describe the standard fatigue test data is demonstrated in Fig. 19. In this figure, the alternating stress predicted by

TABLE 4—Constants for use in correlating striation spacings with cyclic stresses (Eq 7).

Material	Thickness, in.	Frequency, cpm	$p^a$	$S_w^b$
2024-T3 .....	0.050	1000	10.35	$550 \times 10^{-6}$
		10	10.35	$800 \times 10^{-6}$
	0.500	1000	10.35	$1500 \times 10^{-6}$
7075-T6 .....	0.050	1000	9.90	$800 \times 10^{-6}$
		10	9.90	$1000 \times 10^{-6}$
	0.500	1000	...	...
7075-T73.....	0.050	1000	9.73	$800 \times 10^{-6}$
		10	9.73	$1000 \times 10^{-6}$
	0.500	1000	9.73	$2000 \times 10^{-6}$
7079-T6 .....	0.050	1000	10.05	$1000 \times 10^{-6}$
6061-T6 .....	0.050	1000	10.20	$800 \times 10^{-6}$

<sup>a</sup> Constant for Eq 7 when  $\sigma_a$  and  $\sigma_m$  are in units of ksi.

<sup>b</sup> Constant for Eq 7 when  $\ell$ ,  $W$ , and  $s$  are in units of inches.

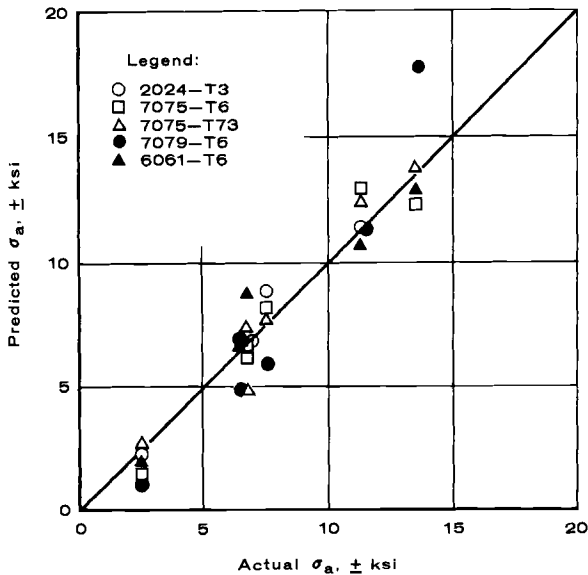


FIG. 19—Comparison of actual and predicted alternating stress for 0.050-in.-thick panels fatigue cracked at 1000 cpm.

Eq 7 is plotted versus the actual alternating stress. Each data point in the figure represents the average predicted alternating stress computed for each striation spacing measurement made in a given test. For most tests, the predicted value of alternating stress is within 1 or 2 ksi of the actual stress.

Predicted and actual alternating stresses for spectrum load tests are compared in Table 5 using the constants developed for a frequency of 1000 cpm.

TABLE 5—Comparison of actual and predicted alternating stress from spectrum load tests.

Material	Mean Stress, $\sigma_m$ , ksi	Actual Alternating Stress, $\sigma_a$ , ± ksi	Average Predicted Alternating Stress, $\sigma_a^a$ , ± ksi
2024-T3 .....	13.75	{ 2.5 7.5 11.25	...
	8.25		7.86
	13.75		16.30
	22.5	6.75	...
7075-T6.....	13.75	{ 2.5 7.5 11.25	...
	8.25		6.42
	13.75		12.33
	22.5	6.75	...
7075-T73 .....	13.75	{ 2.5 7.5 11.25	...
	8.25		7.52
	13.75		10.18
	22.5	6.75	...
7079-T6.....	13.75	{ 2.5 7.5 11.25	...
	8.25		7.60
	13.75		11.78
	22.5	6.75	...
6061-T6.....	13.75	{ 2.5 7.5 11.25	...
	8.25		6.24
	13.75		11.82
	22.5	6.75	...
			8.24
			7.72

<sup>a</sup> Calculated using Eq 7 and constants from Table 4.

Equation 7 can be employed in estimating the alternating stress for a given fatigue crack when the mean stress is known. To use the equation it is necessary to measure striation spacing,  $s$ , at a particular distance,  $\ell/2$ , from the fatigue crack origin. A number of measurements at various distances will improve confidence in the results.

As an example, assume that a fatigue fracture from a 10-in.-wide 7075-T73 structure operating at a mean stress of 18 ksi is to be analyzed to determine the maximum cyclic stress experienced during operation. Five striation spacing measurements are made at  $\ell/2$  distances from the origin.

These  $\ell/2$  distances are 0.5, 0.75, 1.0, 1.25, and 1.5 in. Assume that the resulting striation spacings are 30, 56, 85, 115, and 150  $\mu\text{in.}$ , respectively.

For the total crack length of 1.5 in. ( $\ell/2 = 0.75$ ) and the striation spacing of 56  $\mu\text{in.}$ , the alternating stress is calculated as follows:

$$\begin{aligned} \sigma_a &= \left[ \frac{P}{\sigma_m^{1/3}} \left( \frac{\log \ell/W}{\log s/S_w} \right) \right]^2 \\ &= \left[ \frac{9.73}{(18)^{1/3}} \left( \frac{\log \frac{1.5}{10}}{\log \frac{56 \times 10^{-6}}{800 \times 10^{-6}}} \right) \right]^2 \\ &= 7.01 \text{ ksi} \end{aligned}$$

The results of calculations for the other crack lengths and striation spacings are shown in Table 6. The average calculated alternating stress is 7 ksi. Therefore, the maximum stress is:

$$\begin{aligned} \sigma_{\max} &= \sigma_m + \sigma_a \\ &= 18 \text{ ksi} + 7 \text{ ksi} \\ &= 25 \text{ ksi} \end{aligned}$$

TABLE 6—Calculated alternating stress for idealized example given in text.

Distance from Origin, in.	Total Crack Length, in.	Striation Spacing, $\mu\text{in.}$	Alternating Stress, $\sigma_a \pm \text{ksi}$
0.50 .....	1.00	30	6.78
0.75 .....	1.50	56	7.01
1.00 .....	2.00	85	7.10
1.25 .....	2.50	115	7.04
1.50 .....	3.00	150	7.13
Avg			7.01

## Conclusions

1. The stress intensity range parameter  $\Delta K$  does not satisfactorily describe the relationship between fatigue striation spacing and cyclic stress.

2. If one stress condition is known, such as mean stress, the empirical relationship

$$\sigma_a = \pm \left[ \frac{p}{\sigma_m^{1/3}} \left( \frac{\log \ell/W}{\log s/S_w} \right) \right]^2$$

permits a reasonably accurate calculation of the magnitude of the other stress, that is, alternating stress, in through-crack, thin sheet.

3. The reduction of fatigue frequency from 1000 to 10 cpm results in an increase in the striation spacing at equivalent stress conditions.

4. An increase in thickness from 0.050 to 0.500 in. results in an increase in the striation spacing at equivalent cyclic stress and test frequency.

5. An abrupt decrease of applied fatigue stress can result in a period of arrested crack growth.

6. A fatigue striation is the result of one cycle of stress.

7. The appreciable difference between microscopic and macroscopic growth rates can be explained by the presence of dimple rupture areas on a fatigue surface.

8. Fatigue striations can be observed on both the normal and the oblique mode of fracture.

## Acknowledgment

The authors wish to express their appreciation to the Air Force Materials Laboratory (MAAS), Research and Technology Division, Air Force Systems Command, Wright-Patterson Air Force Base, Ohio, for permission to publish this work. The effort was funded under Contract AF33(615)-3014, with R. L. Henderson as the Air Force project engineer.

## References

- [1] *Handbook for Aircraft Accident Investigators*, U.S. Naval Aviation Safety Center, Office of the Chief of Naval Operations, 1957.
- [2] Phillips, A., Kerlins, V., and Whiteson, B. V., "Electron Fractography Handbook," AFML-TR-64-416, Air Force Materials Laboratory, Wright-Patterson Air Force Base, Ohio, Jan. 1965.
- [3] Gilpin, C. B. et al, "Electron Microautogradiography and Its Application to the Study of Hydrogen Distribution in Steel," *Advances in Electron Metallography*, ASTM STP 396, American Society for Testing and Materials, 1966, pp. 7-20.
- [4] Troiano, A. R., "The Role of Hydrogen and Other Interstitials on the Mechanical Behavior of Metals," *Transactions*, American Society for Metals, Vol. 52, 1960, p. 54.

- [5] Phillips, A. et al, "Electron Fractography Handbook-Specific Applications of Electron Fractography," AFML-TR-64-416, Supplement I, Air Force Materials Laboratory, Wright-Patterson Air Force Base, Ohio, Dec. 1966.
- [6] "Fracture Testing of High Strength Sheet Materials," *ASTM Bulletin*, Jan. and Feb. 1960.
- [7] Paris, P. and Erdogan, F., "A Critical Analysis of Crack Propagation Laws," *Journal of Basic Engineering*. American Society of Mechanical Engineers, Dec. 1963.
- [8] Hertzberg, R. W., "Application of Electron Fractography and Fracture Mechanics to Fatigue Crack Propagation in High Strength Aluminum Alloys," Lehigh University, Bethlehem, Pa., 1965.
- [9] Krafft, J. M., "On Prediction of Fatigue Crack Propagation Rate from Fracture Toughness and Plastic Flow Properties," *Transactions*, American Society for Metals, Vol. 58, 1965.
- [10] Eitman, D. A. and Rawe, R. A., "Plane Stress Cyclic Flaw Growth of 2219-T87 Aluminum and 5A1-2.5Sn Titanium Alloys," NASA CR-54956, National Aeronautics and Space Administration, June 1966.

## Engineering Applications of Fractography

---

**REFERENCE:** Brothers, A. J. and Yukawa, S., "Engineering Applications of Fractography," *Electron Fractography, ASTM STP 436*, American Society for Testing and Materials, 1968, pp. 179–195.

**ABSTRACT:** To date the primary use of microfractography has been qualitative. For this purpose the characteristic features of a specific fracture mechanism are compared with those of the service failure to be identified. However, the optimum use of fractography is that of both a quantitative and qualitative tool. This paper illustrates its usefulness in interpreting quantitatively the microfractographic features of various failure mechanisms, and suggests some currently speculative but promising areas for future work.

The incidence of fatigue striations and their association with cyclic alternating loads provide the basis for quantitative interpretation of fatigue failures. It is shown that fractographic determination of microscopic crack growth rates, coupled with currently available analyses for macroscopic crack growth rates, permits one to estimate relative failure stress or strain level, approximate number of failure cycles, and, in some cases, the relative stress gradient and mode of loading. The general stress dependence of fatigue striations, if determined from component tests, can be used directly for estimating relative operating stress levels of service failed parts. However, the influence on crack growth rate of geometrical factors suggests caution in comparing service failures with fractographic features of laboratory specimens. For this general case the correlations of crack growth rate with Griffith-Irwin fracture mechanics concepts are recommended. Since these analyses consider both component and crack geometry and mode of stressing, they are more generally applicable to a service consideration.

The high magnification used in electron microfractography and its use of replica techniques are shown to be useful in interpreting quantitatively the metallurgical features associated with creep microvoid formation. It is shown that fractography, in combination with standard electron diffraction techniques, permits one to isolate and identify the distribution, size, and content of specific metallurgical phases.

**KEY WORDS:** electron microscopy, fractography, fatigue (materials), cleavage fracture, creep rupture

Since its early use by Zapffe [1]<sup>2</sup> for the examination of cleavage fracture surfaces, fractography, or the study of fracture surfaces, has been developed extensively both in its techniques and applications. Its

<sup>1</sup> Materials and Processes Laboratory, General Electric Co., Schenectady, N.Y.

<sup>2</sup> The italic numbers in brackets refer to the list of references appended to this paper.

general uses have been described previously by Plateau et al [2], Beachem and Pelloux [3], and others. To date, fractography has found its greatest application as a qualitative tool with which to deduce the features of the various fracture mechanisms, or to study in detail the specific features of a single fracture mechanism. Illustration of its use for this latter purpose has been demonstrated by Low [4] for cleavage fracture, by Beachem [5] for ductile fracture, and Forsyth [6] for fatigue. However, to date there have been few attempts to illustrate broadly the direct engineering applications of fractography.

It is the purpose of this paper to review some direct engineering applications of fractography. The general thesis presented is that the optimum practical usefulness of these techniques requires the combined use and relation of quantitative fractographic features to other currently available engineering analyses and correlations. The specific details of fractographic techniques are now generally well known and have been described previously [7-9].

Although the primary emphasis is on the quantitative use of fractography for failure analysis, the general principles illustrated are widely applicable to all general engineering tests.

### Elements of Failure Analysis

The study of service fractures, and their comparison with component tests, provided valuable information regarding weaknesses in engineering design, assessment of operating conditions, and determination of the suitability of specific materials for given applications. The information required from service failures often includes that described below:

1. The fracture initiation mechanism.
2. The mode of loading, that is, bending, tension, torsion, thermal stress, etc.
3. The magnitude of loads causing failure.
4. If a fatigue failure – how many cycles of alternating stresses were involved, that is, is it high- or low-cycle fatigue?
5. The influence of environmental effects on fracture.

In some cases it is possible to assess part of the above information solely from macroscopic examination. For example, the presence of gross chevron markings indicate brittle cleavage, while beach marks suggest fatigue fractures. The extent of deformation near the initiation site and presence of shear lips on a fracture surface indicates some measure of fracture loads and the relative temperature of fracture, respectively. However, the fractographic features of the various modes provide measurable quantities with which to *specifically* characterize a fracture. It is, of course, to be recognized that there are limitations on the uses of fractography, particularly for the examination of service

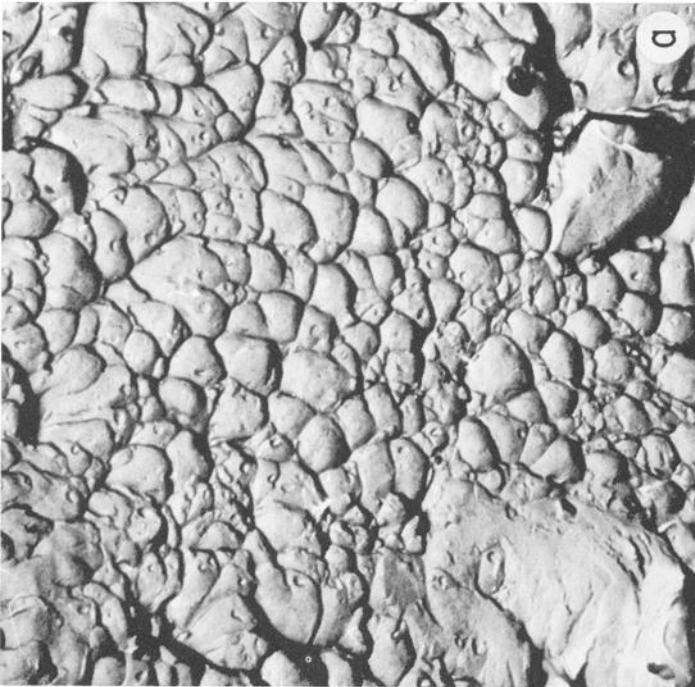
failures. In those cases where local mechanical damage, corrosion, or oxide coatings obscure the fracture surface, useful fractographic analysis is impossible. Furthermore, the successful use of fractography is extremely dependent on the judgment of the investigator. Primarily, it is necessary to distinguish between areas of initiation versus propagation, and to recognize the significance of various macroscopic features of fracture surfaces.

In many cases, as will be shown later, the use of comparison specimens tested under suspected operating conditions permits one to make a direct comparison of fractographic features.

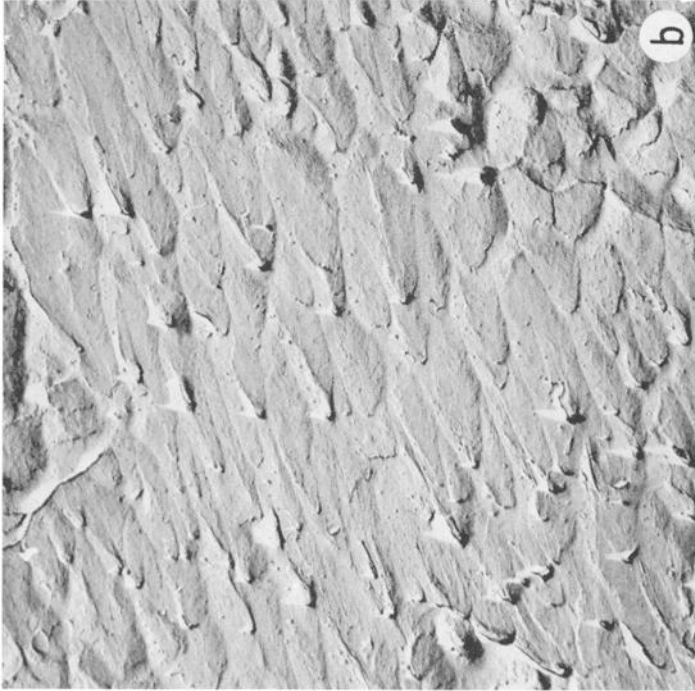
### **Quantitative Features of Static Fracture Modes**

The various modes of static fracture are generally characterized by the manner in which fracture occurs. These include transcrystalline ductile fracture or, so-called dimpled rupture, transcrystalline cleavage fracture and intergranular fracture. The mechanism of transcrystalline ductile fracture has been examined extensively by Gurland and Plateau [10], Rogers [11], and Beachem [3] and found to occur by microvoid coalescence. Although infrequently observed as a primary service failure mode, the incidence of microvoid coalescence or "dimpled rupture" in low and intermediate strength steels is generally indicative of a ductile or tough material which fractured at relatively high stress levels. Although the engineering implications of the fractographic features of dimpled rupture fracture have not been fully explored, there are some applications. It has been observed, for example, that the shape of the dimples is related to the general stress system by which they are formed [3]. Under uniaxial tensile rupture, microvoid growth occurs symmetrically resulting in equiaxed dimples; under shearing or tearing action, parabolic dimples are formed, the directionality of which provides some measure of the local direction of crack propagation. In some cases the presence of extremely elongated parabolas provides clues to the presence of shear loading. These various features are illustrated in Fig. 1.

Qualitatively, the appearance of dimpled rupture in low and intermediate strength steels is indicative of fracture at temperatures above the ductile-to-brittle or cleavage-to-shear transition temperature. However, in high strength steels dimpled rupture may not be indicative of high toughness. Although to date there have been no specific correlations between dimple *size* and test temperature, the work of Edwards [12], Fig. 2, illustrates the dependence of dimple *depth* on test temperature for a high strength steel. Since it is likely that the absolute dimple depth is a function of material strength level, ductility, etc., this empirical correlation will probably have to be established for each material and condition. However, it does suggest that correlations of



(a) Equiaxed dimples illustrating normal tensile fracture in 250M maraging steel ( $\times 15,000$ ).



(b) Parabolic dimples on shear-impact fracture surface of 4340 steel ( $\times 8000$ ).

FIG. 1 — Illustration of equiaxed and parabolic dimples associated with direction of loading.

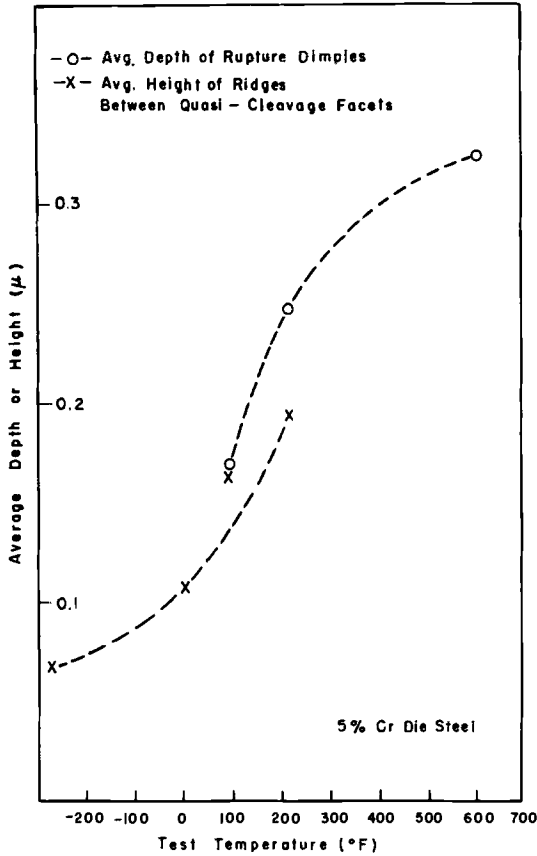


FIG. 2—Plot of average depth of rupture dimples and average height of ridges between quasi-cleavage facets versus test temperatures—Edwards [12].

service fracture dimple depth measurement with that of controlled comparison test specimens could provide a means of assessing fracture temperature, and the local ductility associated with fracture.

The few studies relating dimple diameter to mechanical properties suggest that dimple size merely reflects inclusion or second-phase particle spacing and is not directly related to mechanical properties [3,10]. Birkle et al [13], using fractographic techniques, have shown that the level of fracture toughness is determined primarily by the density and distribution of the sulfide inclusions associated with sulfur content level.

The application of fractography to the examination of cleavage fracture has been performed by Low [4] and others. An example of the engineering application of fractography to cleavage fracture is the determination of the relationship of cleavage facet size or cleavage crack length to the temperature of the ductile-to-brittle transition; in this

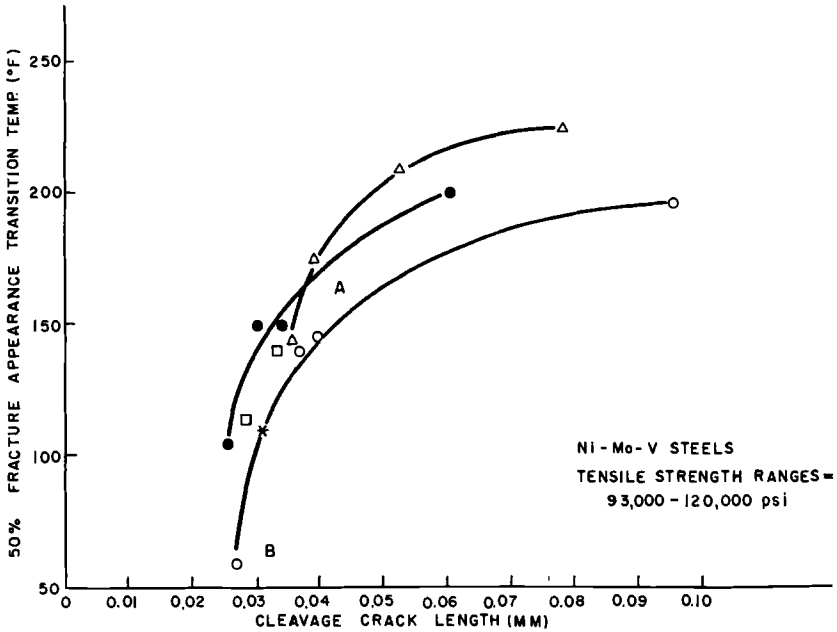


FIG. 3—Relation of transition temperature to cleavage dimensions Ni-Mo-V steels.

case, the 50 per cent fibrous fracture appearance transition temperature measured with Charpy impact specimens. This is illustrated in Fig. 3 which shows the relationship of fracture appearance transition temperature to cleavage crack length for Ni-Mo-V low-alloy steels of the strength range shown. The cleavage microcrack dimensions were determined microscopically from profile cross sections and fractographically by optical examination at magnifications up to  $\times 250$ . The values shown represent the average of a minimum of 25 measurements on fractured Charpy specimens tested at temperatures corresponding to a high percentage of cleavage fracture. Since this variation in cleavage crack length reflects the toughness of the alloy, the measurement of facet size, particularly in regions of complex metallurgical structures (for example, weld regions), can provide a measure of the local toughness in material through which fracture occurred.

The qualitative observations of Lubahn [14] and Crussard [15] of microscopic regions of fibrous fracture and the appearance of curved or deformed cleavage planes in cleavage fracture suggest further quantitative investigation to determine the relative change in microscopic quantities of fibrous fracture with temperature through the brittle-to-ductile range.

### Quantitative Features of Fatigue Fractures

The quantitative fractographic features of fatigue, or failure under alternating stress, have been examined extensively. It has been observed that there are characteristic striations associated with fatigue failure; these general features are shown in Fig. 4, a fractograph of an austenitic alloy component. Since each of these striations represents the fatigue crack front on a local scale, it is possible to derive information of direct engineering value.

By precise orientation of the fractographic shadowing direction relative to macroscopic features of the component, it is possible to estimate the direction of crack growth. If it is assumed that each striation results from a single cycle of loading, it is possible to estimate the relative number of cycles involved in crack propagation. From the spacing of the striations one can estimate the local fatigue crack growth rate. The relative changes in striation spacing with location, that is, their gradient, permits one to determine whether the fatigue crack growth rate is increasing or decreasing with increasing crack length.

Intuitively, one might expect that the fatigue crack growth rate or striation spacing is a function of the nominal alternating stress resulting in fatigue failure. This, in fact, has been observed as shown in Fig. 5.

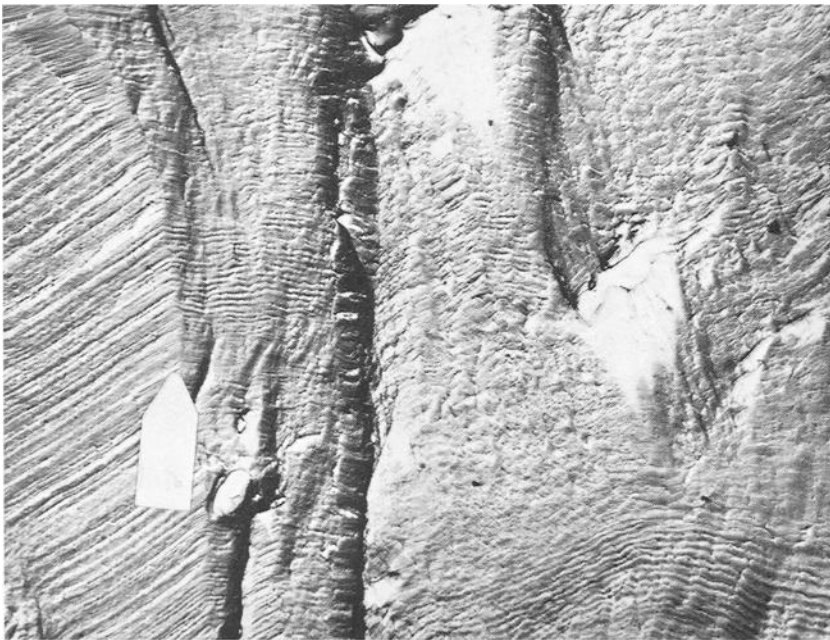
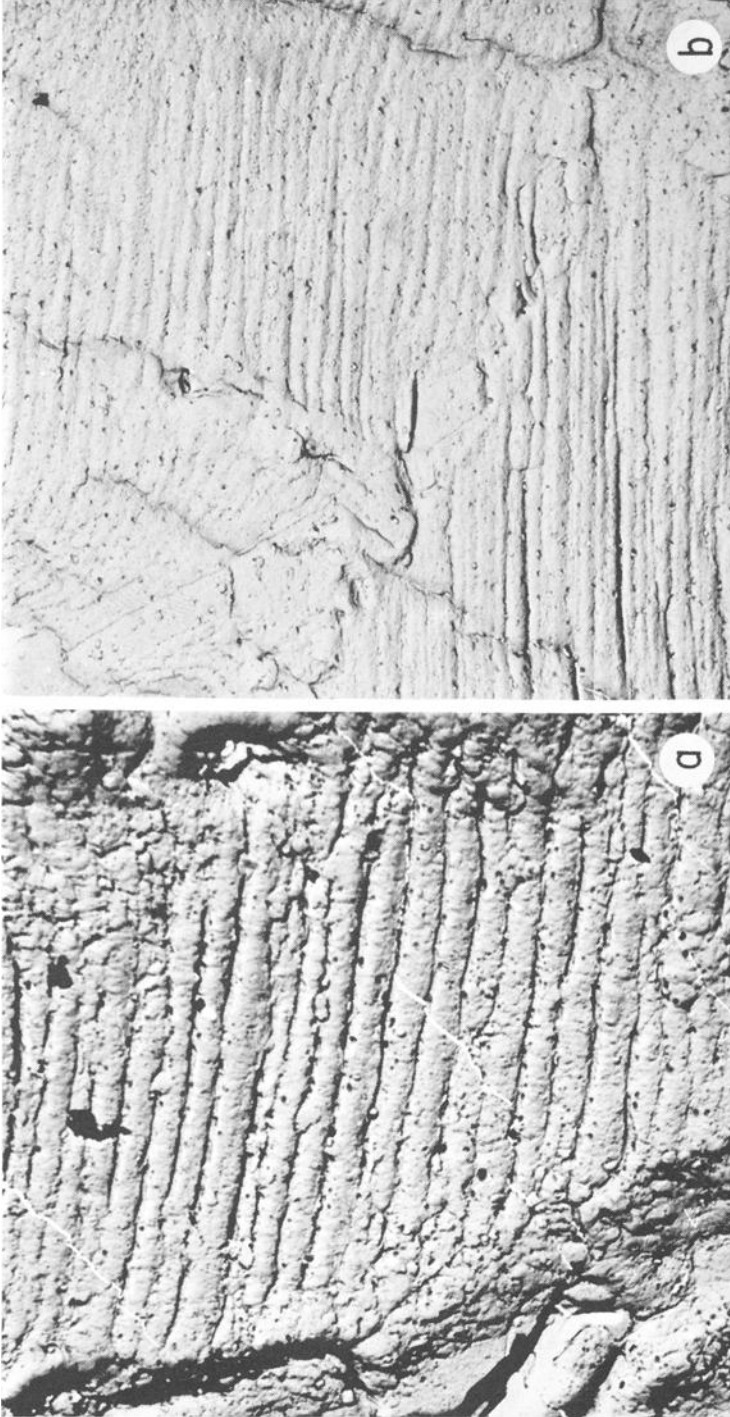


FIG. 4—Fractographic features of austenitic alloy fatigue fracture showing striated features typical of fatigue failures ( $\times 5000$ ).



(a)  $\sigma_{ALT} = 106,000$  psi.  
 $N_F = 6000$  cycles.

(b)  $\sigma_{ALT} = 58,500$  psi.  
 $N_F = 700,000$  cycles.

FIG. 5—Fractographic features of fatigue-failed vane of austenitic alloy ( $\times 7800$ ).

This figure shows the relative striation spacing determined at the site of initiation in two identical vanes tested in zero mean stress, completely reversed bending at two different stress levels. At the higher alternating stresses the crack growth rate is noticeably greater with a correspondingly coarser striation spacing. This general dependence of spacing on alternating stress suggested to Forsyth [16] that fractography could be used to determine the alternating stress associated with component failure. For this purpose and where possible, simulated operating component tests are made at various nominal stresses and the dependence of striation spacing on stress level is determined. Examples of these relationships for various materials tested in reversed bending are shown in Fig. 6. In these cases, the mean stress is zero. The influence of nonzero mean stresses is discussed further below.

The correlation of striation spacing with alternating stress is suitable for direct comparison of service failures with prototype or actual component tests. However, caution should be exercised in attempting direct correlation of the results of laboratory fatigue test specimens with more complex components of different geometry. For these conditions it is suggested that crack growth rates be correlated with the stress intensity factor as proposed by Paris and Erdogan [17] and described in detail in other publications [18,19]. With this procedure

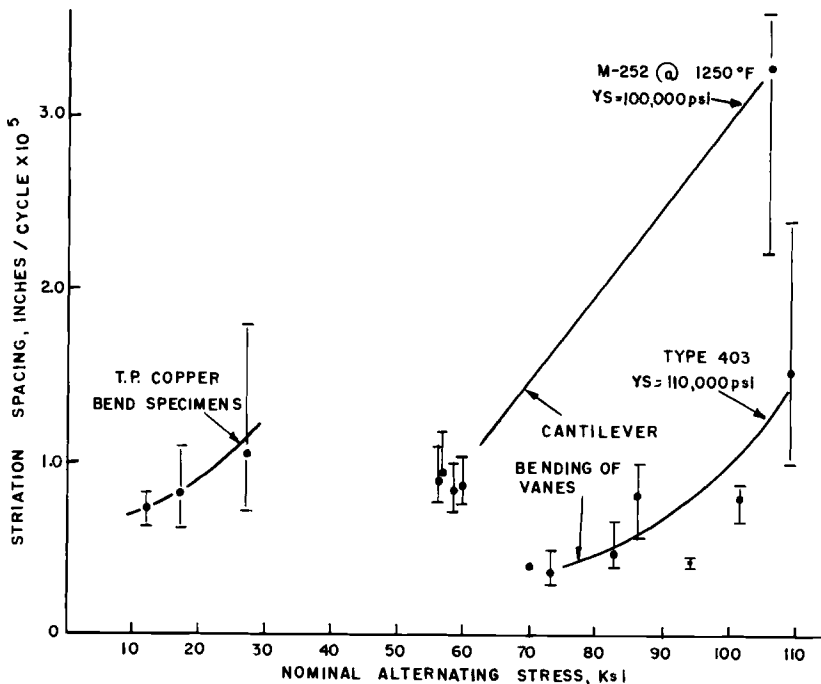


FIG. 6—Relationship between fatigue striation spacing and alternating stress amplitude.

the effects of component or specimen geometry and crack length on crack growth rate can be correlated with the elastically derived stress intensity factor,  $K$ . This term combines in a single parameter both the stress and the effect of geometry, that is, crack length. Conceptually, if one determines empirically the correlation between crack growth rate and stress intensity factor for a given specimen configuration for which  $K$  is known, it is then possible to estimate crack growth rates for other configurations for which an analysis for stress intensity factor is available.

Examples of these correlations for both macroscopic crack growth rates and striation spacing measurements are shown in Fig. 7. Of particular interest is the correlation of fractographically determined crack growth rate as a function of stress intensity factor for part-through surface cracks in Type 304 steel loaded in pulsating tension. For comparison, the correlation of macroscopic crack growth with  $K$  derived from results on 14-in.-wide through-cracked plates is also shown. This reasonably good correlation between macroscopic and microscopic crack growth rates including the effects of specimen geometry and crack type suggest the usefulness of this concept in quantitatively interpreting fatigue service failures. For example, it is possible to predict the gradient in crack growth rate or striation spacing for various modes of loading. This feature is illustrated in Fig. 8 for an idealized simple plate geometry containing a shallow surface crack; the stress intensity factors for these geometries were derived from Ref 20. The corresponding anticipated gradients in crack growth rate resulting from these changes in stress intensity factor are also described here. Although there is little significant difference at very short crack lengths, there is a predicted high variation in relative crack growth rates with increasing crack length. If one considers that edge-loading approximates the condition of thermal loading, it is apparent that there should be a significant difference in crack growth rates under various modes of loading.

Although there have been to the authors' knowledge no systematic investigations to determine the practical applicability of the above described approach, the few isolated examples of Fig. 9 for Type 304 steel suggest that there are, in fact, apparent effects of mode of loading on crack growth rate gradients which correlate generally with the above analysis. In particular, the weak dependence of crack growth rate on crack length for thermal cycling is in agreement with the effect predicted from consideration of the stress intensity factor. Clearly, the specific use of fractography for this application requires additional experimental verification.

The use of a macroscopic crack growth correlation to interpret the significance of various magnitudes and gradients of striation density re-



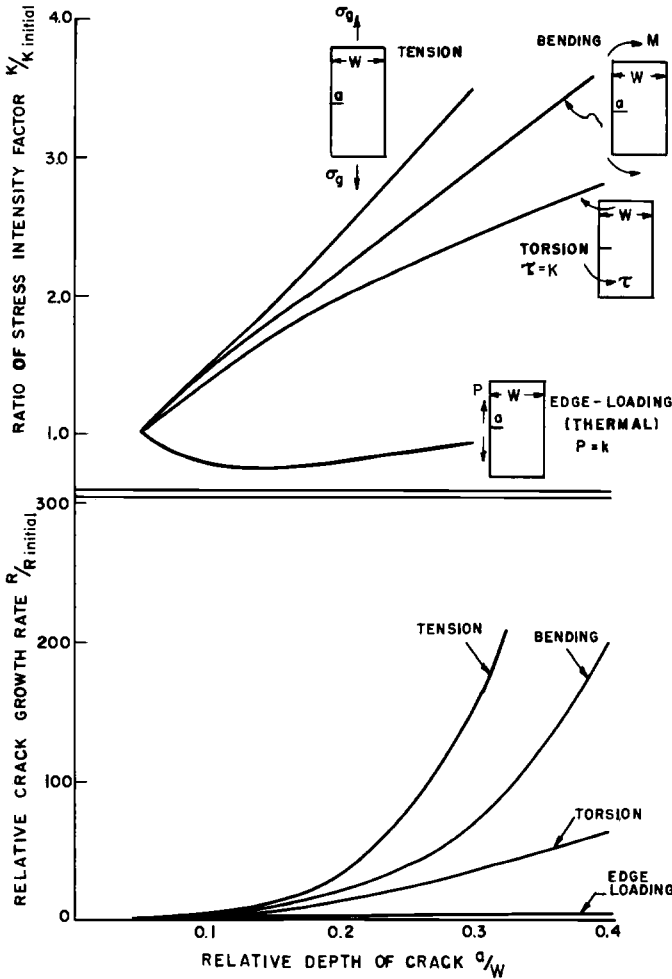


FIG. 8—Illustration of analytical procedures for estimating type of loading in fatigue service failures (schematic).

quires that all variables influencing crack growth rate be known. Although linear-elastic fracture mechanics rationalizes on a semi-empirical basis, the effect of crack length and specimen or part geometry, there is to date no fully satisfactory model or analysis with which to estimate the relative contribution to crack growth rate of mean versus alternating stress. In those cases where service operation includes known levels of mean stress, it may be possible from previous empirical correlations to relate the magnitude of the alternating stress level to the striation frequency. An example of the use of fractography for this purpose is described in Ref 9. Illustration of the effect on crack growth rate of various ratios of mean to alternating to mean stress is shown in Fig. 10. Although the magnitudes of the crack growth rates

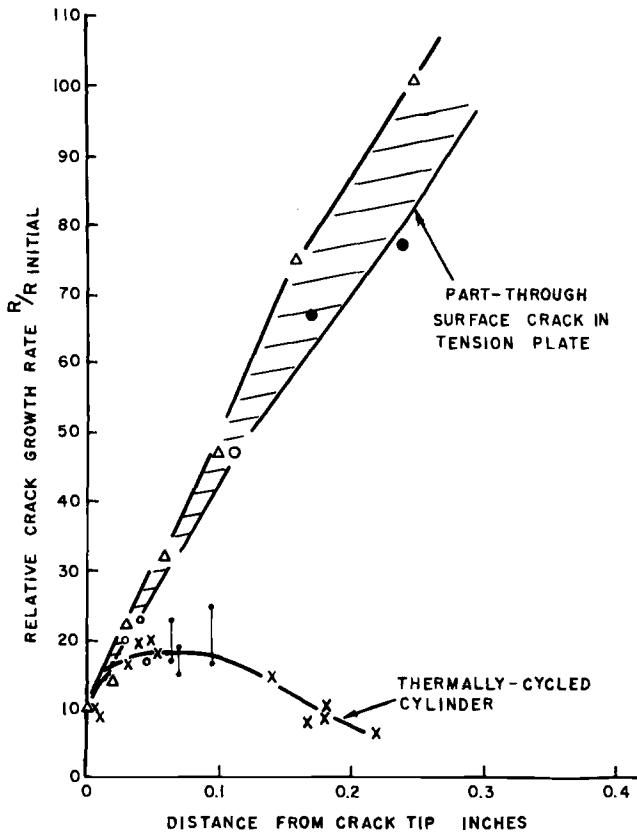


FIG. 9—Comparison of loading procedures on striation frequency gradient in Type 304 steel.

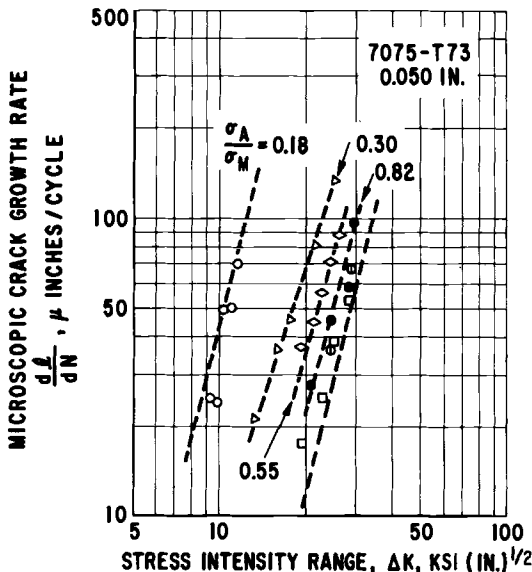


FIG. 10—Relationship between striation spacing and range of stress intensity factor for various stress ratios (Ref 9).

are influenced by mean stress, the nearly similar slopes indicate that the general power dependence of crack growth rate on the range of the stress intensity factor still applies. This conforms generally to the analyses proposed by Krafft [21] and recently by Forman et al [22].

### Application of Fractography to Creep Rupture Fractures

Since creep rupture tests and service failures of most materials at elevated temperatures result in oxidation of fracture surfaces, it is generally not possible to examine these surfaces directly. However, in some cases the creep-induced intergranular microvoids in regions near the fracture surface can be exposed by fracture at low temperatures prior to fractographic examination. This technique was first employed by Hyam [23] to study a 1 per cent aluminum-magnesium alloy. It has also been used on an alloy steel having low creep rupture ductility; the specific fractographic features noted in this alloy are shown in Figs. 11–13. Figure 11 illustrates the general appearance of intergranular microvoids in a polished cross section of a creep rupture specimen of Cr-Mo-V alloy steel tested at 1050 F for about 8000 h. After fracturing in liquid nitrogen to expose the microvoid surfaces, these surfaces were replicated using standard fractographic procedures.

The first of these replicas, a photograph of which is shown in Fig. 12, reveals the metallurgical phases which have been removed *in situ* from the intergranular microcrack surface during the replication pro-



FIG. 11—Intergranular microcracks formed during creep of a CrMoV low-alloy steel at 1050 F stressed for 7700 h at 25,000 psi ( $\times 10$ ).

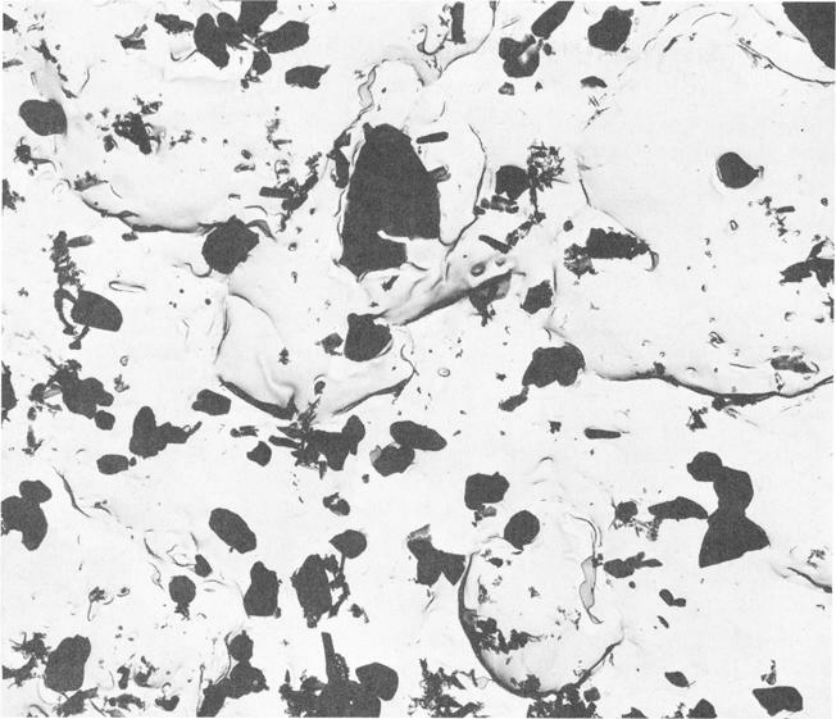


FIG. 12—Extraction replica of exposed intergranular microcracks showing metallurgical phases associated with microvoids. Large plate-like particles are  $M_{23}C_6$ ; filament groups are VC ( $\times 5000$ ).



FIG. 13—Fractographic features of exposed microcrack surface showing distribution of particle sites ( $\times 5000$ ).

cedure. By use of electron diffraction techniques, it was possible to isolate these individual particles and to identify their composition. Subsequent replications removed these particles and revealed the features shown in Fig. 13. From the specific measurement of the number and distribution of particles present on these surfaces, it is possible to determine quantitatively those metallurgical features contributing directly to creep fracture on a microscopic scale.

Similar techniques for metallurgical examination can and have been applied to those materials which can be fractured intergranularly to exposed intergranularly disposed metallurgical phases.

### Summary

Although still in its incipient development stage, the use of fractographically derived features for quantitative engineering applications appears promising. However, the optimum practical usefulness of these techniques will require the combined use and relation of quantitative fractographic features to currently available engineering analyses and correlations.

### References

- [1] Zapffe, C. A. and Clogg, M., Jr., "Fractography—A New Tool for Metallurgical Research," *Transactions, American Society for Metals*, Vol. 34, 1945, p. 71.
- [2] Plateau, J., Henry, G., and Crussard, C., "Several New Applications of Microfractography," *Revue de Metallurgie*, Vol. 55, No. 3, 1957.
- [3] Beachem, C. D. and Pelloux, R. M. N., "Electron Fractography—A Tool for the Study of Micromechanisms of Fracturing Processes," *Fracture Toughness Testing and Its Applications, ASTM STP 381*, American Society for Testing and Materials, 1964, p. 210.
- [4] Low, J. R., Jr., "A Review of the Microstructural Aspects of Cleavage Fracture," *International Conference on Fracture*, Swampscott, Mass., 1959.
- [5] Beachem, C. D., "An Electron Fractographic Study of the Influences of Plastic Strain Conditions upon Ductile Rupture Processes in Metals," *Transactions, American Society for Metals*, Vol. 56, 1963, p. 318.
- [6] Forsyth, P. J. E., "Fatigue Damage and Crack Growth in Aluminum Alloys," *Acta Metallurgica*, Vol. 11, 1963, p. 703.
- [7] Turkalo, A. M., "Electron Microscopy Techniques Applied to the Problem of Brittle Fracture," presented at ASM Symposium on Techniques to Study Fracture and Fatigue, American Society for Metals' Fall Meeting, 1964 (also available as General Electric Research Laboratory Report No. 64-RL-3855M).
- [8] Dahlberg, E. P. and Beachem, C. D., "Fractography, Part XV, Some Artifacts Possible with the Two-Stage Plastic Carbon Replication Technique," Memo Report 1457, National Research Laboratory, 1963.
- [9] Phillips, A. et al, "Electron Fractography Handbook," Technical Report ML-TDR-64-416, Air Force Materials Laboratory, 1965.
- [10] Gurland, J. and Plateau, J., "The Mechanism of Ductile Rupture of Metals Containing Inclusions," *Transactions, American Society for Metals*, Vol. 56, 1963, p. 442.
- [11] Rogers, H. C., "Tensile Fracture of Ductile Metals," *Transactions, American Institute of Mining, Metallurgical, and Petroleum Engineers*, Vol. 218, 1960, p. 498.
- [12] Edwards, A. J., "Depth Measurements on Fracture Surfaces," Report of NRL Progress, National Research Laboratory, 1963.
- [13] Birkle, A. J., Wei, R. P., and Pellissier, G. E., "Analysis of Plane Strain Fracture

- in a Series of 0.45 C-Ni-Cr-Mo Steels with Different Sulfur Contents," *Transactions*, American Society for Metals, Vol. 59, 1966, p. 981.
- [14] Lubahn, J. D., "Room Temperature Crack Propagation and Size Effect in Mild Steel," *Welding Journal Research Supplement*, Vol. 34, 1955, p. 518s.
- [15] Crussard, C. et al, "A Study of Impact Tests and the Mechanism of Brittle Fracture," *Journal of the Iron and Steel Institute*, Vol. 183, 1956, p. 146.
- [16] Forsyth, P. J. E. and Ryder, D. A., "Some Results Derived from the Microscopic Examination of Crack Surfaces," *Aircraft Engineering*, 1960, p. 96.
- [17] Paris, P. C. and Erdogan, F., "A Critical Analysis of Crack Propagation Laws," *Transactions*, American Society of Mechanical Engineers, Vol. 85, 1963.
- [18] Brothers, A. J. and Yukawa, S., "Fatigue Crack Propagation in Low-Alloy Heat-Treated Steels," *Transactions*, American Society of Mechanical Engineers, Vol. 89, 1966.
- [19] Tiffany, C. F. and Masters, J. N., "Applied Fracture Mechanics," *Fracture Toughness Testing and Its Applications*, ASTM STP 381, American Society for Testing and Materials, 1964, p. 249.
- [20] Paris, P. C. and Sih, G. C., "Stress Analysis of Cracks," *Fracture Toughness Testing and Its Applications*, ASTM STP 381, American Society for Testing and Materials, 1964, p. 30.
- [21] Krafft, J. M., "On Prediction of Fatigue Crack Propagation Rate from Fracture Toughness and Plastic Flow Properties," *Transactions*, American Society for Metals, Vol. 58, No. 4, 1965, p. 691.
- [22] Forman, R. G., Kearney, V. E., and Engle, R. M., "Numerical Analysis of Crack Propagation in Cyclic-Loaded Structures," Paper No. 66-WA/Met-4, American Society of Mechanical Engineers, 1966.
- [23] Hyam, E. D., "Discussion in Structural Processes in Creep," *Iron and Steel Institute*, Special Report No. 70, 1961, p. 76.

## Fractography and Microstructure of Aluminum Alloys 7075-T651 and 7075-T7351

---

**REFERENCE:** Hunter, M. S. and McMillan, J. C., "Fractography and Microstructure of Aluminum Alloys 7075-T651 and 7075-T7351," *Electron Fractography, ASTM STP 436*, American Society for Testing and Materials, 1968, pp. 196-211.

**ABSTRACT:** Specimens from 1<sup>3</sup>/<sub>8</sub>-in.-thick plate of 7075-T651 and 7075-T7351 alloys were examined by electron transmission, light microscopy, and electron fractography to relate microstructure, fracture topology, and mechanical and fracture properties. Material in the T7351 temper had a lower yield strength, smaller and more numerous fracture dimples, and an entirely transgranular fracture path. The T651 temper had a higher yield strength, fewer and larger dimples, and a partly intergranular fracture path. It was concluded that the beneficial effect of the lower yield strength more than offset the disadvantage of more numerous fracture dimple sites, and led to greater fracture toughness in the T7351 temper. The partially intergranular fracture was not significant in relation to fracture.

**KEY WORDS:** electron microscopy, fractography, aluminum alloys, microstructure, fracture toughness

One of the primary objectives of Subcommittee II of ASTM Committee E-24 on Fracture Testing of Materials is to obtain an understanding of the relationships that may exist among microstructure, topological features of fracture surfaces, and resistance to crack propagation.<sup>3-5</sup> To achieve this objective, separate task groups were established to examine aluminum and steel specimens. Specimens of a

<sup>1</sup> Scientific associate, Physical Metallurgy Div., Alcoa Research Laboratories, New Kensington, Pa.

<sup>2</sup> Group engineer, Metals Research Group, Commercial Airplane Div., The Boeing Co., Renton, Wash.

<sup>3</sup> Beachem, C. D. and Pelloux, R. M. N., "Electron Fractography—A Tool for the Study of Micromechanisms of Fracturing Processes," *Fracture Toughness Testing and Its Applications, ASTM STP 381*, American Society for Testing and Materials, 1965, pp. 210-244.

<sup>4</sup> Burghard, H. C., Jr., and Davidson, D. L., "Fracture Mechanisms and Fracture Surface Topography," International Conferences on Fracture, Japan, Sept. 1965.

<sup>5</sup> Kerlins, V., Phillips, A., and Whiteson, B. V., "Electron Fractography Handbook," ML-TDR-64-416, Wright-Patterson Air Force Base, Ohio, Jan. 1965.

material of known composition, fabrication history, and mechanical and fracture characteristics were to be examined independently by task group members using whatever techniques each would normally use in fracture-structure diagnosis.

### Material

The specimens selected for the aluminum task group were a group of 7075 alloy specimens in the T651 and T7351 tempers that had been subjected to tension and notch toughness tests, the results of which are given in Table 1. All were from a single lot of 1 $\frac{3}{8}$  in. plate. The speci-

TABLE 1—*Tensile and fracture properties of long transverse specimens of 1 $\frac{3}{8}$ -in.-thick 7075-T651<sup>a</sup> and 7075-T7351<sup>b</sup> plate.*

Identification	7075-T651	7075-T7351
	183201-T	183203-T
Tensile strength, psi .....	86 100	70 100
Yield strength, psi.....	77 750	58 500
Elongation in 4D, %.....	10.8	11.0
Net fracture strength, psi.....	65 500	70 700
$K_{Ic}$ , notched rounds, psi $\sqrt{\text{in.}}$ .....	28 200	31 500
$K_{Ic}$ , center notched panels, psi $\sqrt{\text{in.}}$ .....	26 100	34 400
$K_{Ic}$ , 1-in. panels, psi $\sqrt{\text{in.}}$ .....	30 900	60 400

<sup>a</sup> Solution heat treated 3 h at 870 F, quenched in cold water and aged four days at room temperature plus 24 h at 250 F.

<sup>b</sup> Solution heat treated 3 h at 870 F, quenched in cold water, aged four days at room temperature plus a two-step artificial aging treatment (U.S. Patent 3,198,676).

mens supplied for fractographic examination were 1-in. notched-round fracture specimens taken in the long transverse direction from the plate. In addition to mechanical data, electron transmission micrographs of the two materials were supplied. These specimens promised to be interesting subjects for task group investigation because of the fairly pronounced differences in tensile and fracture properties and in microstructure between the two tempers. With the more vigorous aging to produce the T7351 temper, tensile and yield strengths were reduced appreciably, but fracture properties were increased.

### Methods of Examination

The examination of the fractured specimens involved several metallographic techniques. Electron transmission examinations to reveal alloy structures involved machining to about 0.040 in. thick, chemically etching in a hydrochloric acid solution to about 0.005 in. and finally thinning electrolytically in Lenoir's solution.<sup>6</sup> Specimens for

<sup>6</sup> 722-cm<sup>3</sup> H<sub>3</sub>PO<sub>4</sub>, 134-cm<sup>3</sup> H<sub>2</sub>SO<sub>4</sub>, 150-g CrO<sub>3</sub>, 140-cm<sup>3</sup> H<sub>2</sub>O.

light microstructural examinations were prepared by conventional mechanical techniques and were examined either as-polished or after etching in Keller's etch. Fractographic examinations were made using two-stage, plastic-carbon replicas and anodic oxide replicas.

## Results of Investigation

### *Microstructure*

Comparing the transmission electron microstructure of the two tempers (Figs. 1 and 2) discloses that the principal structural difference lies in the size of precipitate particles within the grains. Both tempers have a considerable number of E-phase particles ( $\text{Cr}_2\text{Mg}_3\text{Al}_{18}$ ) about  $1000 \text{ \AA}$  in size in the form of a randomly distributed dispersoid. In addition, both have considerable grain boundary precipitate, much of which probably developed during quenching because the thickness of

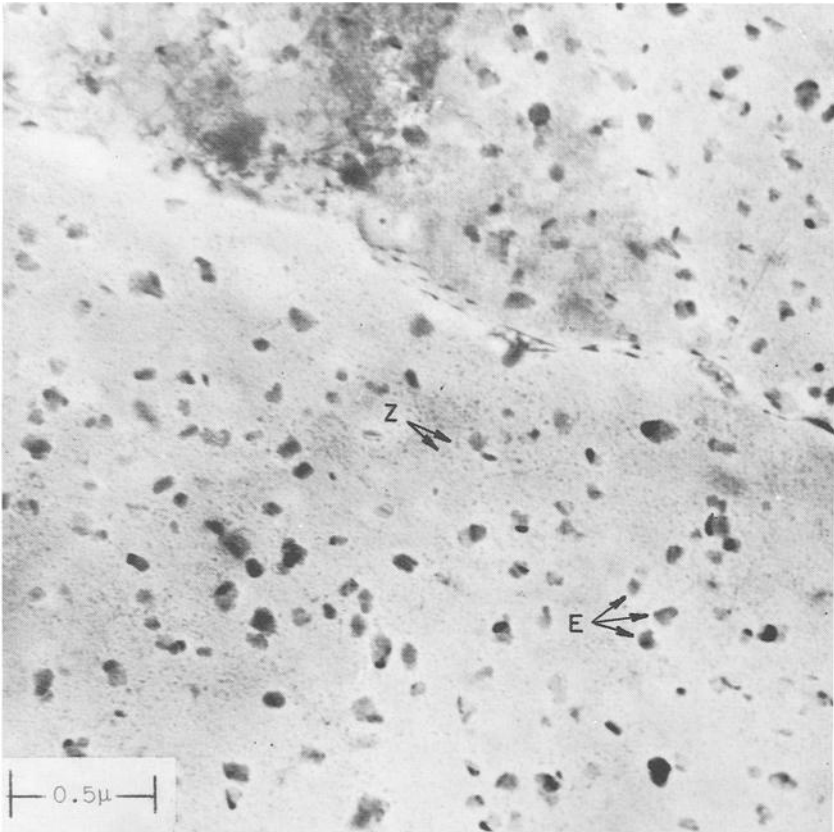


FIG. 1—Electron transmission. Microstructure of 7075-T651 material ( $\times 50,000$ ). E indicates E-phase dispersoids and Z indicates zones.

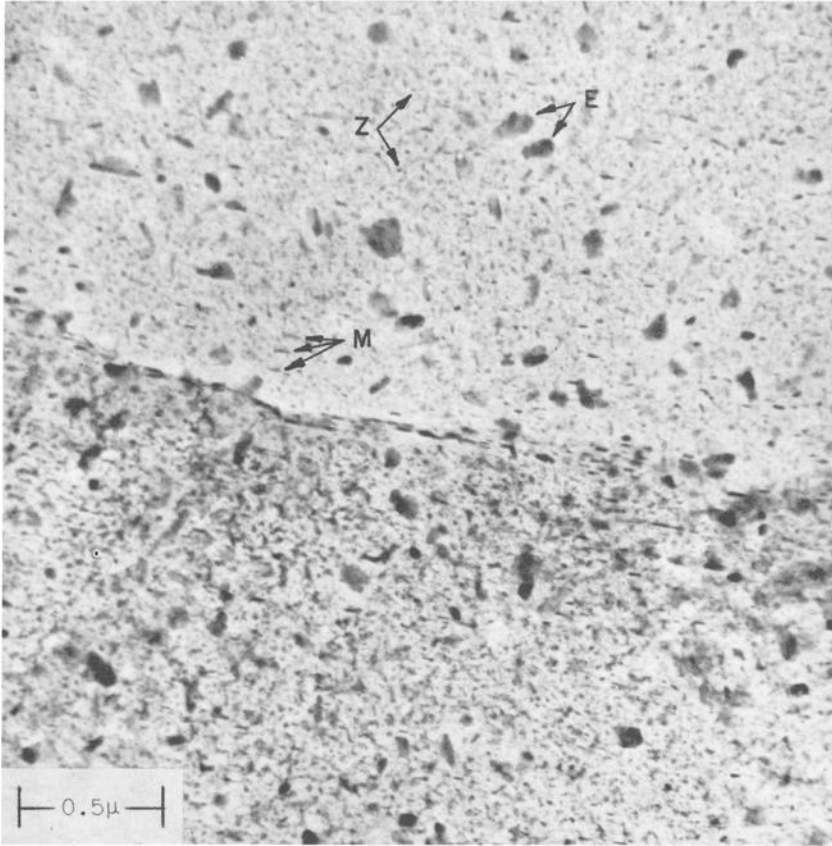


FIG. 2.—*Electron transmission. Microstructure of 7075-T7351 material ( $\times 50,000$ ). Note larger and more distinct zones than T651 temper in Fig. 1. E indicates E-phase dispersoids, Z indicates zones, and M indicates M-phase plates.*

the plate prevented rapid cooling after solution heat treatment. In the T651 temper (Fig. 1), matrix precipitation is in the form of fine zones. In the T7351 temper (Fig. 2), however, the zones are considerably larger and more distinct, and, in addition, numerous small plate-like precipitates of the transition  $M'$ -phase ( $MgZn_2$ ) have developed. Phase identifications are based on previous diffraction work with these alloys and tempers, and the stated compositions for the phases are those prevailing at equilibrium.

#### *Light Microscope Examinations*

Examinations of the fracture surfaces of the fracture specimens were first made under the low power light microscope. Both tempers exhibited fairly rough fracture surfaces, with relatively few smooth areas,

indicating comparatively ductile fractures. In the T651 specimens, however, a number of fine longitudinal fissures were noted.

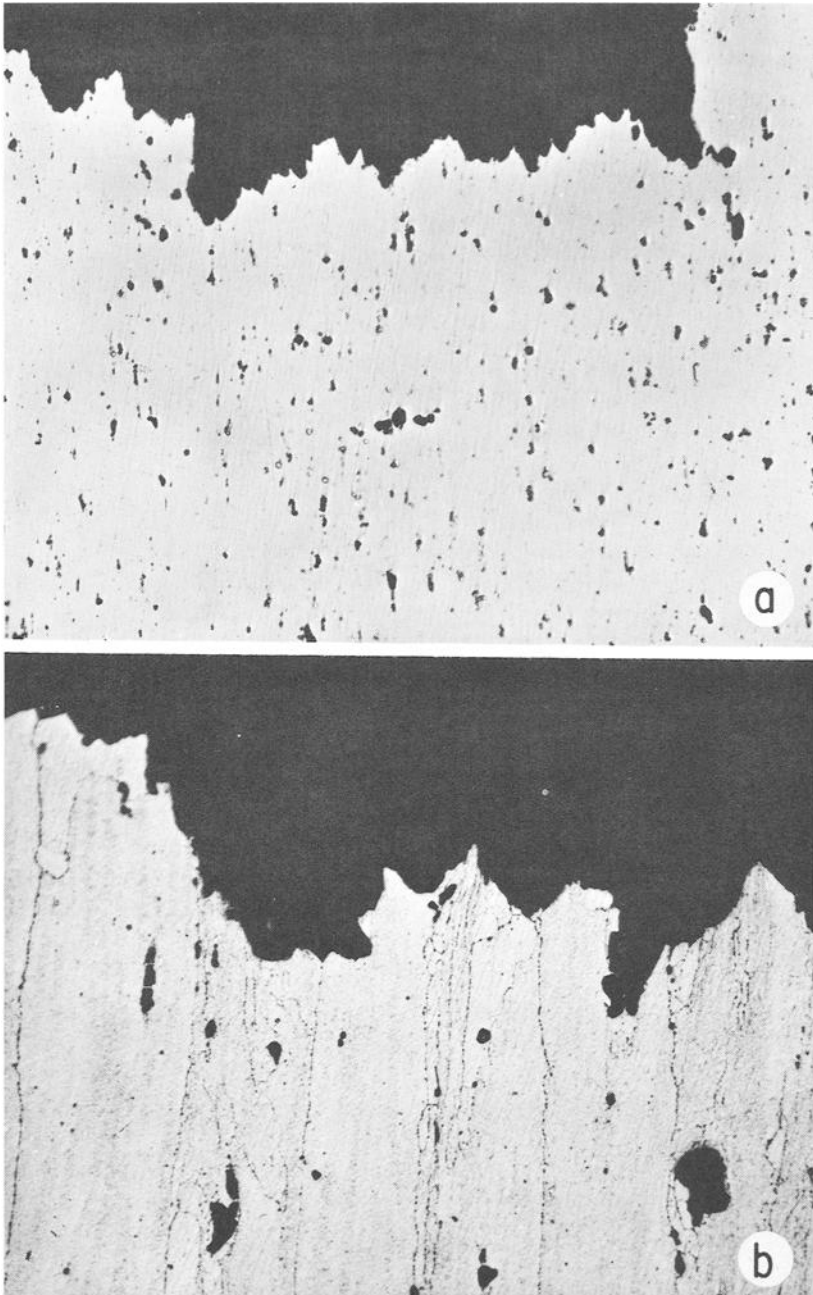
Cross sections of the fracture surfaces were made and were examined under the light microscope at low ( $\times 100$ ) and high ( $\times 500$ ) magnification. The specimen in the T7351 temper had a very ragged fracture and a large number of voids near the fracture (Fig. 3), suggesting more numerous fracture initiation sites. The fracture of the specimen in the T651 temper had about the same general roughness but comparatively few voids near the fracture. Instead, the specimen had smooth intergranular fissures extending normal to the fracture surface and parallel to the stressing direction (Fig. 4). These were presumably the fissures noted during low-power examinations of the fracture surfaces.

#### *Electron Fractographic Examinations*

Replicas of the fracture surfaces of the fracture specimens were examined at several magnifications with the electron microscope. The primary fracture mode throughout the fracture surfaces was the initiation and coalescence of microvoids. Fracture of and around second-phase particles, stretching, and some intergranular fracture was also observed. General views of the fracture appearance at the start of fracture, further along the fracture path, and in the final fracture area are shown by Figs. 5-7. At the  $\times 3000$  magnification of these figures, differences between the two tempers were not readily apparent.

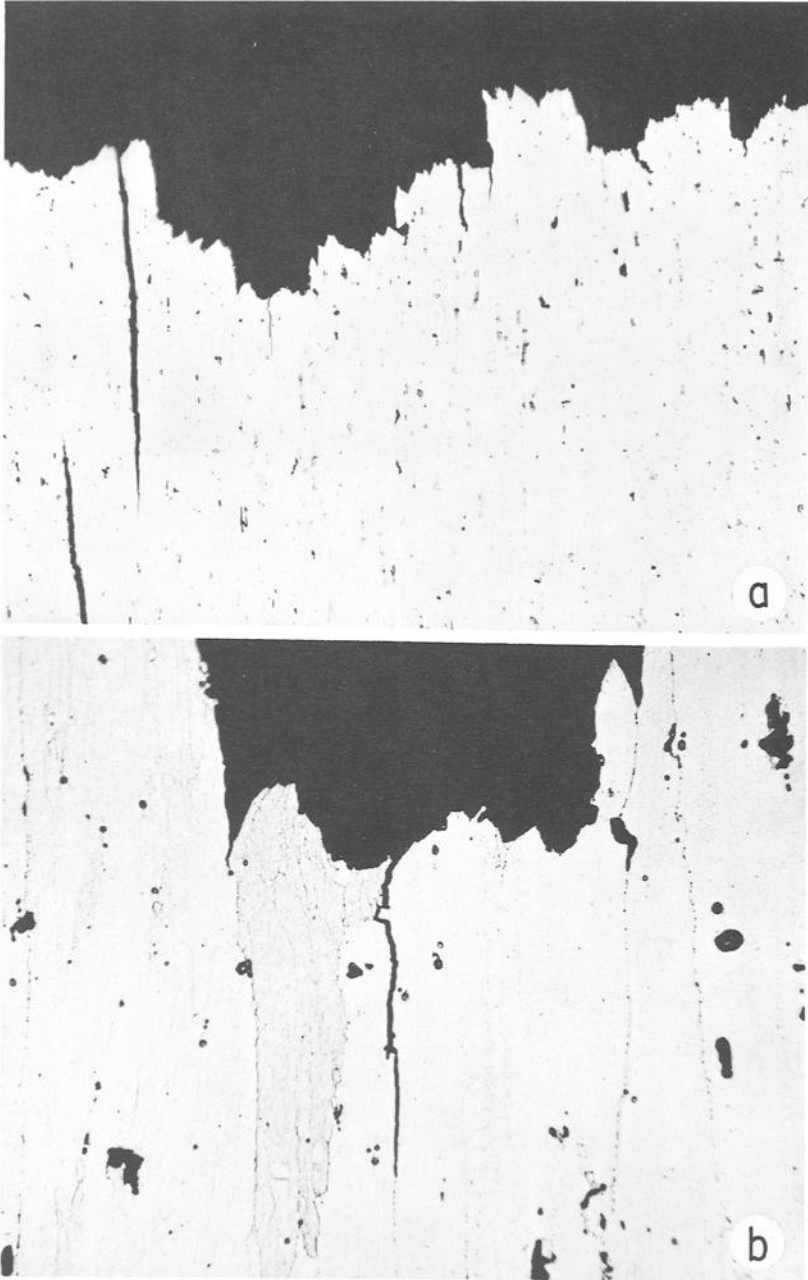
Additional details of the fractures were obtained from examinations at higher magnification. On the basis of extensive scanning with the electron microscope, it was apparent that the fracture of the T7351 material was almost entirely transgranular. That of the T651 material, however, was approximately 80 per cent transgranular and 20 per cent intergranular. In transgranular areas, both tempers had large and small dimples associated with large and small second-phase particles, along with localized regions of shear and tear dimples (Figs. 8 and 9). In certain areas of the T651 fracture, smooth facets at an angle to the general fracture surface were observed as shown at A in Fig. 10. These smooth facets are believed to represent the longitudinal intergranular fissures observed in the cross sections of the fracture region. This is substantiated by the fact that these facets contained many comparatively large particles, probably the grain boundary precipitates.

Examinations at still higher magnification in the dimpled areas revealed a difference in the size and number of dimples between the two tempers. In the T651 specimen (Fig. 11), the dimples were fairly large at this magnification, and the second-phase particles associated with the dimples were the same size as the E-phase dispersoids (Fig. 11 versus Fig. 1). With the specimen in the T7351 temper (Fig. 12), the



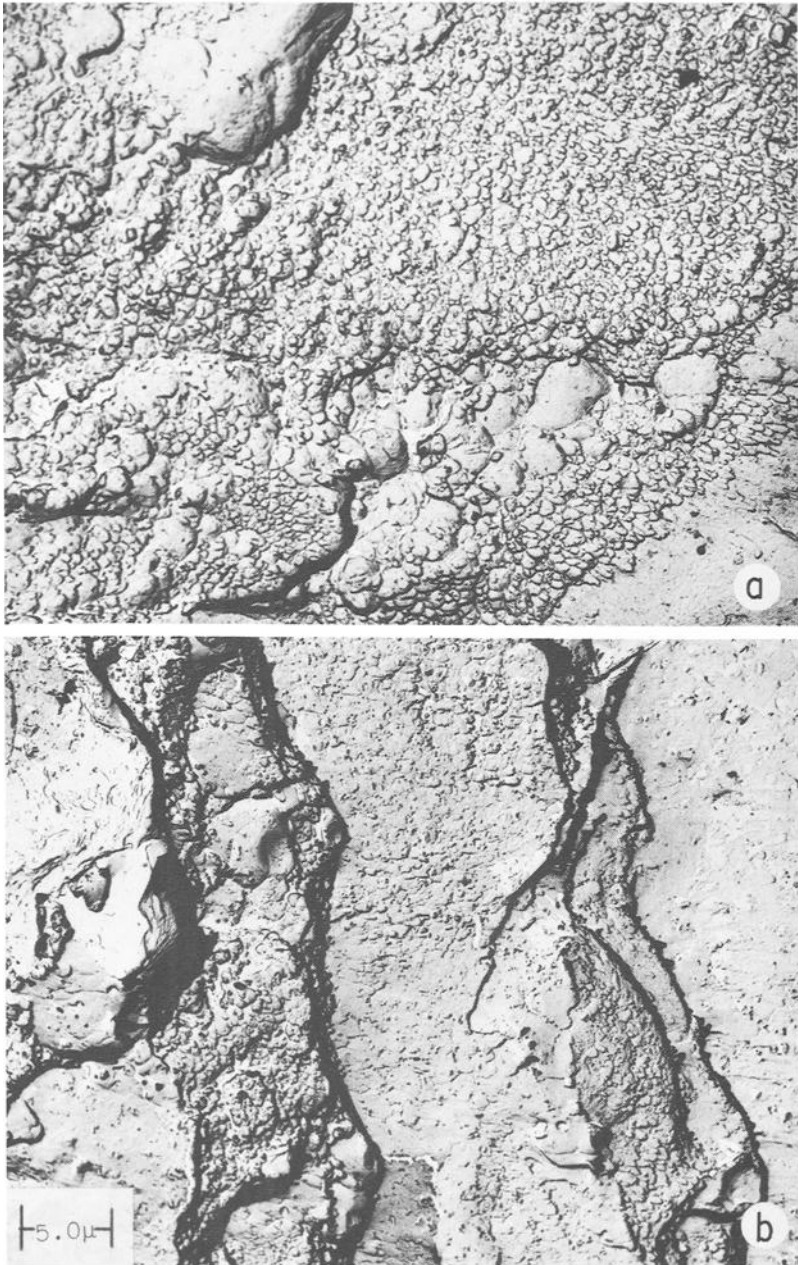
(a) As polished ( $\times 100$ ).  
(b) Keller's etch ( $\times 500$ ).

FIG. 3—Fracture contour and voids in vicinity of fracture of 7075-T7351 specimen.



(a) As polished ( $\times 100$ ).  
(b) Keller's etch ( $\times 500$ ).

FIG. 4—Longitudinal intergranular fissures in vicinity of fracture of 7075-T651 specimen.

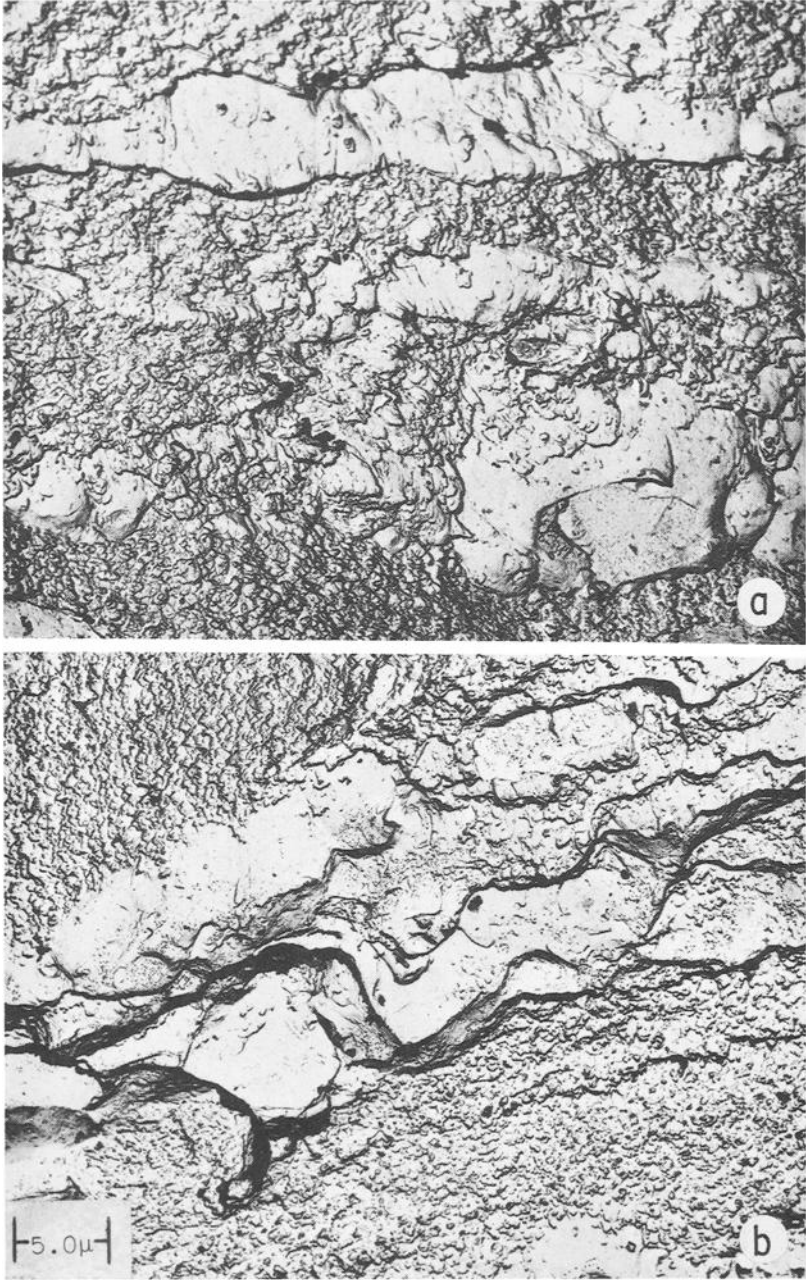


(a) 7075-T651.

(b) 7075-T7351.

Two-stage, plastic-carbon replicas

FIG. 5—Typical fracture topographies from the fracture initiation area ( $\times 3000$ ).

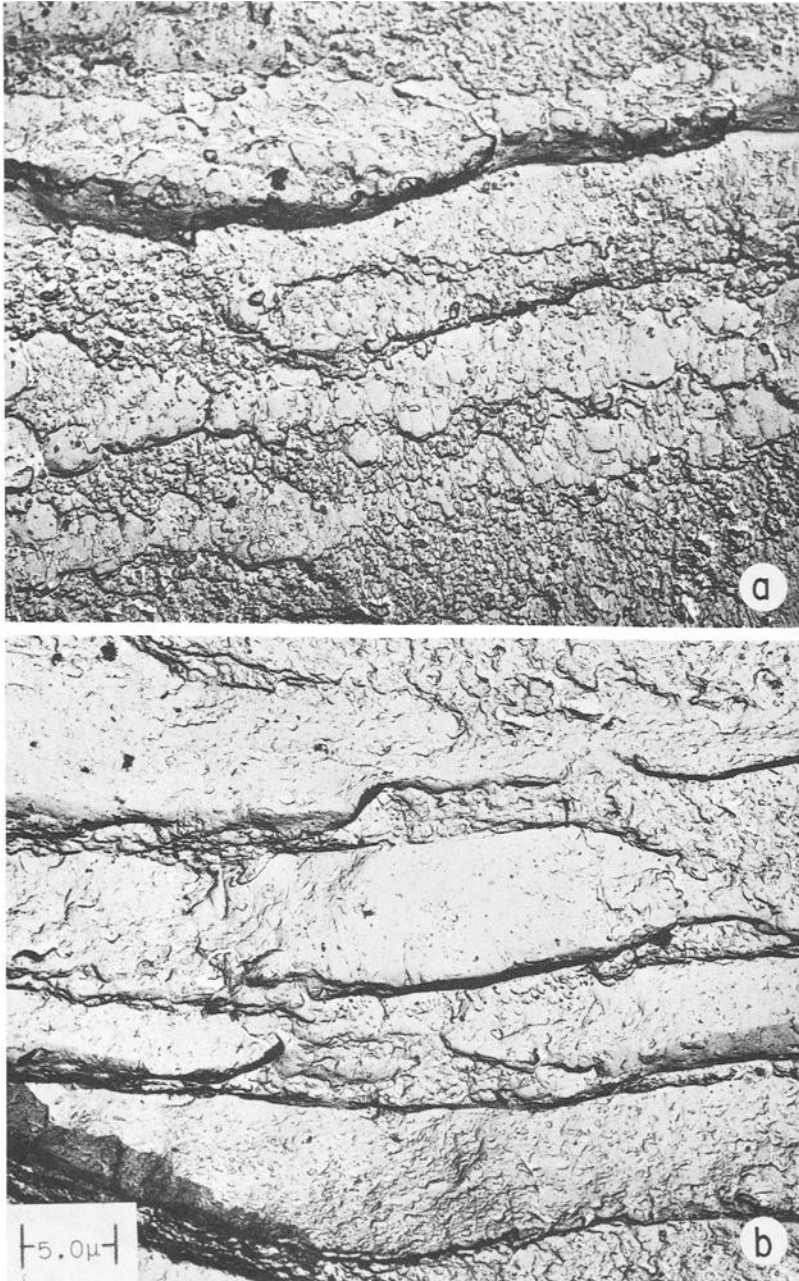


(a) 7075-T651.

(b) 7075-T7351.

Two-stage, plastic-carbon replicas

FIG. 6—Typical fracture topographies from center of fracture ( $\times 3000$ ).



(a) 7075-T651.  
(b) 7075-T7351.

Two-stage, plastic-carbon replicas

FIG. 7—Typical fracture topographies from final fracture area ( $\times 3000$ ).

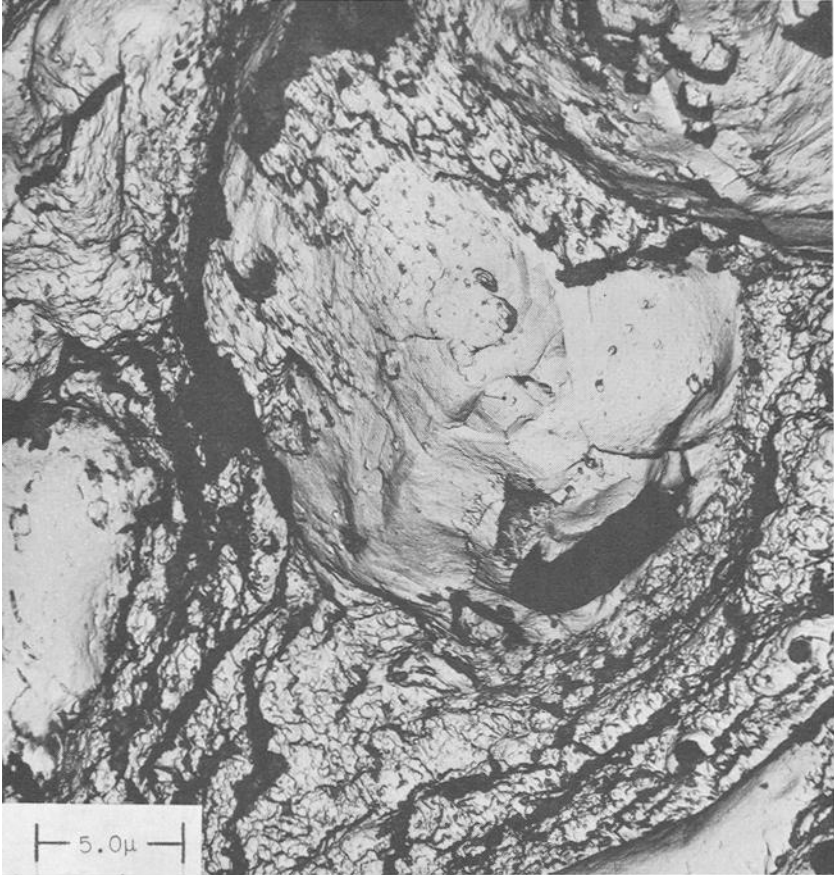


**FIG. 8**—Oxide replica. Typical transgranular fracture appearance in 7075-T7351 specimen ( $\times 5000$ ).

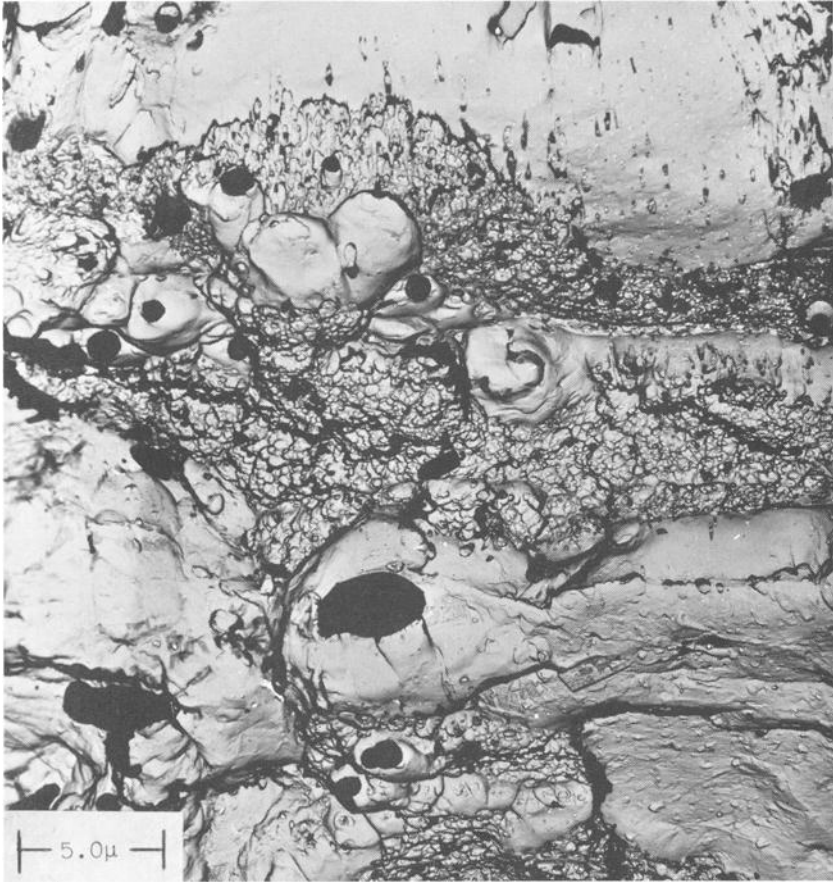


**FIG. 9**—*Oxide replica. Typical transgranular fracture appearance in 7075-T651 specimen ( $\times 5000$ ).*

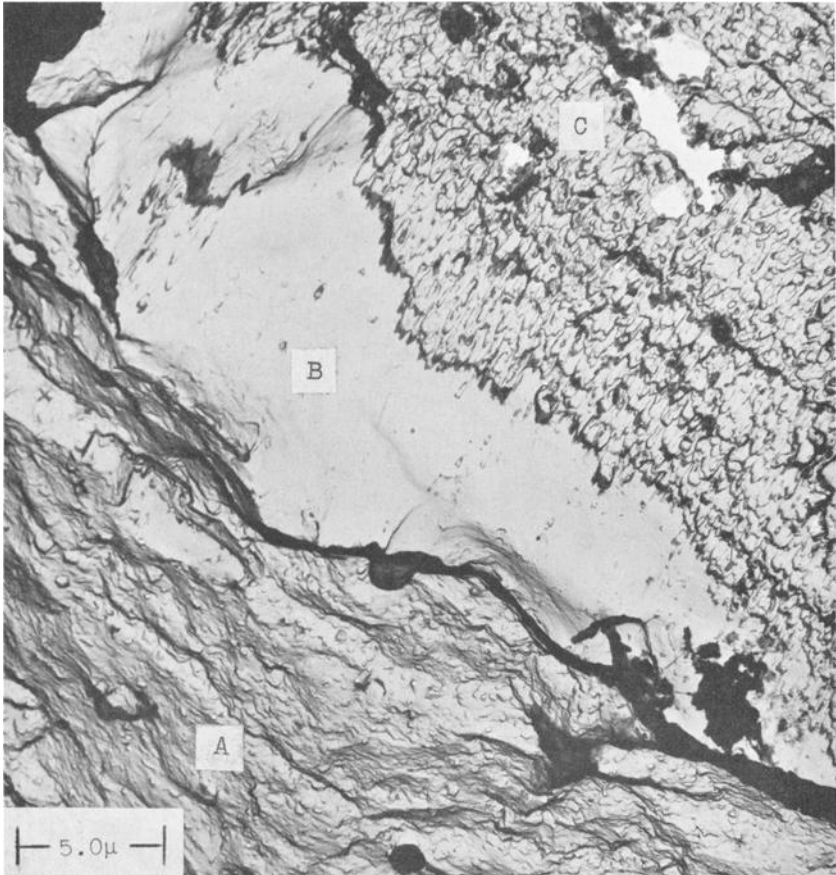


FIG. 10—Oxide replica. Intergranular fracture (a), a stretched region (b), and transgranular dimple rupture (c) in region of longitudinal fissure in 7075-T651 specimen ( $\times 5000$ ).

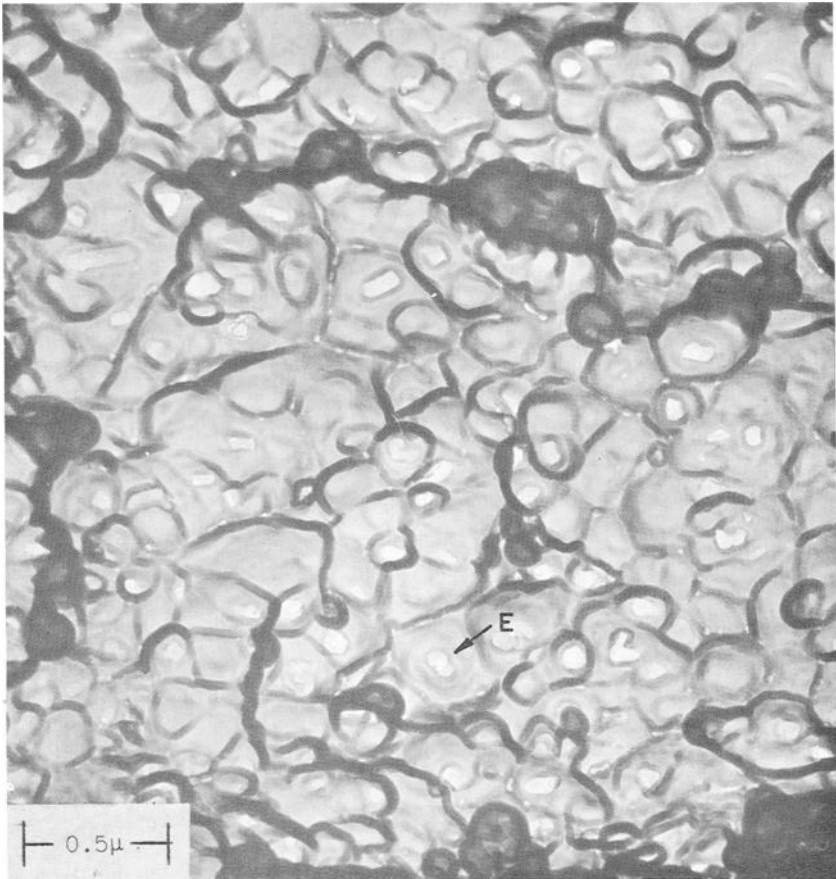


FIG. 11—Oxide replica. Comparatively large dimples associated with dispersoid particles on 7075-T651 fracture ( $\times 50,000$ ). E indicates dimple nucleation site believed to have been an E-phase dispersoid particle.

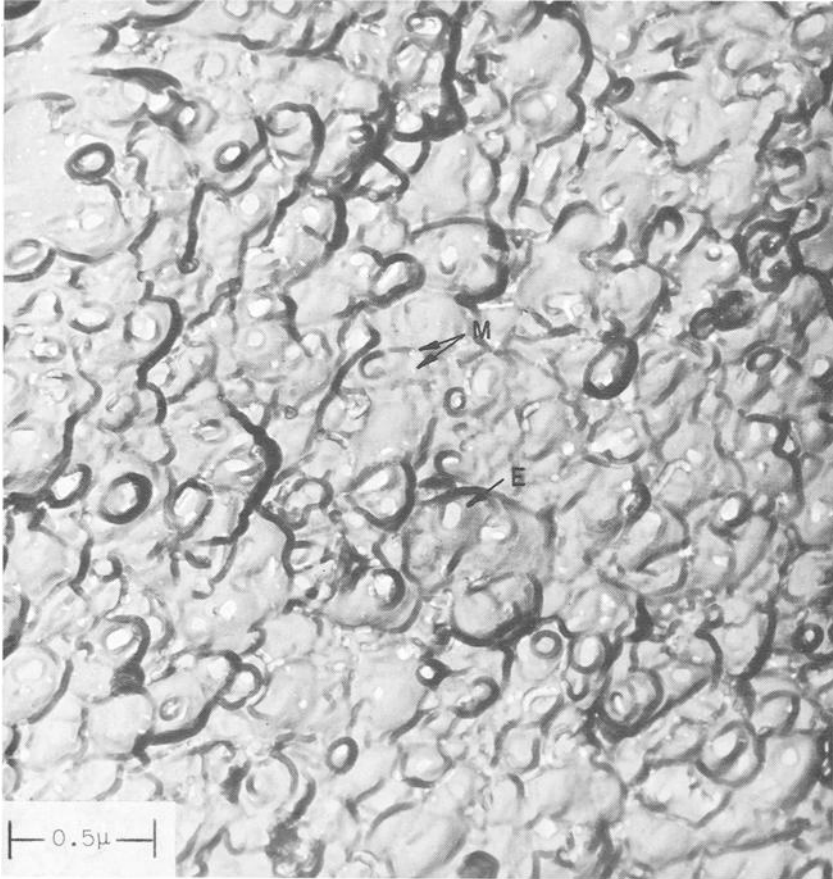


FIG. 12—Oxide replica. Mixture of large and small dimples on 7075-T7351 fracture ( $\times 50,000$ ). *E* and *M* indicate dimple sites believed to have been *E*-phase dispersoid and *M*-phase plates, respectively.

same large dimples were observed, but, in addition, there were a number of smaller dimples associated with smaller second-phase particles, possibly the small plate-like *M'*-phase ( $\text{MgZn}_2$ ) particles (Fig. 2) developed by the higher temperature aging treatment. The net result was more numerous dimples of a smaller average size in the T7351 temper.

### Discussion and Conclusion

In relating microstructural features to the fracture properties of the T651 and T7351 specimens, three factors are apparent, namely, the difference in yield strength of the two tempers, the difference in dimple size, and the partly intergranular fracture in the T651 specimen. The lower yield strength of the T7351 temper would promote greater frac-

ture toughness. The smaller and more numerous dimples in this temper reflect the greater number of fracture initiation sites, which would be expected to give this temper poorer fracture toughness. The partly intergranular fracture of the T651 material would tend to lower fracture toughness if the intergranular path was normal to the direction of stress. Since the intergranular fissures were parallel to the stress, they might be expected to improve fracture properties by blunting of the crack front and by contributing to a biaxial rather than a triaxial stress condition. It is believed, however, that the intergranular fissures were so few and so shallow that they did not help or harm fracture properties. Thus, lower yield strength contributes to improved fracture properties of the T7351 temper, and the larger number of dimples, reflecting additional fracture initiation sites, tends to decrease fracture properties. It is apparent that the yield strength advantage more than offsets the disadvantage of number of fracture sites.

W. R. Warke,<sup>1</sup> N. A. Nielsen,<sup>2</sup> R. W. Hertzberg,<sup>3</sup>  
M. S. Hunter,<sup>4</sup> and M. Hill<sup>5</sup>

## Techniques for Electron Microscopic Fractography

---

**REFERENCE:** Warke, W. R., Nielsen, N. A., Hertzberg, R. W., Hunter, M. S., and Hill, M., "Techniques for Electron Microscopic Fractography," *Electron Fractography, ASTM STP 436*, American Society for Testing and Materials, 1968, pp. 212-230.

**ABSTRACT:** The basic techniques of electron microscopic fractography are reviewed. Steps to be prior to replication for preventing damage and for cleaning are briefly covered. The three most common replication methods are discussed in detail. These methods are the plastic carbon, direct carbon, and oxide techniques. Examination techniques are also discussed covering the range for visual selection of areas to be studied through photography of representative areas. Stereoscopic viewing is given heavy emphasis because of the special advantages of this technique. Finally, the complementary technique of fracture sectioning is described.

**KEY WORDS:** electron microscopy, replication techniques, metals, metallurgy, fracture surfaces, fractography, metallography

Electron microscopic fractography is a metallurgical tool which is finding ever-increasing application in fracture research and service failure analyses. Skill and proficiency in the techniques employed require a good deal of practice and time. However, the ASTM Subcommittee on Fractography felt that a brief description of the basic techniques would be most useful to newcomers to the field and would assist them in avoiding some of the pitfalls which those experienced in fractography have already encountered. This report is intended to be very narrow in scope dealing only with fractographic techniques. For general information on other metallurgical applications of electron microscopy, the reader is referred to previous ASTM publications

<sup>1</sup> Instructor, Illinois Institute of Technology, Chicago, Ill.

<sup>2</sup> Research fellow, E. I. du Pont de Nemours & Co., Inc., Wilmington, Del.

<sup>3</sup> Assistant professor, Lehigh University, Bethlehem, Pa.

<sup>4</sup> Scientific associate, Alcoa Research Laboratory, New Kensington, Pa.

<sup>5</sup> Research metallurgist, Republic Steel Corp., Brecksville, Ohio.

[1,2]<sup>6</sup> and to standard textbooks on the subject [3-5]. Also, the interpretation of fractographs is not considered here, but is covered in the *Air Force Fractography Handbook* [6], in several review articles, and in many articles in the open literature [7-9]. One should become familiar with interpretation as well as techniques before attempting to employ this tool in either research or failure analysis.

The present paper deals with the basic techniques of replication with an introductory section on care and cleaning of fractures and later sections on examination and on fracture sectioning. Throughout this discussion, it should be remembered that three additional important factors are required; the person employing the techniques must always be guided by common sense, patience, and carefulness.

### Care and Cleaning of Fracture Surfaces

Common sense is certainly required in preserving and cleaning fracture surfaces to be examined by electron microscopic fractography. It is recognized that many of the requirements set forth in this section cannot be met in the case of many service failures. However, the more care that is exercised to avoid damage to fracture surfaces, the more meaningful and reliable will be the information obtained.

Unless a fracture is replicated immediately after it is produced, it should be preserved to prevent atmospheric attack. Depending on the nature of the specimen material, varying degrees of care must be exercised in protecting the fracture surface. Any metal or alloy which may react with the environment must be protected as soon as possible after the specimen has been broken. It is especially necessary to protect the fracture surfaces of steels since they rust rapidly in moist air and many fracture surface features are thus obliterated.

One may preserve the fracture surface of the specimen by storing it in vacuum or in a storage vessel containing a desiccant. The latter is obviously less costly and more practical. One may also spray the fracture surface with a protective coating to inhibit oxidation and corrosion. A commercial spray acrylic lacquer has been used for this purpose, and is very suitable since it is readily soluble in acetone. Coating with an oil or grease may suffice if the coating does not contain any compounds which might attack the metal specimen and does not contain any insoluble silicones.

If a particular specimen is to be used for electron fractography and yield meaningful information, mechanical damage to the fracture surfaces must be avoided. The two fractured halves must never be placed back together again as is often done with service failures or when a measurement of total elongation of a tension specimen is desired. If

<sup>6</sup> The italic numbers in brackets refer to the list of references appended to this paper.

such information is necessary then duplicate test pieces should be prepared (that is, one specimen will yield total elongation data while the other will furnish the fractographic information). It is also suggested that satisfactory fractographic information be obtained first and then elongation data measured when only one specimen is available. Also, rubbing, fingering, picking, or erasing on the fractures will destroy vital features which are necessary for fractographic interpretation.

When cleaning the fracture surface, it is imperative that no corrosive chemicals be used. To remove dirt, oil, and other coatings, acetone will usually suffice. Other organic solvents, acids, or alkaline cleaners may also be employed but should always be tested on a trial specimen to be sure that no etching, pitting, or corrosion will result. Commercial ultrasonic cleaners are available and have been used extensively by those working in the field of fractography. Ultrasonic vibration accelerates the action of the solvent and assists in the removal of debris.

Another cleaning technique used by many consists of stripping off and discarding the first few plastic replicas made from the fracture surface. The softened plastic flows around the loose dirt on the fracture surface, and when the replica is stripped the dirt is removed with the plastic. The one disadvantage to this process is that particles involved in the fracture process, which are of great interest to the investigator, will be removed so as to preclude their identification. Surfaces should never be cleaned by rubbing them with an abrasive tool or brush. To be sure, the surface will be cleaned, but the process will introduce scratch marks and obliterate a good portion of the fracture surface.

### **Replication Methods**

There are three techniques of replication which are commonly used for fractographic studies. These are the plastic-carbon method, the direct carbon technique, and the oxide replica techniques. Each of these replication techniques has its limitations and its areas of maximum applicability. The plastic-carbon technique is quite rapid and is nondestructive, the fracture surface being preserved for further study if desired. However, plastic-carbon replicas are more susceptible to artifacts than are the direct-carbon replicas. The direct carbon and the oxide methods give the maximum obtainable fidelity of reproduction of the surface. For example, the resolution of a direct carbon replica is about 50 Å while that for a plastic-carbon replica is about 150 Å. But single step replicas require deep etching or electropolishing of the surface to free the replica. Therefore, plastic-carbon replication is used primarily for service failure analysis and in cases where preservation of the specimen is of prime importance, while the other techniques are used mainly for research work on laboratory-produced fractures where

maximum fidelity is of prime importance and where production of duplicate specimens is not a problem.

### *Plastic-Carbon Replication*

In this two step technique, a piece of cellulose acetate tape is softened on one side by applying a few drops of acetone. After a few seconds, the excess acetone is allowed to run off, and the tape is pressed against the fracture surface. Other plastics, such as nitrocellulose or acetobutyrate may be used with suitable solvents to soften them. Pressure is maintained (usually with one's finger tip or an eraser) for a few moments (10 to 15 s). The specimen is then set aside for 10 to 20 min so that the plastic may be completely hardened. The hardening period will depend upon such things as the degree of softening before application, tape thickness, and ambient temperature. It is important that the tape be moistened with the proper amount of acetone. If too little acetone is used, the tape will not be able to fill in the crevices and other rough surface contours on the surface. If, on the other hand, the tape is too soft it will tend to tear apart when pressed onto the fracture surface, and, in addition, bubble artifacts may be produced. Experience has shown that a good replica can be prepared when the tape (usually two to ten mils thick) is soft and sticky on one side but still firm on the other side. The correct point of stickiness can be judged when the drop of acetone no longer flows freely on the surface of the tape and the tape has lost some of its stiffness.

The replicating tape should be removed only when it has completely dried. If the tape tends to peel off slowly (like removing adhesive tape from a surface) this indicates that the tape has not completely dried. The tape should almost "pop" off when one begins to pry it loose. Removing a tape that has not been completely dried can result in stretch lines and other artifacts. The plastic tape, now having the impression of the fracture surface, is called the primary replica.

The replica is shadowed by vapor depositing a heavy metal or alloy, an oxide, carbon or platinum-carbon in a vacuum evaporator at a pressure of less than  $0.1 \mu\text{m}$ . This procedure enhances the contrast of the final replica and results in easier recognition of various surface characteristics. The material employed for shadowing is not too critical at low magnification but at higher power, granularity and lack of stability under the beam become important considerations. Also the heavier the atoms of the shadowing material are, the greater will be the contrast produced by a given thickness. However, too much contrast should be avoided since important details may be hidden by the shadows. The amount of shadow deposited can be judged by placing a piece of white paper with an object or a drop of oil near the replica in the bell jar and

observing the development of the shadow layer on the paper. With experience the amount of shadow can be controlled more simply by the proper selection of the size of pellet, length of wire or amount of material to be evaporated, and the source-to-replica distance.

Contaminating gases and vapors influence the structure of the shadow layer. Therefore, deposition should be made at the lowest pressure obtainable in a reasonable length of time. For very high resolution studies, a cold trap on the evaporator should be considered.

A shadow angle of 45 deg is usually employed. If the surface is relatively flat, the shadowing angle is often reduced to produce longer shadows from the small elevations. Shadowing in a direction related to some important line on the specimen such as the macroscopic fracture propagation direction is an often used technique. By observing the shadows on the final replica, one is always able to correlate directions in a particular region with this propagation direction. Also, one is able in many cases to trace the fracture to an origin when no directional features exist in the propagation region.

Carbon is then deposited onto the shadowed primary replica. This is usually done at an angle of 90 deg to the replica surface. In cases where the fracture surface is very rough, the replica may be rotated on a motor drive table while the carbon is deposited at an angle less than 90 deg. This insures a continuous uniform layer of carbon on the fracture surface. If rotary deposition is used, the carbon film will be less likely to break up when the plastic tape is removed during final preparation. Also rotary carbon deposition avoids confusing double shadows. The desired thickness of the carbon layer should depend on the particular situation. If high resolution is important, the layer should be as thin as possible without running the risk of breakup during dissolution of the plastic tape. A thin carbon film has a yellowish color. A thicker film is obviously much stronger but does not have the fidelity of the thinner film. A thick carbon film has a gray-black color. The thickness is controlled by the amount of carbon evaporated and by the source-to-replica distance.

The next step, solution of the plastic primary replica, is the most critical and difficult step in the preparation of a replica. A maximum of patience and care is required. In the simplest method, the two layer plastic-carbon composite is carefully cut up into small pieces, about  $\frac{1}{16}$  in. on a side. The shape of these pieces may be used to correlate the orientation and location of the replica with respect to the specimen. The pieces are then placed in a spot plate or Petri dish containing a suitable solvent, acetone in the case of cellulose acetate. With the plastic side down, the preshadowed carbon replica will tend to float freely much more quickly. After three washings in fresh solvent baths the replica is ready to be fished out with a copper grid. This operation

should be carried out under a binocular microscope at  $\times 7$  to  $\times 10$  magnification. The film may be more easily fished out if most of the acetone is removed first, reducing the mobility of the film. Replica motion can also be greatly reduced by placing the clean replica in an alcohol bath.

Difficulty is often encountered during the washing operation since the plastic swells as much as 50 per cent while dissolving and shatters the thin brittle carbon layer into useless small pieces. A number of procedures have been proposed to avoid or alleviate this situation:

1. Balance plastic sheet thickness with fracture surface roughness. Rough surfaces such as ductile ruptures require thick plastic to ensure a continuous replica. Smooth surfaces like many fatigue fractures require a thinner plastic to prevent breaking.

2. Make carbon evaporation at the lowest possible pressure.

3. Cut the acetone by as much as 3 to 1 with alcohol or distilled water.

4. Warm the acetone bath.

5. Use vapors of acetone or an extractor to wash the plastic from the replica.

6. Embed or laminate a specimen grid in the plastic to restrict expansion.

7. Coat the carbon side of the plastic-carbon composite with paraffin before immersing in acetone. The paraffin can be subsequently removed without expansion by washing in benzene.

The experimenter should try the various techniques to find the one which he is best able to employ and which works most satisfactorily on the particular specimens he is attempting to replicate. He should also expect to improvise on the aforementioned list to suit his needs. In any case, the end result is a carbon replica appropriately located on a specimen grid ready to be examined in the electron microscope.

#### *Direct Carbon Replication*

In the case of direct carbon replication, the intermediate plastic replica is eliminated, and the carbon film for examination is prepared directly on the fracture surface. Structure and artifacts which could result from the plastic replica are avoided. Thus, direct carbon replicas are employed when increased fidelity is required and when specimen destruction is permissible.

The shadow and carbon layers for a direct carbon replica are vapor deposited directly on the fracture surface. It is common practice to mask off all of the specimen except the area of interest using stop-off lacquer or tape prior to shadowing. The shape of the unmasked region and the direction of shadow can both be used to relate directions on the replica to the fracture surface. The same rules and precautions for

these operations outlined earlier for plastic-carbon replicas apply to direct carbon replication as well. It is even more important to employ rotary deposition of carbon in this case to ensure a more uniform, continuous coverage of the fracture surface.

The shadowed carbon film is freed from the specimen by etching away the surface to which the replica is attached. It is advantageous to cut the replica into conveniently sized pieces by scribing the shadowed fracture surface prior to etching. Any etchant, chemical polishing solution or electropolish which is suitable for the alloy in question may be employed for stripping direct carbon replicas *provided it does not result in gas evolution at the specimen surface*. Gas bubbles forming and leaving the surface tear the replica rendering it useless. One etching solution which is quite generally applicable but which requires *extreme* care in handling is a 2 to 10 per cent solution of bromine in methanol. CAUTION—severe, slow healing, third degree burns result if this bromine solution comes in contact with the skin. Extreme boiling or bumping can occur when the bromine is added to the alcohol unless it is added slowly with adequate stirring and cooling.

The time required to free the replica is determined by trial and error and may range from a few seconds to several hours. Gentle agitation may be used to assist in freeing a loosely clinging replica. Once the replica is floating in the etchant, it is lifted out and rinsed in a series of alcohol or distilled water baths. Dilute acid may also be used to dissolve debris clinging to the replica, but an acid which does not attack the shadow metal must be used. Often, the carbon film will roll up when stripped, but platinum shadowing will minimize the tendency to curl. Such replicas can be salvaged by alternate immersion in alcohol and distilled water which causes the replica to either straighten or shatter. Once cleaned, the replicas are lifted on specimen support grids and examined or stored in covered containers for future study.

### *Oxide Replication*

Oxide replicas have a unique application and ability in the examination of metal surface structure by electron microscopy. Some general advantages of oxide replicas are the following:

1. The replica consists of a thin oxide film formed to controlled thickness on the metal or alloy surfaces. As such it represents the actual surface layer of the specimen.
2. The oxide films can be chemically or electrochemically stripped from the specimen. Their preparation and isolation introduce a minimum of artifacts to be confused with true replicated structure.
3. Excellent contrast and resolution can be obtained. Variations in surface composition resulting from the presence of secondary phases, precipitates, etc., affect the thickness and structure of the replica and

thereby the electron scattering ability of the film. The films, therefore, have improved image contrast and definition.

4. Oxide replicas are particularly characterized by their dimensional stability. They have the least tendency of all types of replicas to deform or flatten upon positioning and drying on a support grid. The true "three-dimensionality" of the replicated surface topology is maintained in the replica. The use of stereotechniques is very much facilitated.

The prime requirement of oxide replicas is that they should themselves be "structureless" or have minimum electron microstructure. Oxide films which are granular, or porous, or characterized by fine oxide crystallites cannot adequately replicate the structural detail of the substrate metal. These requirements are best fulfilled by the oxide films which form or can be formed by various oxidation treatments on aluminum, titanium, nickel, the stainless steels, high nickel alloys, and the high alloy refractory metals. As a general rule, these metals and alloys whose normal corrosion resistance or useful passivity behavior is associated with the presence of thin, protective surface oxide films are the ones which can be successfully oxide-replicated.

*Aluminum and Aluminum Alloys*—Aluminum and its alloys are especially well suited for oxide replication since they form very tight, structureless, adherent anodic oxide layers. Therefore, oxide replication of these materials is used extensively. A common technique<sup>7</sup> consists of replica formation in a 3 per cent tartaric acid solution adjusted to a pH of 5.5 with ammonium hydroxide (NH<sub>4</sub>OH). The solution is employed at ambient temperature with the specimen as the anode, a high-purity aluminum cathode, and a forming potential of 20 V. The specimen is tapped frequently to dislodge the bubbles which form. Anodization is continued until bubbles no longer form, usually 5 to 10 min.

Areas to be examined are selected and the oxides scraped from the remaining area. The replica is next stripped from the specimen electrolytically in 20 per cent perchloric acid in denatured alcohol. Again the specimen is the anode, and a strip of high-purity aluminum is the cathode. A voltage of 12 to 15 V is applied until the replicas float off from the specimen. The replicas are then washed thoroughly in distilled water.

*Stainless Steels, Nickel, and High-Nickel Alloys*—Mahla and Nielsen [10] in 1948 developed a technique to form and strip oxide films which serve as very satisfactory replicas for the above metals and alloys. While no extensive investigation of oxidation procedures was made, it was found that heat-tinting the specimens in a molten mixture of NaNO<sub>3</sub>KNO<sub>3</sub> (equal parts by weight) produced oxide films that when stripped are sufficiently "structureless" to function as excellent

<sup>7</sup> Hunter, M. S., private communication, Alcoa Research Laboratories.

replicas. In their procedure the metal specimen can be prepared by the usual metallographic techniques or with any degree of surface roughening as by deep etching or a fracture process. The specimen is then immersed in the molten nitrate bath until it is superficially oxidized to the extent that the surface shows a light yellow interference tint. A considerable degree of control of the oxidation conditions is possible, and visual inspection of the specimen is sufficient to determine when it should be removed from the salt bath. For instance, a specimen of deep-etched austenitic stainless steel was oxidized for 5 min at 800 F (425 C) to produce a replica film of satisfactory thickness and properties. However, there is considerable latitude in the time and temperature of oxidation so that an exact specification is not critical. There is reason to believe, however, that the oxidation procedure which produces a replica film of a given thickness, say 250 Å, at the lowest temperature of oxidation should also develop the finest crystallite structure within the oxide. (Room-temperature, air-formed "passive" films on stainless steel are essentially structureless and amorphous.) T. Katsurai [11] has used a 50 KNO<sub>3</sub>, 50 NaNO<sub>3</sub>, 1 MnO<sub>2</sub> (by weight) fused salt bath to study the electron microstructure of four different stainless steels and Armco iron. His oxidation treatment was carried out at 300 C.

Subsequent to oxidation, the specimen is cooled in air, washed with distilled water, and dried. After 1/8 in. squares have been scribed with a razor blade or a sharp-pointed instrument on the oxidized surface, the specimen is wholly immersed in a solution of bromine in methanol. (The concentration of this solution is not critical up to the maximum safe level of 10 per cent. Nickel specimens require rather dilute solutions, 2 to 3 ml of bromine per 100 ml of methanol, while a stronger concentration, 7 to 10 ml of bromine in the 100 ml of methanol is necessary for stainless steel specimens.) As mentioned earlier, extreme care should be exercised to avoid bromine burns. The bromine solution attacks the film-free metal exposed along the scratches and effectively undermines the oxide film, freeing it from the metal. When the film is completely stripped—a matter of several minutes to several hours according to the metal composition—small squares of oxide film float free or cling loosely to the base metal. Gentle agitation of the solution or specimen serves to detach this film. The squares of oxide film are collected with a piece of 200-mesh wire screening and are washed by transfer through successive dishes of fresh methanol. The individual squares of film are then caught on a microscope screen, dried, and examined in the electron microscope.

If a particular area on the metal specimen is to be examined, this area only is originally scribed in the metal surface. The one square of film is easily isolated for investigation.

Further examples of the use of oxide replicas of this kind are given by (a) Mahla and Nielsen [12] in studies of carbide precipitation in stainless steel (the oxide replicas also function as extraction replicas when inert, nonmetallic precipitates are present in the alloy microstructure), (b) by Heindenreich [13] who used thermal oxide replicas to study Widmanstätten precipitates in Alnico V alloy heat-treated in a magnetic field, and (c) by Nielsen [14,15] who used such replicas in stress-corrosion cracking research and in examining platinum-decorated sites of corrosion attack in plastically strained stainless steel.

*Other Metals*—As pointed out, all refractory metals and alloys form protective oxide films which are potentially useful surface replicas. Titanium (and alloys) is one of the best examples. Oxide films from the normal room-temperature oxide to heavier oxides built up by thermal oxidation techniques can provide useful information on the titanium topology and microstructure. Again film-stripping can be accomplished by the bromine-methanol technique in most of these cases. It may also be convenient, however, to experiment with electrolytic stripping techniques. Gulbransen et al [16] have made investigations of oxide films electrolytically isolated from metallographically polished specimens of numerous metals and alloys oxidized at high temperatures in 0.1 atm of oxygen. Their techniques may be applicable to the fractographic examination of these materials.

### *Special Techniques and Applications*

In this section, a number of special replication techniques and applications are described. These methods in some cases entail some steps which differ from those described earlier, but in general the main requirement is a great amount of the common sense, patience, and care which was mentioned previously.

*Origins and Other Specific Areas*—In both fracture research and service failure analysis it is often desired to use fractography to determine the mode of crack initiation as well as propagation. The site of the fracture origin can be ascertained macroscopically by observing radial patterns or arrest marks, or microscopically by tracing back cleavage rivers or fatigue striations. Also, it is sometimes desired to examine a particular fracture facet or other small region on a fracture surface. Two problems are encountered in replicating such areas. First, origins are often located at a free surface (that is, at the edge of the fracture surface). Secondly, the specific area of interest will, in general, be located over a grid bar and not be accessible for examination.

Replicating the entire fracture surface, out to the edge, is not too difficult. Trimming off of the excess plastic with a scalpel or razor blade before stripping is often of assistance. If the excess is not removed it can cause difficulty during shadowing and washing. If an origin is lo-

cated at the edge, shadowing should be done in a direction opposite to the crack propagation direction. This practice avoids shadow deposition on the cut edge of the plastic replica which will often fold over resulting in a double layer at the edge of interest. During washing, replicas tend to crack at the edges. So, to obtain a good replica of an origin at this location, the carbon film should be as thick and as strong as practicable. Also, unnecessary agitation and handling of the replica during immersion washing should be avoided.

Placing of a replica on a specimen grid so that an area of interest is over a grid opening is largely a matter of patience. First of all, the operation should be carried out under a stereo binocular microscope at  $\times 7$  to  $\times 30$ . Secondly, grids of the coarsest mesh possible should be used to maximize the open area. Also it is possible to use grids with one enlarged opening, either purchased or manufactured with a scalpel blade over which the area of interest is placed. Then, either several replicas are prepared to improve chances of success or a replica is carefully strained from an alcohol bath under the binocular microscope, checked for location at about  $\times 30$ , and either refloated, or dried and stored depending on the result obtained.

*Matching Fracture Surfaces*—Although more will be said later about the examination of replicas from matching fracture surfaces, there are some aspects of this technique concerned with replication. If the specimen is of an amenable shape, it is often convenient to clamp the two halves of the fracture together so that corresponding areas on the respective halves are opposite one another. A plastic replica is then made spanning the interface. Some plastic is usually forced down between the two halves of the fracture, and this fin of plastic should be trimmed off with a scalpel prior to shadowing. After carbon deposition small areas spanning the interface are cut out and washed so that the corresponding regions from each half of the fracture are located on the same specimen grid facilitating location and examination. Again, the use of a coarse grid with a greater percentage of open area is advised. This technique is applicable to square bar or sheet specimens but not, in general, to round or irregular pieces.

*Small Specimens*—On occasion wire or foil specimens too small to be replicated by the normal plastic-carbon technique are to be studied. In such cases some success has been obtained by taping a piece of plastic to a glass slide, resting the fracture surface on the plastic, and flowing a drop of acetone under the specimen. The weight of the specimen may be sufficient to press the fracture into the soft plastic. The specimen can be held in self-locking tweezers to provide additional weight. The impression is usually sunk into the plastic, and the excess material must be trimmed away to allow adequate shadowing.

*Etched Fractures*—Comparison of replicas of a fracture surface be-

fore and after etching will in many cases reveal much additional information on the role of the various microconstituents in the fracture process. Also, light etching will facilitate extraction of precipitates. Usually a light etch with the normal metallographic etching solution for the alloy being studied will suffice to delineate the various phases exposed on the fracture surface. Determination of the optimum etchant and etching time will be required for each alloy studied.

### **Examination**

The next aspect of electron microscopic fractography to be discussed is the actual examination of the fracture. In this discussion, it is assumed that the reader has access to a transmission electron microscope and is familiar with its operation.

There are two advantages of the electron microscope over the light microscope which have resulted in electron microscopic fractography being such a useful tool. These advantages are greater magnification and vastly increased depth of field. The high magnifications of which the electron microscope is capable allow the study of submicron sized features on fracture surfaces. However, most of the information to be obtained from fractography is visible at relatively low magnifications for the electron microscope, and it is the depth of field of the instrument which is most important. Under normal conditions, this depth of field is on the order of several microns. The short range level differences on a fracture surface are usually less than this amount so that the entire field of view is in sharp focus even though the surface represented is quite rough.

#### *Visual and Low Magnification Examination*

In general, examination of a fracture surface begins at the visual level and proceeds to succeeding higher magnifications with electron microscopic fractography as the final step in this process. Even prior to replication, as much information as possible should be obtained by optical examination of the fracture at magnifications from  $\times 1$  to  $\times 500$ . Studies with a binocular microscope up to  $\times 50$  will give information on the location of the origin of fracture, shear lips, changes in fracture mode as revealed by changes in texture, and the direction of fracture propagation as indicated by chevron marks, radial markings, and arrest marks. Higher power light microscope studies will give further information on fracture origins and directions and may indicate the general fracture mode (that is, cleavage may be distinguishable from intergranular fracture).

Photomacrography of fracture surfaces becomes difficult at magnifications above  $\times 30$  to  $\times 50$ . Here the principal limitation is depth of field, the lack of which often makes it impossible to clearly show high

points and crack bottoms in the fracture. Also, metallic fractures commonly contain many small mirror-like areas at all possible orientations, and these disperse the light to obscure detail. Among the combinations of illumination which can be tried to avoid this trouble are highly directional light both from the side and from devices like metallurgical illuminators, polarized light, and monochromatic light. Stereoscopic photography obtained by tilting the specimen between exposures will often be helpful. Sometimes carbon, silicon oxide (SiO), or other materials have been vapor deposited on fractures to dull the mirror effect.

The lack of depth of field is the most troublesome problem, however. A greater depth of field may be had for ordinary photographic lenses by stopping them down to a small opening. With modern rapid films the hour-long exposures of the past are obviated. At the higher magnifications this is not feasible, and so Zapffe [17] and co-workers introduced the art of examining interesting regions which were nearly planar by turning the specimen to bring the region in view and then grinding away interfering material so that the microscope objective could be focused on the fracture or aspect to be studied. Successful use of the method requires great patience, manipulative dexterity, practice, and a reasonable concept of what the area being sought should look like. Frequently, it is possible to precede the detail grinding with careful electrical discharge machining so that less time is consumed than if only grinding was used. Another means of improving the depth of field is the use of a scanning microscope which is commercially available. At the time of this writing there are few reports in the literature of its application to fractography. It appears to be capable of use from below  $\times 100$  to above  $\times 1500$  on the specimen surface without special preparation and appears capable of covering a usefully large field. However, the quality, resolution, and ease of use of the instrument for fractography remain to be fully explored.

Low magnification studies of fracture surfaces may also be carried out on replicas. In some cases the study of the fracture's surface may be foregone to permit use of a replica made in the same way as for electron microscopy. A negative plastic or silicone rubber replica can be stripped from the fractured surface and studied. The replica quality with silicone rubber is inadequate above about  $\times 1000$ , but at low magnifications it is more completely pulled out of cracks and crevices than the usual replicating plastics and can serve as a semipermanent record of the overall fracture appearance. These replicas can be studied as units, or by microtomesectioning, contour maps of the fracture can be prepared. This, however, may be too time consuming for most investigations. The quality of either plastic or silicone rubber replicas can be greatly improved by vacuum deposition of a metal such as aluminum to increase the reflectivity and contrast. Plastic replicas may

also be examined with transmitted light, facilitating observations of neighboring noncoplanar facets.

### *Electron Microscopic Examination*

Once these low magnification studies have been carried out and the general location of important features and the fracture growth direction have been ascertained, examination proceeds to the electron microscope. Again, examination begins at the lowest magnification normally available. At  $\times 1500$  to  $\times 4500$ , it is usually possible to distinguish the features characteristic of the major fracture categories (that is, dimpled, cleavage, intergranular, or fatigue). At this magnification, the replica is scanned to ascertain its shape, location, and orientation and to locate the grid openings where replica quality is highest. The relative proportions of the various fracture modes can be evaluated, and the location of a specific feature which was seen using light microscopy can best be found at the lowest available magnification.

Higher magnifications are employed to study features of special interest in detail. Very fine striations can be resolved or the interaction of fatigue striations with precipitates can be studied. The shape and nature of the dimple nuclei in a ductile fracture region may be evident at high magnification. Many other examples could be given of the use of the higher magnifications available in the electron microscope. In any case, as was mentioned earlier, the maximum useable magnification for a replica is set by the resolution of the replica itself. Plastic-carbon replicas do not yield much additional information above about  $\times 12,000$  while the corresponding magnification for direct carbon replicas is about  $\times 40,000$ .

There are situations where it is desirable to employ magnifications on the electron microscope even lower than those normally obtained. This can be accomplished on some microscopes by simply turning one of the lenses down or off. On other microscopes, this is not possible, but the same end can be reached by raising the replica away from the objective lens in a special holder. Low magnifications are employed when studying matching fractures. The magnification is reduced to the point where one grid opening fits on a photographic plate, and the replicas of the two fracture surfaces are mapped out grid opening by grid opening. Prints of these maps are then compared to find the matching regions which can then be examined and compared at normal magnifications. Extra-low magnification is often convenient for locating specific features such as origins since one may employ the same magnification in the electron microscope as was used in a light microscope to locate the feature. Also by going to low magnification and enlarging, it is possible to avoid mounting with its attendant seams and mismatches.

### *Photography*

Facilities for photographic recording of the fracture surface appearance are available on electron microscopes. Much could be said regarding the relative merits of various films, developers, and so forth, but that is not the concern of this report. In this connection it should be pointed out, however, that the same precaution is necessary in fractography as in all metallography. Namely, care should be exercised to photograph typical rather than unusual areas on a fracture surface unless there is clear evidence that the unusual area has some special significance. It can almost be said that areas having the appearance typical of every fracture made can be found on every fracture surface. That is, small regions of brittle fracture are often found in the most ductile specimens, and photographic recording of such a region would be misleading and in the case of service failure analysis could lead to completely erroneous conclusions. So the representative—rather than the outstanding—should be recorded as fractographs, and enough fractographs to adequately present the proportion of various fracture modes in fracture surface should be obtained.

### *Stereoscopic Microfractography*

Manufacturers of present-day electron microscopes incorporate in all but the most inexpensive models simple specimen tilting devices such that stereopairs of micrographs can easily be taken. It is to the user's benefit to take advantage of this feature of the electron microscope (and especially in fractography) as will be summarized in the following section.

*Advantages*—The obvious advantage of stereomicrography is that the observer gets a three-dimensional view of the specimen surface. He is able, almost instantly, to see the true topology, to know what is up and what is down, to distinguish specimen from supporting film, true structure from artifact structure, etc.

Thus, stereomicrography eliminates much of the confusion that often results in ambiguous interpretation of the surface topography in a single micrograph. The various shadings in photographic density become meaningful in terms of topology. Fractography becomes a more complete study and fracture modes more easily identifiable when the fracture surfaces can be visualized in their true spatial geometry.

Another value of electron stereomicrography which is perhaps unappreciated consists of the increased resolution afforded of surface structural detail. Because there are two separate micrographs which the eyes and brain fuse into a single picture, that net image is the result of the contributions of twice the number of electrons and photographic grains. Imperfections and "noise" in the photographic emulsion tend

to cancel out. Even when one micrograph of the pair is off focus, the single fused image appears sharp and clear.

*Procedures*—The first requirement, of course, is a good replica which faithfully reproduces the surface topography of interest and remains dimensionally stable and rigid. On the latter point, oxide replicas are far superior to carbon replicas (particularly on fracture faces where there are re-entrant surfaces). Quantitative measurements will be in considerable error if the replica film flattens or distorts during preparation.

To obtain stereomicrographs, two successive pictures are taken of the same field, tilted between exposures along a line perpendicular to the electron beam. The “built-in” stereoangle in electron microscopes is usually in the 6 to 10 deg range.

The stereomicrographs are viewed as prints or transparencies (positives). In both cases they are positioned or mounted along a base line at right angles to the axis of tilt and to the electron beam. Some points to remember are the following:

1. The stereomicrographs should be taken, if possible, from areas on the replica that lie on the axis of tilt. Otherwise there will be magnification differences between the two micrographs which will have to be compensated for when making exact photographic measurements. Positive transparencies may or may not be capable of correction.

2. The exact same field must be photographed in the two successive pictures. The same area must be brought back to the center of the fluorescent screen for the second micrograph (after the specimen has been tilted through the fixed stereoangle) and usually must be re-focused.

3. The two exposures in the stereo pair should be made to duplicate photographic density.

*Viewing*—Electron stereomicrographs are most commonly viewed as prints using a stereoscope (or stereopticon).<sup>8</sup> When the electron microscope is equipped for 35-mm roll film micrography, it is convenient to make 35-mm transparencies. These are mounted in standard 35-mm stereo-slide mounts which may then be examined in a hand viewer, a table viewer, or by stereo-projection onto an aluminized screen. Table-viewing and projection-viewing both involve superimposed polarized images. The observer must wear polaroid spectacles to see the three-dimensional image.

All of this equipment is commercially available, having been de-

<sup>8</sup> Three sources of supply of such devices are: (1) Air Photo Supply Corp., 158 South Station, Yonkers, N.Y.; (2) Abrams Instrument Corp., 602 East Shiawassee St., Lansing, Mich.; and (3) Wild Heerbrugg Instruments, Inc., 366 Main St., Port Washington, N.Y. The latter two companies market more expensive stereoscopes having parallax bars available for quantitative measurement of differences in elevation of topographical features present in the stereomicrographs.

veloped by several manufacturers for the once popular 35-mm stereo-photography hobby. Those interested in specific equipment for viewing and projection should consult the annual *Industrial Photographic Catalog*.

*Quantitative Surface Relief Measurements*—Stereophotogrammetry is the process of measurement from stereo pairs of micrographs (but more commonly, photographs). Measurements of elevation of topographical features in a surface replica of a fracture face, for example, would be typical of the process. A parallax bar is employed with an appropriate mirror stereoscope. X-direction parallactic displacement (that is, difference in separation perpendicular to the tilt axis) is measured with a micrometer and the value inserted into the following formula [5] to calculate an elevation value:

$$\Delta Z \approx \frac{\csc \gamma}{2M} \Delta X$$

In this equation,  $\Delta Z$  is the difference in elevation of the two points,  $2\gamma$  is the total stereoscopic tilt angle,  $M$  is the magnification, and  $\Delta X$  is the parallactic displacement.

To prepare a contour plot sufficient measurements must be made on the micrograph to connect points of the same elevation for a series of elevations bracketing the range of "roughness" present in the surface topography. Specific instructions on the use of parallax bars are furnished by their manufacturers (two of these were listed earlier).

### Fracture Sectioning

The final technique to be described in this report is fracture sectioning. Although this is not a fractographic technique in the strictest sense of the term, it is closely connected and can contribute much additional information and so is included here. By examining the fracture surface, the appearance characteristic of various fracture modes and testing conditions can be studied and some conclusions regarding the micro-mechanisms of the fracture process can be reached. By combining the study of fracture profiles with fractography at the same magnifications, much more can be learned about the role of microstructure in the fracture process.

Often the best expedient to obtaining good fracture profiles is to plate the fracture with nickel or chromium so that it will not be injured in polishing. Then it may be sectioned and examined by conventional metallographic means. Before plating it is essential that the surface be clean. If there are deep crevices into which replicating plastic has been forced and then broken off or if heavy grease is on the surface, even ultrasonic cleaning may require several changes of solvent.

Frequently the electroplate does not penetrate into recesses but

bridges them forming pockets in the sections which catch etchants and polishing compounds. This may be largely avoided by a preliminary plate of chemical nickel or cobalt sufficiently heavy to smooth the surface outline. This plate will be laid down as deeply as the liquid can penetrate. It may be followed by electro-nickel or hard chrome. When sections are made through cracks it is desirable not to use a pressure-mounting medium. Indeed, application of a room-temperature setting mount under vacuum is desirable. Pressure mounting may bend the parts of the cracked specimen thus opening secondary cracks which will confuse interpretation. Since the section-polishing technique shows the conditions only at a single plane, it is easy to misinterpret evidence of crack paths, the influence of inhomogeneities, and the like. Consequently it is often desirable to polish, replicate, repolish, replicate, and so continue until the photographs present a composite three-dimensional representation of the fracture. The polishing and replicating techniques employed are usually the standard ones for the alloy being studied and so will not be described here. Often it is desirable to polish until some feature shown in an electron fractograph is reached in section. This is always difficult but may be simplified slightly by making a recognizable landmark which will be reached by the polished surface a known distance before the desired feature is reached. Microhardness indentations or electrospark marks are satisfactory as landmarks. If the process is successful, a direct comparison of surface and profile can be made.

## References

- [1] *Advances in Techniques in Electron Metallography*, ASTM STP 339, American Society for Testing and Materials, 1963.
- [2] *Advances in Electron Metallography and Electron Probe Micro-Analysis*, ASTM STP 317, American Society for Testing and Materials, 1962.
- [3] *Techniques for Electron Microscopy*, Kay, D., ed., Blackwell's Scientific Publications, Ltd., Oxford, 1965.
- [4] Thomas, G., *Transmission Electron Microscopy of Metals*, Wiley, New York, 1962.
- [5] Heidenreich, R. D., *Fundamentals of Transmission Electron Microscopy*, Interscience, New York, 1964.
- [6] Phillips, A., Kerlins, V., and Whiteson, B. V., *Electron Fractography Handbook*, ML-TDR-64-416, Air Force Materials Laboratory, Wright-Patterson Air Force Base, Ohio, 1965.
- [7] Beachem, C. D. and Pelloux, R. M. N., "Electron Fractography—A Tool for the Study of Micromechanisms of Fracturing Processes," *Fracture Toughness Testing and Its Applications*, ASTM STP 381, American Society for Testing and Materials, 1965.
- [8] Pelloux, R. M. N., "The Analysis of Fracture Surfaces by Electron Microscopy," *Metals Engineering Quarterly*, Vol. 5, No. 4, Nov. 1965, p. 26.
- [9] Warke, W. R. and McCall, J. L., "Fractography Using the Electron Microscope," Technical Report No. W3-2-65, American Society for Metals.
- [10] Mahla, E. M. and Nielsen, N. A., "An Oxide Replica Technique for the Electron Microscopic Examination of Stainless Steel and High Nickel Alloys," *Journal of Applied Physics*, Vol. 19, No. 4, 1948, pp. 378-382.

- [11] Katsurai, T., "Electron Microscopic Examination of the Surface of Stainless Steel by Means of the Oxide Replica Method," *Transactions*, Chalmers University of Technology, Gothenburg, Sweden, No. 96, 1950, p. 6.
- [12] Mahla, E. M. and Nielsen, N. A., "Carbide Precipitation in Type 304 Stainless Steel—An Electron Microscope Study," *Transactions*, American Society for Metals, Vol. 43, 1951, pp. 290–322.
- [13] Heidenreich, R. D. and Neshitt, E. A., "Physical Structure and Magnetic Anisotropy of Alnico 5. Part 1," *Journal of Applied Physics*, Vol. 23, 1952, pp. 352–365.
- [14] Nielsen, N. A., *Physical Metallurgy of Stress Corrosion Fracture*, Rhodin, T. N., ed., Interscience, New York, 1959.
- [15] Nielsen, N. A., "I. Nature of Initial Corrosion of Stressed Austenitic Steel by Chloride Ions. II. Platinum Decoration of Active Sites," *Corrosion*, Vol. 20, No. 3, March 1964, pp. 104t–110t.
- [16] Gulbransen, E. A., Phelps, R. T., and Hickman, J. W., "Electron Diffraction and Electron Microscopic Study of Oxide Films Formed on Metals and Alloys at Moderate Temperatures," *Industrial and Engineering Chemistry*, analytical edition, Vol. 18, 1946, pp. 391–400.
- [17] Zapffe, C. A. and Clogg, M., "Fractography—A New Tool for Metallurgical Research," *Transactions*, American Society for Metals, Vol., 34, 1945, p. 71.

